UNIVERSIDAD NACIONAL AUTONOMA DE MEXICO

FACULTAD DE CIENCIAS

DIVISION DE ESTUDIOS DE POSGRADO

DINAMICA Y TRANSFERENCIA DE CALOR EN FLUJOS DE METALES LIQUIDOS EN CAMPOS MAGNETICOS INTENSOS

T E S I S

QUE PARA OBTENER EL GRADO ACADEMICO DE:

DOCTOR EN CIENCIAS (FISICA)

P R E S E N T A:

SERGIO CUEVAS GARCIA

DIRECTORES DE TESIS:
DR. BASIL F. PICOLOGLOU
DR. EDUARDO RAMOS MORA

Cuevas

MEXICO, D. F. 1994

UNAM – Dirección General de Bibliotecas Tesis Digitales Restricciones de uso

A Judith, Eugenia

y bebé que nos acompaña

El presente documento constituye una síntesis del trabajo en inglés titulado *Liquid Metal Flow and Heat Transfer in Square Ducts under Strong Magnetic Fields* [Cuevas, 1994]. En esta síntesis se discute el contexto general del estudio y la motivación para llevarlo a cabo, asi como la formulación del problema a resolver y los principales resultados de la investigación. El desarrollo detallado del trabajo, la totalidad de los resultados y el análisis de los mismos, asi como la bibliografía completa, se encuentran en la referencia antes mencionada que se anexa al final de este documento.

Agradecimientos

La presente investigación se llevó a cabo en la *Engineering Physics Division* del *Argonne National Laboratory*, en Illinois, E.U.A. Primeramente, quisiera expresar mi gratitud al Dr. Basil F. Picologlou, quien fungió como mi supervisor de tesis en *Argonne*, por sus contribuciones y continuo apoyo durante el desarrollo de este trabajo. Su guía me permitió convertir mi estancia en *Argonne* en una experiencia enriquecedora. El Dr. Thanh Q. Hua del *Argonne National Laboratory* me ofreció muchos comentarios interesantes y, en particular, me guió en la implementación de los métodos numéricos. El Profesor John S. Walker de la *University of Illinois at Urbana*, contribuyó sustancialmente en la definición del problema dinámico y me introdujo al método espectral de colocación. La Dra. Gita Talmage de la *Pennsylvania State University* me orientó en la implementación del modelo de turbulencia. Agradezco profundamente a todos ellos su amigable y paciente ayuda durante el desarrollo del trabajo asi como sus numerosos y sustanciales comentarios que influyeron positivamente esta investigación. Deseo asimismo agradecer al personal del *Argonne National Laboratory*, especialmente de la *Engineering Physics Division*, por proveerme de todo tipo de apoyo durante mi placentera estancia.

Quisiera expresar un agradecimiento especial a los Drs. Eduardo Ramos Mora y Mariano López de Haro del *Laboratorio de Energía Solar, IIM-UNAM*, por el estímulo y continuo apoyo que me brindaron durante mis estudios de posgrado, al igual que por sus valiosos comentarios sobre esta tesis. Asimismo, deseo agradecer a los Drs. Rosalío Rodríguez, Julio Martinell, Ramón Peralta y Silvia Bravo, de la *Universidad Nacional Autónoma de México*, sus acertados comentarios sobre este trabajo.

Esta investigación fue financiada completamente mediante becas del *Consejo Nacional de Ciencia y Tecnología* (CONACYT) y del *Banco de México*, instituciones a las que agradezco profundamente su apoyo. Finalmente, deseo reconocer ampliamente el apoyo brindado por el *Instituto de Investigaciones Eléctricas*, en particular por el *Departamento de Fuentes No Convencionales*, para la realización de mi investigación doctoral.

DINAMICA Y TRANSFERENCIA DE CALOR EN FLUJOS DE METALES LIQUIDOS EN CAMPOS MAGNETICOS INTENSOS

Sergio Cuevas García

Resumen

Se presenta una investigación teórica sobre la dinámica y la transferencia de calor en flujos de metales líquidos en campos magnéticos intensos, en condiciones relevantes para la operación de los mantos autoenfriados de metal líquido de los reactores de fusión. Se analizan flujos de metal líquido estacionarios y completamente desarrollados, tanto en régimen laminar como en turbulento, en ductos rectangulares bajo la acción de un campo magnético transversal uniforme. Se obtiene una solución conjunta, mediante el método espectral de colocación, para el núcleo y la capa límite lateral que ofrece la posibilidad de analizar flujos en ductos con razones de conductividad eléctrica pared/fluido en el intervalo de interés para aplicaciones en mantos de reactores de fusión (*i.e.* de paredes conductoras delgadas a paredes aislantes). El flujo en las capas límite laterales (paralelas al campo magnético) se resuelve explícitamente aún para números de Hartmann muy grandes. Se estudian los efectos de la variacion de la razón de conductividades, c, de 0 a 0.05, y del número de Hartmann, M, de 10^3 a 10^5, sobre la estructura de flujo laminar. También se considera el problema laminar de transfrencia de calor en un ducto cuadrado con una pared lateral uniformemente calentada y tres paredes adiabáticas. La ecuación tridimensional de transfrencia de calor se resuelve mediante el método de diferencias finitas y se analiza la influencia de la variación de los parámetros c y M sobre la transferencia de calor. También se presentan algunos resultados del problema laminar de transfrencia de calor en un ducto cilíndrico para diferentes condiciones a la frontera. Posteriormente se lleva a cabo una revisión de la teoría de la turbulencia magnetohidrodinámica (MHD) y de resultados experimentales obtenidos en el Argonne National Laboratory, que demostraron la existencia de fluctuaciones de velocidad en las capas laterales. Para explorar los flujos MHD en ductos fuera del régimen laminar, se investiga un flujo turbulento completamente desarrollado. La solución núcleo-capa-lateral se generaliza para incluir efectos turbulentos a través de una viscosidad efectiva proveniente de la teoría de turbulencia del Grupo de Renormalización (GRN). Se realiza un estudio paramétrico de los perfiles turbulentos que, además de c

y M, incluye la variación del número de Reynolds de 5×10^4 a 5×10^5. Los resultados para flujos en ductos de paredes conductoras delgadas muestran el engrosamiento de las capas laterales donde se concentra la turbulencia, mientras que el núcleo permanece esencialmente inalterado. Por otra parte, los resultados turbulentos para ductos con paredes aislantes, esencialmente no presentan diferencias respecto al caso laminar. En general, se encuentran tendencias físicamente razonables. El análisis de transferencia de calor turbulenta se realiza variando los parámetros relevantes, utilizando de entrada los perfiles de velocidad turbulentos y una difusividad térmica efectiva de la teoría GRN. Los efectos turbulentos sobre la transferencia de calor no resultan tan intensos como sobre la dinámica del flujo. Como consecuencia, el mecanismo laminar de transferencia de calor en ductos con paredes conductoras delgadas resulta más eficiente que el turbulento en la mayoría de los casos estudiados.

Contenido

Capítulo 1

Introducción

1.1 La Tecnología de Fusión

Entre los diferentes reactores de fusión explorados durante los últimos años por la comunidad internacional, el sistema de confinamiento Tokamak que utiliza como combustible una mezcla de deuterio y tritio, parece ser la alternativa más viable para el desarrollo a gran escala. En tal sistema, el plasma de deuterio-tritio se confina mediante un campo magnético toroidal generado por imanes superconductores. La reacción de fusión que tiene lugar dentro del Tokamak produce un átomo de helio, un neutrón de alta energía y radiación. Mientras que el deuterio es un elemento que abunda en la naturaleza, el tritio no se encuentra en cantidades significativas y, por consiguiente, debe generarse en el reactor. Esta generación o cría del tritio se lleva a cabo mediante el *manto* (blanket) de litio que rodea al plasma, donde los neutrones de alta energía producidos por la reacción de fusión colisionan produciendo helio y átomos de tritio. El calor liberado por los neutrones durante la colisión se deposita en el litio y puede transferirse a otro fluido (por ejemplo helio a altas temperaturas) que a su vez mueva unas turbuinas para generar electricidad. Básicamente, se pueden considerar tres diferentes tipos de mantos de litio: un compuesto cerámico sólido de litio, litio o una mezcla de litio-plomo en estado líquido en reposo, o bien litio o litio-plomo en estado líquido en movimiento. Mientras que los dos primeros requieren de un sistema secundario de enfriamiento, por ejemplo, agua o helio, el tercer sistema es autorefrigerante, permaneciendo al metal líquido en circulación a través del reactor, el separador de tritio, el intercambiador de calor y la bomba de alimentación. Los mantos de metal líquido autoenfriados han sido favorecidos debido a sus características de operación y a la simplicidad de diseño. Las tres principales funciones del manto, a saber, la absorción de la energía del flujo de neutrones, la cría del tritio y la transferencia de calor al sistema externo de conversión de energía, pueden ser llevadas a cabo por estos sistemas. Sin embargo, es necesario resolver varias cuestiones previas a la implementación de esta tecnología.

1.2 Consideraciones Magnetohidrodinámicas

La principal constricción en el diseño de los mantos de metal líquido autoenfriados proviene del hecho de que al encontrarse dentro de las bobinas superconductoras, el metal líquido fluye en presencia de un campo magnético muy intenso (5-10 Tesla), lo que trae como consecuencia la aparición de efectos magnetohidrodinámicos muy fuertes. En primer lugar, el flujo de metal líquido a través de los ductos que forman el manto interactua con el campo magnético aplicado, induciendo corrientes eléctricas que a su vez interactuan con el campo dando lugar a una fuerza electromagnética, conocida como fuerza de Lorentz. Esta fuerza se opone al flujo del fluido ocasionando grandes pérdidas de presión que incrementan la potencia requerida para bombear al líquido a través del manto y además, dichas caídas de presión pueden originar esfuerzos mecánicos inaceptables en la primera pared que separa al manto del vacío alrededor del plasma. Estos esfuerzos dependen básicamente de las corrientes eléctricas inducidas que circulan en el metal líquido y en las paredes de los ductos. Para determinar los esfuerzos en la primera pared asi como la temperatura y las características de transferencia de calor del manto del reactor, se requieren predicciones precisas de las caídas de presión MHD y de los patrones de flujo. Por consiguiente, un diseño exitoso del manto debe apoyarse en un entendimiento profundo de los fenómenos MHD que tienen lugar en estos sistemas.

En este contexto, en el Argonne National Laboratory se dió inicio en 1984 a un programa teórico-experimental de investigación de flujos MHD de metal líquido en condiciones relevantes para la operación de un reactor de fusión. El programa ha arrojado información experimental valiosa sobre la estructura detallada de tales flujos y, por otra parte, se han desarrollado herramientas predictivas para flujos MHD en campos magnéticos intensos, encontrandose en general un buen acuerdo entre los resultados teóricos y los experimentales. La mayoría de los estudios teóricos se han efectuado suponiendo que pueden despreciarse los términos inerciales, de manera que se tiene un flujo laminar donde la fuerza electromagnética es la interacción dominante que determina el flujo y las distribuciones de presión en el metal líquido, a exepción de delgadas capas límite cercanas a las paredes. En términos de los parámetros adimensionales que caracterizan el flujo, es decir, el número de Hartmann M, cuyo cuadrado puede interpretarse como el cociente de la fuerza electromagnética y la viscosa, y el parámetro de interacción N, que se considera una medida relativa de las interacciones electromagnéticas e inerciales en el flujo, esta aproximación vale, en principio, cuando M y N toman valores muy grandes. Este es el caso para flujos de metales líquidos en mantos autoenfriados, debido a la presencia de campos magnéticos muy intensos, donde M y N toman valores en el rango $10^3 - 10^5$. El número de Hartmann y el parámetro de interacción se definen como

$$M = BL\sqrt{\frac{\sigma}{\rho\nu_o}},$$

y

$$N = \frac{\sigma B^2 L}{\rho U},$$

respectivamente, donde B es la intensidad del campo magnético aplicado, σ, ρ y ν_o son la conductividad eléctrica, la densidad y la viscosidad cinemática del fluido y L y $\bar{U}$ son una longitud y una velocidad características del flujo, respectivamente. Nótese que $N = M^2/Re$, donde Re es el número de Reynolds. Otro parámetro adimensional de interés es el número de Reynolds magnético, definido como

$$Rm = \mu\sigma U L,$$

donde μ es la permeabilidad magnética. Rm comunmente se interpreta como la razón del campo magnético inducido por las corrientes que circulan en el medio y el campo magnético aplicado. En la mayoía de las aplicaciones terrestres, Rm presenta valores muy pequeños, indicando que el campo inducido es despreciable en comparación al campo aplicado. Esto se satisface en los mantos de litio autoenfriados, donde $Rm = 0.001 - 0.1$. De manera que en el presente trabajo se utiliza la aproximación $Rm \ll 1$. Adicionalmente a los números adimensionales definidos arriba, para flujos en ductos comunmente se utiliza otro parámetro conocido como la razón de conductividades pared/fluido, que se define mediante la expresión

$$c = \frac{\sigma_w t_w}{\sigma L},$$

donde σ_w y t_w son la conductividad eléctrica de la pared del ducto y el grosor de la misma, respectivamente. El parámetro c da una medida de la conductividad eléctrica de la pared relativa a la conductividad del fluido. En los ductos que conforman el manto de los reactores de fusión, c puede tomar valores de 0 a 0.1.

1.3 Inestabilidades en Capas Laterales

Es un hecho conocido el efecto de laminarización que, bajo ciertas circunstancias, ejerce un campo magnético sobre el flujo turbulento de un fluido eléctricamente conductor. Por consiguiente, sería razonable esperar que para las condiciones que prevalecen en los mantos de metal líquido de los reactores de fusión, el campo magnético prevendría el crecimiento de cualquier posible inestabilidad, amortiguando las fluctuaciones que podrían llevar a la aparición de turbulencia. Sin embargo, experimentos realizados en el Argonne National Laboratory han confirmado la existencia de fluctuaciones de velocidad que persisten en la región cercana a la pared lateral (paralela al campo magnético) de un ducto rectangular bajo condiciones que se aproximan a las que prevalecen en un reactor de fusión [Reed y Picologlou, 1989]. A la fecha, estas fluctuaciones no se

entienden completamente y merecen una atención más profunda debido a las implicaciones tecnológicas que podrían derivarse de este fenńeno. Los datos experimentales indican que el flujo no es turbulento, al menos en el sentido convencional, presentando una marcada periodicidad y carencia de estructura de pequeña escala. Se especula que las fluctuaciones se originan como resultado de una inestabilidad en los chorros de fluido que se forman en las capas límite asociadas a las paredes laterales y que son característicos de flujos en ductos de paredes conductoras delgadas. Un análisis de estabilidad lineal preliminar de estos flujos constituye un primer intento teórico de caracterizar esta inestabilidad [Ting, et al., 1991]. Aunque el análisis ofrece conclusiones interesantes, está fuertemente limitado por su carácter lineal, mientras que el fenómeno real presenta una naturaleza altamente no-lineal. Estudios experimentales independientes efectuados en la Universidad de Beer-Sheva, han corroborado la existencia de fluctuaciones de velocidad en la región cercana a las paredes laterales, sin embargo, tales estudios fueron llevados a cabo en condiciones alejadas a las condiciones relevantes para la operación de un reactor de fusión. Desde el punto de vista práctico, la existencia de fluctuaciones de velocidad en la región cercana a la pared, podría tener efectos benéficos en términos de un mejoramientos de las tasas de transferencia de calor. Evidentemente, esto tendría implicaciones inmediatas en el diseño del manto del reactor. Sin embargo, todavía son necesarios estudios adicionales teóricos y experimentales para clarificar la naturaleza del fenómeno y valorar las características de transferencia de calor. Existen muchas interrogantes respecto al comportamiento de las capas laterales fuera del régimen laminar pero está claro que estas capas juegan un papel fundamental en la estabilidad y en la determinación de las características de transferencia de calor de estos flujos.

El presente estudio tuvo por objeto la investigación teórica de la dinámica y la transferencia de calor de flujos de metales líquidos en campos magnéticos intensos, tanto en ductos de paredes eléctricamente aislantes como en ductos de paredes conductoras delgadas. Se estudiaron flujos en régimen laminar y turbulento, poniendo especial énfasis en el análisis de las capas límites laterales. Esencialmente, se estudió cómo se ve afectada la estructura de las capas límite laterales debido a la conductividad eléctrica de las paredes, la intensidad del campo magnético y los efectos inerciales, y cómo estos factores afectan el proceso de transferencia de calor. En los capítulos subsiguientes se lleva a cabo una síntesis de los pricipales tópicos y resutados presentados en los capítulos correspondientes del documento fuente antes mencionado [Cuevas, 1994]. En el capítulo 2 se revisan las principales características de los flujos laminares de metal líquido en ductos rectangulares en presencia de campos magnéticos intensos. Se formula el problema dinámico a resolver, es decir, el flujo completamente desarrollado de un metal líquido en un ducto rectangular inmerso en un campo magnético transversal tanto en régimen laminar como en turbulento, y se establecen las condiciones de simetría y de frontera correspondientes que permiten la variación de la conductividad eléctrica de las paredes del ducto, desde ductos aislantes hasta ductos con paredes conductoras

delgadas. Asimismo, se comenta el método espectral de colocación utilizado para la solución de las ecuaciones dinámicas. En el capítulo 3, se discuten las soluciones para el flujo laminar asi como los resultados de transferencia de calor obtenidos mediante el método de diferencias finitas, y se analiza la influencia del número de Hartmann y de la razón de conductividades sobre los perfiles laminares. En el capítulo 4, se resaltan algunas cuestiones de la teoría de la turbulencia MHD que son de relevancia para el presente estudio. En el capítulo 5, se exploran los efectos que tendría sobre el flujo y la transferencia de calor, la eventual aparición de turbulencia. El problema se resuelve con ayuda de un modelo de turbulencia estándar, usando como datos de entrada los perfiles de velocidad laminares MHD. Para el estudio de transferencia de calor se utilizan los perfiles de velocidad turbulentos y una difusividad térmica efectiva dada por el mismo modelo. Finalmente, en el capítulo 6 se exponen las conclusiones del presente estudio.

Capítulo 2

Flujos MHD en Ductos Rectangulares

2.1 Flujo de Metales Líquidos en Ductos con Campos Magnéticos Intensos

Los flujos laminares de metales líquidos en ductos en presencia de campos magnéticos intensos han sido estudiados ampliamente desde hace más de dos décadas debido principalmente a su relevancia en la tecnología de fusión. En el presente estudio se consideran principalmente flujos en ductos de sección transversal rectangular.

La primera característica que puede resaltarse de los flujos de metales líquidos en ductos rectangulares bajo un campo magnético transversal intenso ($M \gg 1$) es la formación de diferentes subregiones dentro del flujo, a saber, el núcleo, las capas límite de Hartmann adyacentes a las paredes superior e inferior (perpendiculares al campo), las capas límite laterales asociadas a las paredes paralelas al campo aplicado, y las esquinas. Una estimación del orden de magnitud de estas subregiones muestra que, en términos adimensionales, el grosor de las capas de Hartmann es $O(M^{-1})$, mientras que las laterales son $O(M^{-1/2})$, en tanto que las esquinas son $O(M^{-1}) \times O(M^{-1/2})$. Cuando M es muy grande, estas capas son my delgadas. El núcleo del flujo puede considerarse invíscido, empatando los valores de la velocidad y el potencial eléctrico con los valores en las paredes a través de las capas límite, donde se concentran los efectos viscosos. Estas capas proveen una trayectoria alternativa para cerrar las corrientes eléctricas y tienen un papel decisivo en la dinámica y en la transfrencia de calor del flujo. Dependiendo de los valores de c y M , la velocidad en las capas límite laterales puede ser mucho mayor que la velocidad en el núcleo y, bajo ciertas circunstancias, una parte sustancial del flujo volumétrico puede ser acarreado en estas capas. Esta característica puede afectar de una manera positiva el proceso de transferencia de calor.

Considérese un ducto rectangular con un sistema coordenado tal que el plano yz se

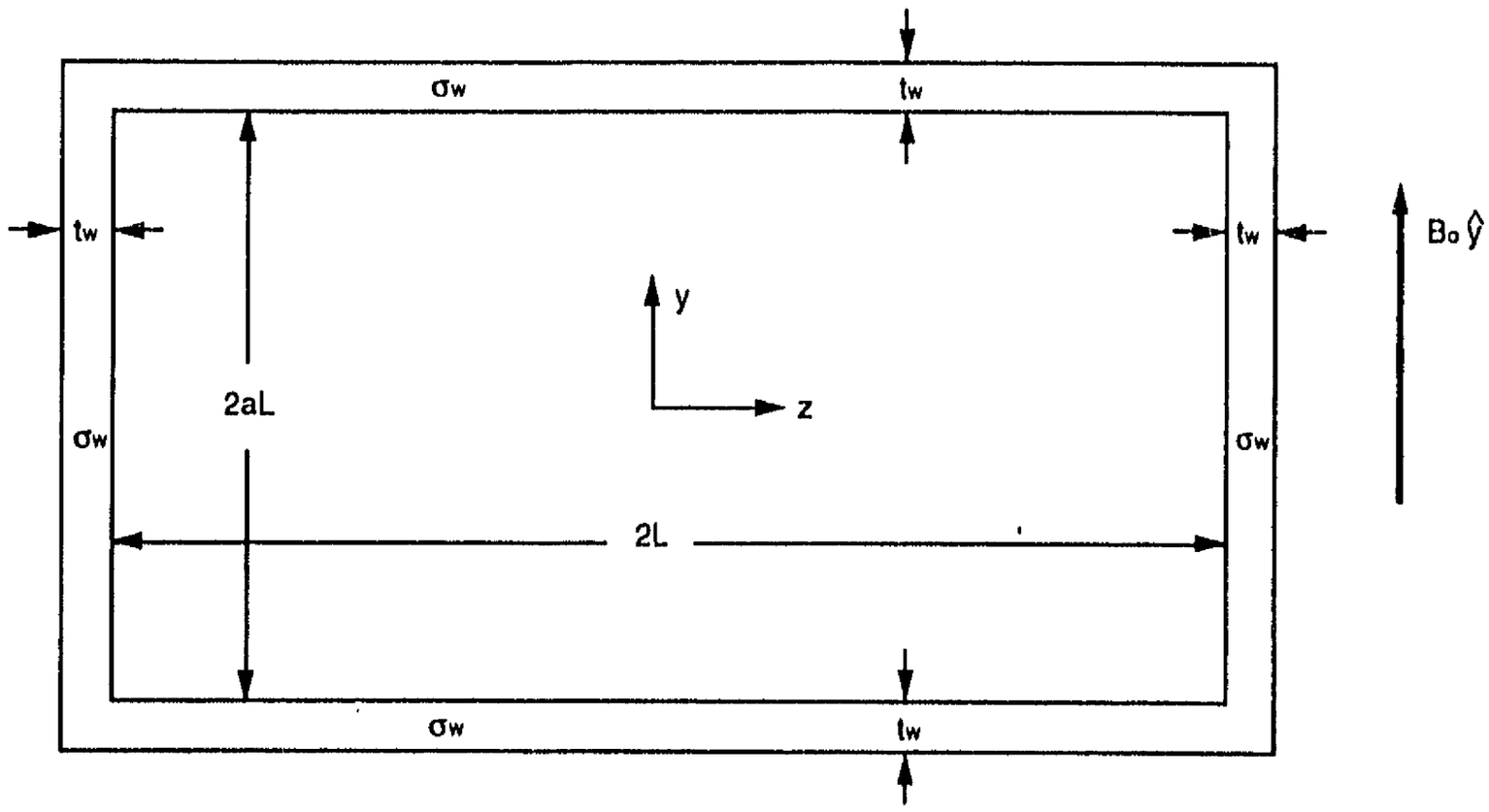

Figura 2.1: Sección transversal del ducto y dimensiones relevantes.

encuentra en la sección transversal del ducto con el origen en el centro del mismo y el eje x en la dirección axial (ver fig. 2.1). Si el metal líquido fluye en la dirección positiva del eje x y el campo magnético se aplica en la dirección y positiva, se inducirá una corriente eléctrica en el núcleo del flujo en la dirección z positiva. La corriente tiene que encontrar una trayectoria de retorno dentro del ducto, ya que no existe un circuito externo. La corriente que sale del núcleo penetra la capa lateral y eventualmente alcanza la pared. El factor que determina si la corriente fluye por la pared o por la capa lateral en dirección y, es la magnitud relativa de las resistencias eléctricas de la pared y la capa, consideradas como resistencias en paralelo. Una vez que la corriente ha alcanzado la pared superior (inferior), fluirá en la dirección z negativa ya sea a través de la pared o bien a través de las capas de Hartmann, o se dividirá entre las dos. Nuevamente, la trayectoria final dependerá de las magnitudes de las resistencias de la pared y la capa en cuestión. Después, la corriente alcanzará la pared lateral opuesta y fluirá en la dirección y negativa (positiva), donde se aplican consideraciones similares. Eventualmente, la corriente saldrá de la región pared-capa-lateral y regresará al núcleo, cerrando el circuito. Nótese que la corriente que fluye a través del metal líquido depende de todas las resistencias, incluyendo la resistencia interna del líquido. Además, esta corriente determinará la fuerza electromagnética ejercida sobre el fluido y la caída de presión adicional requerida para vencer dicha fuerza.

Las resistencias del fluido, capas límite y paredes pueden estimarse en términos de

los parámetros geométricos del ducto y las conductividades eléctricas involucradas. A partir de estas resistencias es posible establecer criterios o aproximaciones en términos de los parámetros adimensionales para determinar por dónde fluirán las corrientes. Así, puede demostrarse que cuando la resistencia de las capas de Hartmann es mucho mayor que la de las paredes superior/inferior, se satisface la condición $c \gg M^{-1}$. En este caso la corriente fluirá por las paredes y no por la capa de Hartmann. El caso opuesto se tendría cuando $c \ll M^{-1}$. Similarmente, si la resistencia en la capa lateral es mucho mayor que en las paredes laterales, se encuentra que $c \gg M^{-\frac{1}{2}}$, en tanto que la condición $c \ll M^{-\frac{1}{2}}$ expresa el hecho de que la resistencia de la capa lateral es mucho menor que la de las paredes laterales. Un caso de gran importancia práctica en los estudios de los mantos de los reactores de fusión núclear, es el de los ductos con paredes conductoras delgadas. En este caso se supone que la resistencia eléctrica de las paredes del ducto es mucho mayor que la resistencia interna del metal líquido pero mucho menor que la de las capas de Hartmann. Esta condición, que se expresa mediante la relación

$$M^{-1} \ll c \ll 1,$$

es una aproximación muy común que permite el establecimiento de condiciones a la frontera que involucran únicamente variables del fluido y ha sido ampliamente utilizada en flujos de metales líquidos en mantos. Si además se satisface $M^{-\frac{1}{2}} \ll c \ll 1$, la velocidad en la capa lateral es $O(M^{\frac{1}{2}})$ y ambas capas acarrean una fracción de $O(1)$ del flujo volumétrico.

La existencia de capas laterales con altas velocidades en ductos de paredes conductoras delgadas puede explicarse de diferentes maneras. Hunt [1965] ofrece una descripción en términos de la fuerza de Lorentz que actua sobre el núcleo y las capas. Sin embargo, él consideró únicamente el caso de un ducto cuyas paredes superior e inferior son perfectamente conductoras mientras que las paredes laterales son de conductividad arbitraria. En tal caso, las líneas de corriente siempre se cierran a través de las paredes superior e inferior. La fuerza de Lorentz que se opone al flujo del líquido está dada por $\mathbf{j} \times \mathbf{B}_o$, donde $\mathbf{j}$ es la densidad de corriente eléctrica y $\mathbf{B}_o$ es el campo magnético aplicado. Mientras que en el núcleo del flujo la componente de la densidad de corriente en la dirección z es máxima ($j_y = 0$), en las capas laterales j_z puede verse disminuida ya que j_y puede tener un valor finito (dependiendo de la razón de conductividades, c). Por lo tanto, en el núcleo la fuerza será mayor, ya que toda la corriente contribuye a $\mathbf{j} \times \mathbf{B}_o$, mientras que en las capas laterales la fuerza disminuirá pues j_y no contribuye a la fuerza de Lorentz. Por ejemplo, si la pared lateral es altamente conductora ($c \gg M^{-\frac{1}{2}}$)), la corriente retornará a través de la pared lateral, dando lugar a una componente j_z muy grande en esta región y consecuentemente a una fuerza grande y una velocidad lateral baja. Por otra parte, al reducir la conductividad de la pared (*i.e.* al reducir c), la corriente regresará a través de la capa lateral. Entonces la componente j_z en la capa lateral será pequeña, dando lugar a una fuerza pequeña y a una velocidad

lateral alta. En un ducto con las cuatro paredes con la misma conductividad arbitraria, este análisis ya no ofrece una descripción adecuada al disminuir la razón de conductividad. La razón es que cuando c es suficientemente pequeña, las corrientes inducidas en el núcleo ya no se cierran a través de las paredes superior e inferior sino a través de las capas de Hartmann y por consiguiente el arrastre electromagnético en el flujo se reduce. Eventualmente, para una c demasiado pequeña ($c \ll M^{-1}$), los excesos de velocidad en las capas laterales serán completamente suprimidos, como es el caso de un ducto con paredes aislantes. Reed y Picologlou [1989] ofrecen un análisis simplificado de los fenómenos presentes en las capas laterales en ductos con paredes conductoras delgadas bajo la condición $M^{-\frac{1}{2}} \ll c \ll 1$. En este análisis, que se reproduce con detalle en [Cuevas, 1994], los chorros laterales se explican debido a una discontinuidad en el valor del potencial eléctrico en el núcleo y el valor en la pared lateral (es decir, a través de la capa lateral) que da lugar, por virtud de la ley de Ohm, a un flujo finito de fluido en la capa lateral.

2.2 Formulación del Problema

El problema principal que se resuelve en el presente estudio es el de un flujo estacionario completamente desarrollado de un metal líquido en un ducto de sección transversal rectangular bajo la acción de un campo magnético transversal. El desarrollo detallado del problema, con las ecuaciones y condiciones a la frontera que gobiernan el flujo se encuentra en [Cuevas, 1994]. El problema se trata tanto en régimen laminar como en turbulento, para lo cual se plantean las ecuaciones que gobiernan la dinámica del flujo en cada régimen, acopladas a las ecuaciones del campo electromagnético, bajo la aproximación MHD. Adicionalmente, se utiliza la aproximación $Rm \ll 1$. La ecuación de la energía se considera en el capítulo 3. Al suponer un flujo estacionario completamente desarrollado, el problema se reduce a dos dimensiones, con un gradiente de presión constante entre los extremos del ducto, siendo diferente de cero únicamente la componente de la velocidad u en la dirección axial x. La velocidad u, al igual que el potencial eléctrico ϕ, depende sólo de las coordenadas y y z. En términos adimensionales, las ecuaciones que gobiernan el problema en régimen laminar bajo las condiciones mencionadas son las siguientes:

$$M^{-2}\left[\frac{\partial^2 u}{\partial y^2}+\frac{\partial^2 u}{\partial z^2}\right]-j_z=\frac{\partial p}{\partial x}=-K \tag{2.1}$$

$$j_y=-\frac{\partial \phi}{\partial y}, \tag{2.2}$$

$$j_z=-\frac{\partial \phi}{\partial z}+u, \tag{2.3}$$

$$\frac{\partial j_y}{\partial y} + \frac{\partial j_z}{\partial z} = 0, \tag{2.4}$$

donde p es la presión, K es una constante, j_y y j_z son las componentes de la densidad de corriente en las direcciones y y z, respectivamente y, además, el campo magnético (adimensional) es de la forma $\mathbf{B} = \hat{\mathbf{y}}$. Además, en la paredes se deben satisfacer la ley de Ohm y la conservación de corriente, es decir,

$$j_{yw} = -\left(\frac{\sigma_w}{\sigma}\right)\frac{\partial \phi_w}{\partial y}, \tag{2.5}$$

$$j_{zw} = -\left(\frac{\sigma_w}{\sigma}\right)\frac{\partial \phi_w}{\partial z}, \tag{2.6}$$

$$\frac{\partial j_{yw}}{\partial y} + \frac{\partial j_{zw}}{\partial z} = 0, \tag{2.7}$$

donde el subíndice w denota una propiedad o variable de la pared, siendo σ y σ_w las conductividades eléctricas del fluido y de la pared, respectivamente. En la interfaz líquido y pared, tanto ϕ como $\mathbf{j} \cdot \hat{\mathbf{n}}$ son contínuas, donde $\hat{\mathbf{n}}$ representa la normal a la pared.

El caso turbulento de trata utilizando el enfoque de Reynolds en el que las variables de flujo instantaneas se expresan como la suma de una parte promedio y una fluctuación con promedio cero. De esta forma se obtienen ecuaciones para las variables promedio, mientras que los efectos turbulentos en la ecuación de balance de momento aparecen a través del tensor de esfuerzos de Reynolds, dado en términos de las fluctuaciones de velocidad. Es decir, en términos adimensionles la ecuación de balance de momento toma la forma

$$M^{-2}\left[\frac{\partial}{\partial y}\left(\frac{\partial \bar{u}}{\partial y} - Re < u'v' >\right) + \frac{\partial}{\partial z}\left(\frac{\partial \bar{u}}{\partial z} - Re < u'w' >\right)\right] - \bar{j}_z - \frac{\partial \bar{p}}{\partial x} = 0, \tag{2.8}$$

donde $\bar{u}$, $\bar{\phi}$, $\bar{j}_z$ y $\bar{p}$ representan las correspondientes variables promedio, en tanto que u', v' y w' son las fluctuaciones de velocidad. Para poder cerrar el sitema de ecuaciones se utiliza el enfoque de Boussinesq que supone que los esfuerzos turbulentos promedio, τ_{xy} y τ_{xz}, dados por el tensor de Reynolds, pueden expresarse en la misma forma que los esfuerzos laminares (*i.e.* mediante gradientes de la velocidad media) pero con una viscosidad efectiva que toma en cuenta los efectos turbulentos, es decir,

$$\tau_{xy} = -Re < u'v' > = \nu_{ey}\frac{\partial \bar{u}}{\partial y}, \tag{2.9}$$

$$\tau_{xz} = -Re < u'w' > = \nu_{ez}\frac{\partial \bar{u}}{\partial z}, \tag{2.10}$$

donde ν_{ej} $(j = y, z)$ es la viscosidad efectiva adimensional (eddy viscosity). Debido al efecto anisotrópico del campo magnético, se consideran viscosidades efectivas diferentes para cada dirección. De esta forma, el problema de cerradura del sistema de ecuaciones se reduce a determinar un escalar, es decir, la viscosidad efectiva ν_{ej}. Introduciendo las ecuaciones (2.9) y (2.10) en la ecuación (2.8) y definiendo las difusividades viscosas totales como

$$\nu_{ty} = 1 + \nu_{ey},$$

$$\nu_{tz} = 1 + \nu_{ez},$$

-que toman encuenta las contribuciones molecular y turbulenta- se puede expresar el sistema de ecuaciones para las variables promedio de la siguiente forma:

$$M^{-2}\left[\frac{\partial}{\partial y}\left(\nu_{ty}\frac{\partial \bar{u}}{\partial y}\right) + \frac{\partial}{\partial z}\left(\nu_{tz}\frac{\partial \bar{u}}{\partial z}\right)\right] - \bar{j}_z = \frac{\partial \bar{p}}{\partial x} = -K \tag{2.11}$$

$$\bar{j}_y = -\frac{\partial \bar{\phi}}{\partial y}, \tag{2.12}$$

$$\bar{j}_z = -\frac{\partial \bar{\phi}}{\partial z} + \bar{u}, \tag{2.13}$$

$$\frac{\partial \bar{j}_y}{\partial y} + \frac{\partial \bar{j}_z}{\partial z} = 0, \tag{2.14}$$

en donde también $\bar{\mathbf{B}} = \hat{\mathbf{y}}$. Similarmente al caso laminar, las variables promedio deben satisfacer la ley de Ohm y la conservación de la corriente en las paredes:

$$\bar{j}_{yw} = -\left(\frac{\sigma_w}{\sigma}\right)\frac{\partial \bar{\phi}_w}{\partial y}, \tag{2.15}$$

$$\bar{j}_{zw} = -\left(\frac{\sigma_w}{\sigma}\right)\frac{\partial \bar{\phi}_w}{\partial z}, \tag{2.16}$$

$$\frac{\partial \bar{j}_{yw}}{\partial y} + \frac{\partial \bar{j}_{zw}}{\partial z} = 0. \tag{2.17}$$

Nótese que haciendo $\nu_t = 1$ y quitando las barras de promedio, las ecuaciones (2.8)-(2.17) se reducen al sistema de ecuaciones laminar (2.1)-(2.7).

La solución del problema se plantea eliminando las densidades de corriente eléctrica en términos de una función de corriente. Debido a las condiciones de simetría, la solución se obtiene sólo para un cuarto de la sección transversal del ducto. En principio, la interacción electromagnética generada por el flujo del metal líquido en el campo

magnético aplicado, se extiende más allá del fluido, a las paredes y al medio circundante. Esto significa que la densidad de corriente eléctrica y el potencial eléctrico del fluido, paredes y medio circundante, están acopladas, y las ecuaciones de Maxwell deben satisfacerse en todo el espacio. Sin embargo, suponiendo que las paredes son conductoras y delgadas y que el medio circundante es un aislante eléctrico, es posible deducir condiciones de frontera en términos únicamente de las variables del fluido, desacoplando el problema del fluido y el de la pared [Walker, 1981]. Es precisamente esta aproximación de paredes conductoras delgadas la que se utilizó para obtener las condiciones a la frontera del problema, aplicándose tanto a la pared lateral como a la pared superior. Ya que en el caso de la pared superior, la aproximación mencionada no permite obtener el límite correcto al hacer tender la conductividad de la pared a cero, es decir, al llegar al límite de una pared aislante, la condición a la frontera tuvo que generalizarse para considerar el límite mencionado. Mientras que al considerar paredes con una conductividad eléctrica finita las corrientes tienen la posibilidad de cerrarse a través de las paredes, al tender la conductividad a cero la corriente no puede atravesar las paredes y debe cerrarse necesariamente dentro del fluido. En la parte superior del ducto, en particular, las corrientes tienen que cerrarse a través de las capas de Hartmann. La extensión que se hizo a las condiciones de frontera fue, precisamente, el permitir que la corriente fluya a través de las capa de Hartmann cuando $c \to 0$. Esta es una modificación muy importante que no se había efectuado previamente y que permite analizar flujos en ductos cuyas paredes presentan conductividades eléctricas dentro del intervalo de interés para la tecnología de fusión, es decir, de paredes aislantes a paredes conductoras delgadas. El sistema de ecuaciones fue planteado en general para el caso turbulento pudiéndose recuperar el caso laminar al hacer la viscosidad efectiva (adimensional) igual a uno, es decir, igual a la viscosidad molecular.

Como ya se mencionó, el objetivo principal del estudio es el análisis de los fenómenos que tienen lugar en las capas laterales que son las responsables de las características de transfrencia de calor y de posibles inestabilidades del flujo. En esta perspectiva, las capas de Hartmann juegan un papel pasivo, en el sentido de servir únicamente como trayectoria de retorno de las corrientes eléctricas. Por otra parte, la resolución numérica de las capas de Hartmann resulta demasiado costosa desde el punto de vista computacional y para los altos números de Hartmann y parámetros de interacción de interés para las aplicaciones de fusión, tal resolución resulta prácticamente imposible. Por tal motivo, en el presente estudio se atacó el problema de una manera simplificada, a saber, considerando una solución conjunta para las capas laterales y el núcleo. En esta aproximación, se ignoran las regiones de intersección (esquinas) y las capas de Hartmann. Realmente, las capas de Hartmann son sólo parcialmente ignoradas pues se permite su existencia como trayectoria de retorno para las corriente pero no se resuelven numéricamente. Esto quiere decir que no se satisface la condición de frontera de no-deslizamiento en la pared superior pero si se satisfacen conservación de corriente y ley de Ohm en tal región. La solución del sistema de ecuaciones re-

sultante para el flujo núcleo-pared-lateral se obtuvo mediante el método espectral de colocación. Este método presenta varias ventajas tales como una fácil implementación numérica, una solución muy eficiente en términos computacionales y la posibilidad de considerar números de Hartmann muy altos $(10^3 - 10^5)$ tanto en flujos laminares como en turbulentos. Esto significa que la estructura de la capa lateral puede explorarse en detalle aún para M muy grande. La solución se obtuvo en la forma de una serie de polinomios de Chebyshev, reduciendo el sistema de ecuaciones diferenciales parciales a un sistema de ecuaciones lineales algebraíco para los coeficientes de la serie que se resolvió mediante el método de eliminación de Gauss. Para la obtención del sistema de ecuaciones algebraíco, se utilizó el método de puntos de colocación [Cuevas, 1994]. Para el caso laminar, las soluciones fueron obtenidas de manera directa en tanto que en el caso turbulento, las soluciones se obtuvieron iterativamente, reescalando al final el número de Reynolds y el gradiente de presión.

Capítulo 3

Análisis de Flujo y Transferencia de Calor en Régimen Laminar

3.1 Flujo Laminar MHD en un Ducto Cuadrado

Primeramente se estudió el flujo laminar en estado estacionario de un metal líquido en un ducto cuadrado con un campo magnético transversal externo. Se analizó cómo se ve afectada la estructura del flujo por la presencia de campos magnéticos intensos y paredes de diferente conductividad eléctrica. En régimen laminar, los parámetros relevantes que gobiernan el comportamiento del flujo son el número de Hartmann, M, y la razón de conductividades, c. El número de Reynolds no es de importancia en este caso pues se asume que todos los flujos son estables independientemente del valor de M y c, siempre y cuando Re sea lo suficientemente pequeño. Los cálculos numéricos fueron validados previamente comparándolos con soluciones analíticas disponibles para los casos $c = 0$ y $c = 0.1$, encontrándose una concordancia bastante aceptable. Una vez efectuada la validación, se procedió a analizar las estructuras de flujo para tres números de Hartmann de interés: 10^3, 10^4 y 10^5. Por otra parte, la razón de conductividades, c, tomó los siguientes valores, que van de paredes aislantes a conductoras delgadas: 0, 0.001, 0.01, 0.05. Al analizar la influencia del número de Hartmann sobre el perfil de velocidades para un ducto con paredes conductoras delgadas con $c = 0.05$ (ver fig. 3.1), se observó que cuando la interacción magnética es despreciable ($M = 1$) el perfil es parabólico. Al ir aumentando M el perfil se aplana primero ($M = 10$) y después aparece un perfil en forma de M en donde la velocidad en la capa lateral es mayor que la velocidad en el núcleo. Esta tendencia se acentua al seguir aumentando M y eventualmente aparece un flujo en retroceso ($M = 10^3$). Para ductos con paredes conductoras delgadas la velocidad en la capa lateral es $O(M^{\frac{1}{2}})$ y alcanza su máximo en el plano medio del canal. Al aproximarse a la pared superior, el exceso de velocidad en la pared va disminuyendo (parabolicamente) hasta desaparecer al llegar a la pared mencionada (ver fig. 3.2). El flujo en el núcleo es prácticamente un flujo tapón, es

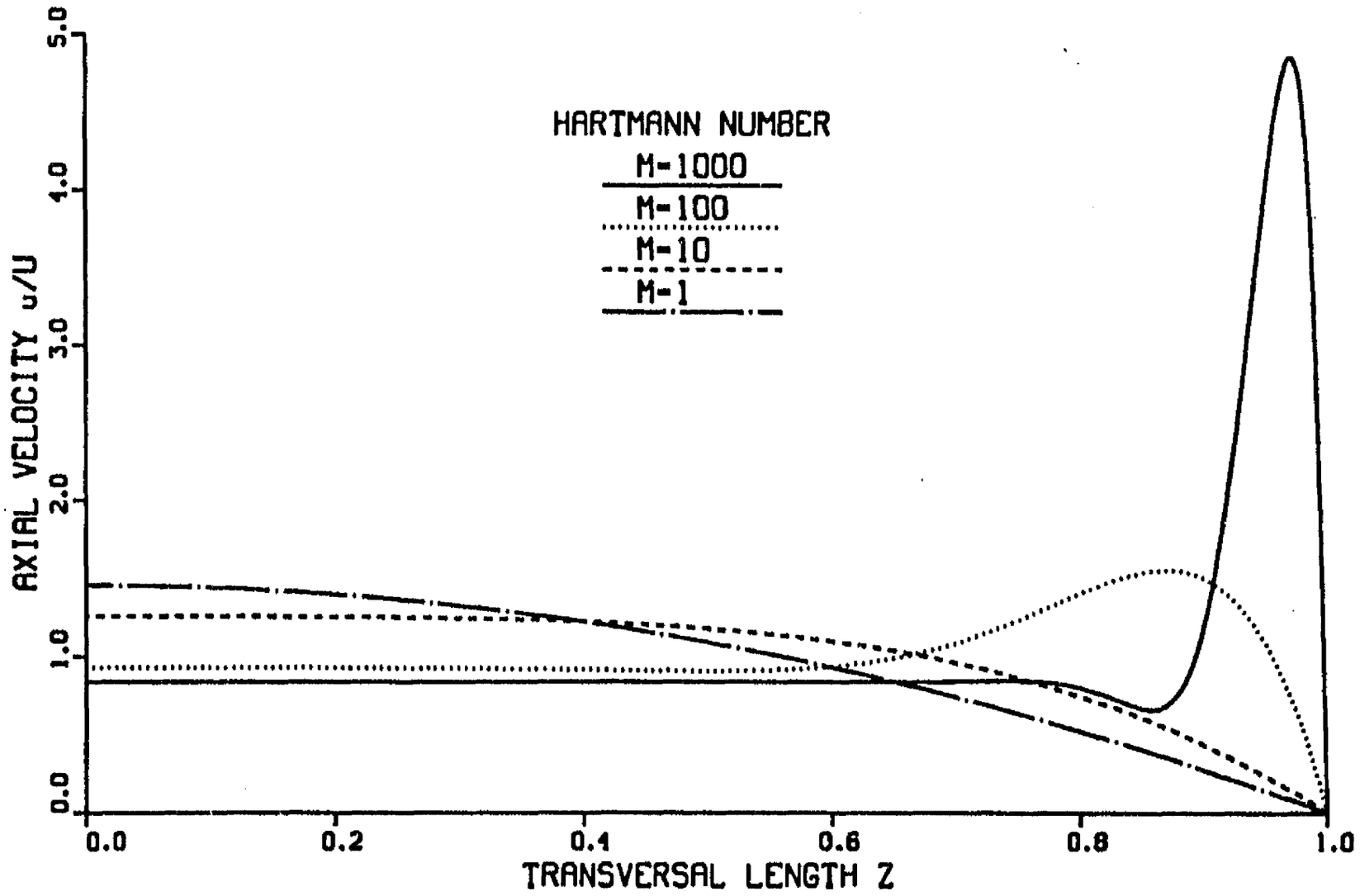

Figura 3.1: Velocidad laminar vs. z en $y = 0$ para diferentes números de Hartmann. $c = 0.05$.

decir, un flujo totalmente plano (sin gradientes). Debido a que la velocidad en la capa lateral es $O(M^{\frac{1}{2}})$, la diferencia en velocidades en dicha capa de $M = 10^3$ a $M = 10^5$ es dramática (ver fig. 3.3). Por otra parte, al considerar un ducto con paredes aislantes ($c = 0$), el perfil de velocidades es esencialmente plano en toda la región, siendo la velocidad en la capa lateral $O(1)$. El efecto del aumento del número de Hartmann en este caso se manifiesta mediante un aplanamiento cada vez mayor del perfil, llegando a ser prácticamente igual a un flujo tapón para el caso $M = 10^5$ (ver fig. 3.4). La transición del perfil de velocidades conforme la razón de conductividades se reduce de 0.05 a 0 para un número de Hartmann dado, muestra la reducción paulatina del exceso de velocidad en la capa lateral hasta desaparecer completamente al llegar a $c = 0$, donde el flujo es esencialmente plano (ver fig. 3.5).

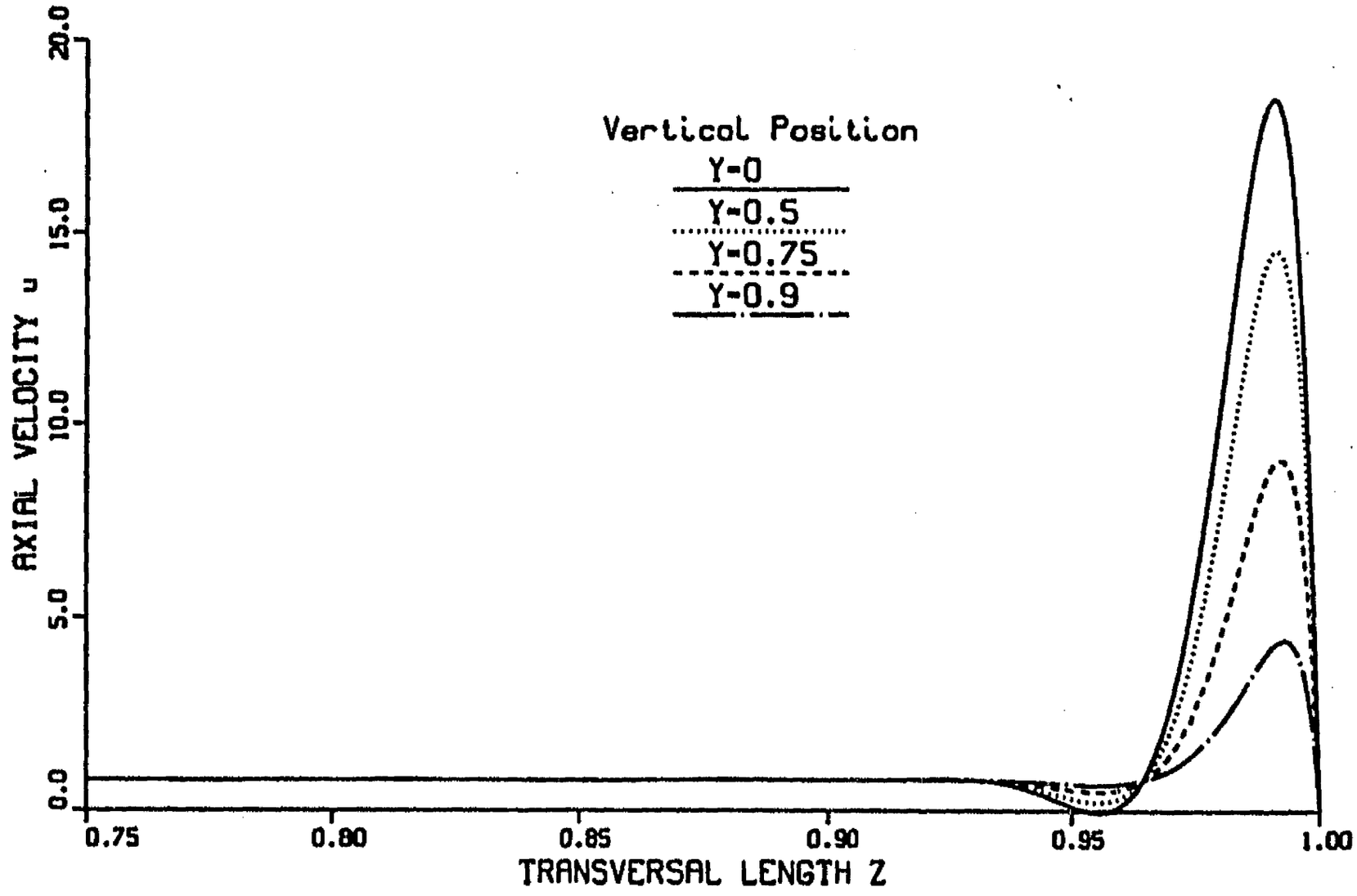

Figura 3.2: Velocidad laminar vs. z para diferentes posiciones en la dirección y. $M = 10^4$, $c = 0.05$.

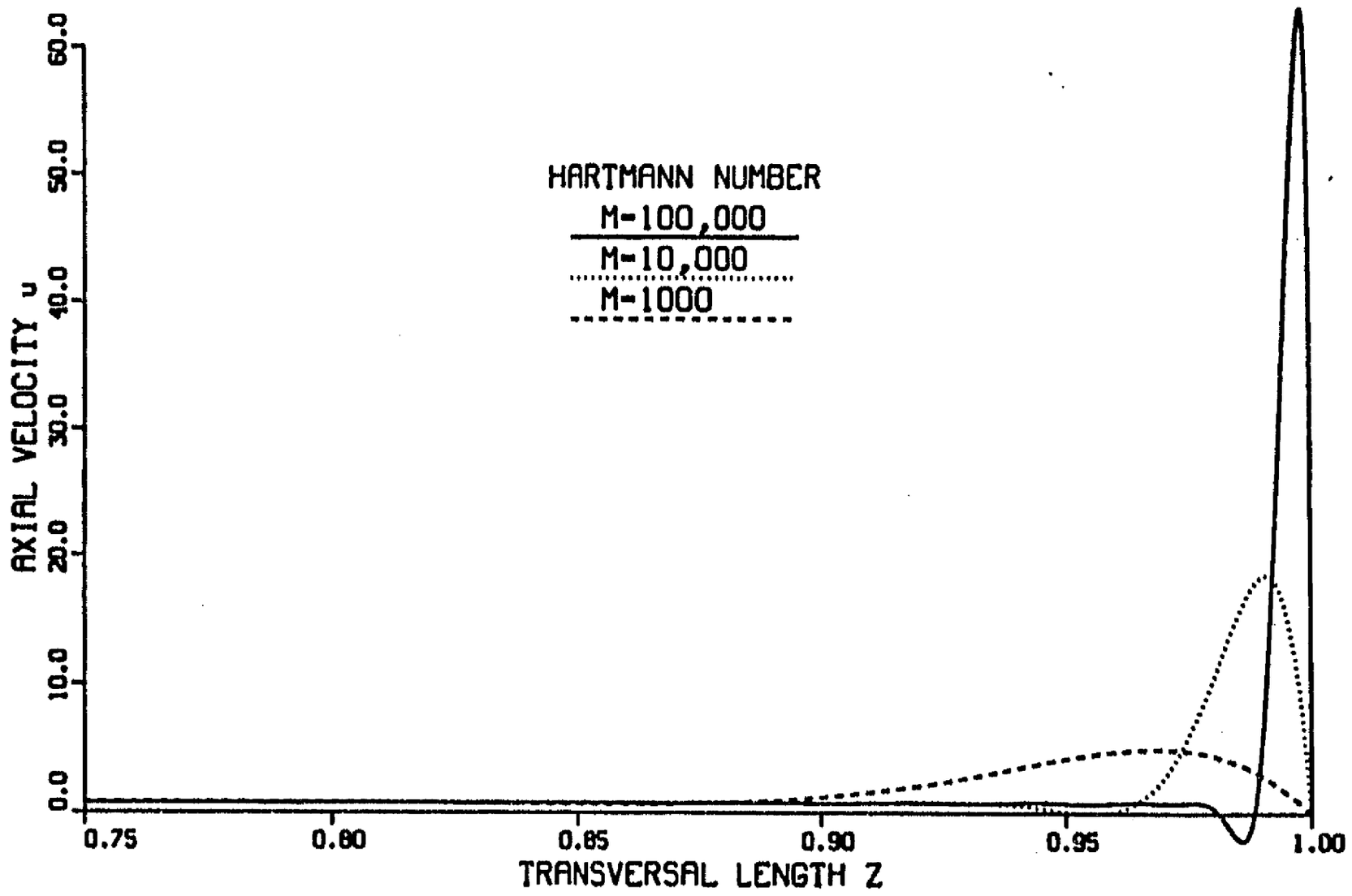

Figura 3.3: Velocidad laminar vs. z en $y = 0$ para diferentes números de Hartmann. $c = 0.05$.

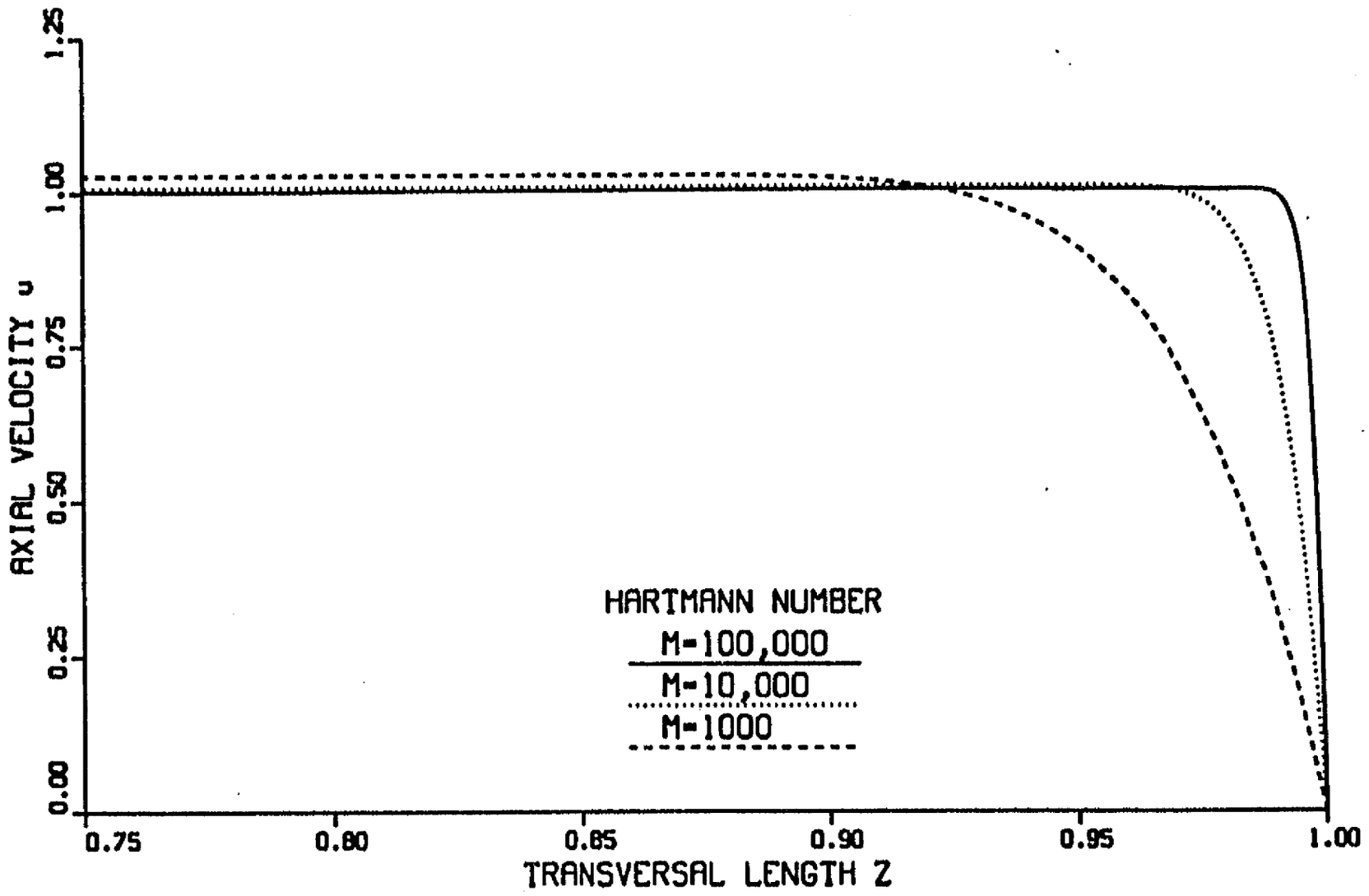

Figura 3.4: Velocidad laminar vs. z en $y = 0$ en un ducto con paredes aislantes para diferentes números de Hartmann.

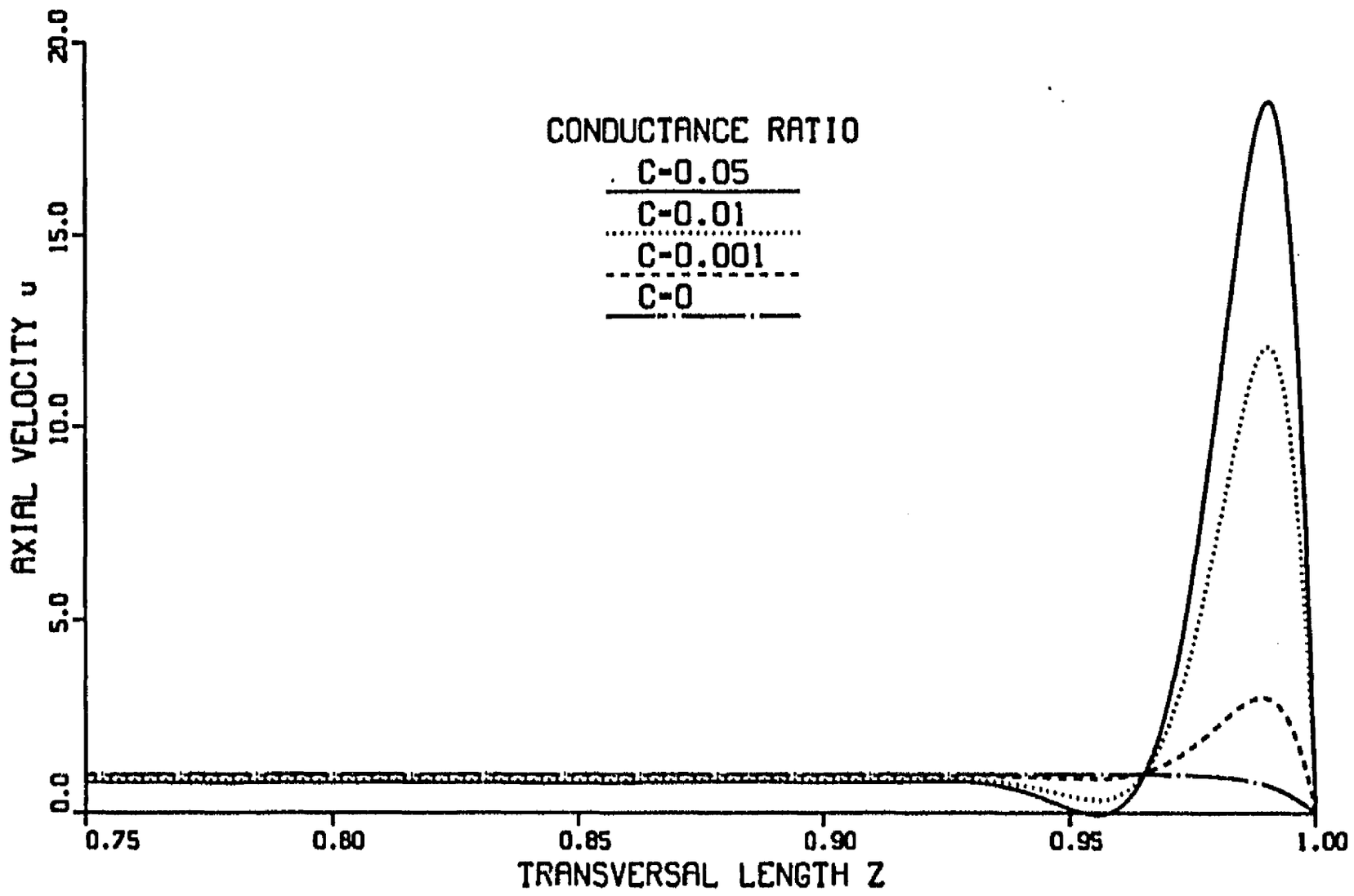

Figura 3.5: Velocidad laminar vs. z en $y = 0$ para diferentes valores de la razón de conductividades. $M = 10^4$.

3.2 Transferencia de Calor en un Flujo Laminar MHD en un Ducto Cuadrado

Previamente se mencionó que el diseño exitoso del manto de un reactor de fusión depende del conocimiento de los efectos MHD en la termohidráulica del sistema. Esto, a su vez, implica el entendimiento de los procesos de transferencia de calor dentro de los ductos que conforman el manto, donde el metal líquido remueve la energía ya sea en forma de un flujo de calor superficial proveniente de la primera pared del reactor o bien debida a la deposición de energía volumétrica en el líquido ocasionada por el flujo de neutrones. Un primer acercamiento al problema se basa en calculos de transferencia de calor por convección laminar forzada. Esto requiere primero resolver las ecuaciones MHD de Navier-Stokes para obtener los campos de velocidad característicos de flujos en ductos con campos magnéticos intensos, tales como los analizados en la sección anterior. El segundo paso involucra la solución de la ecuación de transferencia de calor utilizando los campos de velocidad previamente calculados. Evidentemente, la estructura particular de los flujos MHD afecta la transferencia de calor. De hecho, ya que los perfiles de velocidad MHD presentan distribuciones de flujo no-uniformes en las capas laterales, el problema de transferencia de calor se vuelve tridimensional, de modo que se debe hacer uso de un método numérico para la solución de la ecuación de transferencia de calor. En el presente estudio la solución de la ecuación mencionada se llevó a cabo mediante el método de diferencias finitas propuesto por Patankar [1980]. El problema consistió en resolver la ecuación de transferencia de calor considerando un flujo laminar completamente desarrollado en estado estacionario en un ducto de sección transversal cuadrada con un campo magnético transversal, suponiendo que las propiedades físicas del fluido permanecen constantes. Una de las paredes laterales del ducto recibe un flujo superficial uniforme de calor mientras que las tres paredes restantes se consideran adiabáticas. Como simplificaciones adicionales se supone que no existen fuentes volumétricas de calor y que el grosor de las paredes es despreciable. El resolver el problema sin estas aproximaciones es una extensión directa que puede llevarse a cabo sin mayores complicaciones.

Antes de obtener las soluciones numéricas de los campos de temperatura tomando como dato de entrada los perfiles de velocidad laminares previamente calculados, se procedió a validar el método numérico comparando la solución numérica para un flujo plano contra una solución analítica disponible. Se encontró una excelente concordancia entre ambas soluciones para distintos números de Péclet. Los números de Péclet utilizados fueron 250, 500 y 2500. Posteriormente, se procedió explorar los perfiles de temperatura (principalmente la temperatura en la pared calentada) y el número de Nusselt local en los rangos asignados previamente a los parámetros c, M y Pe. Los perfiles de temperatura en la pared como función de la coordenada axial para una c y un M dados, muestran que la temperatura disminuye al aumentar el número de Péclet, Pe (ver fig. 3.6). Para ductos con paredes conductoras delgadas, el efecto de

los excesos de velocidad en la capa lateral se manifiesta mediante una temperatura mínima en la pared en el plano medio, la cual va aumentando al acercarse a la pared superior en donde la temperatura es máxima, ya que el exceso de velocidad disminuye también y el transporte de calor es menos eficiente (ver fig. 3.7). Por otra parte, se encontró que la capa límite térmica es menor que la dimensión característica del ducto por lo cual sólo es necesario resolver la ecuación de transferencia de calor en una cuarta parte del ducto, lo que simplifica el trabajo computacional (ver fig. 3.8). Mientras que en flujos en ductos aislantes la velocidad en la capa lateral es $O(1)$, en ductos de paredes conductoras delgadas es $O(M^{\frac{1}{2}})$ y conlleva una fracción de $O(1)$ del flujo volumétrico. Esta característica permite que en este último caso, la remoción de calor en la capa lateral sea más eficiente lo que ocasiona una temperatura en la pared más baja que para el caso del ducto aislante (ver fig. 3.10). En general, los flujos en ductos con paredes conductoras delgadas llevan a temperaturas en la pared considerablemente menores que las de un flujo plano, en tanto que los flujos en ductos aislantes llevan a temperaturas en la pared muy cercanas a las calculadas con un flujo plano. Obviamente, estas son consecuencias directas de la distribución de velocidades en cada caso. El aumento del número de Hartmann de 10^3 a 10^5 en el caso de paredes conductoras delgadas lleva a una disminución notoria de la temperatura de la pared, lo que manifiesta el hecho de que al aumentar M, los chorros de fluido cerca de la pared también crecen arrastrando el calor en la capa lateral más eficientemente (ver fig. 3.9). El efecto de esta misma variación de M para el caso de ductos aislantes no es tan drámatico como en el caso anterior. Lo que se observa es que los perfiles de temperatura se acercan al perfil correspondiente a un flujo plano al aumentar M, lo que obviamente se debe a que un incremento en M provoca un flujo cada vez más plano. Finalmente, se observó la transición en el perfil de temperaturas de la pared para un número de Hartmann dado, al disminuir c de 0.05 a 0, es decir, al pasar de un ducto con paredes conductoras delgadas a un ducto aislante. La disminución de c ocasionó un aumento considerable en la temperatura de la pared lo que se explica por la gradual disminución del exceso de velocidad hasta su total desaparición al alcanzar el límite $c = 0$. (ver fig. 3.10) Debido a que el uso de ductos cilíndricos en el manto de los reactores de fusión se ha considreado también como una posibilidad práctica, el análisis de la transferencia de calor en tales ductos para diferentes flujos y condiciones de frontera fue llevado a cabo en [Cuevas, 1994].

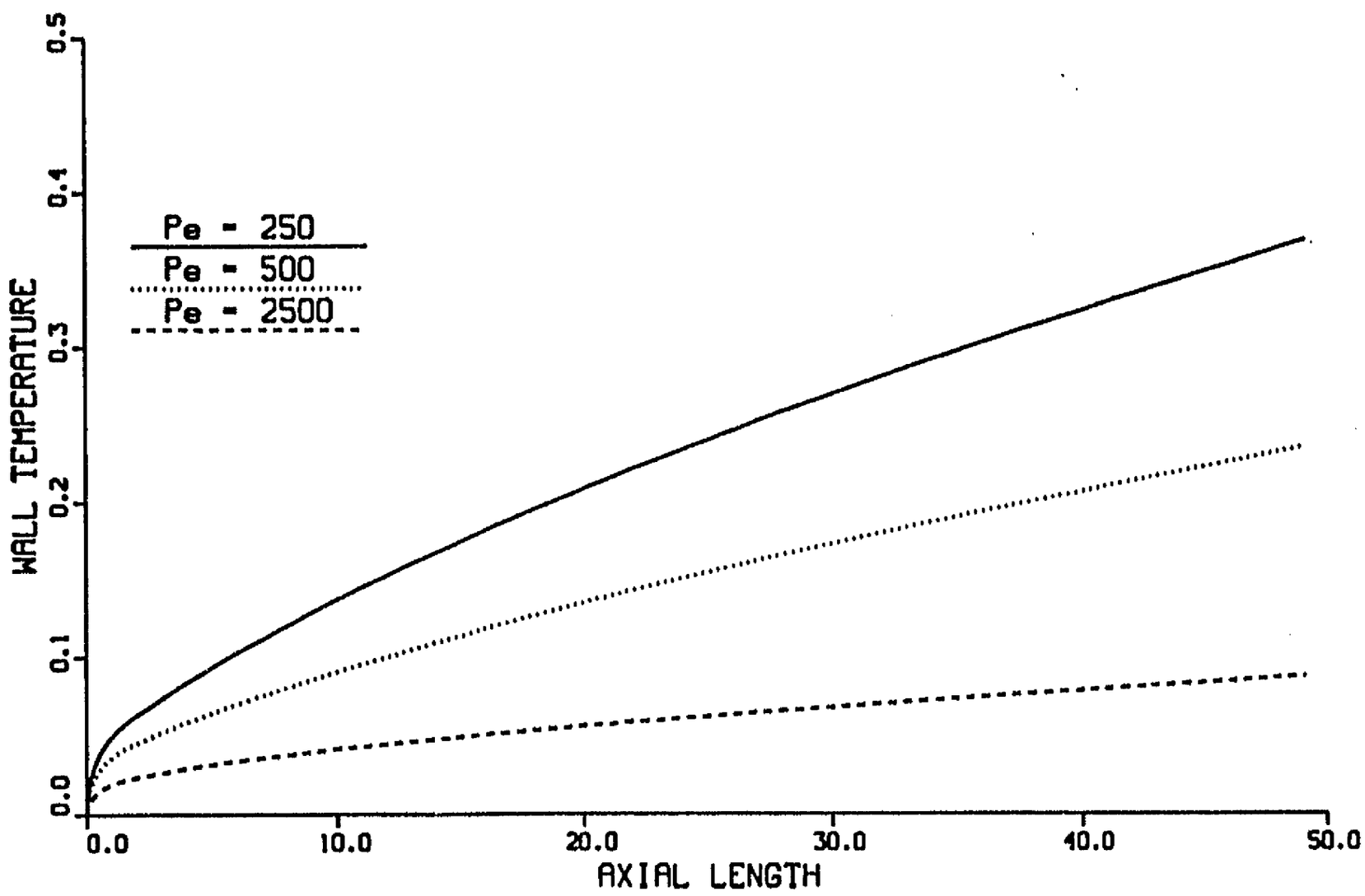

Figura 3.6: Temperatura en la pared vs. x en $y = 0$ para diferentes números de Péclet. $M = 10^3$, $c = 0.05$.

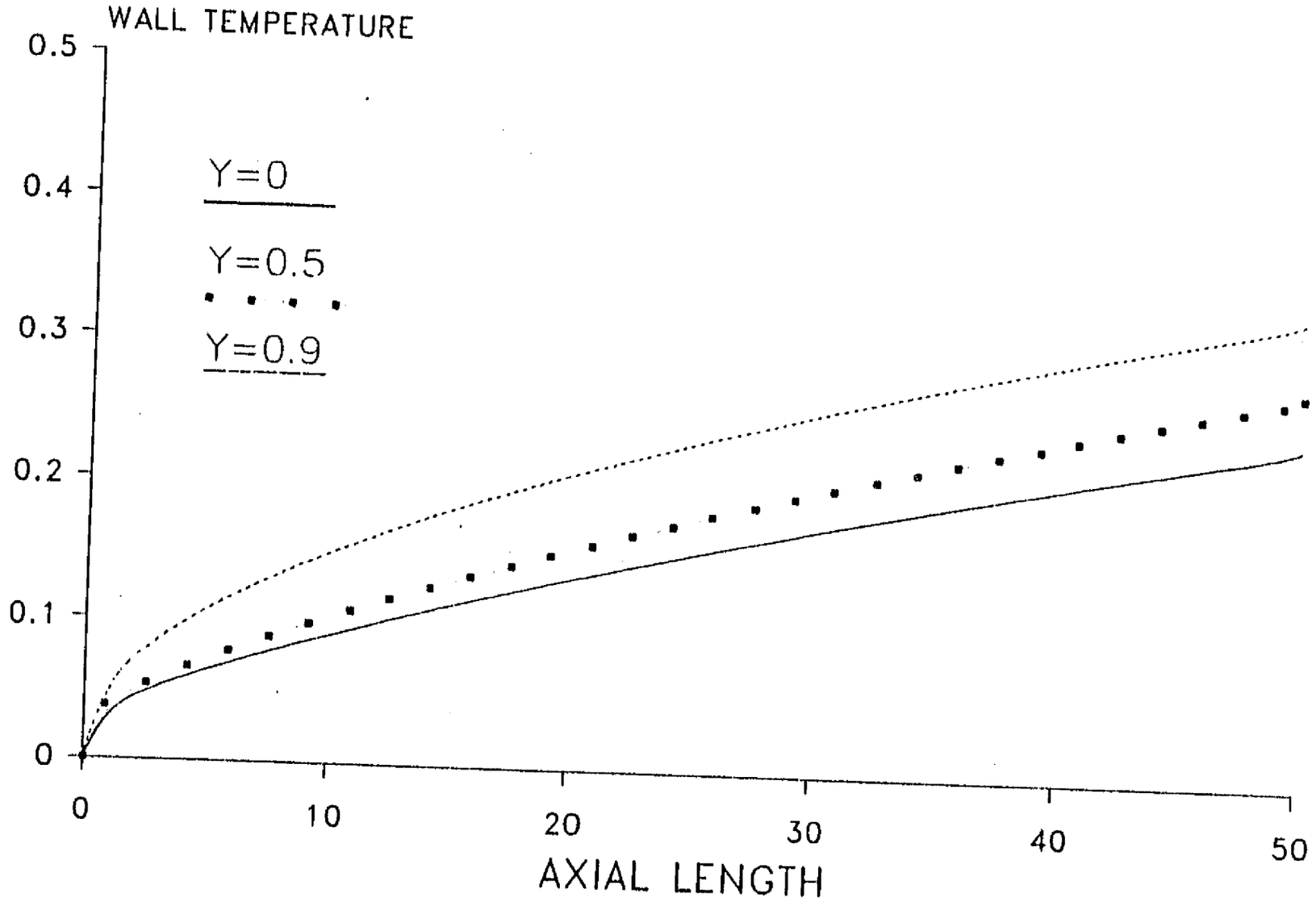

Figura 3.7: Temperatura en la pared vs. x para diferentes posiciones en la dirección y. $M = 10^3$, $c = 0.05$, $Pe = 500$.

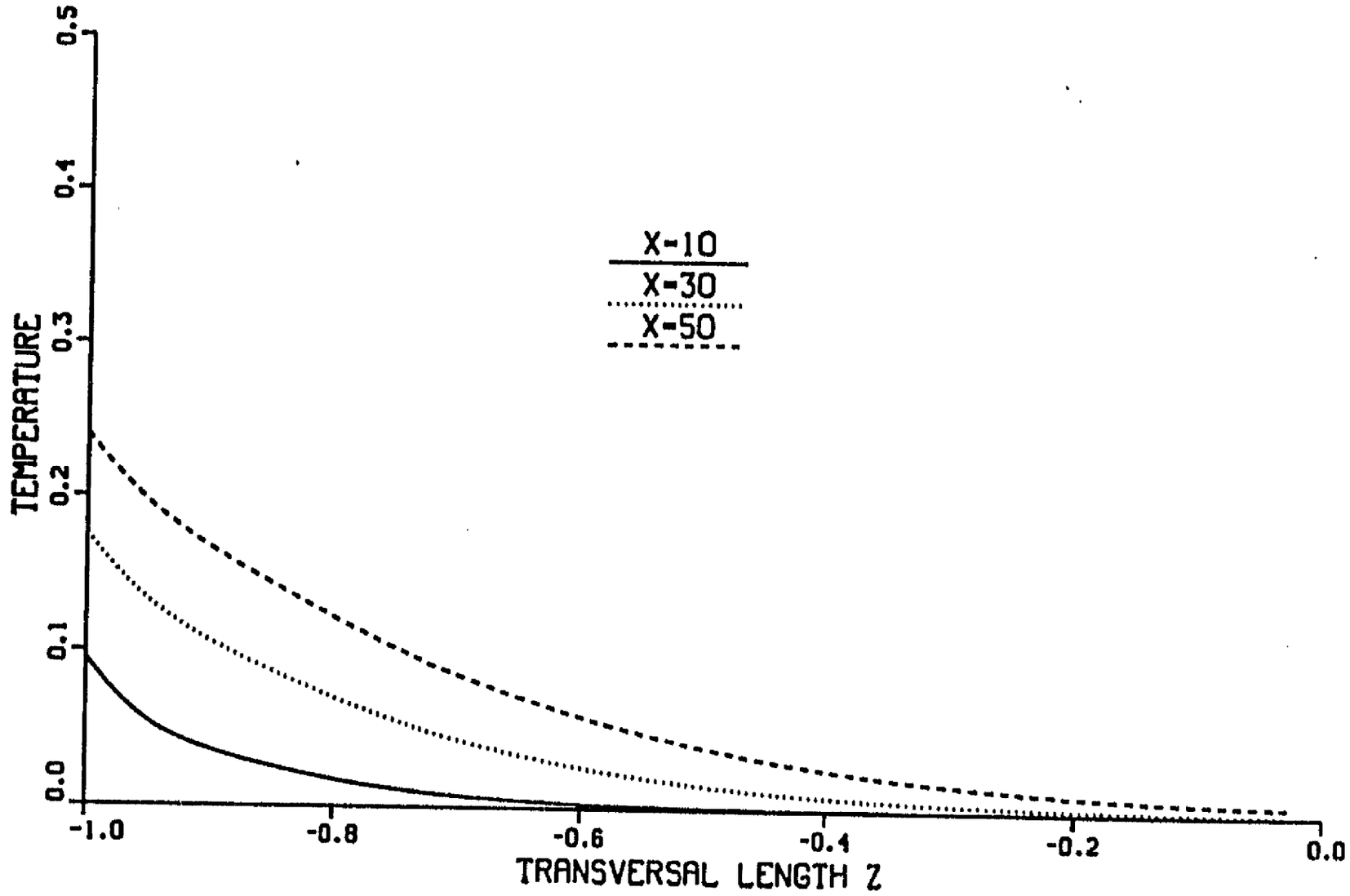

Figura 3.8: Temperatura vs. z en $y = 0$ para diferentes posiciones axiales. $M = 10^3$, $c = 0.05$, $Pe = 500$.

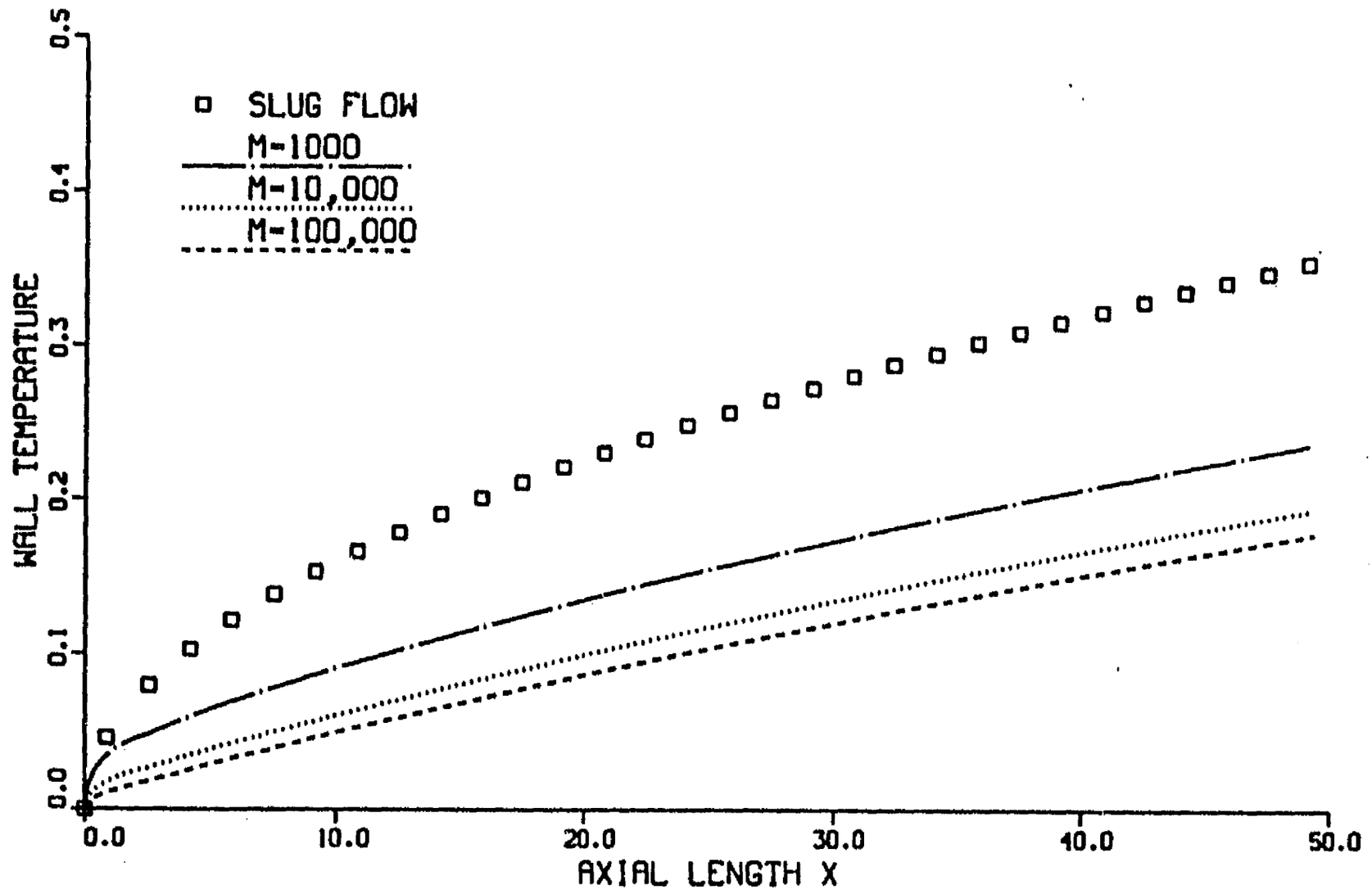

Figura 3.9: Temperatura en la pared vs. x en $y = 0$ con un flujo tapón y flujos MHD con diferentes números de Hartmann. $c = 0.05$, $Pe = 500$.

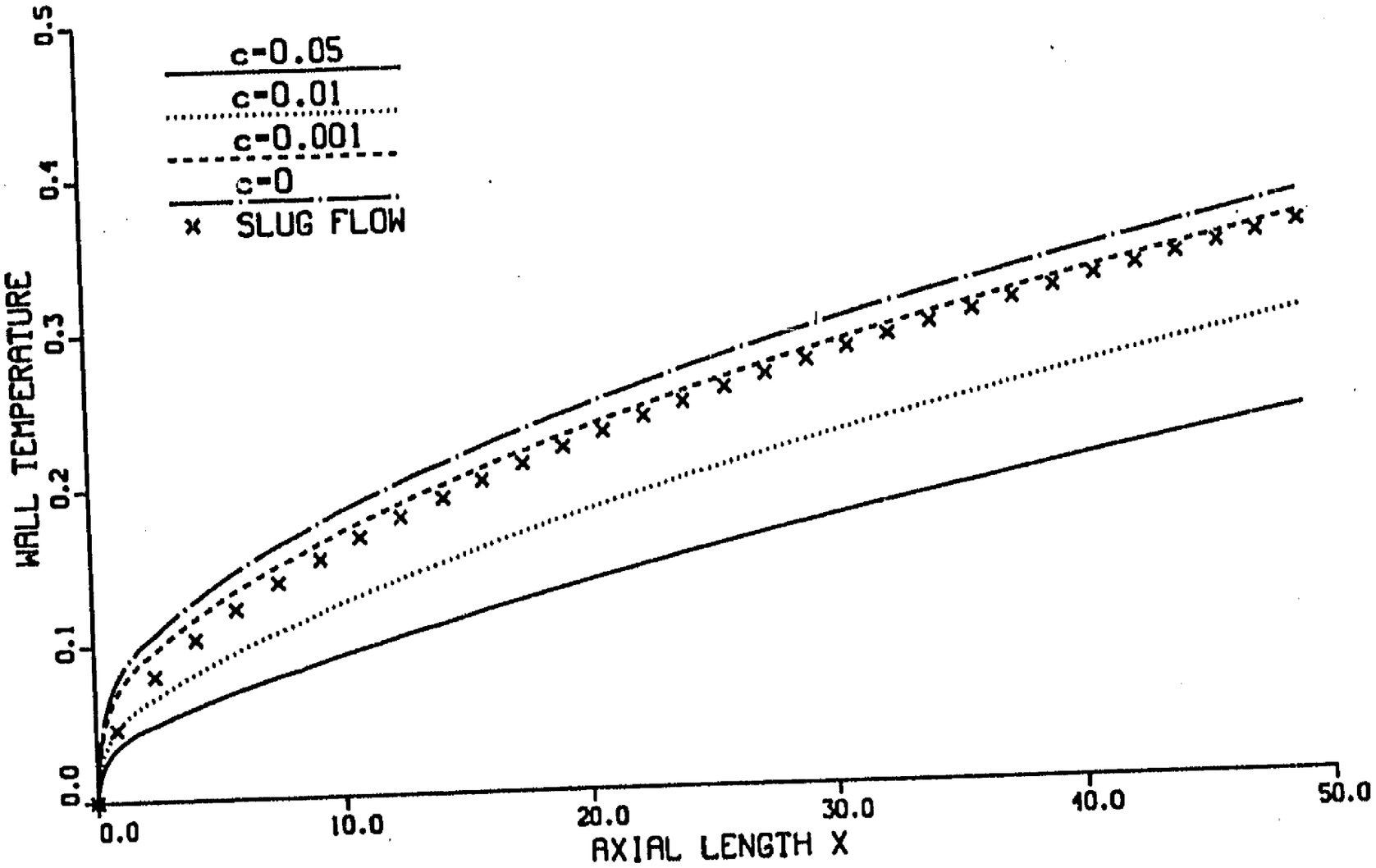

Figura 3.10: Temperatura en la pared vs. x en $y = 0$ con un flujo tapón y flujos MHD con diferentes valores de la razón de conductividades. $M = 10^3$, $Pe = 500$.

Capítulo 4

Turbulencia MHD y Tópicos Afines

En este capítulo se exponen algunas ideas y conceptos acerca de la teoría de turbulencia MHD que pueden tener relevancia para el análisis y modelación de los fenómenos que se presentan fuera del régimen laminar en los ductos que conforman el manto de los reactores de fusión.

Un campo magnético puede afectar sustancialmente la naturaleza de la turbulencia. El campo introduce una dirección preferencial en el espacio y modifica la dinámica así como los fenómenos de transporte dentro del flujo. Los efectos de laminarización representan algunas de las características que, bajo ciertas condiciones, pueden obtenerse en un flujo turbulento debido a la acción de un campo magnético. El campo magnético afecta la estabilidad de un fluido conductor al interactuar con las fluctuaciones turbulentas y con el flujo promedio. Además de la disipación viscosa, en un campo magnético la energía se disipa por efecto Joule, lo que ocasiona un amortiguamiento más rápido de las perturbaciones que en ausencia de campo magnético. Muchos experimentos han confirmado la supresión de turbulencia mediante la acción de un campo magnético transversal, tanto en ductos con paredes aislantes como conductoras. Sin embargo, también se ha observado que aún cuando el factor de fricción alcanza su valor laminar, permanece un nivel de turbulencia significativo. Esta turbulencia residual parece ser originada en la entrada del flujo al campo magnético, como resultado de una fuerte inestabilidad de los perfiles de velocidad en forma de M.

Por otra parte, existe la creencia de que la turbulencia MHD a bajo número de Reynolds magnético presenta una tendencia hacia la bidimensionalidad. Muchos resultados experimentales apoyan esta conclusión y en los últimas décadas han sido propuestas algunas explicaciones teóricas de este fenómeno. La bidimensionalidad en la turbulencia MHD es vista más como un límite idealizado que como un estado físico real. De hecho, aunque la tendencia de la turbulencia MHD hacia la bidimensionalidad ha sido bien establecida, no existe un consenso general, al menos para flujos en ductos,

de que el estado final alcanzado en la turbulencia MHD presente todas los rasgos característicos de la turbulencia bidimensional. En general, a pesar de los avances recientes, la turbulencia MHD (al igual que la turbulencia ordinaria) es un tópico polémico y no totalmente entendido.

En general, se puede afirmar que el comportamiento bidimensional de la turbulencia MHD se debe a las fuerzas de cuerpo y a las condiciones de frontera impuestas sobre el sistema, que impiden el crecimiento de fluctuaciones tridimensionales. Se puede demostrar que si un fluido presenta un movimiento enteramente paralelo o enteramente perpendicular a las líneas de fuerza de un campo magnético uniforme, el movieniento no se ve afectado por el campo: en el primer caso, la fuerza de Lorentz es cero mientras que, en el segundo, la fuerza es irrotacional, por lo que en ambos casos la fuerza no afecta la distribución original de velocidades. De hecho, un campo magético uniforme vertical favorece un movimiento puramente bidimensional. La tendencia hacia la bidimensionalidad de la turbulencia MHD puede entenderse utilizando una descripción en el espacio de Fourier. En tal caso, puede mostrarse la existencia de un término disipativo de Joule que depende del coseno cuadrado del ángulo que forma un vector de onda dado con el campo aplicado. De esta forma, la disipación será máxima para aquellos vectores de onda que sean paralelos al campo, mientras que los vectores de onda perpendiculares al campo magnético no se verán afectados por tal disipación. Este fenómeno propicia la bidimensionalidad. Este hecho también puede explicarse en términos de vorticidad ya que el campo magnético suprime las componentes de vorticidad perpendiculares al campo. Existen ciertas evidencias de que la turbulencia MHD presenta una estructura particular en la que los vórtices turbulentos tienden a alinearse y alargarse en la dirección del campo magnético. La formación de estas estructuras turbulentas alargadas se explica mediante la acción de un mecanismo de difusión electromagnética a lo largo de las líneas de campo. El efecto del mecanismo de difusión es la supresión de las diferencias de velocidades entre planos transversales y se presenta en ductos con paredes aislantes asi como conductoras. Sin embargo, la tasa de decaimiento de los vórtices alargados es menor en paredes aislantes que en paredes conductoras ya que los efectos disipativos son más intensos en estas últimas. Esto hace pensar en que estas estructuras bidimensionales son más propensas a formarse en ductos aislantes que en ductos con paredes conductoras. Sin embargo, existen evidencias experimentales de que estas estructuras turbulentas pueden persistir también en ductos con paredes conductoras.

Experimentos realizados en la Universidad de Beer-Sheva, Israel, apuntan hacia la existencia de una cascada inversa de energía (característica de la turbulencia bidimensional) en flujos de metales líquidos en ductos con paredes no conductoras en condiciones en que existe una inyección de energía. Por otra parte, experimentos realizados en canales con paredes eléctricamente conductoras muestran la persistencia de la turbulencia en condiciones en que el flujo debía estar laminarizado. Al parecer, el campo magnético suprime la turbulencia en el núcleo del flujo mientras que promueve

el aumento de la intensidad de la turbulencia cerca de las paredes sin la necesidad de medios perturbativos externos. Se especula que la turbulencia en ductos conductores es creada continuamente a lo largo del canal, probablemente debido a los fuertes gradientes de velocidad de los perfiles en forma de M.

Por otra parte, experimentos realizados en el Argonne National Laboratory demostraron la existencia de una inestabilidad en el flujo MHD de un metal líquido en un ducto rectangular, en condiciones cercanas a las requeridas para la operación de un reactor de fusión. La inestabilidad se desarrolló en el chorro existente en la capa límite asociada a la pared lateral, paralela al campo magnético y se especula que este fenómeno podría tener efectos benéficos para la termohidráulica del manto del reactor mediante un mejoramiento de la transferencia de calor. Entre las principales características de la inestabilidad resaltan el presentar oscilaciones de gran amplitud, respecto a la velocidad media y además un carácter fuertemente periódico de las oscilaciones que se mantiene conforme el flujo procede corriente abajo. Al irse acercando al núcleo del flujo, las oscilaciones disminuyen su amplitud hasta que desaparecen por completo. Uno de los principales efectos de la presencia de la inestabilidad en la distribución de flujo medio es el engrosamiento de la capa lateral. Al incrementar progresivamente el parámetro de interacción, la inestabilidad tiende a desaparecer. Un análisis preliminar de estabilidad lineal indica que el flujo en el núcleo es incondicionalmente estable ante perturbaciones en la capa lateral. El análisis muestra también que la inestabilidad involucra únicamente movimientos en planos perpendiculares al campo magnético. Además, la inestabilidad de las capas laterales involucra una vorticidad paralela al campo magnético que está confinada en la capa mencionada. El análisis implica la existencia de grandes fluctuaciones periódicas dentro de la capa lateral de alta velocidad, las cuales producirían un mezcaldo excelente en tal región, lo que mejoraría la transferencia de calor.

Capítulo 5

Análisis de Flujo y Transferencia de Calor en Régimen Turbulento

5.1 Modelo de Turbulencia de la Teoría del Grupo de Renormalización

Para el análisis del flujo y la transferencia de calor en régimen turbulento se utilizó un modelo de turbulencia de la teoría del Grupo de Renormalización (GRN) que provee expresiones para la viscosidad total (laminar + turbulenta) así como para la difusividad térmica total [Yakhot and Orszag, 1986]. La idea básica detrás de la teoría GRN es la eliminación de modos de pequeña escala y la inclusión de su influencia en una viscosidad o difusividad térmica (renormalizada) efectiva, de manera que únicamente permanecen las escalas grandes. El procedimiento GRN involucra escalamiento dinámico e invariancia, junto con métodos perturbativos iterativos y permite la eliminación sistemática de fluctuaciones de escalas isotrópicas pequeñas, considerando su influencia promediada sobre las escalas grandes, dando lugar a coeficientes de transporte renormalizados. La eliminación de las escalas isotrópicas fluctuantes tiene lugar primordialmente en el intervalo inercial. Como resultado del proceso de eliminación de escalas, se obtiene una ecuación de movimiento renormalizada y una expresión para la viscosidad total. Un proceso similar se realiza para la ecuación de la energía, obteniendose una difusividad térmica total. De esta forma la viscosidad y difusividad térmica se incrementan de su valor molecular a un valor efectivo.

En el estudio fueron consideradas dos distintas versiones del modelo de viscosidad total y después de un análisis cuidadoso se eligió a la primera versión como la más adecuada para describir el flujo turbulento en las capas laterales. Para la obtención de la viscosidad total en cada punto se requiere la solución de una ecuación algebráica que depende del gradiente de velocidades, una longitud integral, el número de Reynolds y ciertas constantes del modelo. Para la determinación de la longitud integral se utilizó

un modelo que toma en cuenta la estructura específica de la capa límite. Las constantes fueron elegidas tomando en cuenta ciertos estudios previos donde se utilizó el modelo GRN para el análisis de flujos turbulentos MHD.

5.2 Flujo Turbulento MHD en un Ducto Cuadrado

El análisis del flujo en régimen turbulento se llevó a cabo variando el número de Hartmann y la razón de conductividades en los mismos rangos que para el caso laminar. Adicionalmente se estudió el efecto de tres números de Reynolds, a saber, 5×10^4, 10^5 y 5×10^5. En el caso de ductos con paredes conductoras delgadas, para un número de Hartmann dado, la existencia de turbulencia se manifestó principalmente mediante dos efectos: una disminución drámatica de la velocidad en la capa lateral respecto al caso laminar y un engrosamiento de dicha capa. Ambos efectos son más pronunciados mientras mayor es el número de Reynolds (ver fig. 5.1). Por otra parte, la viscosidad turbulenta en la capa lateral extendida aumenta considerablemente y, similarmente, un incremento en el número de Reynolds lleva a un aumento en la viscosidad total. Sin embargo, el núcleo del flujo permanece esencialmente imperturbado y la viscosidad en tal región mantiene el valor molecular (ver fig.5.2). Los efectos turbulentos mencionados se mantienen al disminuir c pero su intensidad es cada vez menor (ver figs. 5.3 y 5.4) de tal suerte que al alcanzar el límite $c = 0$, el modelo predice que el flujo turbulento coincide con el laminar, o dicho de otra forma, no es posible obtener un flujo turbulento cuando $c = 0$ en el intervalo de números de Reynolds analizado (ver fig. 5.5). Este resultado tiene que ver con el hecho de que al disminur c disminuyen los chorros de fluido en la capa lateral, que son la causa principal de promoción de turbulencia. Un flujo en un ducto aislante no presenta chorros en las paredes y por consiguiente no existen gradientes pronunciados de velocidad en la capa lateral que promuevan la aparicón de turbulencia. Puede decirse entonces que mientras más pequeña es la razón de conductividades, los efectos turbulentos son menos pronunciados. Esta conclusión concuerda con el análisis cualitativo efectuado por Hunt [1965]. Por otra parte, respecto al efecto del número de Hartmann puede decirse que para ductos con paredes conductoras delgadas, al disminuir M se reducen los efectos turbulentos para un Re dado (ver fig. 5.6). En términos más físicos, la afirmación anterior implica que mientras más altos y más delgados son los chorros laterales, mayor es la susceptibilidad del flujo en la capa lateral de promover un alto nivel de turbulencia. En este sentido, en ductos de paredes conductoras delgadas a $M \gg 1$, un incremento en el campo magnético puede ser un factor desestabilizante.

Las principales conclusiones del análisis del flujo en régimen turbulento se pueden resumir de la siguiente forma:

- En un ducto de paredes conductoras delgadas para un M dado, la presencia de

turbulencia ocasiona una reducción drámatica de la velocidad en la capa lateral, un engrosamiento de dicha capa y un aumento considerable de la viscosidad total en dicha región. Los efectos turbulentos son más fuertes mientras mayor es Re.

- Los efectos turbulentos se restringen a la capa lateral, permaneciendo el núcleo imperturbado.

- Flujos en ductos con paredes aislantes o cuasi-aislantes preservan el comportamiento laminar, aún con Re altos. El campo magnético impide la aparición de turbulencia en ductos aislantes con $M \gg 1$.

- Para un M y un Re dados, mientras más pequeña es c, los efectos turbulentos son menos pronunciados. Una reducción en c tiende a reducir el nivel de turbulencia.

- Para un Re dado, en flujos en ductos con paredes conductoras delgadas, mientras más pequeño es M, más débiles son los efectos turbulentos. En tales ductos, cuando $M \gg 1$, un incremento del campo magnético promueve la aparición de turbulencia.

5.3 Transferencia de Calor en un Flujo Turbulento MHD en un Ducto Cuadrado

Las consecuencias de los efectos turbulentos en la transferencia de calor fueron explorados utilizando los perfiles de velocidad promedio previamente calculados junto con el modelo de difusividad térmica efectiva para un número de Prandtl específico, que en este caso fue el del litio. Los resultados numéricos obtenidos con el modelo GRN predicen que la existencia de turbulencia afecta más fuertemente la dinámica que el comportamiento térmico del flujo. En otras palabras, a pesar de que la viscosidad total se incrementa notablemente debido a la turbulencia en la capa lateral, para un fluido con un número de Prandtl pequeño como el litio, la difusividad térmica total no se incrementa en la misma proporción. No obstante, el comportamiento físico de las difusividades totales, viscosa y térmica, es muy similar, es decir, ambas incrementan notablemente su valor respecto al valor molecular, en la capa límite lateral y disminuyen gradualmente al aproximarse al núcleo del flujo hasta alcanzar el valor molecular. Sin embargo, mientras que para el número de Reynolds más alto ($Re = 5 \times 10^5$) la viscosidad total es $O(10^3)$, para el mismo Re la difusividad total es $O(10)$ (ver fig. 5.7). Este comportamiento no resulta sorprendente después de analizar la fórmula GRN para el número de Prandtl turbulento y la difusividad térmica, ya que en el límite $Pr_o \to 0$, donde Pr_o es el número de Prandtl molecular, la teoría GRN predice que la difusividad térmica total es del mismo orden que la molecular. Evidentemente, este hecho se reflejó en los cálculos de transferencia de calor, donde se analizó el efecto de los perfiles

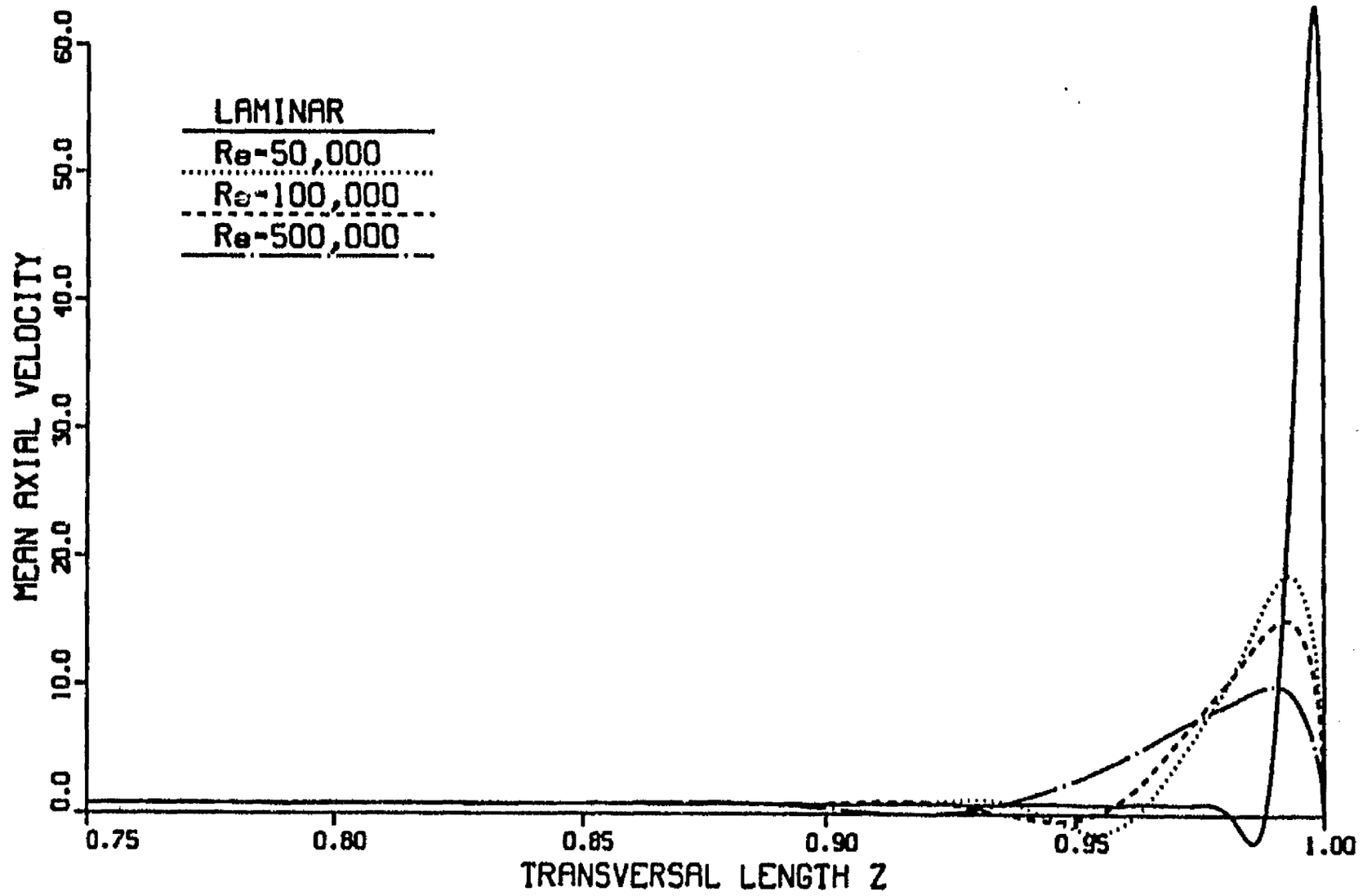

Figura 5.1: Velocidad axial laminar y promedio vs. z en $y = 0$ para diferentes números de Reynolds. $M = 10^5$, $c = 0.05$.

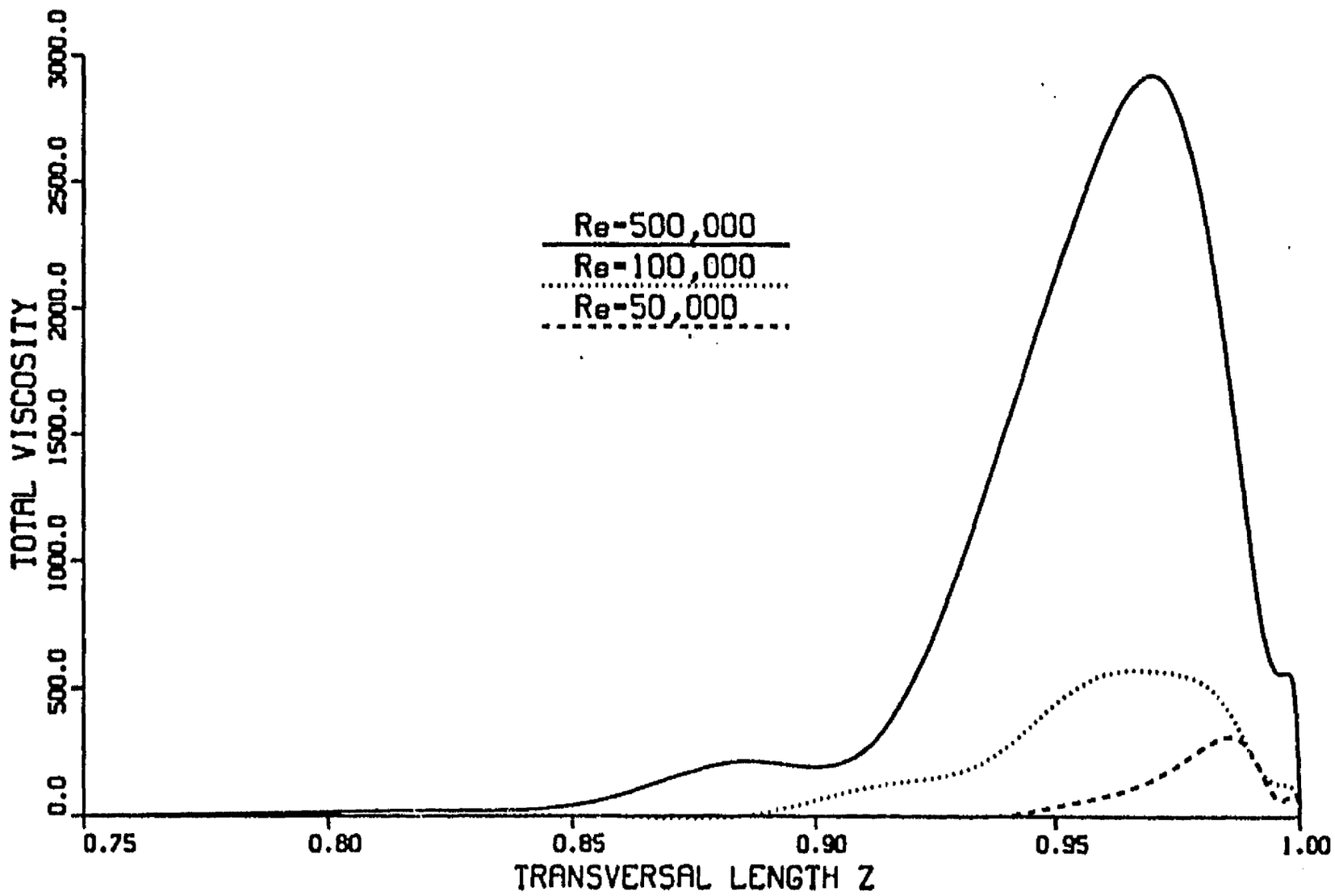

Figura 5.2: Viscosidad total vs. z en $y = 0$ para diferentes números de Reynolds. $M = 10^5$, $c = 0.05$.

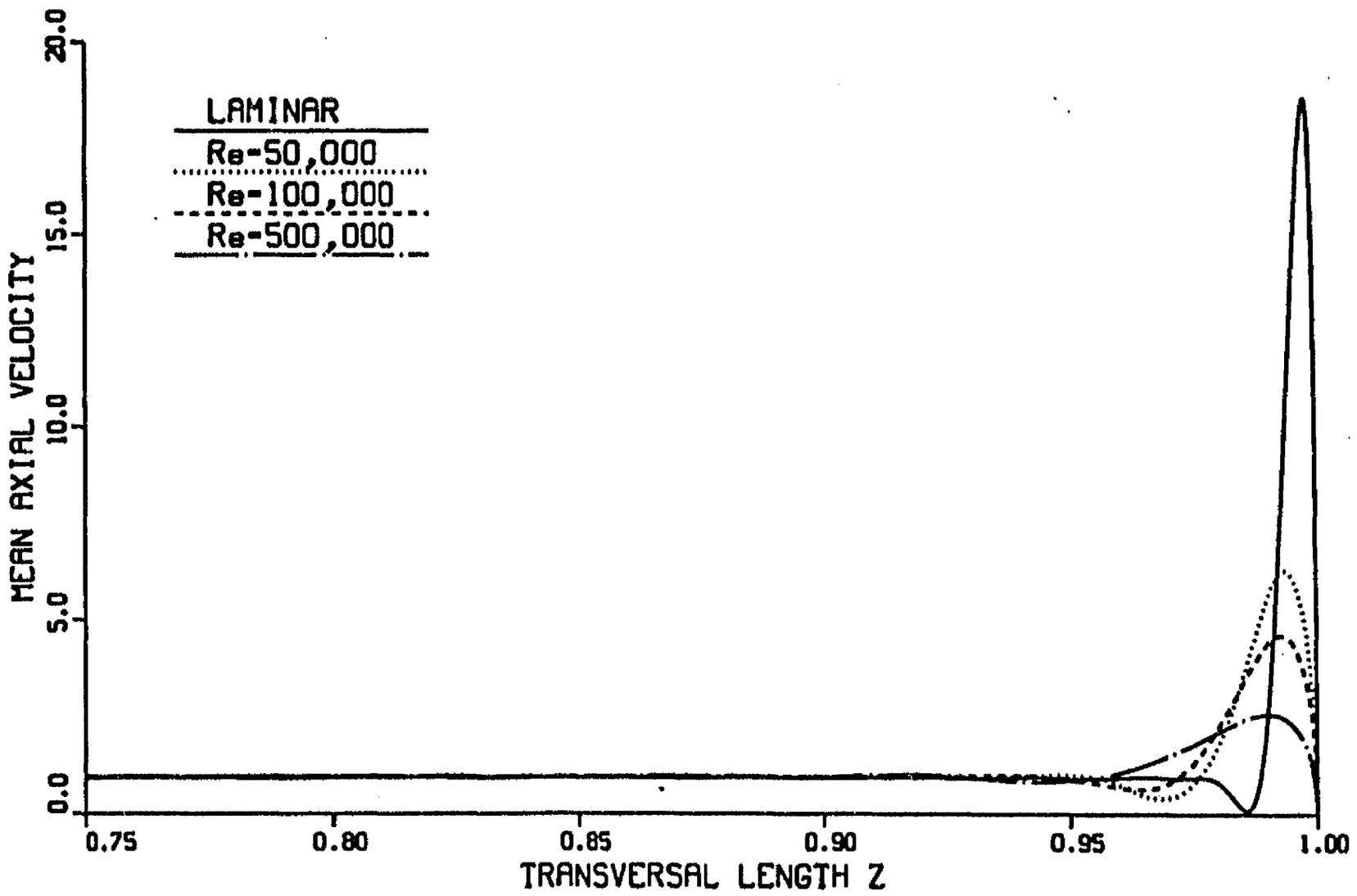

Figura 5.3: Velocidad axial laminar y promedio vs. z en $y = 0$ para diferentes números de Reynolds. $M = 10^5$, $c = 0.001$.

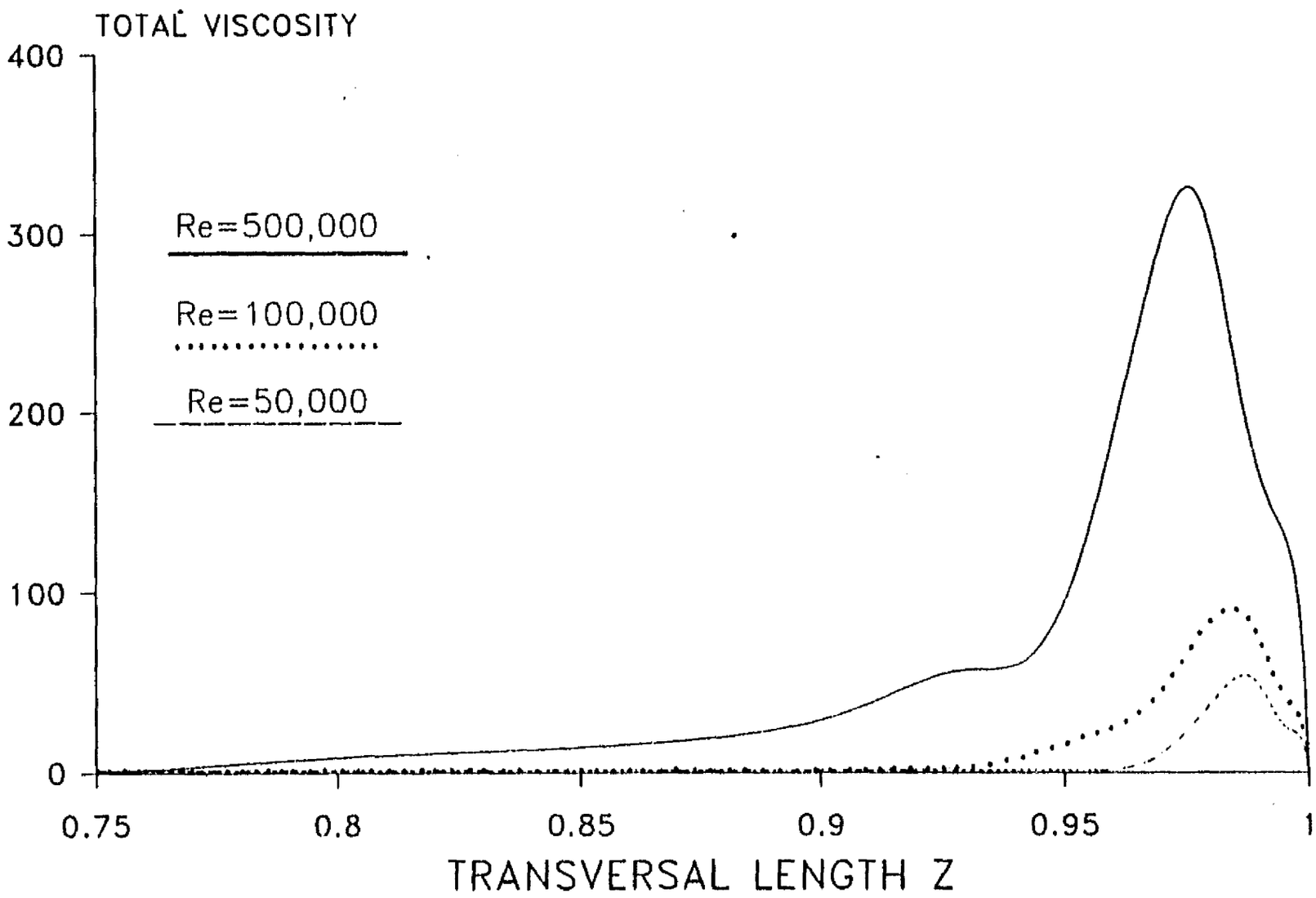

Figura 5.4: Viscosidad total vs. z en $y = 0$ para diferentes números de Reynolds. $M = 10^5$, $c = 0.001$.

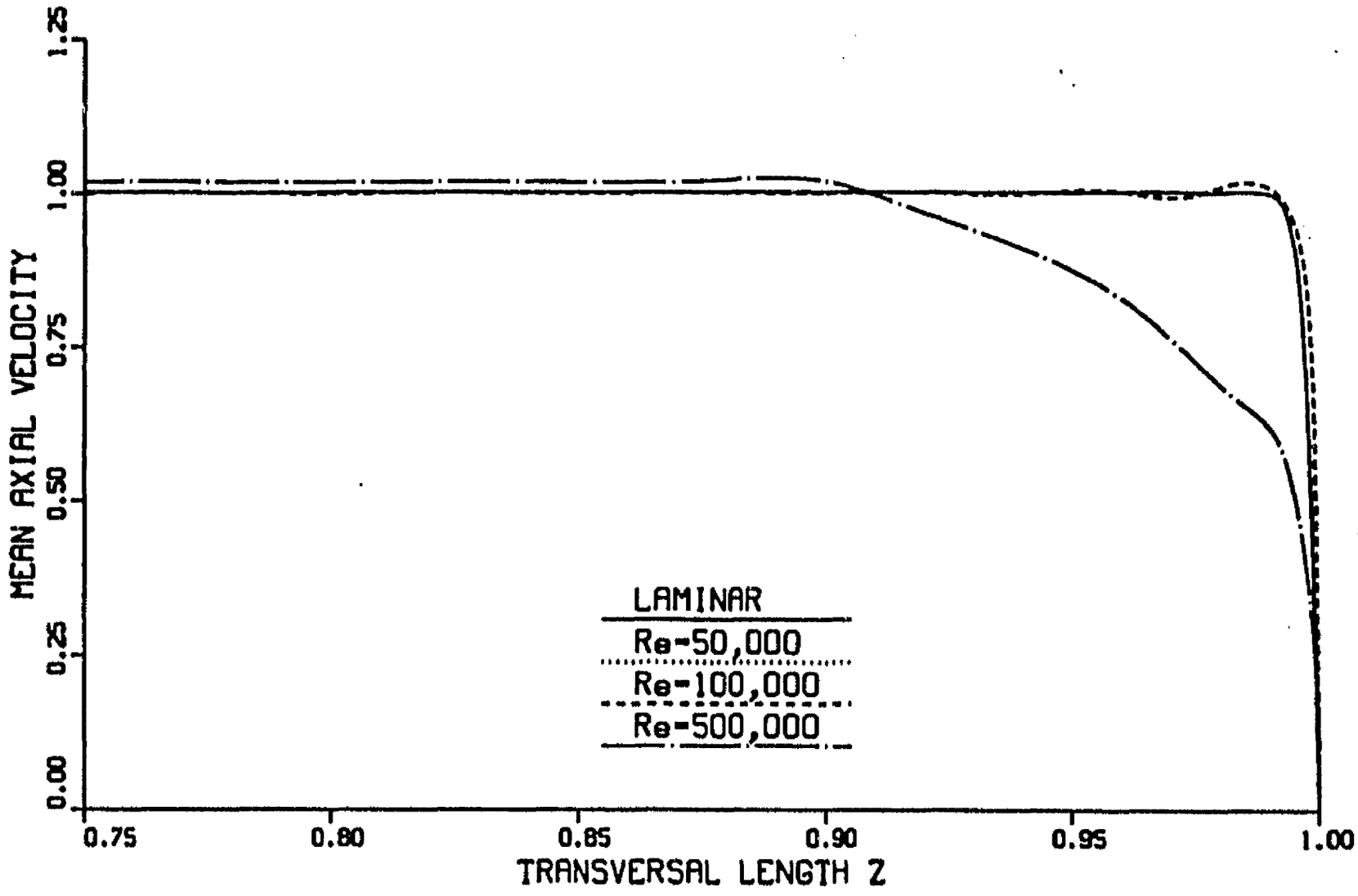

Figura 5.5: Velocidad axial laminar y promedio vs. z en $y = 0$ para diferentes números de Reynolds. $M = 10^5$, $c = 0$.

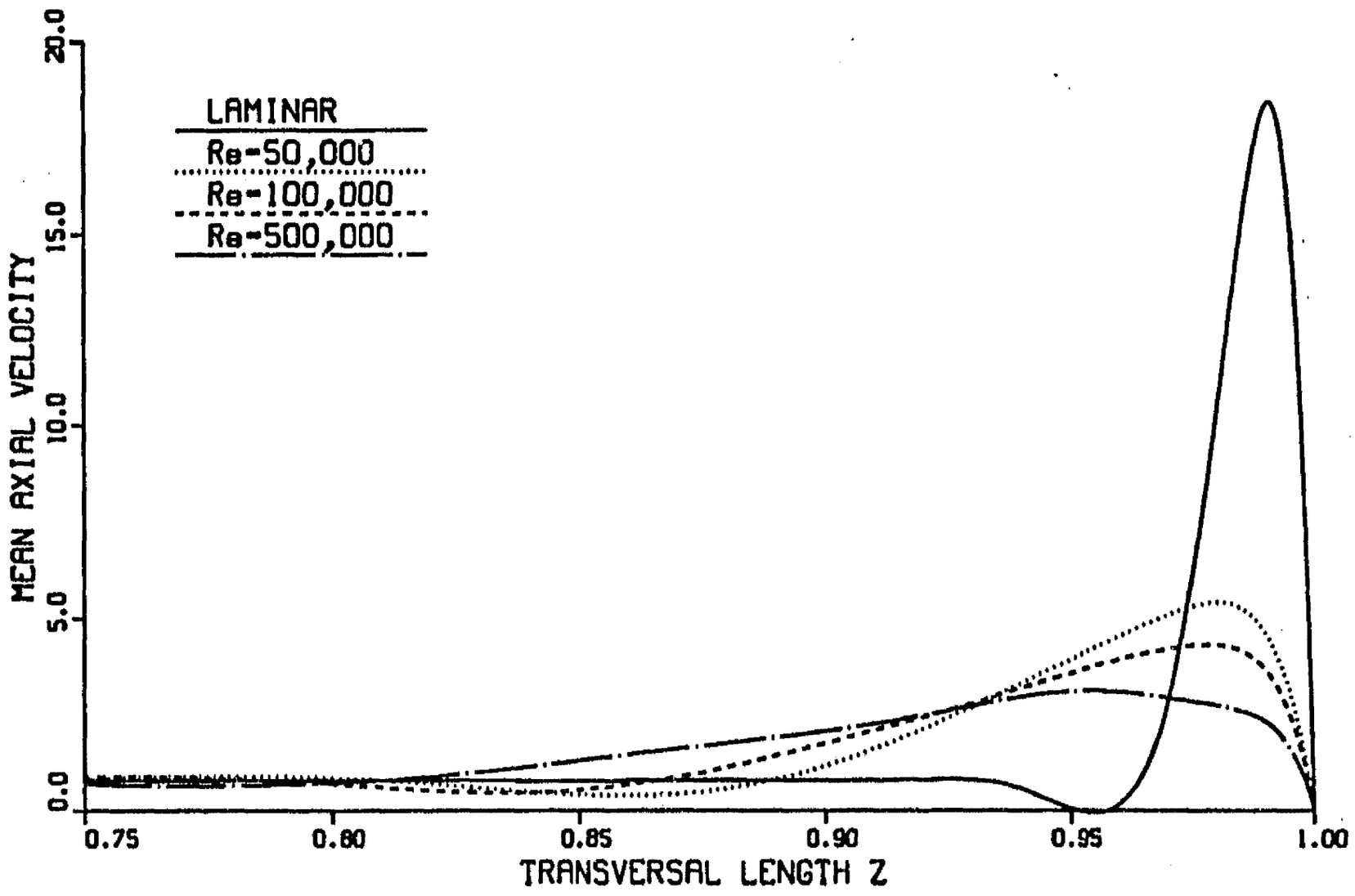

Figura 5.6: Velocidad axial laminar y promedio vs. z en $y = 0$ para diferentes números de Reynolds. $M = 10^4$, $c = 0.05$.

de velocidad promedio y la difusividad térmica total sobre los perfiles promedio de temperatura en ductos de paredes conductoras delgadas y aislantes.

El efecto de incrementar el número de Péclet, Pe (o equivalentemente, el número de Reynolds, $Re = Pe/Pr_o$) para un M y un c dados, fue obviamente el mismo que para el caso laminar, es decir, mientras mayor es Pe, los efectos convectivos son más fuertes y la temperatura de la pared es más baja. En otras palabras, cuando Pe (Re) es grande, los efectos turbulentos son más intensos por lo que una mayor cantidad de energía es arrastrada en la capa lateral, disminuyendo la temperatura de la pared. Similarmente al caso laminar, se encontró que el grosor de la capa límite térmica es menor que la longitud caracertística del canal y, por lo tanto, la presencia de la pared opuesta no es de relevancia en el problema de transferencia de calor. Por otra parte, al comparar los perfiles de temperatura turbulentos contra los laminares en ductos de paredes conductoras delgadas para M y Pe dados, en general se observó que, en contra de lo que podría esperarse, los perfiles turbulentos de temperatura en la pared fueron más altos que los perfiles laminares (ver fig. 3.8). La turbulencia no parece mejorar la transferencia de calor en la capa lateral, es decir, el efecto conjunto del perfil promedio de velocidades y la difusividad térmica total no llevan a un mejoramiento de la transferencia de calor en la región cercana a la pared a pesar de que la viscosidad total es muy grande en tal región. Esta tendencia continua al disminuir c para Pe y M dados y, de hecho, mientras más pequeño es c, más grande es la diferencia entre el perfil laminar y el turbulento, siendo este último más alto (ver fig. 3.9). Sólo para uno de los casos analizados ($M = 10^5$, $c = 0.05$, $Pe = 2500$) la temperatura turbulenta en la pared fue ligeramente menor que la del caso laminar (ver fig. 3.10). Puede decirse que en general, el flujo laminar remueve el calor más eficientemente que el flujo turbulento en ductos con paredes conductoras delgadas. Tal parece que el incremento de la difusividad térmica total en la capa leteral no compensa la reducción en la velocidad promedio en la misma región, ocasionada por la turbulencia. Para ductos con paredes conductoras aislantes, se encontró que los perfiles de temperatura laminares y turbulentos coinciden y se sobreponen a los perfiles calculados con un flujo plano para números de Péclet grandes ($Pe = 2500$, ver fig. 3.11), en tanto que para Péclet pequeños ($Pe \leq 500$) el flujo plano lleva a temperaturas en la pared ligeramente más bajas que los flujos MHD (ver fig. 3.12). Previamente se mencionó que el modelo de turbulencia predice un perfil de velocidad laminar independientemente de Re (dentro del rango analizado) en ductos con paredes aislantes. Por lo tanto, los perfiles de velocidad turbulentos y laminares coinciden y la difusividad térmica total toma el valor molecular en todo punto, lo que explica la coincidencia de los perfiles de temperatura laminares y turbulentos en este caso. Por otra parte, se encontró que tanto para flujos laminares como turbulentos, una reducción en la razón de conductividades lleva a un incremento de la temperatura en la pared. Este efecto está relacionado con el perfil de velocidades, ya que al disminuir c, el máximo de velocidad en la capa lateral disminuye y el perfil se hace más angosto, por lo tanto, los efectos convectivos se aminoran y la temperatura en la pared aumenta.

Asimismo, para flujos laminares y turbulentos una reducción en el número de Hartmann lleva a temperaturas más altas, independientemente de c y Pe. Este efecto también se explica por los cambios en el perfil de velocidades.

Las principales conclusiones del análisis de transferencia de calor con flujos turbulentos son las siguientes:

- Los efectos turbulentos en la transferencia de calor no son tan intensos como en la dinámica del flujo, ocasionando cambios más dramáticos en los perfiles promedio de velocidad que en las distribuciones promedio de temperatura, con respecto a los casos laminares. Las difusividades totales viscosa y térmica presentan comportamientos similares aunque la primera es varios órdenes de magnitud mayor que la segunda.

- Para flujos laminares y turbulentos, mientras mayor es Pe, los efectos convectivos son más fuertes y la temperatura en la pared es menor, para M y c dados.

- Para flujos laminares y turbulentos, conforme c disminuye, la temperatura en la pared se incrementa, para M y Pe dados.

- Para flujos laminares y turbulentos, una reducción en M lleva a temperaturas en la pared más altas, para c y Pe dados.

- El mecanismo laminar de transferencia de calor en flujos en ductos con paredes conductoras delgadas es más eficiente que el turbulento para la mayoría de los casos estudiados. El incremento en la difusividad térmica total en la capa límite producida por la turbulencia, no compensa la reducción en la velocidad media en la capa lateral. El mezclado turbulento en la capa límite no es suficientemente fuerte para reducir la temperatura en la pared a niveles más bajos que los obtenidos con flujos laminares, caracterizados por chorros de alta velocidad en las capas laterales.

- Para Pe y M dados, los flujos laminares y turbulentos en ductos con paredes aislantes, son equivalentes a un flujo plano, desde el punto de vista de transferencia de calor. Para Pe bajos (≤ 500), la remoción de calor mediante un flujo plano es más eficiente que los flujos MHD.

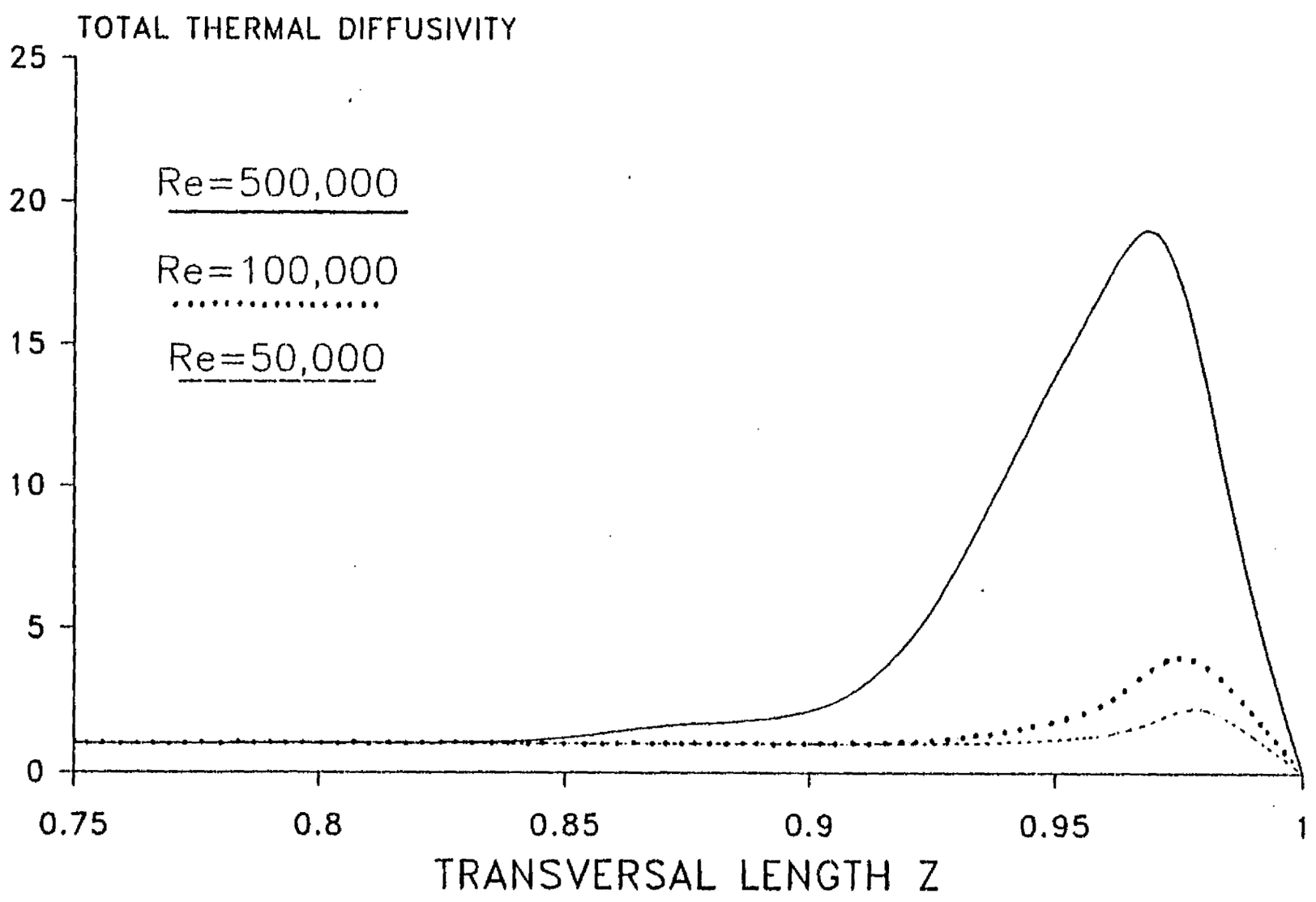

Figura 5.7: Difusividad térmica total vs. z en $y = 0$ para diferentes números de Reynolds. $M = 10^5$, $c = 0.05$.

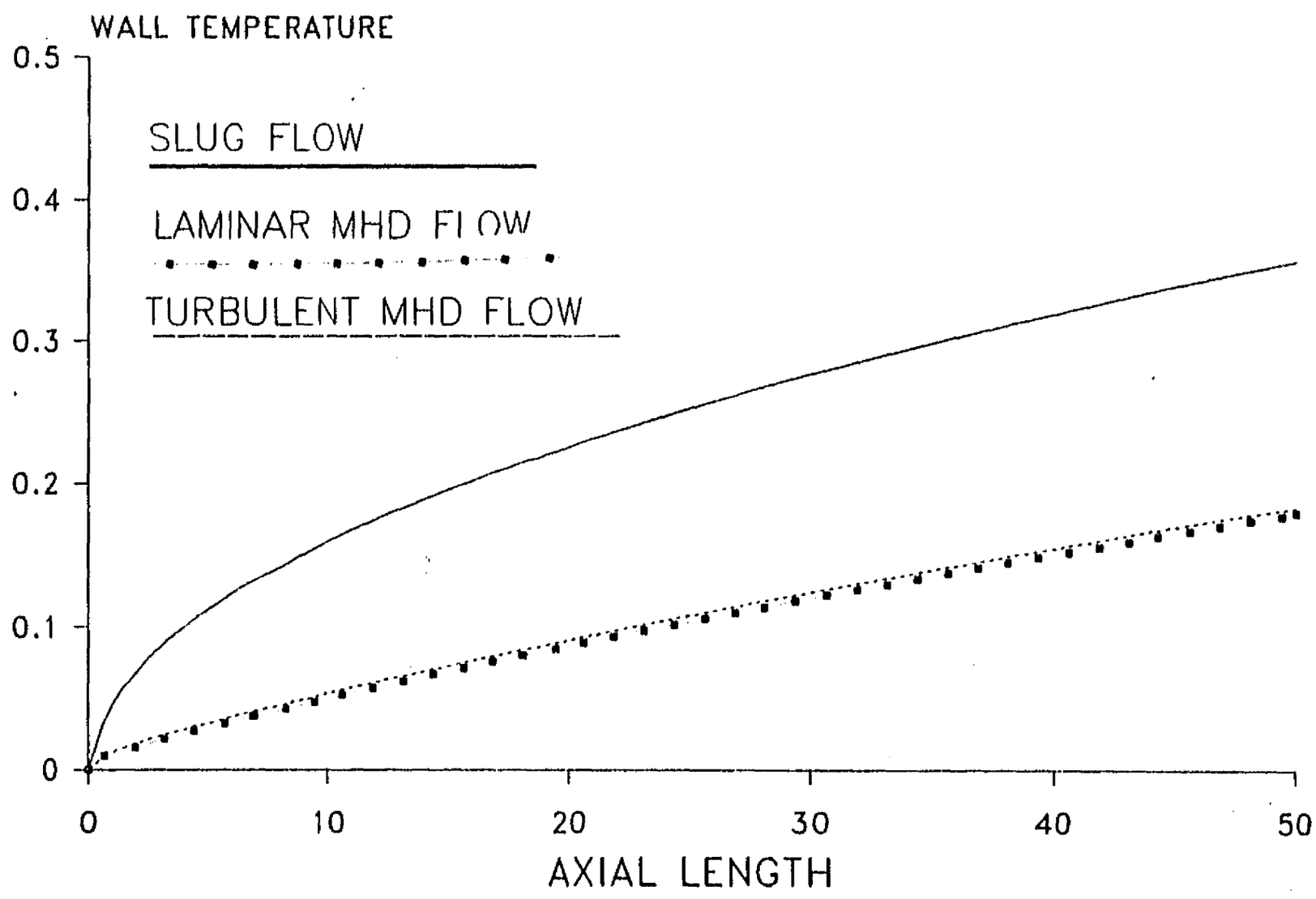

Figura 5.8: Temperatura promedio en la pared vs. z en $y = 0$ para flujo plano, laminar y promedio. $M = 10^5$, $c = 0.05$, $Pe = 500$.

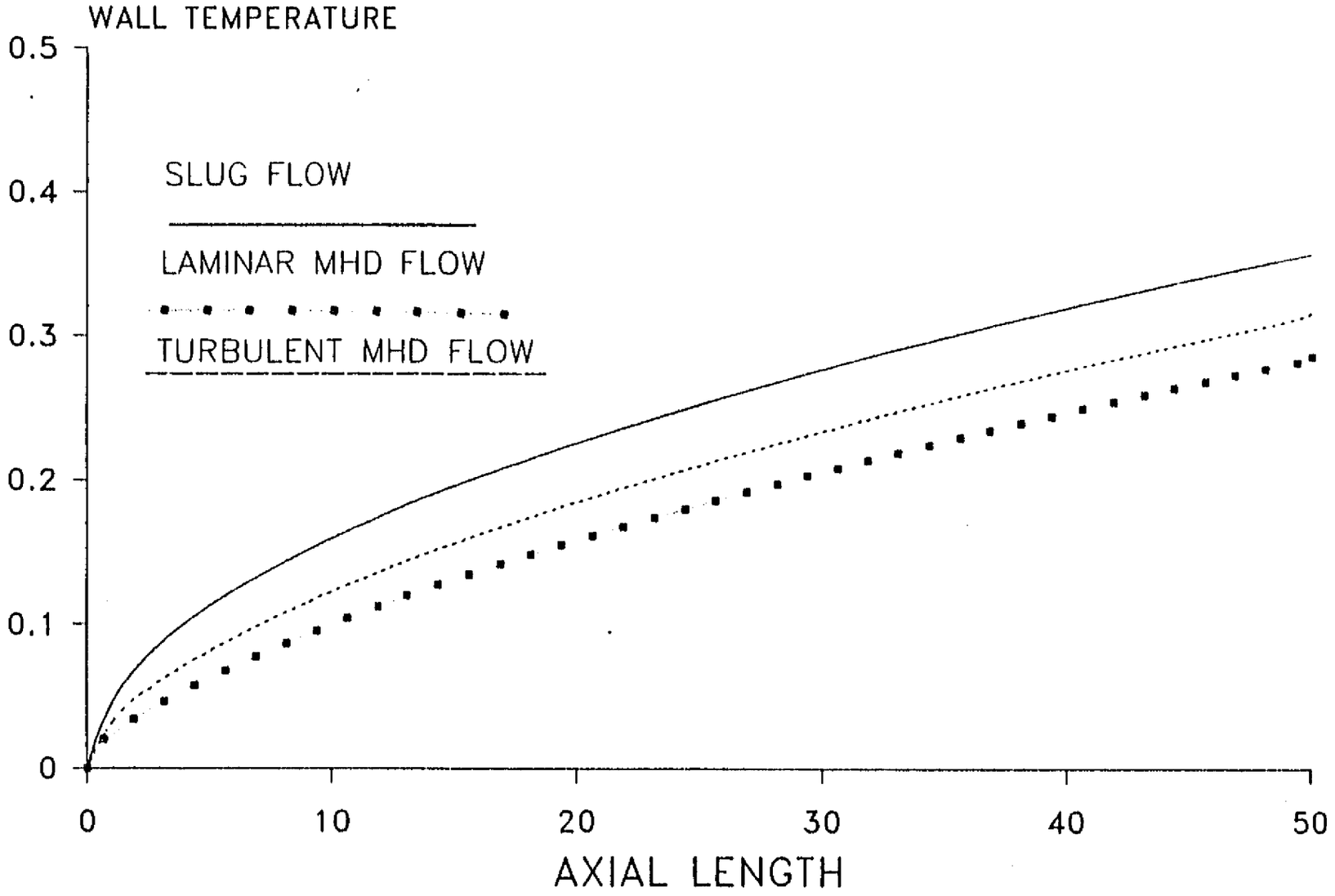

Figura 5.9: Temperatura promedio en la pared vs. z en $y = 0$ para flujo plano, laminar y promedio. $M = 10^5$, $c = 0.001$, $Pe = 500$.

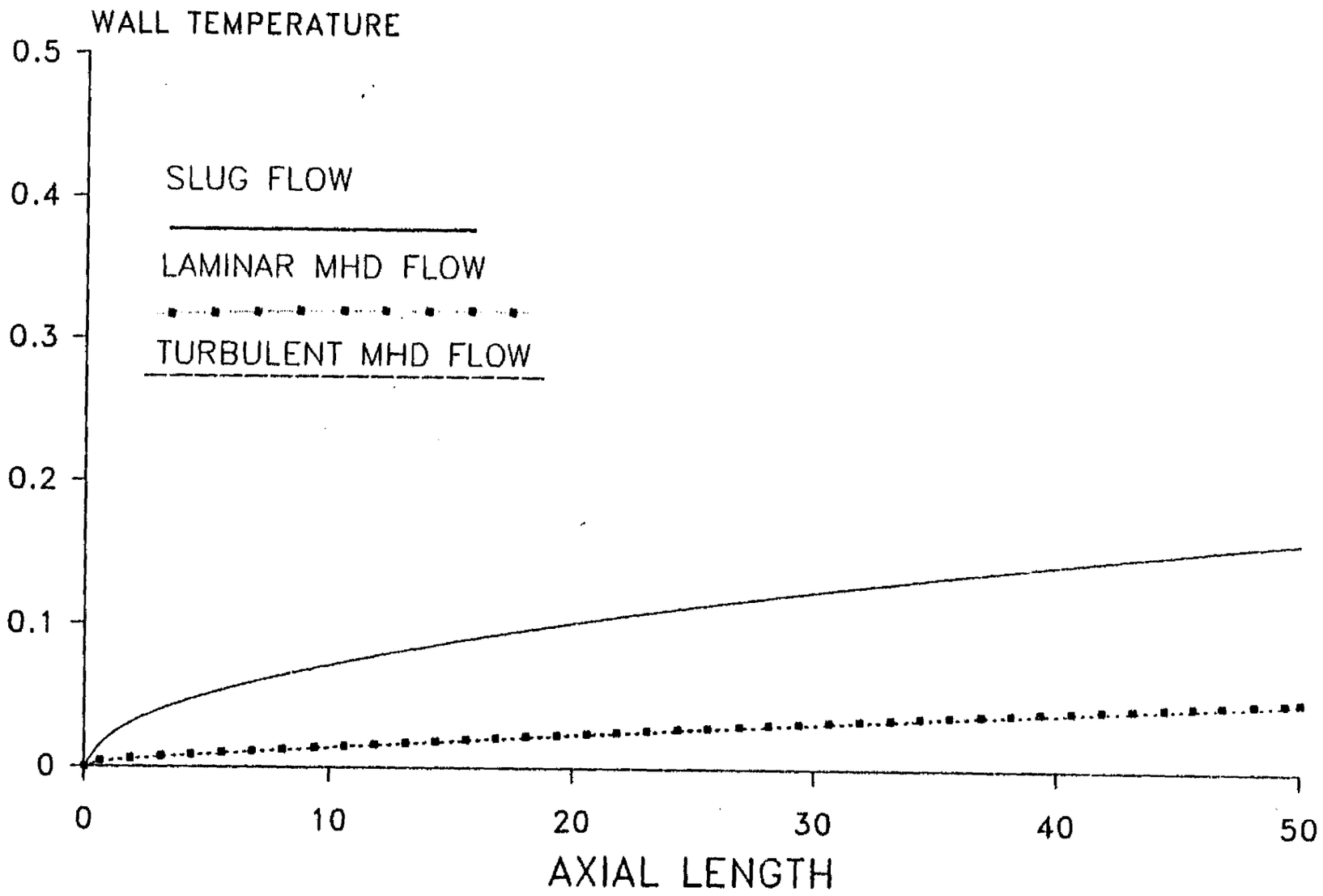

Figura 5.10: Temperatura promedio en la pared vs. z en $y = 0$ para flujo plano, laminar y promedio. $M = 10^5$, $c = 0.05$, $Pe = 2500$.

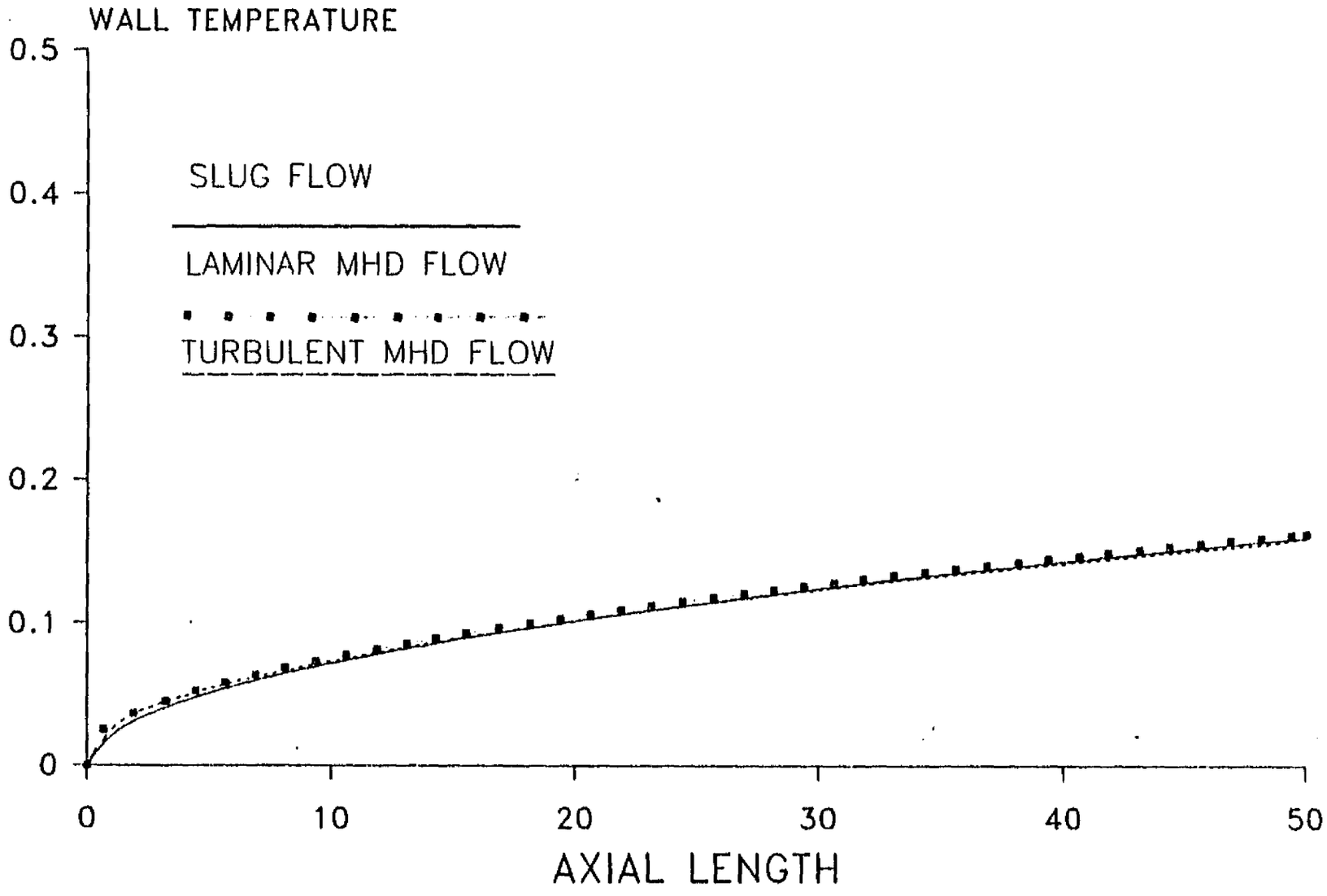

Figura 5.11: Temperatura promedio en la pared vs. z en $y = 0$ para flujo plano, laminar y promedio. $M = 10^5$, $c = 0$, $Pe = 2500$.

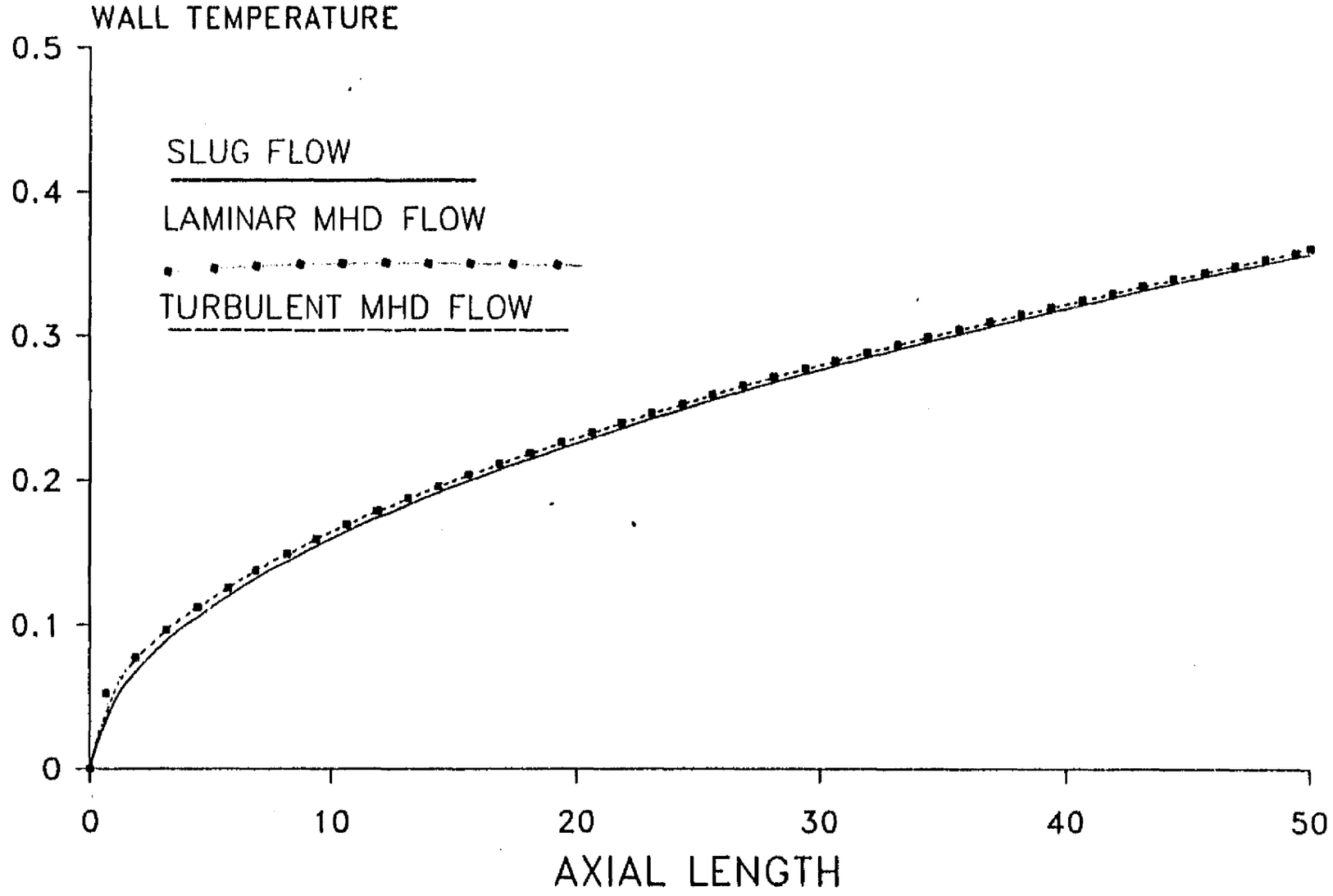

Figura 5.12: Temperatura promedio en la pared vs. z en $y = 0$ para flujo plano, laminar y promedio. $M = 10^5$, $c = 0$, $Pe = 500$.

Capítulo 6

Conclusiones

En este estudio se investigó el flujo completamente desarrollado de un metal líquido en un ducto de sección transversal cuadrada en presencia de un campo magnético transversal intenso. Se obtuvo una solución para el flujo compuesto núcleo-capa-límite-lateral mediante el método espectral de colocación. La solución ofrece la posibilidad de analizar flujos tanto en régimen laminar como en turbulento y además permite considerar ductos con paredes conductoras delgadas asi como ductos con paredes eléctricamente aislantes. De esta forma, fue posible explorar flujos en ductos cuya razón de conductividades se situa en el rango de interés práctico para el diseño de los mantos de los reactores de fusión ($c = 0.05 - 0$). La solución también permitió considerar flujos con números de Hartmann muy altos ($M = 10^3 - 10^5$), del mismo orden que los encontrados en las aplicaciones de fusión. Se encontró una concordancia muy buena entre los perfiles laminares calculados con el método espectral de colocación y las soluciones analíticas disponibles. La solución compuesta núcleo-capa-límite-lateral permitió la resolución de las capas límite laterales de una manera bastante eficiente desde el punto de vista computacional, aún para números de Hartmann de orden 10^5, contrastando con las soluciones de diferencias finitas que resultan ineficientes aún para $M \leq 10^3$. La transición de un ducto con paredes conductoras delgadas a uno con paredes aislantes revela un cambio dramático en la estructura del flujo, de un flujo con chorros de alta velocidad en las capas límite laterales a un flujo plano en casi toda la región del ducto. Un incremento en el número de Hartmann lleva a velocidades más altas en la capa lateral en los casos de ductos con paredes conductoras delgadas mientras que en ductos asilantes un incremento en M produce un mayor aplanamiento del flujo. El análisis de la estabilidad de los flujos no se llevó a cabo en el presente trabajo pero es de gran importancia práctica y deberá realizarse en una futura investigación. La influencia de los perfiles laminares de velocidad en la transferencia de calor fue estudiada resolviendo la ecuación de transferencia de calor mediante el método de diferencias finitas, en un ducto cuadrado con una pared lateral uniformemente calentada y las tres paredes restantes adiabáticas. Los resultados numéricos confirmaron los efectos

benéficos en la transferencia de calor de los flujos en ductos de paredes conductoras delgadas (donde la velocidad en la capa límite lateral es $O(M^{\frac{1}{2}})$ y acarrea una fracción del flujo volumétrico de $O(1)$) respecto a los cálculos efectuados con un flujo plano, en el intervalo de números de Hartmann analizados. Los efectos son mayores en el plano medio donde los chorros asociados a las paredes laterales alcanzan su velocidad máxima. Por otra parte, en flujos en ductos con paredes aislantes donde la velocidad en la capa límite lateral es $O(1)$, el flujo plano y los flujos MHD presentaron un comportamiento muy similar en sus características de transferencia de calor. Los perfiles de temperatura para un M dado y diferentes c's, claramente muestran la transición entre flujos en ductos con paredes conductoras delgadas y flujos en ductos con paredes aislantes.

Los efectos turbulentos fueron introducidos en la solución mediante un modelo de viscosidad efectiva proveniente de la teoría del Grupo de Renormalización (GRN). Aunque no se tiene evidencia experimental de que bajo condiciones relevantes para un rector de fusión se presente un flujo turbulento completamente desarrollado, el enfoque seguido en este estudio ofrece la posibilidad de explorar el comportamiento del flujo fuera del régimen laminar. Ciertamente se requieren más estudios para determinar si la inestabilidad en la capa lateral puede evolucionar, bajo ciertas condiciones, en un flujo turbulento completamente desarrollado. Las limitaciones intrínsecas del modelo para flujos MHD impidieron que se obtuviera una descripción cuatitativa completa del problema. Sin embargo, los resultados turbulentos mostraron tendencias físicamente razonables. De hecho, la presencia de turbulencia en flujos en ductos con paredes conductoras delgadas se manifestó mediante una marcada disminución de la velocidad en la capa límite lateral, un engrosamiento de esta capa límite y un notable incremento de la viscosidad total. Estos efectos se amplificaron al aumentar el número de Reynolds, aunque la turbulencia afectó únicamente a la región de capa límite, permaneciendo el núcleo inalterado. La reducción de la razón de conductividad de la pared trajo consigo un efecto de laminarización, en el sentido de que los efectos turbulentos se redujeron para un M y un Re dados. Esta es una clara consecuencia de la reducción de los chorros laterales que son la fuente principal de producción de turbulencia. En el caso límite de flujos en ductos con paredes aislantes, donde los chorros laterales desaparecen, el modelo predice un comportamiento laminar para cualquier Re, en el rango estudiado. Por otro lado, para flujos en ductos con paredes conductoras delgadas y $M \gg 1$, el campo magnético puede jugar un papel de promotor de turbulencia en el sentido de que un incremento en M ocasiona efectos turbulentos más intensos para un Re dado. Esto, a su vez, manifiesta el hecho de que mientras más grandes son los chorros laterales, son más susceptibles de volverse turbulentos y el nivel de turbulencia generada es también más alto. Las tendencias presentadas por los resultados turbulentos concuerdan, en general, con el análisis de estabilidad cualitativo realizado por Hunt [1965], aunque él únicamente consideró flujos en ductos con paredes asilantes o perfectamente conductoras. Los resultados turbulentos muestran cierta semejanza con el compor-

tamiento de la inestabilidad de los chorros laterales encontrada experimentalmente. Sin embargo, debido a las diferencias en condiciones físicas entre las dos situaciones, las extrapolaciones serían arriesgadas. No obstante, la presente investigación puede considerarse como un primer paso hacia la modelación de flujos de metales líquidos en ductos en campos magnéticos intensos fuera del régimen laminar. Entre las tareas futuras que pueden resultar interesantes se encuentra, por una parte, la introducción en el modelo GRN de un mecanismo magnético de supresión de turbulencia que considere la disipación de vórtices elongados y, por otra, el estudio de modelos adicionales de turbulencia.

Los resultados de transferencia de calor obtenidos a partir de los perfiles turbulentos de velocidad y viscosidad total junto con el modelo de difusividad térmica total de la teoría GRN, mostraron que las características de transferencia de calor son menos afectadas por la turbulencia que la dinámica del flujo. Aunque tanto la viscosidad total así como la difusividad térmica total presentaron un notable incremento en la región de capa límite, la primera es varios órdenes de magnitud mayor que la última. Este comportamiento es predicho por el modelo GRN cuando se consideran fluidos con números de Prandtl pequeños. Al variar la razón de conductividades y los números de Hartmann y Péclet se observaron tendencias globales físicamente razonables de los perfiles de temperatura en la pared, tanto para flujos laminares como para turbulentos. Asimismo, como una consecuencia directa de los resultados dinámicos turbulentos, los resultados de transferencia de calor en flujos en ductos con paredes aislantes fueron los mismos tanto en régimen laminar como en turbulento y los perfiles de temperatura en la pared fueron prácticamente los mismos para un flujo plano y para los flujos MHD. Los resultados de transferencia de calor obtenidos con el modelo GRN para flujos en ductos con paredes conductoras delgadas no son alentadores, ya que una clara mejora en la tasa de transferencia de calor sólo se obtuvo para $M = 10^5$, $c = 0.05$ y $Pe = 2500$. En la mayoría de los casos analizados, el mecanismo laminar MHD de transferencia de calor, caracterizado por chorros laterales de alta velocidad, es más eficiente que el mezclado turbulento en la capa límite. Podría esperarse que, en la mayoría de los casos, el mezclado turbulento reflejado mediante un notable incremento en la viscosidad total en la capa límite, llevara a temperaturas en la pared más bajas que los flujos laminares, para ductos con paredes conductoras delgadas. Sin embargo, los resultados predicen, en general, el comportamiento opuesto. Aquí se presenta la cuestión acerca de la validez del modelo utilizado. En este estudio se ha ofrecido una interpretación física consistente de los resultados arrojados por el modelo GRN y, bajo estas circunstancias, no se encontraron mayores objeciones. Sin embargo, existe la posibilidad de que el modelo GRN no sea adecuado para el problema investigado en este estudio. Discernir acerca de este punto requiere un trabajo teórico y experimental adicional. Puesto que estamos utilizando el modelo GRN de turbulencia para flujos ordinarios en flujos MHD, los resultados de transferencia de calor podrían estar indicando la necesidad de escalar la fórmula GRN para flujos MHD o bien de introducir modificaciones en

el modelo que tomen en cuenta los efectos de campo magnético sobre la transfrencia de calor. Los cambios en el modelo deben validarse sobre una base experimental. Un enfoque alternativo en términos de una difusividad térmica efectiva basada en los resultados experimentales sobre la inestabilidad en los chorros laterales, por ejemplo mediante la teoría de longitud de mezclado, podría servir para valorar la influencia en la transferencia de calor de las fluctuaciones de velocidad en las capas límite laterales.

Bibliografía

- Cuevas, S. (1994) "*Liquid Metal Flow and Heat Transfer in Square Ducts under Strong Magnetic Fields*". Anexo al presente documento.

- Hunt, J.C.R. (1965) "*Magnetohydrodynamic Flows in Rectangular Ducts*", J.Fluid Mech., **21**, pp. 577-590

- Patankar, S.V. (1980) "*Numerical Heat Transfer and Fluid Flow*", Hemisphere Publishing Corporation.

- Reed, C.B. y Picologlou, B.F. (1989) "*Sidewall Flow Instabilities in Liquid Metal MHD Flow under Blanket Relevant Conditions*", Fusion Technology, **15**, pp. 705-715

- Ting, A., Walker, J.S., Moon, T.J., Reed, C.B. and Picologlou, B.F. (1991) "*Linear Satbility Analysis for High-Velocity Boundary Layers in Liquid-Metal Magnetohydrodynamic Flows*", Int. J. Engng. Sci., **31**, pp. 357-372

- Walker, J.S. (1981) "*Magnetohydrodynamic Flows in Rectangular Ducts with Thin Conducting Walls. Part I. Constant Area and Variable Area Ducts with Strong Magnetic Fields*", J. Méc., **20**, pp. 79-112

- Yakhot, V. y Orszag, S. (1986) "*Renormalization Group Analysis of Turbulence. I. Basic Theory*", J. Sci. Comput., **1**, pp. 3-51

Liquid-Metal Flow and Heat Transfer in Square Ducts under Strong Magnetic Fields

Sergio Cuevas García

LIQUID-METAL FLOW AND HEAT TRANSFER IN SQUARE DUCTS UNDER STRONG MAGNETIC FIELDS

Sergio Cuevas García

Abstract

A theoretical investigation on liquid metal flow and heat transfer in strong magnetic fields in conditions of relevance for self-cooled liquid-metal fusion blankets is carried out. Steady fully developed flows in ducts of square cross-section under uniform transverse magnetic fields are analyzed in laminar as well as in turbulent flow regimes. A core-side-layer solution which offers the possibility of analyzing flows in ducts with wall conductance ratios in the range of interest for fusion blanket applications (*i.e.* from thin conducting to insulating wall ducts) is obtained through the spectral collocation method. The flow in the side-layers (parallel to the magnetic field) is explicitly resolved even for very large Hartmann numbers. The effects of variation of the wall conductance ratio from 0 to 0.05, and the Hartmann number from 10^3 to 10^5, on the laminar flow structure are studied. The laminar heat transfer problem in a duct with one side wall uniformly heated and three adiabatic walls, is also considered. The three-dimensional heat transfer equation is solved with a finite difference method and the influence of the variation of the former parameters on the heat transfer characteristics is analyzed. Some results for the laminar heat transfer problem in a cylindrical duct for different boundary conditions are also shown. A survey of magnetohydrodynamic (MHD) turbulence theory and of experimental results, obtained at Argonne National Laboratory, that demonstrated the existence of velocity fluctuations in the side layers, is conducted. In order to explore MHD duct flows beyond the laminar regime, a fully developed turbulent flow is studied. The core-side-layer solution is extended to include turbulent effects through an eddy viscosity model from the Renormalization Group (RNG) theory of turbulence. A parametric study of the turbulent profiles which, in addition, includes variation of the Reynolds number from 5×10^4 to 5×10^5, is carried out. Results for thin conducting wall ducts show the turbulence concentrated on the increased side layers while the core is essentially unperturbed. On the other hand, turbulent results for the insulating wall duct case present essentially no difference with respect to the laminar case. In general, a reasonable physical behavior was found. The heat transfer analysis is addressed using as an input the turbulent profiles and the RNG effective thermal diffusivity formula. The effect of the relevant parameters on the turbulent heat transfer, as predicted by the model, is investigated. Numerical results reveal stronger effects of turbulence on the flow dynamics than on the heat transfer. As a matter of fact, the laminar MHD heat transfer mechanism in thin conducting wall ducts results more efficient than the turbulent mechanism in most of the studied cases.

Contents

Chapter 1

Introduction

1.1 Fusion Technology

Controlled fusion reactions are one of the most challenging technological developments of our time. The construction of a safe and efficient fusion reactor may transform the energetic panorama for future generations. International cooperation programs [Conn, et al., 1992][1] are in the way to convert this technological challenge into a reality but the technical problems that still have to be overcome can in no way be considered simple.

Among different fusion reactor systems explored over the years by the international fusion research community, the Tokamak toroidal confinement system fueled with a deuterium-tritium (D-T) mixture appears to be the most feasible alternative [Cordey, Goldston and Parker, 1992]. In such system, the D-T plasma is confined by a toroidal magnetic field generated by a set of separated superconducting magnetic coils. The fusion D-T reaction that takes place inside the Tokamak produces a helium atom, a high-energy neutron and radiation. While deuterium is a stable and plentiful atom, tritium is not found in significant quantities in nature. Consequently, tritium must be generated in the reactor. This generation or breeding of tritium is accomplished by means of the lithium *blanket* surrounding the plasma where the high-energy neutrons from the fusion reaction collide, producing helium and tritium atoms. Tritium is then extracted and feed back to the plasma. The heat released by neutrons during the collision and by the exothermic reactions that breed the tritium, is deposited in the lithium and can be transferred to another fluid such as high-temperature helium which in turn, can drive turbines to generate electricity. Basically, three different types of lithium blankets can be considered [Talmage and Walker, 1988] namely, a solid, ceramic lithium compound, an essentially stagnant liquid lithium or a lithium-lead mixture, and a flowing liquid lithium or lithium-lead alloy. While the first two require a secondary cooling system using, for instance, water or helium, the third one is self-cooled, having the liquid-metal in circulation through the reactor, tritium separator, heat exchanger and feed pump. Self-cooled liquid metal blankets have been favored due to their performance characteristics and simplicity of design [Smith et al., 1984]. The

[1] References are listed alphabetically at the end of the manuscript by the first author's last name. Multiple citations to the same author(s) are given chronologically.

three essential functions of blankets, namely, absorption of the energy of the neutron flux, breeding of tritium, and transfer of heat to the external energy conversion system, can be carried out properly by these systems. In self-cooled liquid-metal blankets liquid lithium (or lithium-lead) flows through an arrange of ducts located immediately after the first wall which separates the blanket from the vacuum around the plasma. External to the blanket are the second wall, shielding and magnets. Due to the extreme operation conditions prevailing in the blanket (hot liquid lithium and high-density neutron flux), ducts must be manufactured with metal walls since no insulator material is able to withstand such conditions. Hence, a proper design of self-cooled liquid-metal blankets must necessarily be based on a deep knowledge of the physical phenomena present under relevant operation conditions.

1.2 Magnetohydrodynamic Considerations

The main constraints in the design of self-cooled liquid-metal blankets appear from the fact that, being located inside the windings, the liquid metal flows in the presence of a very strong magnetic field (5-10 Tesla). As a consequence, very strong magnetohydrodynamic (MHD) effects will be originated [Picologlou et al., 1985a]. In the first place, the flow of liquid metal through the ducts that form the blanket interacts with the applied magnetic field, inducing electric currents that, in turn, interact with the field producing an electromagnetic force, usually known as Lorentz force. This force will oppose the flow of the fluid giving rise to strong pressure losses that increases the required power to pump the liquid through the blanket. In addition, the large MHD pressure drops may originate unacceptable mechanical stresses in the first wall. These stresses depend primarily on the induced electrical currents that circulate in the liquid-metal and the duct walls. Actually, in an MHD duct flow the pressure drop is proportional to the thickness of the duct's walls, therefore, an additional requirement is to make the metal walls as thin as possible. In order to determine the first-wall stresses as well as the temperatures and heat transfer characteristics of the blanket, accurate predictions of MHD pressure drops and flow patterns are required. Therefore, a successful blanket design must be supported by a deep understanding of the MHD related phenomena that take place in these systems [Picologlou et al., 1989]. Actually, instead of being considered as a shortcoming, MHD effects can even be used as a positive blanket design tool [Walker and Picologlou, 1985].

In this context, a theoretical and experimental program has been carried out at Argonne National Laboratory since 1984, aimed at the investigation of liquid-metal MHD flows at reactor relevant conditions [Reed, *et al.*, 1985; Picologlou,*et al.*, 1989]. The program has thrown valuable experimental information about the detailed structure of these flows [Reed et al., 1987; Reed and Picologlou, 1989;] and, on the other hand, predictive tools for MHD flows at strong magnetic fields have been developed [Hua et al., 1988; Picologlou et al., 1989; Hua and Picologlou, 1991]. In general, a very good

agreement between experimental results and theoretical predictions has been found. Most of the theoretical studies have been performed within the inertialess approximation [Hua et al., 1988] which assumes a laminar flow where the electromagnetic force is the dominant interaction that determines the flow and pressure distributions in the liquid-metal, except for thin boundary layers.

Liquid metal duct flows in self-cooled fusion blankets are properly characterized by their relevant dimensionless parameters, namely, the Hartmann number, the interaction parameter, the magnetic Reynolds number and the wall conductance ratio, defined as

$$M = B_o L \sqrt{\frac{\sigma}{\rho \nu_o}}, \tag{1.1}$$

$$N = \frac{\sigma B_o^2 L}{\rho \bar{U}}, \tag{1.2}$$

$$Rm = \mu \sigma \bar{U} L, \tag{1.3}$$

$$c = \frac{\sigma_w t_w}{\sigma L}, \tag{1.4}$$

respectively. Here, B_o is the applied magnetic field strength, $\bar{U}$ is the average flow velocity, σ, ρ, ν_o and μ are the electrical conductivity, mass density, molecular kinematic viscosity and magnetic permeability of the fluid, respectively; L is a characteristic length of the flow that will be defined in the next Chapter in terms of duct's geometry and σ_w and t_w are the electrical conductivity and thickness of the duct walls, respectively. The square of the Hartmann number M, can be interpreted as the quotient of the electromagnetic force over the viscous force, while the interaction parameter, N, is considered as a relative measure of the electromagnetic and inertial interactions in the flow. Notice that $N = M^2/Re$, where Re is the ordinary Reynolds number,

$$Re = \bar{U} L / \nu_o. \tag{1.5}$$

For liquid-metal flows in self-cooled blankets, due to the presence of very strong magnetic fields, M and N take very high values, ranging from 10^3 to 10^5 [Picologlou, 1985b]. At these high values of M and N, the dominant electromagnetic force is much larger than the viscous and inertial interactions, and will affect the flow characteristics in a very peculiar way that we will describe in the next chapter. In the inertialess approximation, the assumption $N \gg 1$ allows us to neglect the inertial term in the equation of motion everywhere. Similarly, assuming $M \gg 1$, it is possible to neglect the viscous term in the equation of motion, except inside thin boundary layers. Strictly, the inertialess approximation is valid when $N \gg M^{\frac{3}{2}}$. This condition is not satisfied in liquid metal fusion blankets but the inertialess solution have proved to be in good agreement with experimental results for $N = O(M^{\frac{3}{2}})$ or even smaller [Walker, 1981].

The magnetic Reynolds number, Rm, is usually interpreted as the ratio of the magnetic field induced by the currents flowing in the liquid, to the applied magnetic field. In most terrestrial applications Rm presents very low values, indicating that the induced magnetic field is negligible in comparison to the applied field. This is satisfied for liquid metal flows where, for example, $Rm = 0.001 - 0.1$ in fusion lithium blankets [Walker, 1981]. Therefore, in this kind of flows the low-magnetic Reynolds number approximation, $Rm \ll 1$, is commonly used. Finally, the wall conductance ratio, c, gives a measure of the electrical conductivity of the wall, relative to the conductivity of the fluid. For electrically conducting wall ducts in fusion reactors, c ranges form 0.01 to 0.1 [Walker, 1981]. Most of the theoretical studies on liquid metal fusion blankets are based on the thin conducting wall approximation, which will be discussed in Chapter 2. Since insulating wall ducts may eventually become a feasible option, the range of interest of c for fusion applications can be extended from 0 to 0.1.

1.3 Side Layer Instabilities

It is a rather well known fact the laminarization effect that, under certain conditions, a magnetic field exerts over a turbulent conducting fluid [Branover, 1978]. Hence, in a simplistic approach it could be expected that, for the conditions prevailing in liquid-metal blankets, the magnetic field will prevent the growth of any possible instability, damping out the fluctuations that could lead to the appearance of turbulence. However, experimental results have confirmed the existence of velocity fluctuations that persist in the region near the walls parallel to the magnetic field of a rectangular conducting duct under conditions approaching those that prevail in a fusion reactor [Reed and Picologlou, 1989]. These fluctuations are not fully understood and deserve more attention. The experimental data indicate that the flow is not turbulent, at least in the conventional way, presenting strong periodicity and lack of small scale structure. It is speculated that the fluctuations are originated as a result of an instability in the side layer jets attached to the side walls parallel to the magnetic field. This kind of high velocity jets are characteristic of MHD flows in thin conducting wall ducts and will be described in the next Chapter. A preliminary linear stability analysis of these flows constitutes a first theoretical attempt to characterize this instability [Ting, et al. 1991]. Although the analysis offers some interesting conclusions, it is strongly limited by its linear character, while the actual phenomenon is of a highly non-linear nature. Independent experimental studies have corroborated the existence of near-the-wall velocity fluctuations in MHD flows in ducts with conducting walls [Sukoriansky, et al., 1988], though these experiments were carried out at conditions very different from the reactor relevant operation conditions. From the practical point of view, the existence of velocity fluctuations in the near-the-wall region could have beneficial effects in terms of enhancement of the heat transfer rates. Evidently, this would have immediate implications in the blanket design. However, further experimental and theoretical studies are

necessary in order to clarify the nature of the phenomenon and assess the heat transfer characteristics. The experimental evidence of persisting side-layer velocity fluctuations arises the necessity of extending previous studies to consider flows beyond the laminar regime. There are many open questions regarding the behavior of the side layers beyond the laminar regime but it is clear that these layers play a fundamental role on the stability and heat transfer characteristics of these flows.

Even though, due to stresses considerations, new tendencies in the fusion reactor design community point toward the utilization of insulating ducts as well as conducting cylindrical ducts for blanket purposes,the study of MHD flows in insulating and thin conducting wall ducts with rectangular cross-section is still a relevant technological issue. On the other hand, advancement in the understanding and modeling of the side-wall flow instability problem may constitute, by itself, a worth pursuing goal from the basic point of view.

The present study is aimed at the theoretical investigation of the dynamic and heat transfer characteristics of liquid-metal flows in strong, uniform magnetic fields, in both insulating and thin conducting wall ducts. Fully developed flows in laminar as well as in turbulent regime in constant-area rectangular ducts are considered. We are mainly interested on how the structure of the side-layers is influenced by the electrical conductivity of the walls, the magnetic field strength and the inertial effects, and how these factors affect the heat transfer processes. The main objective of this investigation is to extend some previous studies of liquid metal flows in self-cooled fusion blankets, firstly, by analyzing both laminar and turbulent flows, secondly, by stating boundary conditions that allow us a unified analysis of duct flows with wall conductance ratios in the range of interest for fusion applications, that is, from insulating to thin conducting wall ducts, and finally, by considering values of M and N in the range of relevance for fusion applications ($10^3 - 10^5$). The dynamic problem is addressed considering a composite core-side-layer flow and using the spectral collocation method to solve the boundary value problem. This approach has proved to be suitable for two- and three-dimensional MHD problems with uniform and non-uniform magnetic fields [Ting, 1991].

The document is organized in the following way. In Chapter 2, we first review the main characteristics of laminar liquid-metal flows in rectangular ducts in strong magnetic fields. The governing MHD equations are then presented and, afterwards, the dynamic problem is formulated, namely, the fully developed liquid metal flow in a constant-area rectangular duct whose walls range from thin conducting to insulating, under a uniform, transverse magnetic field. The equations governing the composite core-side-layer flow are obtained and the spectral collocation solution method is exposed. In Chapter 3, we present the spectral collocation flow solutions and the heat transfer finite difference results for the laminar regime, and analyze the influence of the relevant parameters, namely, the Hartmann number and the wall conductance ratio, on the laminar profiles. Some laminar heat transfer results for cylindrical ducts are also

included. In Chapter 4, we conduct a survey of MHD turbulence theory and of experimental results on the side layer instability. In Chapter 5, we explore the effect that the eventual appearance of turbulence would have on the flow and heat transfer. We simulate a fully developed turbulent MHD flow in a square duct, approaching the problem with an iterative scheme and a standard turbulence model [Yakhot and Orszag, 1986], and using as an input the MHD laminar velocity profiles. Likewise, turbulent velocity profiles and a total thermal diffusivity model are used to investigate the turbulent heat transfer problem. Finally, in Chapter 6 we expose the main conclusions of the present study.

Chapter 2

MHD Flows in Rectangular Ducts

2.1 Introduction

We begin this Chapter with a general review of the characteristic features that appear in laminar liquid-metal flows in strong magnetic fields, in order to offer a better physical picture of the phenomena considered in the present study. Afterwards, we present the basic equations that govern the flow of a conducting fluid in a magnetic field in both laminar and turbulent regimes and write them in dimensionless terms. We formulate the main problem to be solved in this study, namely, the fully developed liquid metal flow in a rectangular duct in a uniform magnetic field, in laminar as well as in turbulent regimes. For the turbulent case, we use the approaches of Reynolds and Boussinesq from which we obtain equations for the averaged variables, including turbulent effects through an eddy viscosity. The simplified set of equations with the approximations and boundary conditions used for this problem is then established. We consider a single core-side-layer flow solution with boundary conditions which allows us to deal with thin conducting as well as insulating wall ducts and explore the transition between these two cases. Finally, we present the method of solution for the system of equations, namely, the spectral collocation method, and discuss some aspects related to its numerical implementation.

2.2 Main Characteristics of Liquid Metal Flows in Ducts with Strong Magnetic Fields

Laminar liquid-metal duct flows in the presence of strong magnetic fields have been thoroughly studied in the past two decades, mainly due to their relevance to fusion technology. In order to provide a better understanding for the subject of this study, we will describe here in a rather qualitative way, some of the most characteristic features of these flows.

In most of the blanket, the liquid metal flows through constant-area ducts where the magnetic field is mainly transverse and uniform. Under these conditions, the flow is fully developed. However, there are regions of the blanket where the magnetic field is

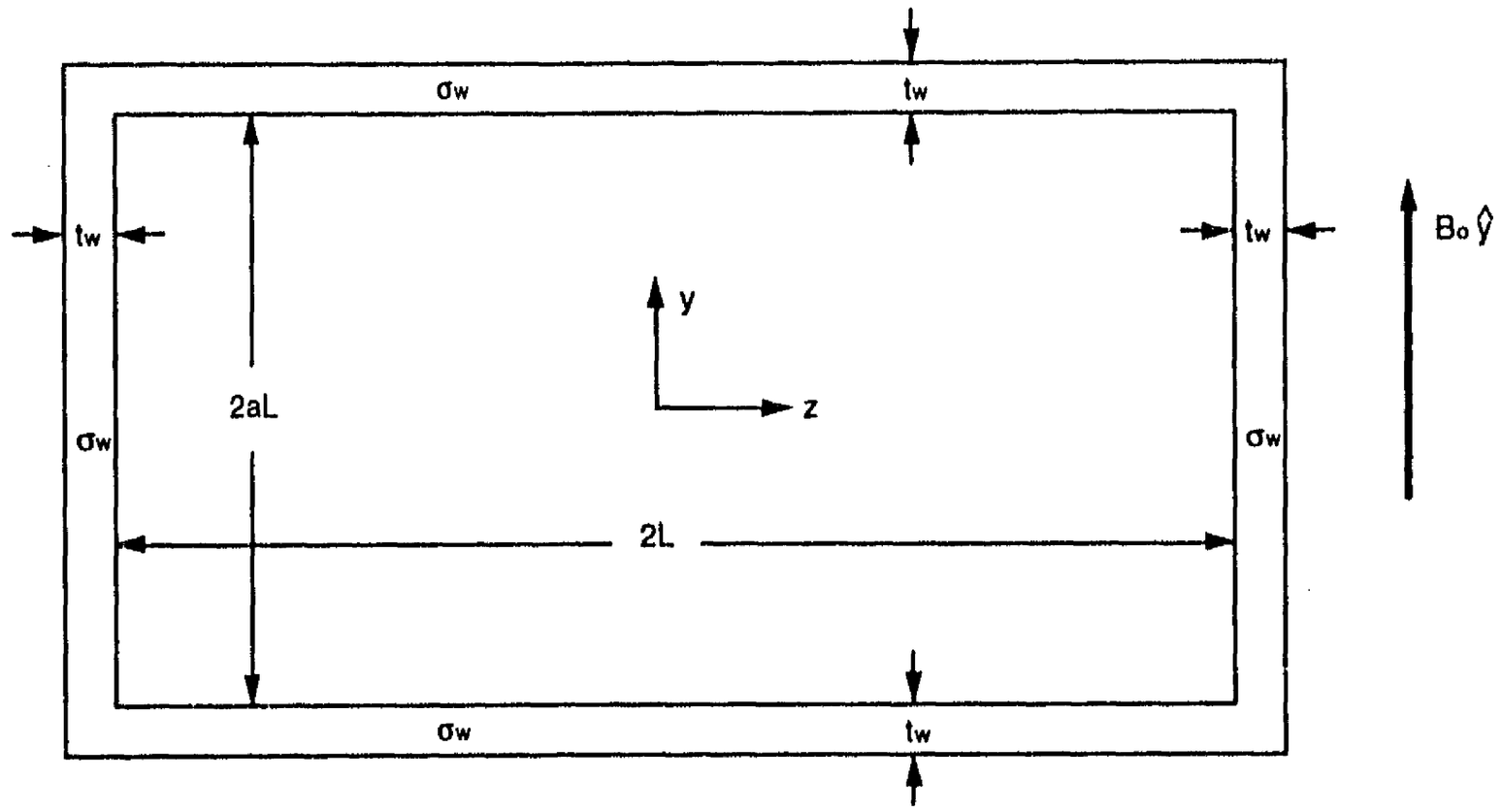

Figure 2.1: Duct cross-section and relevant dimensions.

non-uniform and the flow is not fully developed. A complete study of liquid metal flows in uniform and non-uniform magnetic fields was carried out by Ting [1991]. For the sake of conciseness, in this section we will concentrate only on fully developed laminar flows in constant-area rectangular ducts immersed in a uniform, transverse magnetic field. Figure 2.1 shows the geometric arrangement considered and the disposition of the applied magnetic field and coordinate system. The characteristic length of the flow, denoted by L, is taken as the half spacing between the walls parallel to the magnetic field while the aspect ratio of the channel is denoted by a.

Liquid-metal flows in rectangular ducts with strong magnetic fields ($M \gg 1$) can be divided into different subregions, namely, the core, the Hartmann layers adjacent to the top and bottom walls perpendicular to the applied magnetic field, the side-wall layers parallel to the magnetic field and the corner regions [Roberts, 1967, Walker, 1981]. Figure 2.2 shows the division of the flow in these subregions. An estimation of the order of magnitude of these subregions shows that, in dimensionless terms, the thickness of the Hartmann and side-wall layers are $O(M^{-1})$ and $O(M^{-\frac{1}{2}})$, respectively, while the corner regions are $O(M^{-1}) \times O(M^{-\frac{1}{2}})$. These orders of magnitude are justified in the next subsection. Note that at very high M, these layers will be very thin. The core of the flow can then be considered inviscid, matching the values of the velocity and electrical potential with the values at the walls through the boundary layers, where

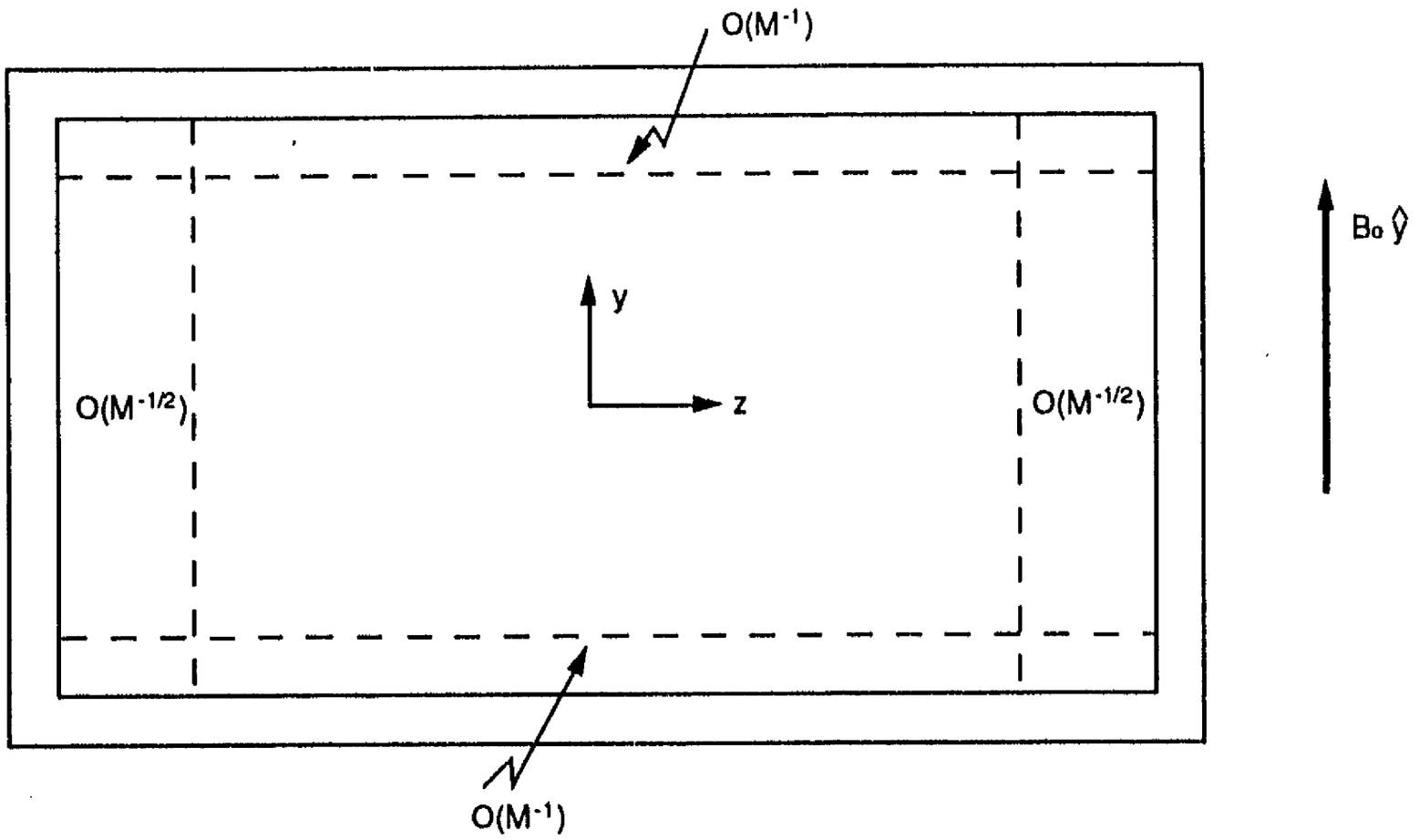

Figure 2.2: Different flow subregions in a rectangular duct flow under a strong transverse magnetic field.

viscous effects (*i.e.* steep velocity gradients) are concentrated. These layers provide an alternative path for the closure of electrical currents and have a decisive role in the dynamic and heat transfer characteristics of the flow. In particular, it can be shown that in contrast to the layers found in ordinary fluid mechanics, which adapt to the properties of the exterior flow, the Hartmann layers control the outer flow [Moreau, 1990], in the sense that there is a proportionality relation between the current flowing in the layer and the core velocity. On the other hand, as we will show later, depending on the magnitudes of c and M, the velocity in the side wall layers can be much larger than the core velocity and, under certain circumstances, can carry a substantial part of the total volume flux. This characteristic may strongly affect the heat transfer process in a positive way [Hua and Picologlou, 1989].

2.2.1 Electric Current Paths and Flow Structures

Let us now consider in more detail the path of the electric currents, originated by the interaction of the flowing liquid metal and the applied magnetic field. In the MHD flows we are interested, a pressure drop drives a liquid metal with a velocity field $\mathbf{u}$, through a duct with a transverse magnetic field $\mathbf{B}_o$, produced by an external magnet. The interaction of the conducting fluid with the magnetic field produces an induced

electric field given by $\mathbf{u} \times \mathbf{B}_o$, which is the source driving all electrical currents. Due to the symmetry with respect to the xz plane, we discuss only the upper region of the duct, $y \geq 0$ (see figure 2.1). Assuming that the liquid flows in the positive x direction while the magnetic field is applied in the y direction, an electric current will be induced in the core of the flow in the positive z direction. The current has to find a return path inside the duct, since no external circuit is connected. The current leaving the core, will penetrate the side layer and will eventually reach the wall. That the current will flow in the positive y direction either through the side layer or through the side wall (or through both), will be determined by the relative magnitudes of the electrical resistances of the wall and the layer, considered as parallel resistors [Picologlou, 1985b]. Once the current has reached the top wall, it will flow in the negative z direction either through the wall or through the Hartmann layer or be splitted through both. Again, the actual path will depend on the magnitudes of the electrical resistance of the wall and the layer in question. Afterwards, the current will reach the opposite side-wall and flow in the negative y direction, where similar considerations apply. Eventually, it will leave the side-wall region and return to the core, closing the circuit. The magnitude of the electric current density, $\mathbf{j}$, flowing through the liquid metal and walls will depend on the magnitude of the induced electric field $\mathbf{u} \times \mathbf{B}_o$ as well as on the total electrical resistance of the internal circuit consisting of the liquid metal and the walls in series. In addition, this current will determine the electromagnetic force opposing the flow of the liquid metal, given by $\mathbf{j} \times \mathbf{B}_o$. As a matter of fact, the increased pressure drop required to surmount that force is proportional to $\mathbf{j}$.

The resistance of the wall and the internal resistance (per unit axial length) of the liquid metal are given by $\mathcal{R}_w = 2aL/\sigma_w t_w$ and $\mathcal{R}_{int} = 2aL/\sigma L$, respectively. On the other hand, the electrical resistance of the layers can be estimated by $\mathcal{R}_l = 2aL/\sigma d_l$, where d_l is the thickness of the given layer. An estimation of the order of magnitude of the thicknesses of the Hartmann and side layers can be obtained by comparing the order of magnitude of the electromagnetic and viscous forces acting per unit volume in each layer [Shercliff, 1962; Branover, 1978]. For simplicity, we consider an insulating wall duct, so that currents close completely inside the liquid. As we mentioned, the electromagnetic force per unit volume acting on the fluid is $\mathbf{j} \times \mathbf{B}_o$, where the electric current density is given through Ohm's law, $\mathbf{j} = \sigma(-\nabla\phi + \mathbf{u} \times \mathbf{B}_o)$. Here ϕ is the electric potential. In the Hartmann layers, the order of magnitude of the current density is $\sigma \bar{U} B_o$.[1] Hence, the electromagnetic force per unit volume in the flow direction is of order $\sigma \bar{U} B_o^2$. On the other hand, the specific viscous force in the Hartmann layers is of order $\rho \nu_o \bar{U}/\delta_{Ha}^2$, taking $\bar{U}/\delta_{Ha}$ as a representative velocity gradient, where δ_{Ha} is the thickness of the Hartmann layer. Assuming that both forces are comparable, $\sigma \bar{U} B_o^2 \approx \rho \nu_o \bar{U}/\delta_{Ha}^2$, we get in dimensional terms

[1] Assuming that the electrostatic field is of the same order of the induced field $\bar{U} B_o$.

$$\delta_{Ha} \approx \frac{L}{M}. \tag{2.1}$$

The thickness of the side-wall layers, δ_{sl}, is greater than that of the Hartmann layers since the electric current density in the side layers has not only a component in the z-direction, j_z, but also a component in the y-direction, j_y, which does not interact with the field. We mentioned that in the Hartmann layers $j_z \approx \sigma \bar{U} B_o$, therefore, the total current per unit length of duct in these layers is of order $\sigma B_o \bar{U} L M^{-1}$. This is also the order of magnitude of the total current in the core and the side layers. Thus j_z in the core and the side layers is of order $\sigma B_o \bar{U} M^{-1}$ and, consequently, the order of magnitude of the electromagnetic force per unit volume is $\sigma B_o^2 \bar{U} M^{-1}$. Since this force is comparable to the specific viscous force in the side layers, $\rho \nu_o \bar{U} / \delta_{sl}^2$, the thickness δ_{sl} can be estimated as

$$\delta_{sl} \approx \frac{L}{M^{\frac{1}{2}}}. \tag{2.2}$$

The estimates of δ_{Ha} and δ_{sl} are confirmed by the exact solutions [Moreau, 1990]. Taking into account equations (2.1) and (2.2), the resistances of the Hartmann and side layers can be estimated as

$$\mathcal{R}_{Ha} = \frac{2aL}{\sigma(L/M)}, \quad \mathcal{R}_{sl} = \frac{2aL}{\sigma(L/M^{\frac{1}{2}})},$$

respectively. Since the thickness of the Hartmann layer is $O(M^{-1})$ while that of the side layer is $O(M^{-\frac{1}{2}})$, the resistance of the former will be larger than that of the latter.

The assumption that the Hartmann layers present a much higher resistance than the top/bottom walls ($\mathcal{R}_{Ha} \gg \mathcal{R}_w$), leads to the condition

$$\frac{M}{\sigma L} \gg \frac{1}{\sigma_w t_w},$$

that is,

$$c \gg M^{-1}.$$

In this case, most of the current will flow through the top/bottom walls, as occurs in ducts with walls of a high electrical conductivity. On the other hand, if we assume that $\mathcal{R}_{Ha} \ll \mathcal{R}_w$, we get the condition $c \ll M^{-1}$. This would imply that no current will go through the wall, flowing instead through the Hartmann layers, as in the case of a duct with insulating walls. A similar analysis can be performed for the side walls and the side layers. In that case, a much higher resistance in the side layer than in the side wall ($\mathcal{R}_{sl} \gg \mathcal{R}_w$), is expressed by the condition $c \gg M^{-\frac{1}{2}}$, while the case $\mathcal{R}_{sl} \ll \mathcal{R}_w$ gives $c \ll M^{-\frac{1}{2}}$. Figure 2.3 shows schematically a situation where part of the current flows through the side layer and part through the side wall and returns through top and

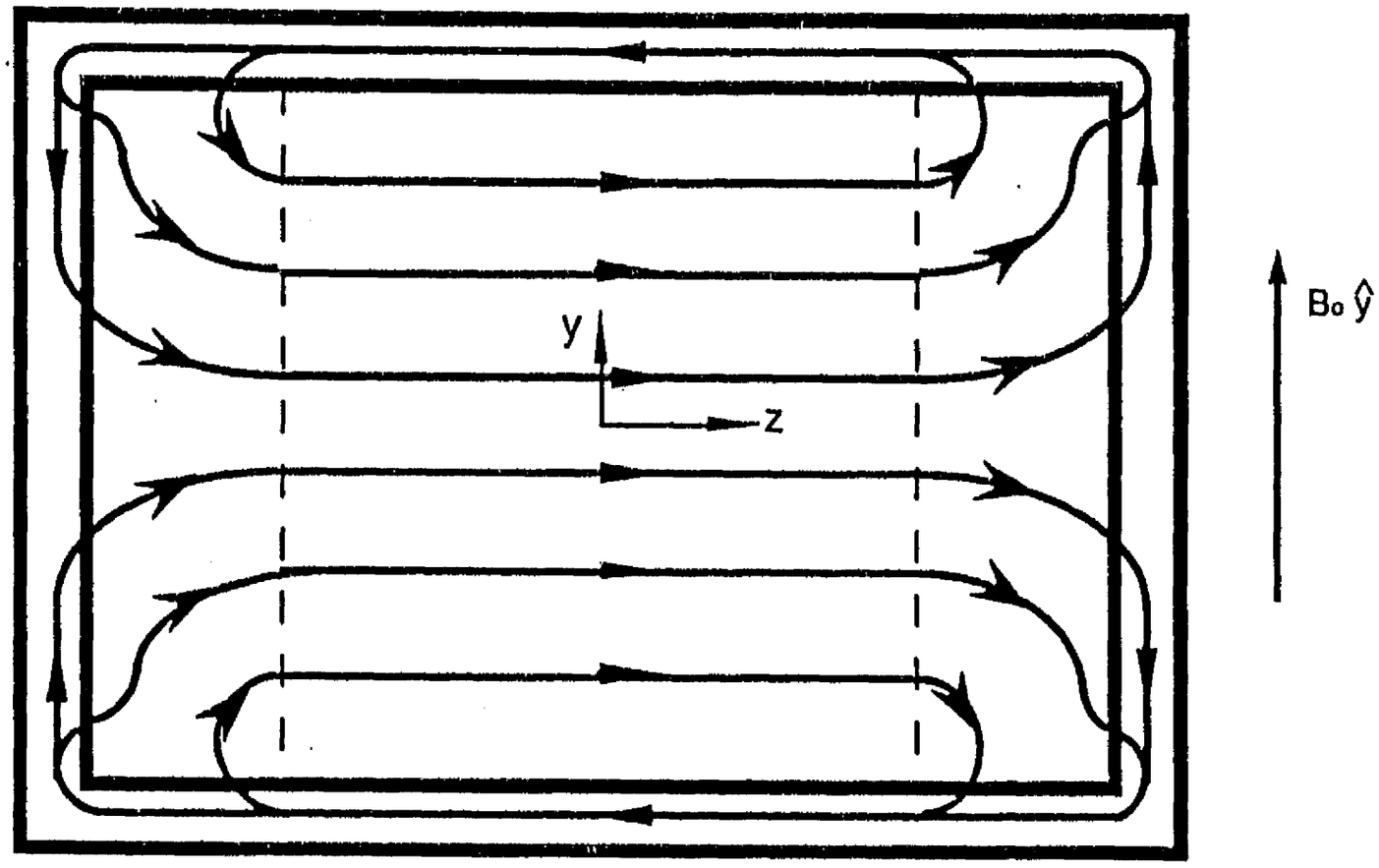

Figure 2.3: Electric current paths with currents in the y direction divided between the side layer and side wall [Ting, A., 1991].

bottom walls of high electrical conductivity. The existence of different paths for the current, depending on the relation of c and M, will originate different flow structures.[2]

The evolution of fully developed flow in rectangular ducts as the conductance ratio c increases from zero for fixed M, has been thoroughly described by Walker [1981]. Picologlou [1985b] has presented a simplified analysis for some interesting cases in terms of an electrical circuit model that allows the estimation of the pressure drop. For instance, for the insulating wall case ($c \ll M^{-1}$) this analysis shows that the pressure drop is $O(M^{-1})$ and is controlled by the resistance of the Hartmann layer. In addition, the side layer velocity is $O(1)$. Another relevant case is that of a duct with thin conducting walls. In this case, it is assumed that the electrical resistance of the duct walls is much greater than the resistance of the bulk of the liquid metal but much less than that of the Hartmann layers, that is, $R_{int} \ll R_w \ll R_{Ha}$ [Picologlou, 1985b; Talmage and Walker, 1988]. This is equivalent to the condition

$$M^{-1} \ll c \ll 1.$$

This is a very common approximation that allows the establishment of boundary conditions involving only fluid variables [Shercliff, 1956; Walker, 1981] and has been used

[2]In the former considerations we have assumed, for simplicity, that the conductance ratio of all the walls is the same, but this is not necessarily the case.

in many problems related with the flow of liquid metals in fusion blankets, particularly, using asymptotic expansions in powers of $c^{\frac{1}{2}}$. Here the current closes through the top (bottom) wall whose resistance controls the magnitude of the current and the pressure drop. The latter is larger by a factor of cM than the pressure drop of the insulating wall case, being $O(c)$. The top and bottom currents can flow into the side layers at $z = -L$ either from the top and bottom or from the side wall, depending on the relation between c and $M^{-\frac{1}{2}}$. Actually, the structure of the side layers will be determined by the conductivities of the side walls. Within the thin wall approximation, we can identify different ranges, namely, $M^{-1} \ll c \ll M^{-\frac{1}{2}}$, $c = \alpha M^{-\frac{1}{2}}$ (where α is a $O(1)$ constant) or $M^{-\frac{1}{2}} \ll c \ll 1$. For $M^{-1} \ll c \ll M^{-\frac{1}{2}}$ a significant amount of current in the top and bottom flows into the side layer at $z = -L$ and originates a large side layer velocity of $O(cM)$ [Walker, 1981]. However, this velocity is not sufficiently large to convey any of the $O(1)$ volume flux. For $c = \alpha M^{-\frac{1}{2}}$ the side layer velocity is large enough to carry a significant part of the total volume flow, and this part grows as α increases. On the other hand, for $M^{-\frac{1}{2}} \ll c \ll 1$ the current in the top and bottom enters first into the side wall and then into the side layer as a uniform current. The side layer velocity in this case is $O(M^{\frac{1}{2}})$ and a fraction of the $O(1)$ volume flux is conveyed by both side layers. It can be shown [Walker, 1981; Picologlou, 1985b] that the perfectly conducting wall case is expressed by the condition $c \gg M^{\frac{1}{2}}$. The pressure gradient is $O(1)$ and is controlled, as well as the current, only by the resistance of the liquid metal while the side layer velocity is $O(1)$. Additional cases are discussed in detail in the original references.[3]

From the previous discussion it is clear that, since the insulating ducts present the lower pressure drop, they should be the best option for fusion blanket applications. However, utilization of insulating ducts is constrained to the availability of insulating materials capable of withstanding the extreme working conditions of fusion reactors. For this reason, thin wall metal ducts are still good candidates.

2.2.2 Side Layer Characteristics

The existence of high velocity side layers in thin conducting wall ducts deserves further explanation. A description of this phenomenon in terms of the Lorentz force applied on the core and the layers was offered by Hunt [1965] and Sterl [1990]. However, they considered a different case, namely, a duct with perfectly conducting top and bottom walls and side walls of arbitrary conductivity. In such a case, the current lines always close through the top and bottom walls. The Lorentz force opposing the flow of the liquid is given by $\mathbf{j} \times \mathbf{B}_o$. While in the core of the flow the component of the current density in the z-direction is maximum ($j_y = 0$), in the side layers j_z may be diminished since j_y may have a finite value (depending on the conductance ratio). Therefore, in

[3] In Chapter 3 we will show concrete examples of some of the previously discussed cases.

the core, the force will be higher since the whole current contributes to $\mathbf{j} \times \mathbf{B}_o$ while in side layers the force will be diminished for j_y does not contribute to the Lorentz force. For instance, if the side wall is highiy conducting ($c \gg M^{-\frac{1}{2}}$) the current will return through the side wall, giving a high j_z component in this region and consequently a large force and a low side layer velocity. On the other hand, if we reduce the conductivity of the side wall, (*i.e.* if we reduce c) the current will return through the side layer. The j_z component in the side layer will then be small, giving rise to a small force and a high side layer velocity. For a duct with the four walls of the same arbitrary conductivity, this analysis fails in giving the correct picture as the conductance ratio is decreased. The reason is that when c is sufficiently reduced, the currents induced in the core are no longer closed through the top and bottom walls but through the Hartmann layers, and hence the electromagnetic drag on the flow is reduced. Eventually, for a small enough c ($c \ll M^{-1}$), the velocity overshoots will be completely suppressed, as in the flow in a duct with insulating walls. This effect will be shown in the results of Chapter 3.

Reed and Picologlou [1989] offered a simplified picture of the side layer phenomena in ducts with thin conducting walls when $M^{-\frac{1}{2}} \ll c \ll 1$. Here we follow their analysis to show that many essential characteristics of these flows can be extracted without information about the detailed structure of the side layers.

Let us assume that both side walls have different thickness t_1 and t_2 and different conductivities, σ_{w1} and σ_{w2}, while the top and bottom walls have the same thickness and conductivity, t_w and σ_w, respectively. The conductance ratio of the top and bottom walls is then $c = \sigma_w t_w / \sigma L$ while those of the side walls are $c_i = \sigma_{wi} t_{ni} / \sigma L$, where $i = 1, 2$ corresponds to the left and right walls, respectively. Since the viscous effects are relevant only in the boundary layers, in the core, the equation of motion reduces to

$$\nabla p = \mathbf{j} \times \mathbf{B}_o, \tag{2.3}$$

where p is the pressure. In fully developed flow $\mid \nabla p \mid = K = constant$ while the conservation of mass $\nabla \cdot \mathbf{u} = 0$ is identically satisfied, where $\mathbf{u} = u\hat{\mathbf{x}}$ is the velocity field and $\hat{\mathbf{x}}$ is a unit vector in the axial direction. On the other hand, equation (2.3) along with the conservation of current $\nabla \cdot \mathbf{j} = 0$, and the symmetry condition with respect to $y = 0$, lead to the conclusion that the only component of the current density different from zero is $j_z = K/B_o$. Actually, uniformity of j_z in the core implies uniformity of u in that region. In addition, Ohm's law

$$j_z = \sigma(-\frac{\partial \phi}{\partial z} + uB_o), \tag{2.4}$$

must be satisfied, where ϕ is the electric potential in the fluid. Equation (2.4) along with the conservation of current lead to a linear variation of ϕ in the core, that is, $\phi = \gamma z$, where γ is a constant and at $z = 0$, $\phi = 0$ has been taken as the reference voltage.

Now, in the top or bottom walls the voltage gradient is continuous at the wall/fluid interface, that is, there is no voltage drop across the Hartmann layer (at $O(M^{-1})$). Since all the current (per unit length) I will return through the top (bottom) wall, application of Ohm's law at this wall gives a current density

$$j_w = -\frac{I}{t_w} = \sigma_w \left(-\frac{\partial \phi_w}{\partial z}\right) = \sigma_w \left(-\frac{\partial \phi}{\partial z}\right) = -\sigma_w \gamma.$$

But in the core the total current is $I = j_z aL$. Since the current is conserved, we get $\gamma = j_z aL/\sigma_w t_w$, and from equation (2.4) we find

$$j_z = \frac{\sigma u B_o c}{a + c}. \tag{2.5}$$

Let us now apply Ohm's law to the side wall where we assume that the condition $c_i \gg M^{-\frac{1}{2}}$ $(i = 1, 2)$ is satisfied. The current entering the side layers will close through the side walls, presenting a linear variation from $I = 0$ at $y = 0$ (due to symmetry) to $I = j_z aL$ at $y = aL$. For instance, at the right-hand side wall, conservation of current means that $j_z y = j_{sw} t_2$, that is

$$j_{sw} = \frac{j_z y}{t_2} = -\sigma_{w2} \frac{\partial \phi_{w2}}{\partial y}.$$

Therefore, the electric potential in the side wall is given by

$$\phi_{w2} = -\frac{j_z y^2}{2\sigma_{w2} t_2} + \beta,$$

where β is a constant. At the corner $y = aL$, $z = L$ the electric potential at the side matches the potential at the top which is equal to $-\gamma L$, due to the continuity of the potential at the core/top wall interface. This allows to determine β, namely

$$\phi_{w2} = -\alpha L + \frac{j_z}{2\sigma_{w2} t_2}(a^2 L^2 - y^2). \tag{2.6}$$

Because the side layer thickness, δ, is very small, $-\gamma L$ is also the potential at the top wall at $z = aL - \delta$ and, for continuity, it is the potential in the fluid at the core/side layer interface. Notice that in the core, $\partial\phi/\partial y = 0$, which means that the electric potential is constant along the magnetic field lines. Since at the interface between the core and the side layer the potential is constant and equal to γL, the second term in equation (2.6) can be interpreted as a jump in the potential across the side layer

$$\Delta\phi_{sl} = \frac{j_z}{2\sigma_{w2} t_2}(a^2 L^2 - y^2). \tag{2.7}$$

where the subindex sl denotes the side layer variables. This jump will give rise, by virtue of Ohm's law, to a finite flow rate in the layer. This can be seen by integration of Ohm's law across the side layer

$$\int_0^{\delta} u_{sl} dz = \frac{1}{B_o}\left(\frac{j_z}{\sigma}\delta + \Delta\phi_{sl}\right).$$

Notice that the left hand side of this equation is the volumetric flow rate in the side layer per unit y. The first term in the parenthesis can be neglected since it is $O(c_2 M^{-\frac{1}{2}})$ compared to the second one. Hence the flow rate per unit y in the side layer, q_2, presents a parabolic distribution in y, that is

$$q_2 = \frac{j_z}{2\sigma_{w2} t_2 B_o}(a^2 L^2 - y^2), \tag{2.8}$$

and the total flow in the side layer, Q_2, is given by

$$Q_2 = \frac{2}{3}\frac{c}{c_2}\frac{a^3}{a+c} u L^2, \tag{2.9}$$

where equation (2.5) has been used. A similar analysis follows in the left side layer. Since the flow in the core is given by $Q_{core} = 4L^2 a u$, we can write

$$Q_i = \frac{1}{6}\frac{c}{c_i}\frac{a^2}{a+c} Q_{core}, \quad i = 1, 2. \tag{2.10}$$

Equation (2.10) states that for a square duct with the same wall thicknesses and conductivities ($a = 1, c = c_1 = c_2$) each side layer conveys one-sixth of the core flow. This means that each side layer carries a flow of the same order of magnitude as that of the core but through a cross sectional area $M^{\frac{1}{2}}$ times smaller. Therefore the velocities in the side layers will be larger by a factor $M^{\frac{1}{2}}$ than the velocities in the core. It is clear now that a change in the conductance ratio of the walls will produce a change in the flow rate carried by the side layers. The previous considerations also allow the estimation of the pressure gradient $dp/dx = j_z B_o$ through equation (2.5), showing its dependence on the conductance ratios of the walls.

2.3 Governing Equations

In this section we present the governing equations of a liquid metal flowing in a magnetic field, first in laminar and later in turbulent regime. In both cases, equations are expressed in dimensionless form and simplified to the case we are interested in, namely, a fully developed flow in a constant-area rectangular duct with a uniform transverse magnetic field.

The equations governing the flow of an electrically conducting fluid in the presence of a magnetic field result from the coupling of the fluid dynamic conservation equations and the electromagnetic field equations. Under the physical conditions we are considering, namely, liquid metal flows in stationary magnetic fields, the set of equations can be simplified through the MHD approximation [Shercliff, 1965; Hughes and Young, 1989].

Essentially, this approximation assumes non-relativistic flows and quasi-stationary or low frequency magnetic fields. In addition, it is assumed that the electric fields are of the same order of magnitude of the induced electromotive force, $\mathbf{u} \times \mathbf{B}$. Hence, under the MHD approximation, the dimensional equations governing the flow of an electrically conducting, incompressible newtonian fluid immerse in a magnetic field are

$$\rho\left(\frac{\partial \mathbf{u}}{\partial t} + \mathbf{u}\cdot\nabla\mathbf{u}\right) = -\nabla p + \eta_o \nabla^2 \mathbf{u} + \mathbf{j}\times\mathbf{B}, \tag{2.11}$$

$$\nabla\cdot\mathbf{u} = 0, \qquad \nabla\cdot\mathbf{j} = 0, \tag{2.12a, b}$$

$$\mathbf{j} = \sigma(\mathbf{E} + \mathbf{u}\times\mathbf{B}), \tag{2.13}$$

$$\nabla\cdot\mathbf{B} = 0, \qquad \nabla\times\mathbf{B} = \mu\mathbf{j}, \tag{2.14a, b}$$

$$\nabla\cdot\mathbf{E} = \rho_e/\epsilon, \qquad \nabla\times\mathbf{E} = -\partial\mathbf{B}/\partial t, \tag{2.15a, b}$$

where η_o, ρ, σ, μ and ϵ are the molecular dynamic viscosity, mass density, electrical conductivity, magnetic permeability and electric permitivity of the fluid. In turn, ρ_e and $\mathbf{j}$ are the electric charge and electric current densities, respectively, and $\mathbf{u}$, p, $\mathbf{B}$ and $\mathbf{E}$ are the velocity, pressure, magnetic induction and electric fields, respectively. All transport coefficients are assumed to be constant. The momentum balance is expressed through equation (2.11) where the Lorentz force $\mathbf{j}\times\mathbf{B}$ accounts for the magnetic interaction. Conservation of mass and electric charge are given through equations (2.12a) and (2.12b), respectively. Equation (2.13) represent Ohm's law in a moving media and equations (2.14a, b) and (2.15a, b) are Maxwell's equations within the MHD approximation which, essentially, neglects the displacement current in the Ampère-Maxwell law, (2.14b). Notice that the conservation of electric charge, (2.12b), follows from equation (2.14b). However, in our solution scheme we need the conservation of electric charge as an independent equation. The electric field is fully determined through the rotational equations and Ohm's law, so that equation (2.15a) is only necessary if we are interested in determining the electric charge density, ρ_e. If, in addition, we are dealing with time-independent fields, as it is actually the case we are interested in, time derivatives in equations (2.11) and (2.15b) are zero. Hence, Faraday's law, (2.15b), reduces to

$$\nabla\times\mathbf{E} = 0, \tag{2.16}$$

which implies that the electric field has the form

$$\mathbf{E} = -\nabla\phi, \tag{2.17}$$

where ϕ is the electric potential function. Taking into account the previous considerations, the system of equations (2.11)-(2.15) can be simplified, namely,

$$\rho(\mathbf{u}\cdot\nabla)\mathbf{u} = -\nabla p + \eta_o\nabla^2\mathbf{u} + \mathbf{j}\times\mathbf{B}, \tag{2.18}$$

$$\nabla \cdot \mathbf{u} = 0, \quad \nabla \cdot \mathbf{j} = 0, \tag{2.19a,b}$$

$$\mathbf{j} = \sigma(-\nabla\phi + \mathbf{u} \times \mathbf{B}), \tag{2.20}$$

$$\nabla \cdot \mathbf{B} = 0, \quad \nabla \times \mathbf{B} = \mu\mathbf{j}. \tag{2.21a,b}$$

The energy or heat transfer equation is not considered here since we are assuming that the fluid is incompressible and therefore, this equation can be decoupled from the dynamic problem. The solution of the heat transfer equation in laminar and turbulent regimes is addressed in Chapters 3 and 5, respectively.

2.3.1 Laminar Liquid Metal Flow in a Constant-Area Rectangular Duct with a Uniform, Transverse Magnetic Field

In the laminar regime, equations (2.18)-(2.21) are directly used to determine the flow variables in a given fluid flow problem. In order to get the dimensionless version of the former equations, let us define the following dimensionless variables:

$$\mathbf{x}^* = \frac{\mathbf{x}}{L}, \quad t^* = \frac{t}{L/\bar{U}}, \quad \mathbf{u}^* = \frac{\mathbf{u}}{\bar{U}}, \quad p^* = \frac{p}{\sigma \bar{U} B_o^2 L},$$

$$\mathbf{j}^* = \frac{\mathbf{j}}{\sigma \bar{U} B_o}, \quad \phi^* = \frac{\phi}{\bar{U} B_o L}, \quad \mathbf{B}^* = \frac{\mathbf{B}}{B_o}.$$

where L is the characteristic length of the flow, $\bar{U}$ is the average flow velocity and B_o is the uniform applied magnetic field. Substituting the former variables in equations (2.18)-(2.21), we get the set of equations in dimensionless form:

$$N^{-1}(\mathbf{u} \cdot \nabla)\mathbf{u} = -\nabla p + M^{-2}\nabla^2\mathbf{u} + \mathbf{j} \times \mathbf{B}, \tag{2.22}$$

$$\nabla \cdot \mathbf{u} = 0, \quad \nabla \cdot \mathbf{j} = 0, \tag{2.23a,b}$$

$$\mathbf{j} = -\nabla\phi + \mathbf{u} \times \mathbf{B}, \tag{2.24}$$

$$\nabla \cdot \mathbf{B} = 0, \quad \nabla \times \mathbf{B} = Rm\mathbf{j}, \tag{2.25a,b}$$

where we have dropped the $*$ in order to simplify the notation. Here, the magnetic induction field $\mathbf{B}$ represents the superposition of an applied magnetic field produced by the external magnets and an induced magnetic field generated by the electric currents circulating in the liquid metal and, if that is the case, in the metal duct walls. If we assume that the induced magnetic field is sufficiently small to be neglected in comparison to the applied magnetic field, or in other words, that the approximation $Rm \ll 1$ holds, equation (2.25b) becomes

$$\nabla \times \mathbf{B} = 0. \tag{2.26}$$

In this way, the problem of determining the magnetic induction field $\mathbf{B}$ is governed by equations (2.25a) and (2.26) with suitable boundary conditions at the pole faces of the magnet, and is decoupled from the flow problem. Therefore, in order to solve the flow problem, a known magnetic induction field must be given either by an assumed function or by solving the corresponding boundary value problem for $\mathbf{B}$. Once $\mathbf{B}$ is known, we can address a boundary value problem for variables $\mathbf{u}$, p, ϕ and $\mathbf{j}$, governed by equations (2.22)-(2.24) and suitable boundary conditions at the duct walls. Ting [1991] has addressed these boundary value problems for the laminar regime (within the inertialess approximation) for two interesting three-dimensional cases, namely, a liquid metal flow in a constant-area rectangular duct with a non-uniform, transverse magnetic field, $\mathbf{B} = B_y(x)\hat{\mathbf{y}}$, and with a non-uniform, planar magnetic field $\mathbf{B} = B_x(x,y)\hat{\mathbf{x}} + B_y(x,y)\hat{\mathbf{y}}$, where $\hat{\mathbf{x}}$ and $\hat{\mathbf{y}}$ are unit vectors in the axial x-direction and transverse y-direction, respectively. In the present study, we consider a liquid metal flowing steadily in the x-direction in a constant-area rectangular duct with a uniform, transverse magnetic field, namely,

$$\mathbf{B} = \hat{\mathbf{y}}.$$

With these assumptions, the flow becomes fully developed and the problem is reduced to two dimensions.[4] The coordinate system and geometry of the transversal cross-section of the duct, in dimensionless terms, is given in figure 2.4.

As a matter of fact, in a fully developed flow in a constant-area duct with a uniform, transverse magnetic field, the boundary value problem for $\mathbf{B}$ can be decoupled from the flow problem without invoking the $Rm \ll 1$ approximation (Shercliff [1956]; Walker [1981]). In that case, the magnetic field has the form $\mathbf{B} = B_x(y,z)\hat{\mathbf{x}} + \hat{\mathbf{y}}$, where $B_x(y,z)$ is the field induced by the movement of the liquid through the applied magnetic field. Then, B_x is decoupled from all other variables, which can be determined without reference to the induced field. In addition, Hunt [1969] showed that if the magnetic field, the conductance ratio and the cross-section are independent of x, there exists only one time-independent flow, namely, $\mathbf{u} = (u(y,z),0,0)$, $\phi = \phi(y,z)$ and $\nabla p = (-K,0,0)$, where K is a constant. With these assumptions, the inertial term in equation (2.22) identically vanishes and equations (2.22)-(2.24) reduce to

$$M^{-2}\left[\frac{\partial^2 u}{\partial y^2} + \frac{\partial^2 u}{\partial z^2}\right] - j_z = \frac{\partial p}{\partial x} = -K, \tag{2.27}$$

$$j_y = -\frac{\partial \phi}{\partial y}, \tag{2.28}$$

[4]The fully developed laminar flow was also considered by Ting [1991] but her analysis restricted to thin conducting wall ducts and Hartmann numbers up to 6400.

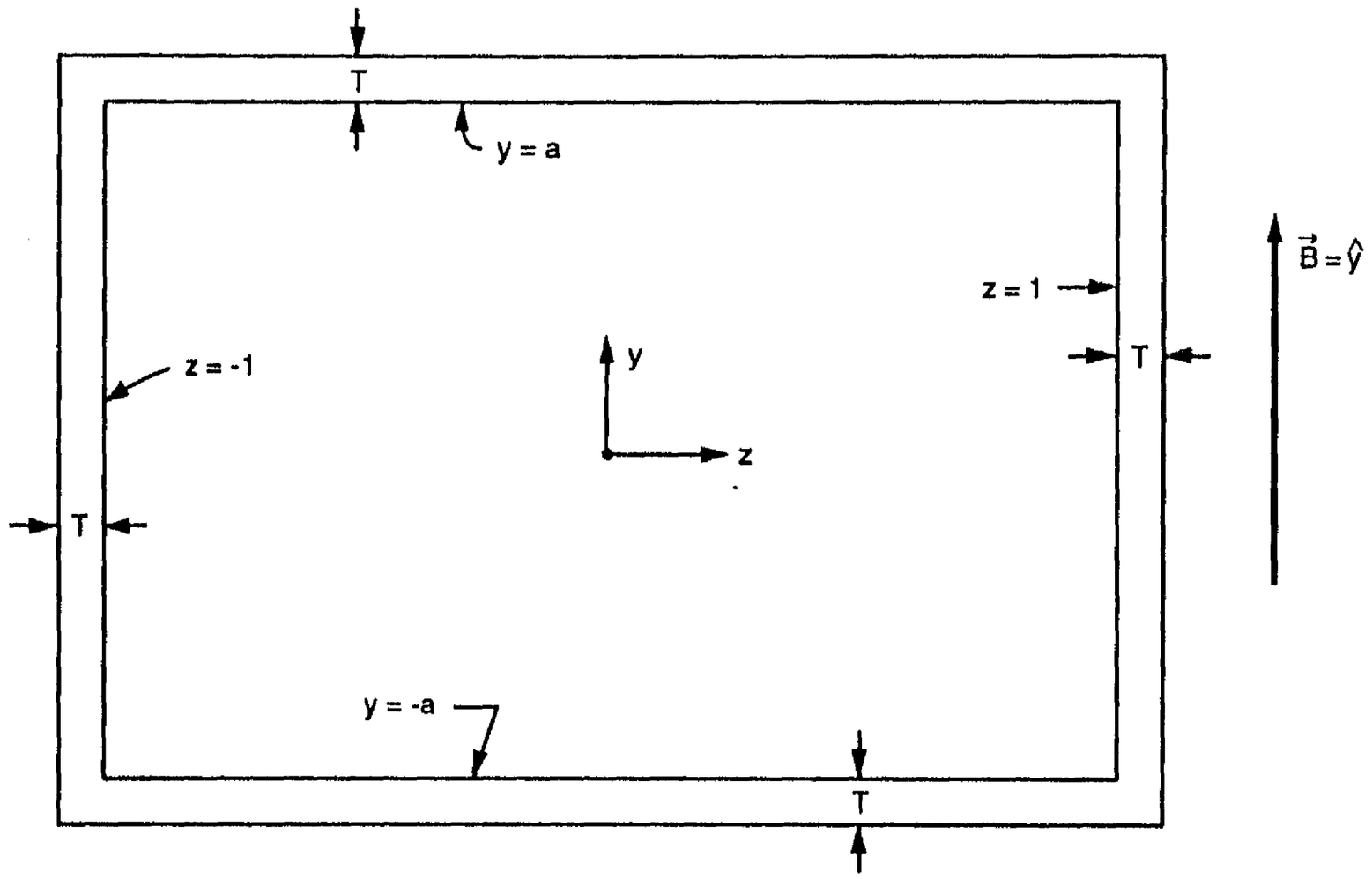

Figure 2.4: Dimensionless duct cross-section.

$$j_z = -\frac{\partial \phi}{\partial z} + u, \tag{2.29}$$

$$\frac{\partial j_y}{\partial y} + \frac{\partial j_z}{\partial z} = 0, \tag{2.30}$$

In addition, we also have to satisfy Ohm's law and current conservation at the walls, that is

$$j_{yw} = -\left(\frac{\sigma_w}{\sigma}\right)\frac{\partial \phi_w}{\partial y}, \tag{2.31}$$

$$j_{zw} = -\left(\frac{\sigma_w}{\sigma}\right)\frac{\partial \phi_w}{\partial z}, \tag{2.32}$$

$$\frac{\partial j_{yw}}{\partial y} + \frac{\partial j_{zw}}{\partial z} = 0, \tag{2.33}$$

where the subindex w indicates a property or variable of the wall.[5]

[5] Dimensionless wall variables $\mathbf{j}_w^*$ and ϕ_w^* are defined in a similar way as fluid variables, namely

$$\mathbf{j}_w^* = \frac{\mathbf{j}_w}{\sigma \bar{U} B_o}, \quad \phi_w^* = \frac{\phi_w}{\bar{U} B_o L}.$$

At a wall-liquid interface, both ϕ and $\mathbf{j} \cdot \hat{\mathbf{n}}$ are continuous, where $\hat{\mathbf{n}}$ stands for the normal to the surface. The complete set of equations that governs the present problem is established in section 2.4, where boundary conditions are deduced.

2.3.2 Turbulent Liquid Metal Flow in a Constant-Area Rectangular Duct with a Uniform, Transverse Magnetic Field

In order to get the governing equations for the turbulent regime, we address the problem within the Reynolds approach [Hinze, 1975]. Hence, we consider the flow variables $\mathbf{u}$, p and ϕ to consist of a mean part, which will be denoted by an overbar, and a fluctuating part with a zero average, denoted by a prime. Then we have

$$\mathbf{u} = \bar{\mathbf{u}} + \mathbf{u}', \quad p = \bar{p} + p', \quad \phi = \bar{\phi} + \phi', \tag{2.34}$$

where, by definition,

$$\bar{\mathbf{u}}' = \bar{p}' = \bar{\phi}' = 0. \tag{2.35}$$

Since we assume that the low magnetic Reynolds number approximation holds ($Rm \ll 1$), pulsations of the magnetic induction field can be neglected in comparison with its averaged value, that is, $\mathbf{B} = \bar{\mathbf{B}}$ [Branover, 1978]. Substituting equations (2.34) in (2.18)-(2.21) we get the dimensional set of equations:

$$\rho(\bar{\mathbf{u}} \cdot \nabla)\bar{\mathbf{u}} = -\nabla\bar{p} + \nabla \cdot (\eta_o \nabla\bar{\mathbf{u}} + \tilde{\tau}) + \bar{\mathbf{j}} \times \bar{\mathbf{B}}, \tag{2.36}$$

$$\nabla \cdot \bar{\mathbf{u}} = 0, \quad \nabla \cdot \bar{\mathbf{j}} = 0, \tag{2.37a,b}$$

$$\bar{\mathbf{j}} = \sigma(-\nabla\bar{\phi} + \bar{\mathbf{u}} \times \bar{\mathbf{B}}), \tag{2.38}$$

$$\nabla \cdot \bar{\mathbf{B}} = 0, \quad \nabla \times \bar{\mathbf{B}} = \mu\bar{\mathbf{j}}, \tag{2.39a,b}$$

where $\tilde{\tau}$ in equation (2.36) is the Reynolds stress tensor given by

$$\tau_{ij} = -\rho u_i' u_j'. \tag{2.40}$$

Defining the dimensionless variables in an analogous form to the laminar case, equations (2.36)-(2.39) become

$$N^{-1}(\bar{\mathbf{u}} \cdot \nabla)\bar{\mathbf{u}} = -\nabla\bar{p} + M^{-2}\nabla \cdot (\nabla\bar{\mathbf{u}} - Re\overline{\mathbf{u}'\mathbf{u}'}) + \bar{\mathbf{j}} \times \bar{\mathbf{B}}, \tag{2.41}$$

$$\nabla \cdot \bar{\mathbf{u}} = 0, \quad \nabla \cdot \bar{\mathbf{j}} = 0, \tag{2.42a,b}$$

$$\bar{\mathbf{j}} = -\nabla\bar{\phi} + \bar{\mathbf{u}} \times \bar{\mathbf{B}}, \tag{2.43}$$

$$\nabla \cdot \bar{\mathbf{B}} = 0, \quad \nabla \times \bar{\mathbf{B}} = Rm\bar{\mathbf{j}}, \tag{2.44a,b}$$

where, again, the $*$ has been dropped.

As in the laminar case, we assume $Rm \ll 1$, so that the **B**-boundary value problem is decoupled from the flow problem. In addition, we assume the applied magnetic field to be $\mathbf{B} = \hat{\mathbf{y}}$. Hence, we end up at the steady, fully developed turbulent liquid metal flow in a constant-area rectangular duct with a uniform, transverse magnetic field. If we assume that the same conditions of the laminar problem are still valid, that is, $\bar{\mathbf{u}} = (\bar{u}(y,z), 0, 0)$, $\bar{\phi} = \bar{\phi}(y,z)$ and $\nabla\bar{p} = (-K, 0, 0)$, equation (2.41) reduces to

$$M^{-2}\left[\frac{\partial}{\partial y}\left(\frac{\partial\bar{u}}{\partial y} - Re\overline{u'v'}\right) + \frac{\partial}{\partial z}\left(\frac{\partial\bar{u}}{\partial z} - Re\overline{u'w'}\right)\right] - \bar{j}_z - \frac{\partial\bar{p}}{\partial x} = 0. \tag{2.45}$$

Here we have to address the *closure* problem in order to determine the turbulent Reynolds stresses. One of the simplest and most common approaches was introduced by Boussinesq. In this approach, one assumes that the mean turbulent stress can be expressed in the same form as the laminar stress with a turbulent viscosity. Hence, using the Boussinesq's assumption τ_{ij} can be written in the form

$$\tau_{xy} = -Re\overline{u'v'} = \nu_{ey}\frac{\partial\bar{u}}{\partial y}, \tag{2.46}$$

$$\tau_{xz} = -Re\overline{u'w'} = \nu_{ez}\frac{\partial\bar{u}}{\partial z}, \tag{2.47}$$

where ν_{ej} $(j = y, z)$ is known as the dimensionless eddy viscosity (normalized by the molecular kinematic viscosity ν_o). Here, due to the anisotropic effect of the magnetic field, we allow for different eddy viscosities in each direction. Once we accept the Boussinesq postulate expressed by equations (2.46) and (2.47), the closure problem is reduced to determining the scalars ν_{ej}. Nevertheless, the problem of determining the eddy viscosity and the mean flow should be coupled, since, in principle, ν_{ej} depends on the fluctuating part of the solution, as can be seen from equations (2.46) and (2.47). In our case, this problem will be solved using the RNG turbulence model [Yakhot and Orszag, 1986] which is introduced in Chapter 5. Introducing equations (2.46) and (2.47) in equation (2.45) and defining the total viscous diffusivities as

$$\nu_{ty} = 1 + \nu_{ey},$$

$$\nu_{tz} = 1 + \nu_{ez},$$

-which take into account the molecular and turbulent contributions- we can finally reduce the set of equations (2.41)-(2.43) for the problem under consideration to the form

$$M^{-2}\left[\frac{\partial}{\partial y}\left(\nu_{ty}\frac{\partial \bar{u}}{\partial y}\right)+\frac{\partial}{\partial z}\left(\nu_{tz}\frac{\partial \bar{u}}{\partial z}\right)\right]-\bar{j}_z=\frac{\partial \bar{p}}{\partial x}=-K, \tag{2.48}$$

$$\bar{j}_y=-\frac{\partial \bar{\phi}}{\partial y}, \tag{2.49}$$

$$\bar{j}_z=-\frac{\partial \bar{\phi}}{\partial z}+\bar{u}, \tag{2.50}$$

$$\frac{\partial \bar{j}_y}{\partial y}+\frac{\partial \bar{j}_z}{\partial z}=0, \tag{2.51}$$

Similarly to the laminar case, the mean variables have also to satisfy Ohm's law and current conservation at the walls:

$$\bar{j}_{yw}=-\left(\frac{\sigma_w}{\sigma}\right)\frac{\partial \bar{\phi}_w}{\partial y}, \tag{2.52}$$

$$\bar{j}_{zw}=-\left(\frac{\sigma_w}{\sigma}\right)\frac{\partial \bar{\phi}_w}{\partial z}, \tag{2.53}$$

$$\frac{\partial \bar{j}_{yw}}{\partial y}+\frac{\partial \bar{j}_{zw}}{\partial z}=0. \tag{2.54}$$

Notice that by setting $\nu_t = 1$ and dropping the overbars, equations (2.45)-(2.54) reduce to the laminar set of equations (2.27)-(2.33).

2.4 Symmetry and Boundary Conditions

In this section we establish the conditions and approximations that lead to the complete set of equations defining our problem, in both laminar and turbulent regimes. The set of equations is obtained in general for the turbulent case, that is, for the mean flow variables, but the laminar case is recovered through the condition $\nu_t = 1$. Numerical solutions for laminar and turbulent regimes are presented in Chapters 3 and 5, respectively.

Equations (2.51) and (2.54) allow the elimination of the electric current density by the introduction of an electric current stream function h and h_w for the fluid and the walls, respectively, defined as

$$\bar{j}_y=-\frac{\partial h}{\partial z}, \quad \bar{j}_z=\frac{\partial h}{\partial y}, \tag{2.55}$$

$$\bar{j}_{yw}=-\frac{\partial h_w}{\partial z}, \quad \bar{j}_{zw}=\frac{\partial h_w}{\partial y}. \tag{2.56}$$

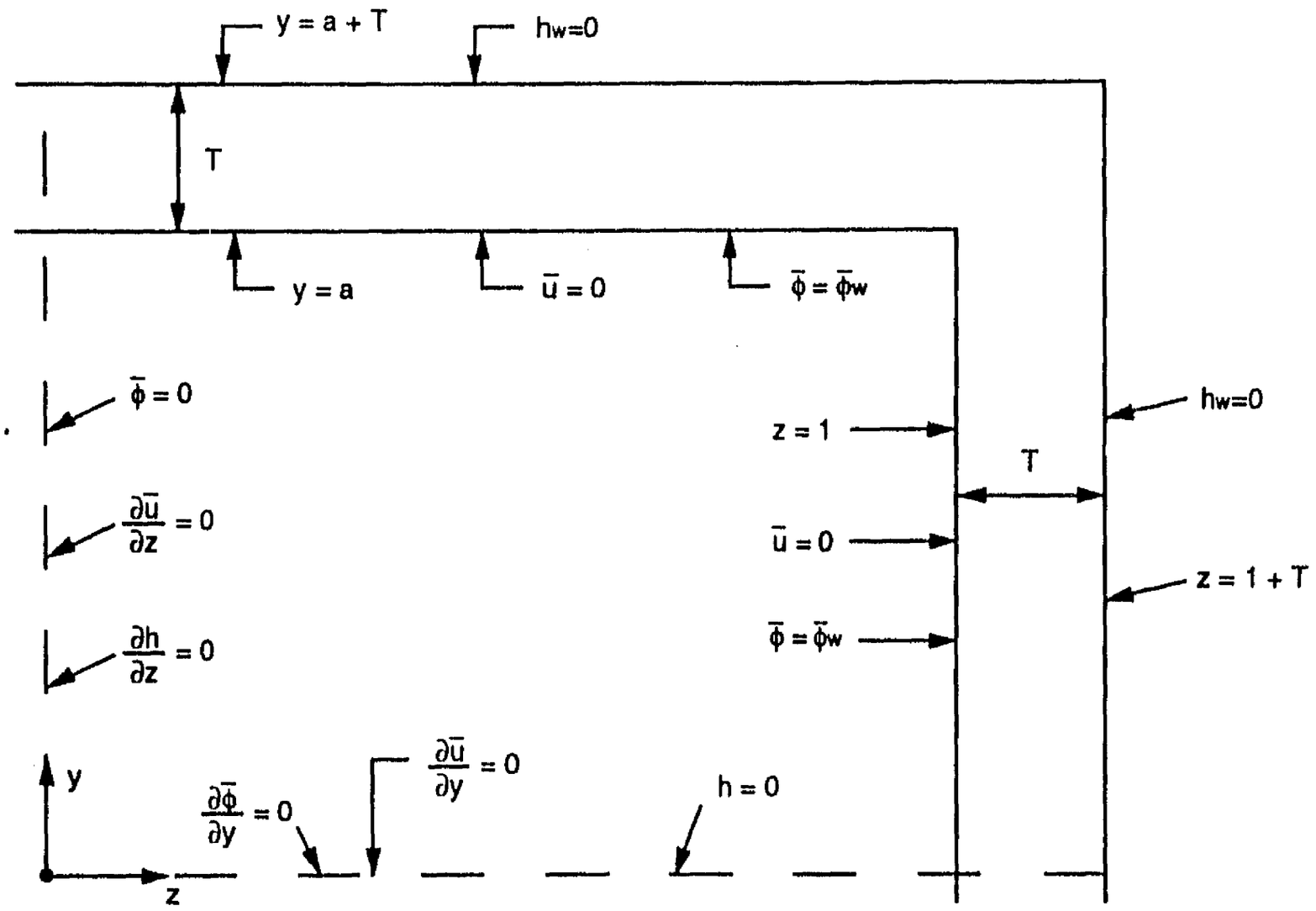

Figure 2.5: Boundary and symmetry conditions in a quarter-duct cross-section.

Because of symmetry conditions in both directions y and z we need to consider only one quarter of the cross section of the duct, for instance $y \geq 0$ and $z \geq 0$. Figure 2.5 shows the conditions that hold in the treated region.

In terms of the electric current stream function, Navier-Stokes equation (2.48) and Ohm's law (2.49)-(2.50), can be rewritten as

$$M^{-2}\left[\frac{\partial}{\partial y}\left(\nu_{ty}\frac{\partial \bar{u}}{\partial y}\right)+\frac{\partial}{\partial z}\left(\nu_{tz}\frac{\partial \bar{u}}{\partial z}\right)\right]-\frac{\partial h}{\partial y}=-K \tag{2.57}$$

$$\frac{\partial h}{\partial z}=\frac{\partial \bar{\phi}}{\partial y}, \tag{2.58}$$

$$\frac{\partial h}{\partial y}+\frac{\partial \bar{\phi}}{\partial z}=\bar{u}, \tag{2.59}$$

for $0 \leq y \leq a$ and $0 \leq z \leq 1$.

In the wall region, Ohm's law equations (2.52)-(2.53) become

$$\frac{\partial h_w}{\partial z}=\left(\frac{\sigma_w}{\sigma}\right)\frac{\partial \bar{\phi}_w}{\partial y}, \tag{2.60}$$

$$\frac{\partial h_w}{\partial y} + \left(\frac{\sigma_w}{\sigma}\right)\frac{\partial \bar{\phi}_w}{\partial z} = 0, \tag{2.61}$$

for $a \leq y \leq a+T$ and $0 \leq z \leq 1+T$, as well as for $1 \leq z \leq 1+T$ and $0 \leq y \leq a$, where $T = t_w/L$ is the dimensionless wall thickness (see fig. 2.5). In addition, we have:
At $y = 0$:

$$\tfrac{\partial \bar{u}}{\partial y} = 0, \qquad \tfrac{\partial \bar{\phi}}{\partial y} = 0, \qquad h = 0; \tag{2.62a, b, c}$$

at $z = 0$:

$$\tfrac{\partial \bar{u}}{\partial z} = 0, \qquad \bar{\phi} = 0, \qquad \tfrac{\partial h}{\partial z} = 0; \tag{2.63a, b, c}$$

at $y = a$ and at $z = 1$:

$$\bar{u} = 0, \qquad \bar{\phi} = \bar{\phi}_w, \qquad h = h_w; \tag{2.64a, b, c}$$

and at $y = a+T$ and at $z = 1+T$:

$$h_w = 0. \tag{2.65}$$

Equation (2.62a) expresses the symmetry condition of the velocity field with respect to the horizontal center line $y = 0$; the symmetry of the electric current density with respect to $y = 0$ is expressed by equation (2.62b), which states that no current in the y-direction can cross the center line $y = 0$, that is, the line $y = 0$ constitutes an electric current stream line; so that, equation (2.62c) sets a reference value (zero) for that electric current stream line in the fluid. Similarly, the symmetry condition of the velocity field with respect to the center line $z = 0$ is expressed through equation (2.63a) while equation (2.63b) sets a reference value for the electric potential and, in turn, (2.63c) establishes the symmetry of the electric current density with respect to the vertical center line $z = 0$, in such a way that the component j_y is zero in $z = 0$ (the only component of the current density in the core is j_z). On the other hand, equation (2.64a) expresses the non-slip condition of the fluid at the walls while (2.64b) and (2.64c) state the continuity of the electric potential and the current stream function at the fluid-wall interface. Finally, since the normal component of the electric current density vanishes outside of each wall, the outside wall surfaces become electric current stream lines. Hence, equation (2.65) sets the reference value for these electric current stream lines as zero.

Let us now introduce a suitable potential function $F(y, z)$ for h and $\bar{\phi}$, defined in the following way:
In the liquid:

$$h = \frac{\partial F}{\partial y}, \qquad \bar{\phi} = \frac{\partial F}{\partial z}. \tag{2.66}$$

In the walls:

$$h_w = \frac{\partial F_w}{\partial y}, \qquad \bar{\phi}_w = \left(\frac{\sigma}{\sigma_w}\right) \frac{\partial F_w}{\partial z}. \tag{2.67}$$

In order to assure the uniqueness of F and F_w, the following condition must be satisfied:

$$F_w(0, 1+T) = 0, \qquad F(0,1) = F_w(0,1), \tag{2.68}$$

which is equivalent to

$$F_w(a+T, 0) = 0, \qquad F(a,0) = F_w(a,0). \tag{2.69}$$

In terms of the new potential, the equations and boundary conditions (2.57)-(2.65) take the form

$$M^{-2}\left[\frac{\partial}{\partial y}\left(\nu_{ty}\frac{\partial \bar{u}}{\partial y}\right) + \frac{\partial}{\partial z}\left(\nu_{tz}\frac{\partial \bar{u}}{\partial z}\right)\right] = \frac{\partial^2 F}{\partial y^2} - K, \tag{2.70}$$

$$\bar{u} = \frac{\partial^2 F}{\partial y^2} + \frac{\partial^2 F}{\partial z^2}, \tag{2.71}$$

for $0 \le y \le a$ and $0 \le z \le 1$.

$$\frac{\partial^2 F_w}{\partial y^2} + \frac{\partial^2 F_w}{\partial z^2} = 0, \tag{2.72}$$

for $a \le y \le a+T$ and $0 \le z \le 1+T$, or $1 \le z \le 1+T$ and $0 \le y \le a$.
At $y = 0$:

$$\frac{\partial \bar{u}}{\partial y} = 0, \qquad \frac{\partial F}{\partial y} = 0, \qquad \frac{\partial F_w}{\partial y} = 0; \tag{2.73}$$

at $z = 0$:

$$\frac{\partial \bar{u}}{\partial z} = 0, \qquad \frac{\partial F}{\partial z} = 0, \qquad \frac{\partial F_w}{\partial z} = 0; \tag{2.74}$$

at $y = a+T$:

$$\frac{\partial F_w}{\partial y} = 0; \tag{2.75}$$

at $z = 1+T$:

$$F_w = 0; \tag{2.76}$$

at $z = 1$:

$$\bar{u} = 0, \quad F = F_w, \quad \frac{\partial F_w}{\partial z} = \left(\frac{\sigma_w}{\sigma}\right)\frac{\partial F}{\partial z}; \tag{2.77}$$

and at $y = a$:

$$\bar{u} = 0, \quad \frac{\partial F}{\partial y} = \frac{\partial F_w}{\partial y}, \quad \frac{\partial F_w}{\partial z} = \left(\frac{\sigma_w}{\sigma}\right)\frac{\partial F}{\partial z}. \tag{2.78}$$

2.4.1 Thin Conducting and Insulating Wall Conditions

In principle, the electromagnetic interaction generated by the flow of the liquid metal in the applied magnetic field, extends beyond the fluid into the walls and the surrounding medium. This means that the electric current density and electric potential function of the fluid, walls and surrounding medium are coupled, and the Maxwell's equations have to be satisfied everywhere in space. However, assuming that the walls are thin (*i.e.* $T \ll 1$) and the surrounding medium is an electrical insulator, it is possible to derive a boundary condition on the fluid variables only [Walker, 1981, 1992a], decoupling the fluid problem from the wall problem.

In order to do that, let us consider first the region $1 \leq z \leq 1 + T$ and define the *stretched* coordinate

$$, \ Z = \frac{1}{T}(z - 1),$$

so that, $\partial/\partial z = 1/T\partial/\partial Z$. Then, from equation (2.72) we get

$$\frac{\partial^2 F_w}{\partial Z^2} = -T^2\frac{\partial^2 F_w}{\partial y^2}, \tag{2.79}$$

and from equation (2.77) we have

$$\frac{\partial F_w}{\partial Z} = \left(\frac{\sigma_w}{\sigma}\right)T\frac{\partial F}{\partial z}(y, 1) = c\frac{\partial F}{\partial z}(y, 1), \tag{2.80}$$

where the wall conductance ratio is defined as $c = T(\sigma_w/\sigma)$. Integrating equation (2.79), we get

$$F_w = -\frac{T^2}{2}\left(\frac{\partial^2 F_w}{\partial y^2}\right)Z^2 + \alpha_1 Z + \alpha_2. \tag{2.81}$$

Now, at $Z = 0$, $\partial F_w/\partial Z = \alpha_1$ and using equation (2.80) we get $\alpha_1 = c\partial F(y, 1)/\partial z$. Neglecting terms $O(T^2)$ and noting from equation (2.76) that at $Z = 1$, $F_w = 0$, we have $\alpha_1 = -\alpha_2$. Hence

$$F_w = c\frac{\partial F}{\partial z}(y, 1)(Z - 1), \tag{2.82}$$

but at $Z = 0$, $F_w = F(y, 1)$, so we finally have

$$F(y,1) = -c\frac{\partial F}{\partial z}(y,1). \tag{2.83}$$

As a matter of fact, equation (2.83) is an integral of a boundary condition of the kind previously found by Shercliff [1956] in terms of the current stream function h, namely

$$h(y,1) = -c\frac{\partial h}{\partial z}(y,1). \tag{2.84}$$

Notice that equations (2.83) or (2.84) can be written in the form originally given by Walker [1981]:

$$j_z(y,1) = -c\frac{\partial^2 \phi}{\partial y^2}(y,1). \tag{2.85}$$

In physical terms, equation (2.85) (*i.e.* (2.83)) expresses nothing else but the conservation of electric charge and Ohm's law at the wall within the thin conducting wall approximation.

Now we consider the region $a \leq y \leq a + T$ and define the stretched coordinate $Y = (y - a)/T$. From (2.72) we have

$$\frac{\partial^2 F_w}{\partial Y^2} = -T^2\frac{\partial^2 F_w}{\partial z^2}, \tag{2.86}$$

In addition, from equation (2.75), at $Y = 1$

$$\frac{\partial F_w}{\partial Y} = 0, \tag{2.87}$$

and, from equation (2.78), at $Y = 0$

$$\frac{\partial F_w}{\partial Y} = T\frac{\partial F}{\partial y}(a,z), \tag{2.88}$$

$$\frac{\partial F_w}{\partial z} = \left(\frac{\sigma_w}{\sigma}\right)\frac{\partial F}{\partial z}. \tag{2.89}$$

Now we express F_w as a series in the parameter T, that is

$$F_w = F_{w0}(z) + T^2 F_{w1}(Y,z) + O(T^4). \tag{2.90}$$

Then, equation (2.86) becomes

$$\frac{\partial^2 F_{w1}}{\partial Y^2} = -\frac{\partial^2 F_{w0}}{\partial z^2}, \tag{2.91}$$

while equation (2.87) gives

$$\frac{\partial F_{w1}}{\partial Y} = 0, \quad at \;\; Y = 1, \tag{2.92}$$

and, neglecting terms $O(T^2)$, equation (2.89) reads

$$\frac{\partial F_w}{\partial z} = \left(\frac{\sigma_w}{\sigma}\right) \frac{\partial F}{\partial z}. \tag{2.93}$$

Integrating equation (2.91) and using boundary condition (2.92) we get

$$\frac{\partial F_{w1}}{\partial Y} = -\frac{\partial^2 F_{w0}}{\partial z^2}(z)\,(Y-1). \tag{2.94}$$

Then from equations (2.88), (2.90), (2.93) and (2.94) we finally obtain

$$\begin{aligned} \frac{\partial F}{\partial y}(a,z) &= \frac{1}{T}\frac{\partial F_w}{\partial Y}(0,z) = \frac{1}{T}\frac{\partial}{\partial Y}\left(F_{w0}(z) + T^2 F_{w1}(0,z) + O(T^4)\right) \\ &= T\frac{\partial F_{w1}}{\partial Y}(0,z) + O(T^3) = T\frac{d^2 F_{w0}}{dz^2}(z) + O(T^3) \\ &= c\frac{\partial^2 F}{\partial z^2}(a,z) + O(cT^2), \end{aligned} \tag{2.95}$$

that is,

$$\frac{\partial F}{\partial y}(a,z) = c\frac{\partial^2 F}{\partial z^2}(a,z). \tag{2.96}$$

Notice that from equation (2.71)

$$\frac{\partial^2 F}{\partial y^2}(a,z) = -\frac{\partial^2 F}{\partial z^2}(a,z) + \bar{u}(a,z),$$

but $\bar{u}(a,z) = 0$, and then

$$\frac{\partial F}{\partial y}(a,z) = c\frac{\partial^2 F}{\partial z^2}(a,z) = -c\frac{\partial^2 F}{\partial y^2}(a,z),$$

and since $h = \partial F/\partial y$, we get the following boundary condition of the Shercliff's kind in terms of the electric current stream function:

$$h(a,z) = -c\frac{\partial h}{\partial y}(a,z). \tag{2.97}$$

At this point, some comments become necessary. Boundary condition (2.96) (*i.e.* (2.97)) is valid within the thin wall approximation. As we mentioned previously, this is expressed by the condition $M^{-1} \ll c \ll 1$. Hence this approximation ignores the jump in $\vec{j}_y$ across the Hartmann layer which means that the Hartmann layer is completely

disregarded. It is clear that boundary condition (2.96) does not give the correct limit when $c \to 0$, that is, when the walls become insulators. In such a case, all the return currents should flow through the Hartmann layers but equation (2.96) predicts no current at all when $c = 0$. Since we are interested in exploring the transition of the flow patterns as the conductance ratio decreases, we must modify boundary condition (2.96) to take into account the Hartmann layers. In order to do this, we need to estimate the amount of current flowing through this layer. The $\bar{j}_z$ component of the current density is

$$\bar{j}_z = \bar{u} - \frac{\partial \phi}{\partial z},$$

where $\bar{u}$ is the core-layer velocity profile given by [Moreau, 1990]

$$\bar{u} = \bar{u}_c(1 - e^{-M\xi}).$$

Here $\bar{u}_c$ is the external or core velocity and ξ is the coordinate perpendicular to the top wall, measured from the wall. Since ϕ is continuous across the Hartmann layer within an error of $O(M^{-2})$, $\partial\phi/\partial z$ can be considered constant. On the other hand, the current density outside the layer is

$$\bar{j}_{zc} = \bar{u}_c - \frac{\partial \phi}{\partial z},$$

and then, the total current through the Hartmann layer is

$$\int_0^\infty (\bar{j}_z - \bar{j}_{zc}) d\xi = \bar{u}_c \int_0^\infty e^{-M\xi} d\xi = \frac{\bar{u}_c}{M},$$

that is,

$$\Delta h = M^{-1} u_c(a, z) = M^{-1} \left(\frac{\partial^2 F}{\partial y^2}(a, z) + \frac{\partial^2 F}{\partial z^2}(a, z) \right),$$

where equation (2.71) has been used. Finally, adding this contribution to equation (2.96), we get

$$\frac{\partial F}{\partial y}(a, z) - (c + M^{-1}) \frac{\partial^2 F}{\partial z^2}(a, z) = M^{-1} \frac{\partial^2 F}{\partial y^2}. \tag{2.98}$$

Hence, in the limit $c = 0$ (insulated duct), boundary condition (2.98) states that all the return currents will close through the Hartmann layer. Strictly, this modification holds only for a laminar Hartamnn layer and we should be able to devise a proper modification for a turbulent layer. However, there are some physical reasons to expect that an instability in the Hartmann layer is not very likely to grow into a turbulent boundary layer. The argument is that the shear layers in the Hartmann layers have vorticity that is perpendicular to the magnetic field. Therefore, if the Hartmann layers become

unstable, the resultant instability will have vorticity predominantly perpendicular to the magnetic field and, as we will discuss in Chapter 4, will be quickly damped. On the other hand, we are mainly concerned with the phenomena that take place in the side wall layers and, with this approach, we consider the Hartmann layers to have a passive role. Furthermore, the consideration of a turbulent -or laminar- Hartmann layer would require its numerical resolution but, because of their thickness, this is a very difficult task [Sterl, 1989]. Actually, such an effort may not be valuable for the purpose of this study. In conclusion, we consider (2.98) as a reasonable boundary condition for both laminar and turbulent cases.

Therefore the system of equations and boundary conditions that govern our problem is:

$$M^{-2}\left[\frac{\partial}{\partial y}\left(\nu_{ty}\frac{\partial \bar{u}}{\partial y}\right)+\frac{\partial}{\partial z}\left(\nu_{tz}\frac{\partial \bar{u}}{\partial z}\right)\right]=\frac{\partial^2 F}{\partial y^2}-K, \tag{2.99}$$

$$\bar{u}=\frac{\partial^2 F}{\partial y^2}+\frac{\partial^2 F}{\partial z^2}, \tag{2.100}$$

for $0 \leq y \leq a$ and $0 \leq z \leq 1$.
At $y = 0$:

$$\frac{\partial \bar{u}}{\partial y}=0, \qquad \frac{\partial F}{\partial y}=0; \tag{2.101}$$

at $z = 0$:

$$\frac{\partial \bar{u}}{\partial z}=0, \qquad \frac{\partial F}{\partial z}=0; \tag{2.102}$$

at $z = 1$:

$$\bar{u}=0, \qquad F+c\frac{\partial F}{\partial z}=0; \tag{2.103}$$

and at $y = a$:

$$\bar{u}=0, \qquad \frac{\partial F}{\partial y}-(c+M^{-1})\frac{\partial^2 F}{\partial z^2}=M^{-1}\frac{\partial^2 F}{\partial y^2}. \tag{2.104}$$

In addition, we also have to satisfy the volume flux conservation condition:

$$\int_0^a \int_0^1 \bar{u}\,dz\,dy = a. \tag{2.105}$$

In the following subsections we will consider a single core/side-layer solution that allows us to obtain a turbulent solution of the former system of equations for a given eddy viscosity through numerical iteration.

2.5 Composite Core-Side-Layer Flow

We previously mentioned that our main interest lies in the understanding of the phenomena occurring in the side-wall layers which are responsible for the heat transfer characteristics and the eventual appearance of instabilities. On these respects, the Hartmann layers play a rather passive role. On the other hand, the complete numerical resolution of all the regions inside the flow, especially of the Hartmann layers, involves a very expensive task in terms of computing time and storage. For the very high Hartmann numbers and interaction parameters of interest for fusion applications ($10^4 - 10^5$), this approach becomes practically impossible [Sterl, 1989]. Here we address the problem in a simplified way by considering a joint core-side-layer flow which occupies the region $0 \leq y \leq a$, $0 \leq z \leq 1$. In this approximation, assuming that M is sufficiently large, the Hartmann layers and corner regions are ignored. Actually, the Hartmann layers are only partially ignored because we allow their existence as a return path for the electric currents (since we are interested in the limit $c \rightarrow 0$), but we do not resolve them numerically. Therefore we do satisfy boundary condition (2.104*b*) but we do not satisfy the non-slip condition (2.104*a*) at the top (bottom) wall. The composite core-side-layer flow does not distinguishes between the core and the side layer and is governed by a boundary value problem with M as a parameter. It appears that this approach coincides more closely with realistic flow situations [Ting, 1991]. On the other hand, in matched asymptotic expansion solutions the side layer flow problem is separated from the core flow problem provided the Hartmann number is extremely large. In that approach, the condition that the electrical resistance of the side wall is much lower than that of the side layer, expressed by $c \gg M^{-\frac{1}{2}}$, is implicitly assumed. This means that the $O(1)$ electric current leaving the core flows across the side layer and penetrates into the side wall. In other words, the current lines remain horizontal across the side layer and no current flows directly from the side layer to the top or bottom. The assumption $c \gg M^{-\frac{1}{2}}$ leads to overestimate the side layer flow and the resistance of the complete circuit which brings about the underestimation of the total current and the associated pressure drop needed to drive the flow. These problems are overcome by the composite core-side-layer solution which correctly predicts the division of the electric currents between the side layer and the side wall, since it does not make any assumptions about the relationship between $M^{-\frac{1}{2}}$ and c [Ting, 1991].

Within the composite core-side-layer flow approach, we can simplify the system of equations (2.99)-(2.104) at different orders of magnitude. For instance, we could retain terms up to $O(M^{-2})$ and neglect all the other smaller terms. In this case, we substitute the velocity field given by equation (2.100) in equations (2.99) and (2.101)-(2.103), and neglect terms smaller than $O(M^{-2})$ compared to the other terms in both the core and the side layer. In this way, taking into account that $F = O(M^{-1})$, $\frac{\partial}{\partial z} = O(M^{\frac{1}{2}})$ and $\frac{\partial}{\partial y} = O(1)$, we find the following governing equations for the composite core-side-layer flow:

$$\frac{\partial^2 F}{\partial y^2} - M^{-2}\left[\frac{\partial \nu_{ty}}{\partial y}\frac{\partial^3 F}{\partial y \partial^2 z} + \frac{\partial \nu_{tz}}{\partial z}\frac{\partial^3 F}{\partial y^3} + \nu_{tz}\frac{\partial^4 F}{\partial z^4} + (\nu_{ty}+\nu_{tz})\frac{\partial^4 F}{\partial y^2 \partial z^2}\right] = K, \quad (2.106)$$

for $0 \leq y \leq a$ and $0 \leq z \leq 1$.
At $y = 0$:

$$\frac{\partial^3 F}{\partial y^3} + \frac{\partial^3 F}{\partial y \partial z^2} = 0, \quad \frac{\partial F}{\partial y} = 0; \quad (2.107)$$

at $z = 0$:

$$\frac{\partial^3 F}{\partial z \partial y^2} + \frac{\partial^3 F}{\partial z^3} = 0, \quad \frac{\partial F}{\partial z} = 0; \quad (2.108)$$

at $z = 1$:

$$\frac{\partial^2 F}{\partial y^2} + \frac{\partial^2 F}{\partial z^2} = 0, \quad F + c\frac{\partial F}{\partial z} = 0, \quad (2.109)$$

and, at $y = a$:

$$\frac{\partial F}{\partial y} - (c + M^{-1})\frac{\partial^2 F}{\partial z^2} - M^{-1}\frac{\partial^2 F}{\partial y^2} = 0. \quad (2.110)$$

Once F is found, the velocity profile $\bar{u}$ is given by equation (2.100). On the other hand, we can consider the system of equations at a higher order, namely, $O(M^{-1})$. At this order, equation (2.99) takes the form

$$M^{-2}\frac{\partial}{\partial z}\left(\nu_{tz}\frac{\partial \bar{u}}{\partial z}\right) = \frac{\partial^2 F}{\partial y^2} - K, \quad (2.111)$$

and using equation (2.100) we have

$$\bar{u} = K + M^{-2}\frac{\partial}{\partial z}\left(\nu_{tz}\frac{\partial \bar{u}}{\partial z}\right) + \frac{\partial^2 F}{\partial z^2}.$$

However,

$$M^{-2}\frac{\partial}{\partial z}\left(\nu_{tz}\frac{\partial \bar{u}}{\partial z}\right) \leq O(M^{-1}) \times \bar{u};$$

then, at the present order we have

$$\bar{u} = K + \frac{\partial^2 F}{\partial z^2}. \quad (2.112)$$

Substituting (2.112), equation (2.111) becomes

$$\frac{\partial^2 F}{\partial y^2} - M^{-2}\left[\nu_{tz}\frac{\partial^4 F}{\partial z^4} + \frac{\partial \nu_{tz}}{\partial z}\frac{\partial^3 F}{\partial z^3}\right] = K, \tag{2.113}$$

for $0 \leq y \leq a$ and $0 \leq z \leq 1$. In addition, at $y = 0$:

$$\frac{\partial^3 F}{\partial y \partial z^2} = 0, \quad \frac{\partial F}{\partial y} = 0; \tag{2.114}$$

at $z = 0$:

$$\frac{\partial^3 F}{\partial z^3} = 0, \quad \frac{\partial F}{\partial z} = 0; \tag{2.115}$$

at $z = 1$:

$$\frac{\partial^2 F}{\partial z^2} = -K, \quad F + c\frac{\partial F}{\partial z} = 0; \tag{2.116}$$

and at $y = a$:

$$\frac{\partial F}{\partial y} - (c + M^{-1})\frac{\partial^2 F}{\partial z^2} = M^{-1}K. \tag{2.117}$$

Notice that, at this order, there is no dependence on ν_{ty}.

2.6 Spectral Collocation Method

Different approaches have been used for the solution of the equations governing the laminar duct flow of a liquid metal in strong magnetic fields. Many studies involving the thin wall approximation utilize the asymptotic expansions method, based on conjectures on the orders of magnitude of different terms in the equations [Walker, 1981]. In addition, semi-analytical or semi-numerical methods have been developed in order to overcome some limitations of the asymptotic analysis [Talmage and Walker, 1988, Hua et al., 1988]. In these approaches, inertial and viscous effects are commonly disregarded and the velocity profile near the walls is not obtained in detail but only the volumetric flow rate is given. There are also some fully numerical solutions of the MHD equations [Winowich and Hughes, 1982; Ramos and Winowich, 1990; Sterl, 1990]. However, even though this approach allows the exploration of the detailed flow in the near wall region, the high requirements of storage and computing time strongly limit these solutions to rather small Hartmann numbers ($M < 10^3$).

In the present investigation, the solution of the governing equations for both laminar and turbulent regimes was obtained through the Spectral Collocation Method [Canuto et al., 1987; Walker, 1992b]. This approach presents many advantages for the purpose of this study, for instance, a very easy numerical implementation, a very efficient solution

in terms of computing time and storage, and the possibility of considering very high Hartmann numbers ($10^3 - 10^5$) for both laminar and turbulent flows. This means that the structure of side layers can be explored in detail even for high M. This method has already been used in the study of laminar MHD duct flows with uniform and non-uniform magnetic fields, in two- and three-dimensional problems [Ting, 1991; Ting et al., 1993;]. A brief explanation of the method is provided here, addressing the details to the former references.

In this method, the unknown function $F(y,z)$ that satisfies the boundary value problem defined by equations (2.113)-(2.117) (or (2.106)-(2.110)) is approximated by a finite series of the form

$$F(y,z) = \sum_{l=0}^{NY} \sum_{n=0}^{NZ} A_{ln} T_{2l}(y/a) T_{2n}(z), \tag{2.118}$$

where A_{ln} are coefficients to be determined and

$$T_{2l}(y/a) = \cos[2l \arccos(y/a)], \quad 0 \leq \arccos(y/a) \leq \pi, \tag{2.119}$$

and

$$T_{2n}(z) = \cos[2n \arccos(z)], \quad 0 \leq \arccos(z) \leq \pi, \tag{2.120}$$

are the even Chebyshev polynomials of order $2l$ and $2n$, respectively. NY and NZ are the truncation limits in the Chebyshev series in y and z, respectively. The objective is to reduce the system of partial differential equations to a system of simultaneous, linear algebraic equations governing the coefficients A_{ln}. Since the number of unknown coefficients A_{ln} is $NT = (NY+1)(NZ+1)$, we have to supply the same number of algebraic equations. Once this system of equations is known, it can be solved for A_{ln} by Gauss elimination. Some of these equations are obtained by substitution of equation (2.118) in the boundary conditions (2.114)-(2.117). The rest of the equations have to be extracted from the governing equation (2.113). There are essentially two methods for the extraction of the system of linear algebraic equations, namely, the Galerkin or Tau methods and the Collocation method. The Galerkin or Tau methods involve the calculation of integrals with a weighting function for the determination of the coefficients. However, in some cases, the evaluation of the integrals can be a very difficult task. Some examples of the Galerkin method applied to an MHD heat transfer problem can be found in [Cuevas and Ramos, 1991; 1993]. The Collocation method provides an alternative approach. In this method, we choose a set of collocation points in the domain of interest, namely, y_i for $i = 0$ to NY and z_k for $k = 0$ to $(NZ-1)$. Then we apply the governing equations and boundary conditions at these points, by substituting first y_i and z_k into (2.118)-(2.120) and afterwards, equation (2.118) in the system (2.113)-(2.117). In this way we get a well defined linear system of simultaneous, algebraic equations for the coefficients A_{ln}. While the Galerkin method guarantees a

small error everywhere in the solution domain, the Collocation method only insures that the error is zero at the collocation points, but places no bound on the error between these points. So that, a bad selection of collocation points or insufficient collocation points can originate a considerable error, manifested as an oscillating solution. However, while the Galerkin method shows a progressive improvement as the number of terms increases, the Collocation method frequently shows a sudden improvement as the number of points grows. This fact, together with the spectral convergence of Chebyshev polynomials, implies that only a few terms in the series solution are needed to get a small truncation error. A family of orthogonal functions with algebraic convergence would require far more terms for the same accuracy.

A convenient set of points is provided by the Gauss-Lobatto Collocation points [Canuto et al., 1987]

$$y_i = a\cos\left(\frac{i\pi}{2NY}\right), \quad for \;\; i = 0 \;\; to \;\; NY, \tag{2.121}$$

$$z_k = \cos\left[\frac{k\pi}{2(NZ-1)}\right], \quad for \;\; k = 0 \;\; to \;\; (NZ-1). \tag{2.122}$$

which yield a good numerical resolution for the boundary layers by concentrating points near the walls ($y = a$, $z = 1$). With this choice, the Chebyshev polynomials (2.119)-(2.120) become

$$T_{2l}(y_i/a) = \cos\left(\frac{il\pi}{NY}\right), \quad i = 0 \;\; to \;\; NY. \tag{2.123}$$

$$T_{2n}(z_i) = \cos\left[\frac{kn\pi}{(NZ-1)}\right], \quad k = 0 \;\; to \;\; NZ-1. \tag{2.124}$$

We can visualize the coefficients A_{nl} to be determined in the series solution (2.118), as a vector of unknowns, namely,

$$\mathbf{V}(JC) = A_{nl}, \qquad JC = l(NZ+1) + n + 1.$$

Since l runs form 0 to NY, and n from 0 to NZ, the index JC runs from 1 to $NT = (NY+1)(NZ+1)$, where NT is the number of coefficients A_{nl}. Hence, the required linear system of simultaneous, algebraic equations can be concisely expressed as

$$\sum_{JC=1}^{NT} \mathbf{C}(IR, JC)\mathbf{V}(JC) = \mathbf{K}(IR),$$

where $IR = 1$ to NT, $\mathbf{C}(IR, JC)$ is the matrix of coefficients associated to $\mathbf{V}(JC)$, and $\mathbf{K}(IR)$ is a known vector. Let us show explicitly how to get the former system of

linear equations. Introducing (2.118) into governing equation (2.113) and evaluating at collocation points, we obtain

$$\sum_{l=0}^{NY}\sum_{n=0}^{NZ}\left\{\frac{1}{a^2}T_{2l}^{(2)}\left(\frac{y_i}{a}\right)T_{2n}(z_k)-M^{-2}T_{2l}\left(\frac{y_i}{a}\right)\right.$$
$$\left.\left[\nu_{tz}(y_i,z_k)T_{2n}^{(4)}(z_k)+\frac{\partial\nu_{tz}}{\partial z}(y_i,z_k)T_{2n}^{(3)}(z_k)\right]\right\}A_{nl}=K, \qquad (2.125)$$

for $i=1$ to NY and $k=1$ to $(NZ-1)$, that is, excluding the boundaries. The terms $T_{2n}^{(j)}$, $T_{2l}^{(j)}$ denote j-order derivatives of Chebyshev polynomials:

$$T_{2l}^{(2)}\left(\frac{y_i}{a}\right)=8l\sum_{p=0}^{(l-1)}(l^2-p^2)\frac{1}{c_p}\cos\left(\frac{ip\pi}{NY}\right),$$

$$T_{2n}^{(3)}(z_k)=8n\sum_{p=0}^{(n-2)}[(n^2-1)n^2-(p+1)p(2n^2-p^2-p)]\cos\left[\frac{(2p+1)k\pi}{2(NZ-1)}\right],$$

$$T_{2n}^{(4)}(z_k)=\frac{16}{3}\sum_{p=0}^{(n-2)}(n^2-p^2)[(n-p)^2-1][(n+p)^2-1]\frac{1}{c_p}\cos\left[\frac{kp\pi}{(NZ-1)}\right],$$

where $c_0=2$ and $c_p=1$ for $p\geq 1$. Up to here, the index IR takes the values

$$IR=(i-1)(NZ-1)+1=1 \quad to \quad NY(NZ-1).$$

Symmetry conditions (2.114) and (2.115) at $y=0$ and $z=0$, respectively, are identically satisfied when (2.118) is introduced, and no equations are generated. From the boundary condition given by equation (2.116a), we get

$$\sum_{l=0}^{NY}\sum_{n=0}^{NZ}A_{nl}T_{2l}\left(\frac{y_i}{a}\right)n^2(4n^2-1)=-\frac{3}{4}K, \quad for \ \ i=1 \ \ to \ \ NY, \qquad (2.126)$$

and

$$IR=NY(NZ-1)+i=NY(NZ-1)+1 \ \ to \ \ NY(NZ-1)+NY=NY\ NZ.$$

From the equation (2.116b) we have

$$\sum_{l=0}^{NY}\sum_{n=0}^{NZ}A_{nl}[1+4n^2c]T_{2l}\left(\frac{y_i}{a}\right)=0 \quad for \ \ i=0 \ \ to \ \ NY, \qquad (2.127)$$

$$IR = NY\ NZ + i + 1 = NY\ NZ + i + 1\ \ to\ \ NY\ NZ + NY + 1\ NZ.$$

where the relations $T_{2n}(1) = 1$ and $T_{2n}^{(1)}(1) = 4n^2$, have been used. Finally, from boundary condition (2.117), it follows that

$$\sum_{l=0}^{NY}\sum_{n=0}^{NZ} A_{nl}\left[\frac{4l^2}{a}T_{2n}(z_k) - (c + M^{-1})T_{2n}^{(2)}(z_k)\right] = M^{-1}K,$$

$$for\ \ k = 0\ \ to\ \ (NZ - 1), \qquad (2.128)$$

$$IR = NY\ NZ + NY + 1 + k + 1 = NY\ NZ + NY + 2\ \ to\ \ (NY + 1)(NZ + 1),$$

where

$$T_{2l}(1) = 1, \qquad T_{2l}^{(1)}(1) = 4l^2,$$

$$T_{2n}^{(2)}(z_k) = 8n\sum_{p=0}^{(n-1)}(n^2 - p^2)\frac{1}{c_p}\cos\left[\frac{kp\pi}{(NZ-1)}\right].$$

Equations (2.125)-(2.128) fully determine the linear system of simultaneous, algebraic equations for the coefficients A_{nl}. The solution of the system was performed through the Gauss-Jordan elimination method. Once we have the final solution at the collocation points, it can be interpolated at any other set of points.

In the laminar case, in order to get the velocity profile we input the Hartmann number, the wall conductance ratio and the dimensionless pressure gradient, K. We set the total viscosity $\nu_{tz}(y_i, z_k)$ equal to 1 and $\frac{\partial \nu_{tz}}{\partial z}(y_i, z_k) = 0$, introduce the information in the matrix associated to A_{nl}, solve the linear system of equations, satisfy the volume flux condition (2.105) and get the solution in a direct way. On the other hand, the turbulent flow solution involves an iterative procedure. We need to input also an *initial* Reynolds number Re_* that, at the end, is properly rescaled. We begin the iteration procedure by calculating the matrix elements corresponding to a laminar flow, $\nu_t(y_i, z_k) = 1$, for the given Hartmann number and conductance ratio, and solve the linear system of equations by Gauss-Jordan elimination. So, we get the laminar velocity profile at the collocation points and, in order to assure the conservation of mass, the volume flux condition (2.105) is satisfied. Afterwards, we calculate the velocity gradients and the *integral length*,[6] l_o, at the collocation points and add them as, along with Re_*, into the turbulence model from which we get an effective viscosity

[6]The integral length is a length scale required by the turbulence model and is disscused in Chapter 5.

$$\nu_{tz} = \nu_{tz}\left(Re_*, l_o, \frac{\partial u}{\partial y_i}, \frac{\partial u}{\partial z_i}\right).$$

We then proceed to calculate the viscosity gradients at the collocation points. The new values of $\nu_{tz}(y_i, z_k)$ and $\frac{\partial \nu_{tz}}{\partial z}(y_i, z_k)$ are fed into the matrix elements and, once the system of equations is solved, a modified velocity profile is obtained. We continue the iterations until convergence is reached. Finally, the Reynolds number and the pressure gradient are rescaled, based on the average velocity. This rescalation is accomplished in the following way. The *initial* Reynolds number and pressure gradient are based on a certain velocity U_*, different from the average velocity $\bar{U}$, that is,

$$Re_* = \frac{U_* L}{\nu_o},$$

$$-K_* = \frac{1}{\sigma U_* B_o^2} \frac{\partial p'}{\partial x'},$$

where p' and x' stand for the dimensional pressure and axial coordinate. Instead of $-K$, it is more common to deal with the friction factor, namely,

$$\lambda_{f*} = -\frac{L}{2\rho U_*^2} \frac{\partial p}{\partial x} = \frac{2\sigma B_o^2 L}{\rho U_*} K = \frac{N_* K}{2},$$

where N_* is the interaction parameter based on U_*. Once the turbulent solution has converged, the volume flux condition (2.105) gives

$$\int \bar{u} dA = \frac{1}{U_* A_o} \int \bar{u}' dA' = \frac{\bar{U}}{U_*} = m, \tag{2.129}$$

where dA is the differential area element and the primes denote dimensional variables, A_o being the dimensional cross-section. The *actual* average velocity is then given by

$$\bar{U} = m U_*,$$

and the Reynolds number and friction factor based on the average velocity are finally computed as

$$Re = m Re_*, \qquad \lambda_f = \frac{\lambda_{f*}}{m},$$

respectively.

Chapter 3

Laminar Flow and Heat Transfer Analysis

3.1 Introduction

In this Chapter we present the flow and heat transfer results for the laminar steady-state flow of a liquid metal in a square duct with an imposed transverse magnetic field. The walls of the duct are considered to range from thin conducting to insulating. First, we address the laminar MHD flow in a square duct by solving the system of equations given in subsection 2.4.3, using the spectral collocation method. We validate the numerical procedure by comparing the collocation velocity profiles with some available analytical solutions and afterwards analyze the effect of the Hartmann number and the wall conductance ratio in the structure of the laminar velocity profiles. Later, we present the laminar heat transfer analysis which involves the finite difference solution of the heat transfer equation. After introducing and validating the numerical method, we use the laminar MHD velocity profiles to solve the heat transfer equation and get the temperature profiles for different Péclet numbers. We explore the effect of the Hartmann number and wall conductance ratio on the heat transfer process and compare the wall temperature profiles obtained with a laminar MHD flow against the profiles obtained with slug flow. Finally, some laminar heat transfer results for the cylindrical duct with different boundary conditions and flows are presented.

3.2 Laminar MHD Flow in a Square Duct

This section shows how the structure of liquid metal flows in square ducts is affected by the presence of strong magnetic fields and walls of different electrical conductivity. The results presented here correspond only to the laminar regime. Under this condition, the relevant parameters governing the behavior of the flow are the Hartmann number and the wall conductance ratio. The Reynolds number is not an issue here. Actually, it is assumed that all flows are stable whatever the values of M and c, provided the Reynolds number is sufficiently small. However, due to practical implications, the flow

stability problem deserves a careful analysis. It is particularly relevant for flows in thin conducting wall ducts with high velocity side layers, specially at the very high Hartmann numbers considered in this study. The stability problem is not explored in this investigation and should be addressed in a future study. Some aspects about the stability of liquid metal flows in thin conducting wall ducts with strong magnetic fields have been investigated by Ting [1991] and Ting *et al.* [1991]. In the present work, an analysis beyond the laminar regime is performed in Chapter 5, where inertial effects are introduced in order to investigate the fully developed turbulent liquid metal flow in thin conducting as well as in insulating wall ducts under strong magnetic fields.

The velocity profiles were obtained by solving the $O(M^{-1})$ system of equations (2.111)-(2.117), simplified by the laminar condition $\nu_{tz} = 1$ which means that only molecular viscosity is considered. As a matter of fact, numerical computations showed essentially no distinction between results obtained by solving the former system of equations and those obtained through the $O(M^{-2})$ system (2.106)-(2.110) (with $\nu_{ty} = 1$) for most of the cases of interest. Laminar solutions were obtained directly (no iterations) using the spectral collocation method described in 2.4.3. All the solutions correspond to a duct with a square cross-section (*i.e.* the aspect ratio is $a = 1$) and with the four walls of uniform thickness and conductivity (uniform c).[1] In addition, the velocity profiles were normalized by applying condition (2.105).

In order to validate the numerical calculation method we compare our numerical solutions for the velocity profiles for two specific cases where analytical solutions are available. Figure 3.1 shows the comparison of the collocation solution as a function of z at the plane $y = 0$, for the case $M = 10^4$ and $c = 0$, against the analytical solution provided by Roberts [1967], for the insulating wall duct case, namely,

$$u(y,z) = 1 - \frac{1}{2}\left[G(y,z) + G(-y,-z),\right] \tag{3.1}$$

where

$$G(y,z) = (1-y)\left[(1+2q^2)erfc\ q - \frac{2q}{\sqrt{\pi}}e^{-q^2}\right],$$

$$q = \frac{1}{2}(1-z)\left[\frac{M}{a(a-y)}\right]^{\frac{1}{2}}.$$

The figure shows only one eighth of the duct, from $z = 0.75$ to $z = 1$, that is, a portion of the core-flow and the side-wall layer. The rest of the core-flow presents no variations. The collocation velocity profile shown in figure 3.1 was obtained with $NY = 3$ (*i.e.* four collocation points in the y-direction) and $NZ = 25$ (*i.e.* 26 collocation points in the z-direction).[2] Notice that the numerical solution compares very

[1] Results are shown in dimensionless units.

[2] The points showed in the figure do not correspond to the collocation points.

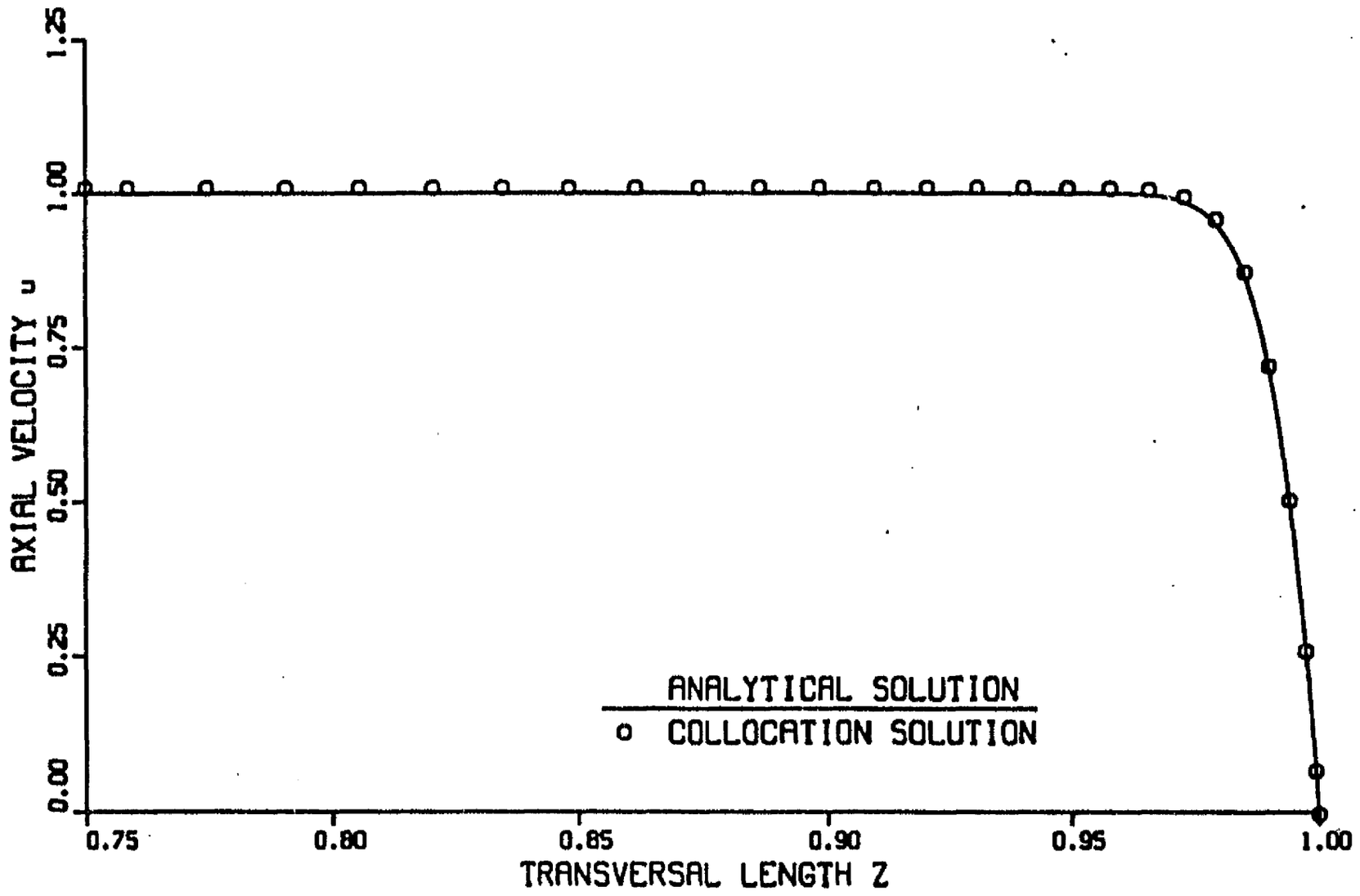

Figure 3.1: Comparison of collocation and Roberts' [1967] analytical solution for an insulating wall duct flow. $M = 10^4$.

well with the analytical one even though we used just a few points in the y-direction. Actually, since in the core-side-layer solution we are not resolving the Hartmann layers, a few collocation points in the y-direction are sufficient to get a good agreement, as far as a large enough distance from the upper (bottom) wall is maintained ($\gg O(M^{-1})$). On the other hand, since we are interested in resolving the side-wall layers, we need to provide enough points in the z-direction. Figure 3.2 shows the comparison of the velocity profile at $y = 0$ for a thin conducting wall case ($M = 10^4$, $c = 0.1$) obtained through the collocation method, against the analytical solution provided by Hua and Picologlou [1989], which corresponds to an approximate form of the asymptotic expansions solution given by Walker [1981]:

$$u(y,z) = u_{so}(a^2 - y^2)\sin[\gamma(z+1)]e^{-\gamma(z+1)} + u_{co}[1 - e^{-\gamma(z+1)}], \qquad (3.2)$$

where

$$\gamma = \frac{(\pi M)^{\frac{1}{2}}}{2a}, \qquad u_{so} = 3\gamma\left[1 - u_{co}\left(1 - \frac{1}{\gamma}\right)\right].$$

Here, u_{co} is the core velocity which depends on the wall conductance ratios:

$$u_{co} = \mathcal{K}\left(1 + \frac{a}{c_t}\right),$$

where

$$\mathcal{K} = \left[1 + \frac{a}{c_t} + \frac{a^2}{6} + \left(\frac{1}{c_1} + \frac{1}{c_2}\right)\right]^{-1}.$$

c_t, c_1 and c_2 are the wall conductance ratios of the top wall ($y = a$), the side wall at $z = -1$, and the side wall at $z = 1$, respectively. In the case we are analyzing, the wall conductance ratios are all the same and equal to $c = 0.1$.

In figure 3.2, the electromagnetic effect leading to the side-wall jets is clearly shown. Again, the collocation solution was obtained for $NY = 3$ and $NZ = 25$. Here the agreement is also very good although there is a slight difference in the value of the peak velocity near the wall. This may be due to the approximate form of the analytical velocity profile, expressed as the superposition of two solutions, namely, the leading terms of the Walker's asymptotic expansions solution for the side layer and a solution for the inertialess, inviscid core flow.

Once we found that our numerical method reproduces well known solutions satisfactorily, we now proceed to explore the behavior of the velocity profiles by varying the parameters involved in the laminar problem, namely, the Hartmann number and the wall conductance ratio. In order to perform a parametric study, we consider only three high values of the Hartmann number M (with the exception of figure 3.3), namely, 10^3, 10^4 and 10^5, characteristic of fusion applications where strong magnetic fields are

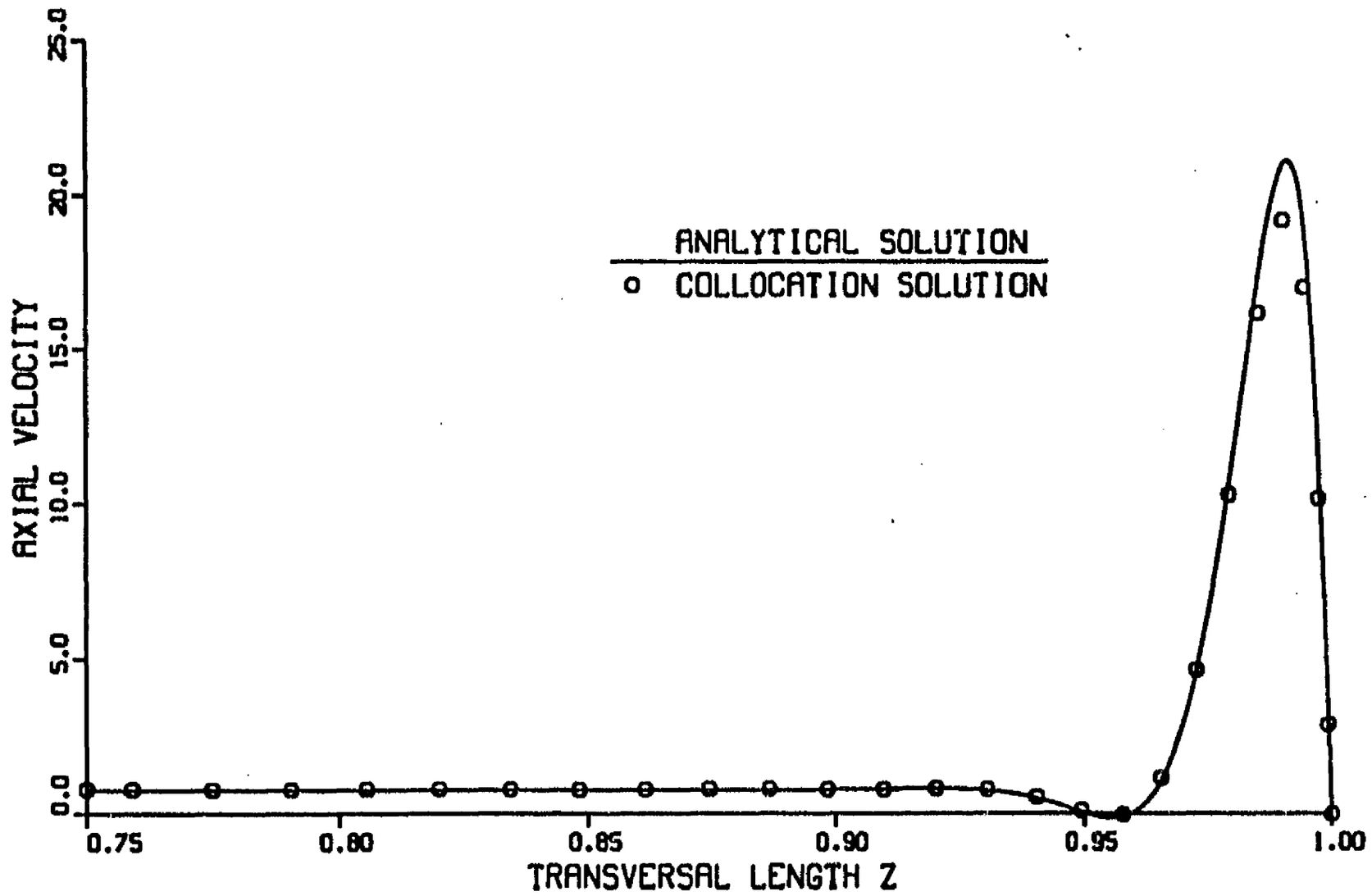

Figure 3.2: Comparison of collocation and analytical solutions [Walker, 1981; Hua and Picologlou, 1989] for a thin conducting wall duct flow. $M = 10^4$, $c = 0.1$

involved. Likewise, since we are interested in exploring the transition from the thin conducting to the insulating wall case, we choose the values of the wall conductance ratio c as 0.05, 0.01, 0.001 and 0. We hope that with this range of parameters we can offer a clear idea of the main MHD effects that may appear in flows of liquid-metal-cooled blankets. A similar flow analysis for laminar MHD flows in rectangular ducts was performed by Ting [1991] but these results are restricted to thin conducting wall ducts and a maximum Hartmann number of 6400.

The number of collocation points in the z-direction varied depending on the Hartmann number. It was found that for $M = 10^3$, $NZ = 15$ was enough to provide a good agreement with the analytical solutions. On the other hand, for $M = 10^4$ it was necessary to increase NZ up to 25, while for $M = 10^5$, NZ was increased up to 45. In all cases $NY = 3$. For the analysis of the results, we rely on the discussion performed in section 2.2 and in [Walker, 1981].

The behavior of the solutions as the Hartmann number grows is presented in figure 3.3 where the velocity profiles as a function of z for different M are shown. The results correspond to the plane $y = 0$ and the Hartmann number takes the values $1, 10, 10^2$ and 10^3 while c is fixed at 0.05. At $M = 1$ the magnetic interaction is negligible and the velocity profile is parabolic; at $M = 10$ the magnetic effects are weak and the profile gets flatter in the core. As M is increased to 100, the MHD effects are considerable and an M-shaped profile appears, decreasing the velocity in the core and increasing in the side-wall layer. When $M = 10^3$ the MHD effects are stronger, the decrease in the core velocity and the increase in the side layer velocity are even more pronounced while the side layer's width is $O(M^{-\frac{1}{2}})$.[3] In addition, a back flow appears in the intersected core-side-layer region.

Figure 3.4 shows an expanded view of the former case, that is, the core-side-layer profile for $M = 10^3$ and $c = 0.05$ for different vertical (y) positions. In this thin conducting wall case, the higher overshoot as well as the more intense back flow, correspond to the position $y = 0$, that is, to the mid-plane position. As we approach the upper wall, the peak velocity in the side layer decreases parabolically, as can also be corroborated from the analytic solution [Walker, 1981]. Therefore, at the top wall $y = 1$, there is no flow in the side layer. At $y = 0.90$ the back flow has completely disappeared, though an M-shaped profile persists. The core-flow is uniform and independent of the y-coordinate. Notice that the extra flow carried by the side layer is compensated by a reduction in the core velocity ($u_c < 1$).

Figures 3.5 and 3.6 are similar to figure 3.4, the same wall conductance ratio, $c = 0.05$, but different Hartmann numbers. Figure 3.5 corresponds to $M = 10^4$ while figure 3.6 to $M = 10^5$. Compare the width of the side layer in figures 3.4, 3.5 and 3.6. Since it is $O(M^{-\frac{1}{2}})$, for a Hartmann number as low as 10^3, one laminar side layer occupies less than 10 % of the cross-section of the duct while for $M = 10^5$ occupies

[3] Notice that these are only order of magnitude estimations and should not be considered as accurate measures.

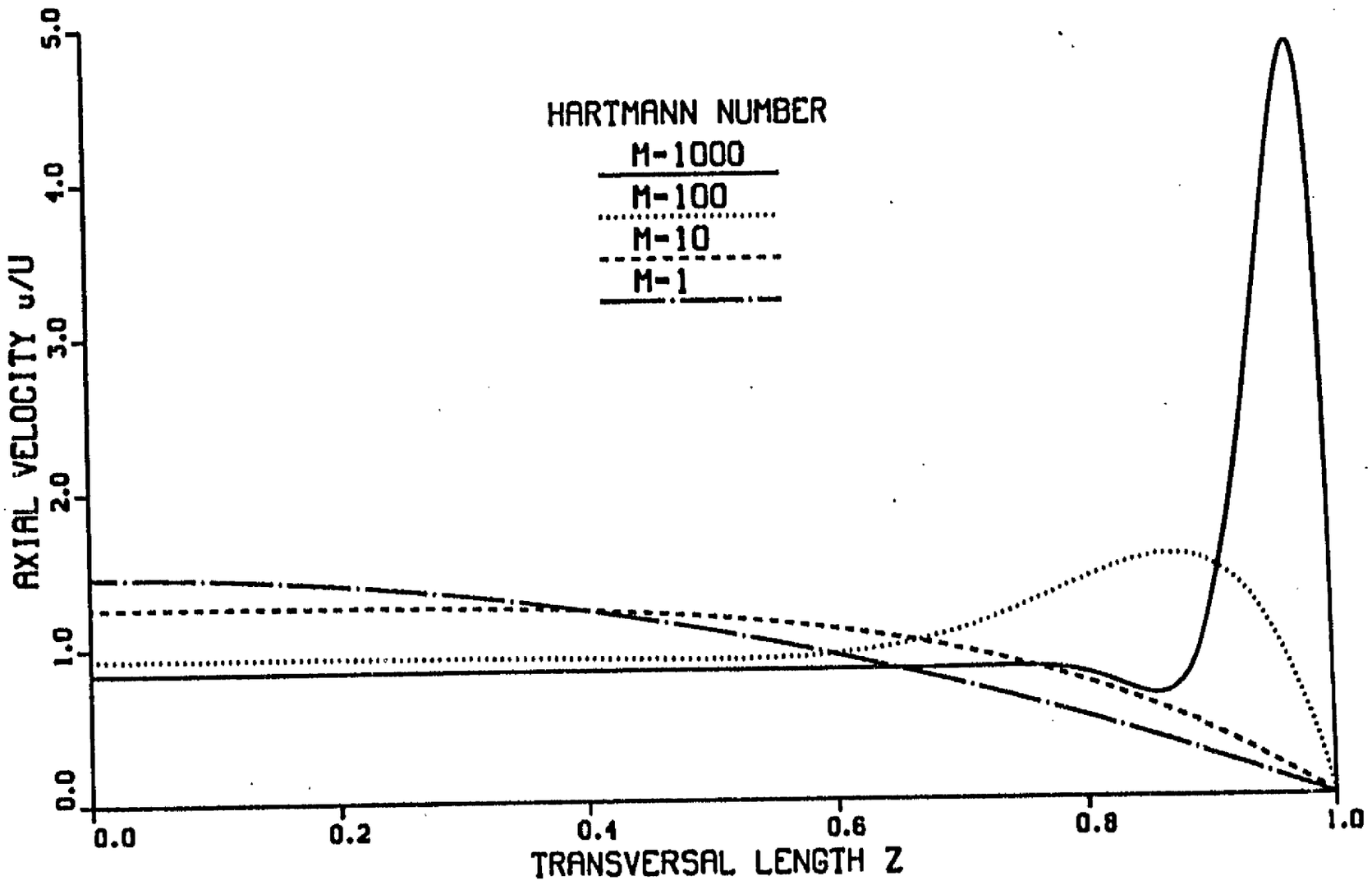

Figure 3.3: Laminar velocity vs. z at $y = 0$ for different Hartmann numbers. $c = 0.05$.

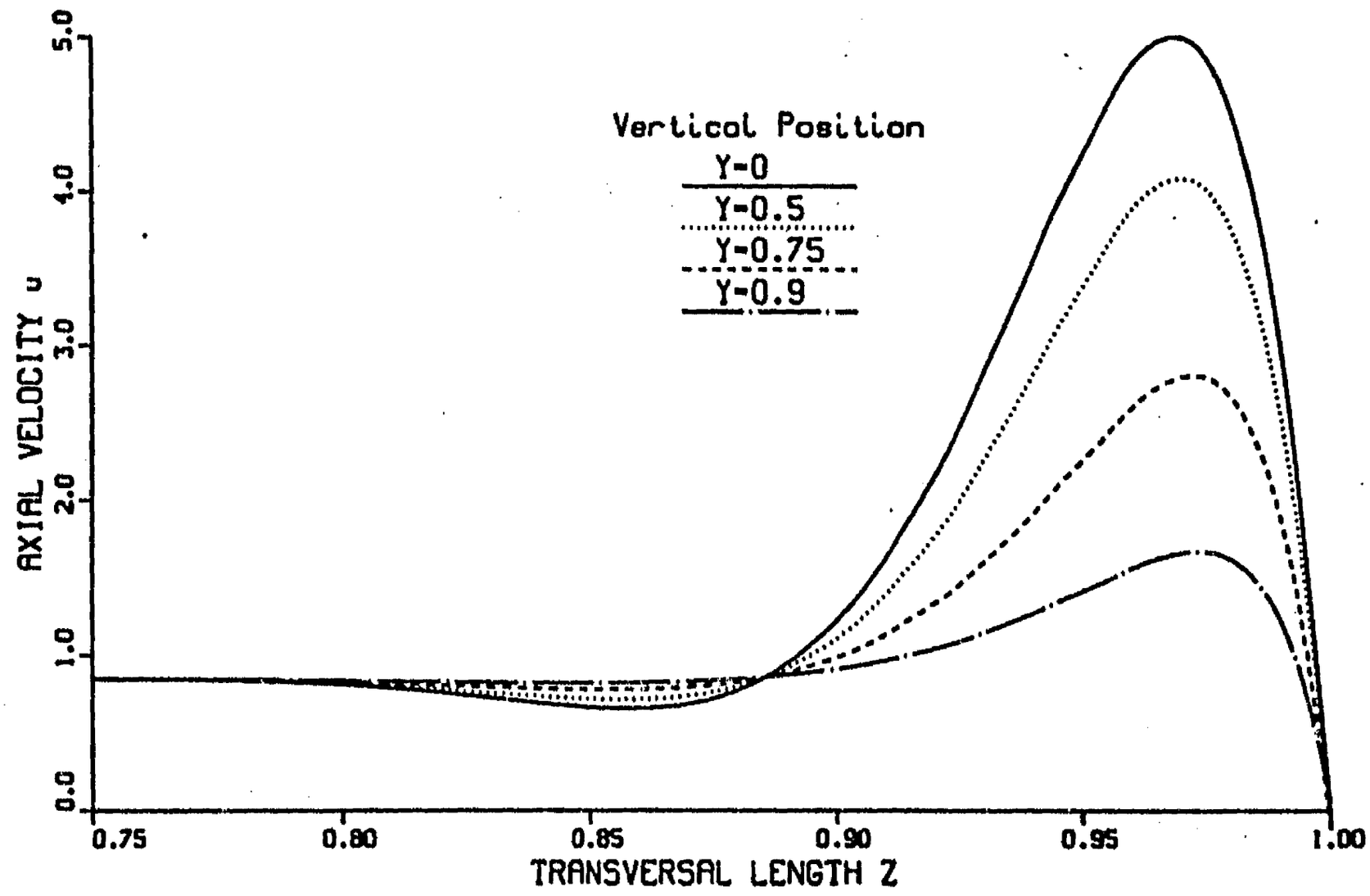

Figure 3.4: Laminar velocity vs. z for different y-positions. $M = 10^5$, $c = 0.05$.

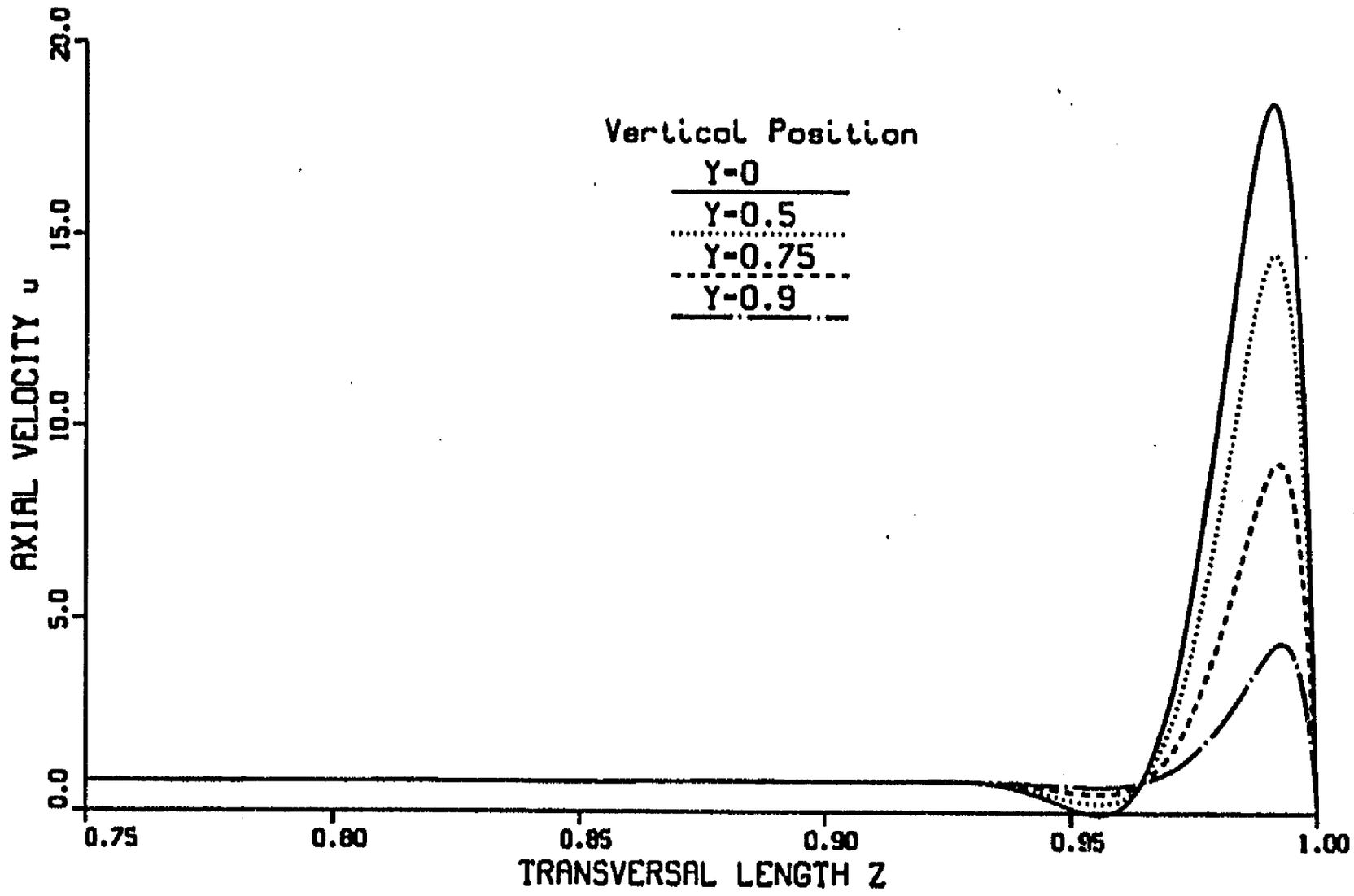

Figure 3.5: Laminar velocity vs. z for different y-positions. $M = 10^4$, $c = 0.05$.

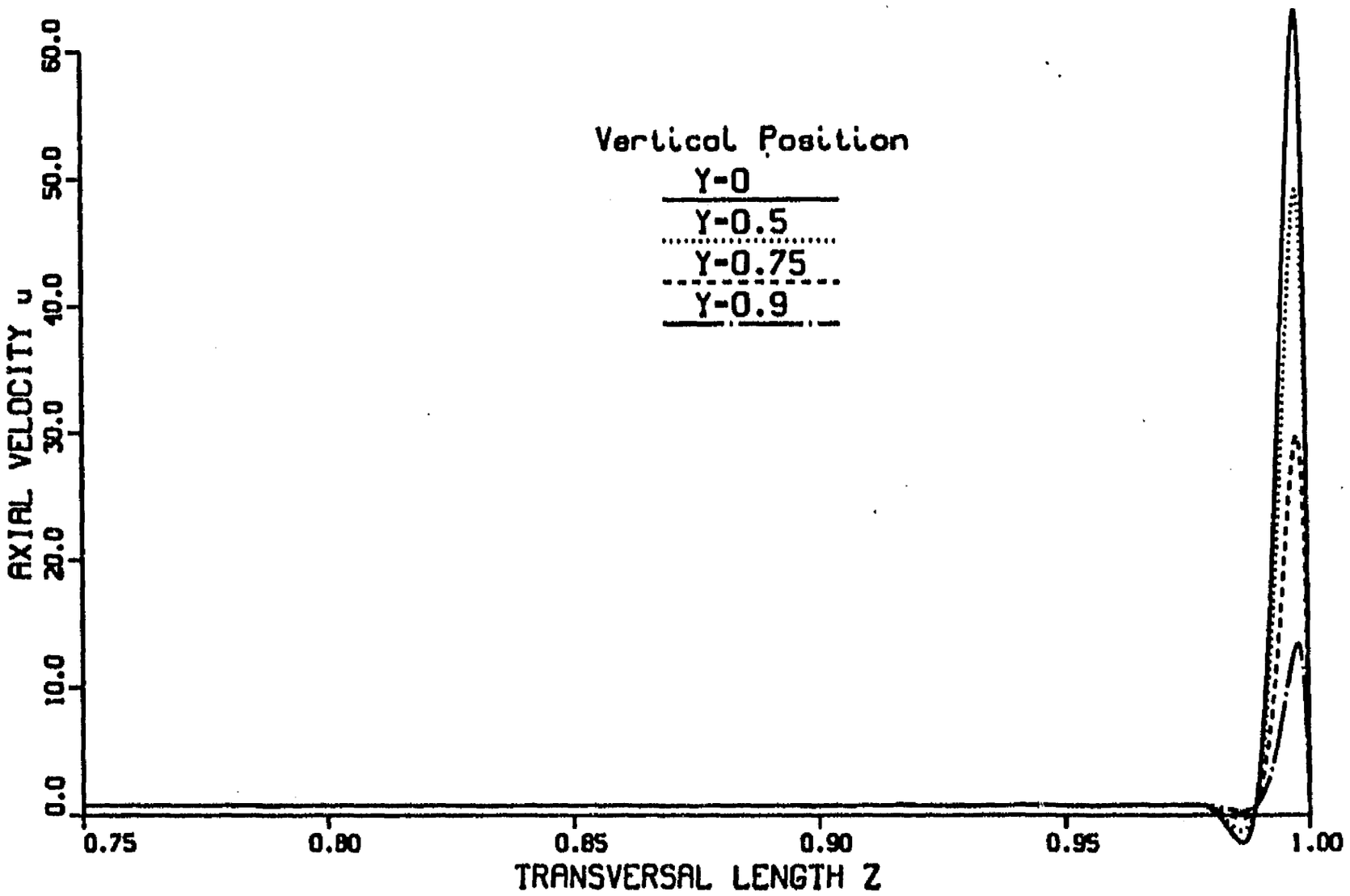

Figure 3.6: Laminar velocity vs. z for different y-positions. $M = 10^5$, $c = 0.05$.

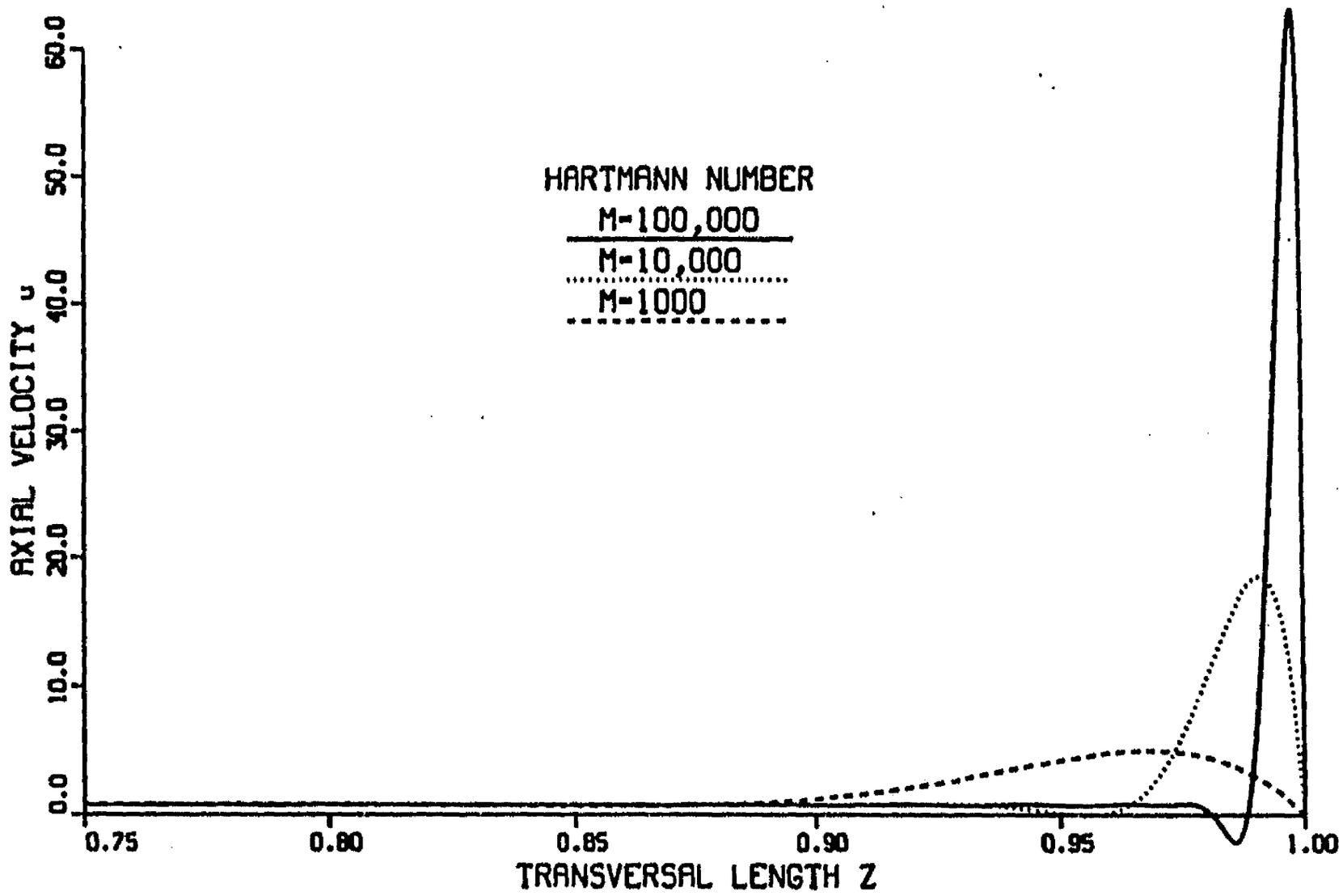

Figure 3.7: Laminar velocity vs. z at $y = 0$ for different Hartmann numbers. $c = 0.05$.

less than 2 %. On the other hand, the side layer velocity is $O(M^{\frac{1}{2}})$, hence, its increase with the Hartmann number is dramatic, the peak velocity for $M = 10^3$ being about 10 % the maximum velocity for the case $M = 10^5$. These characteristics are clearly condensed in figure 3.7 where the velocity profiles at $y = 0$ for the three different Hartmann numbers are presented for $c = 0.05$.

Figure 3.8 presents the velocity profile for $M = 10^3$ at different vertical positions for the insulating wall case, namely, $c = 0$. As we mentioned before, in this case the electric currents close completely within the fluid (through the Hartmann layers) reducing the electromagnetic drag. In this limit the velocity overshoots are completely suppressed and the non-slip condition at the side wall is matched smoothly through the side layer with the uniform flow at the core. Here the defect flow in the side layer is compensated by an increase in the core velocity ($u_c > 1$). Figures 3.9 and 3.10 show similar velocity profiles for the case $c = 0$, and for Hartmann numbers 10^4 and 10^5, respectively. Notice that as the Hartmann number is increased, the side layer is reduced and becomes flatter and flatter while the y-dependence is less marked. The side layer velocity matches the core velocity closer to the wall and $u_c \approx 1$. Actually, for $M = 10^5$ the MHD velocity profile for an insulating wall duct is very close to that of a slug flow, that is, a completely flat flow, without gradients in the flow region. Figure 3.11 condenses the effect of the Hartmann number on the insulating wall duct velocity profiles.

Figure 3.12 shows the transition of the velocity profiles at $y = 0$, as the wall conductance ratio decreases from 0.05 to 0 for $M = 10^3$. For this Hartmann number, the thin conducting wall approximation holds for those values of c in the range $M^{-1} = 0.001 \ll c \ll 1$. Therefore, in the range of wall conductance ratios we are exploring, the curves corresponding to $c = 0.05$ and $c = 0.01$ fit within this approximation. Actually, in these two cases $c = \alpha M^{-\frac{1}{2}}$, where α is a different constant for each c. For $c = 0.05$, $\alpha \approx 1.6$ while for $c = 0.01$ $\alpha \approx 0.35$. Here, the inner side layer velocity is $O(M^{\frac{1}{2}})$ and carries a fraction of the $O(1)$ volume flux. On the other hand, the insulating wall case is represented by the curve $c = 0$, where the inner side layer velocity is $O(1)$. The curve $c = 0.001$ lies in the case $c = O(M^{-1})$ that, essentially, is the same as the insulating wall case, although the inner side layer velocity presents a slight difference with respect to that of the insulating duct. Figures 3.13 and 3.14 present results similar to those of figure 3.12 but for Hartmann numbers $M = 10^4$ and $M = 10^5$, respectively. For $M = 10^4$, the thin conducting wall approximation holds for $10^{-4} \ll c \ll 1$. Consequently, the curves $c = 0.05$, $c = 0.01$ and $c = 0.001$ in figure 3.13 can be considered within the approximation. It can be seen that even for $c = 0.001$ there is a velocity overshoot in the side layer. In this case, c lies in the range $M^{-1} \ll c \ll M^{-\frac{1}{2}}$, then, the side layer velocity is $O(cM^{\frac{1}{2}})$ and is not large enough to convey any of the $O(1)$ volume flux. For $c = 0.01$, we have that $c = M^{-\frac{1}{2}}$ ($\alpha = 1$), the side layer velocity is $O(M^{\frac{1}{2}})$ and carries a fraction of the $O(1)$ volume flux. The case $c = 0.05$ can be considered to fit in the range $M^{-\frac{1}{2}} \ll c \ll 1$. Here

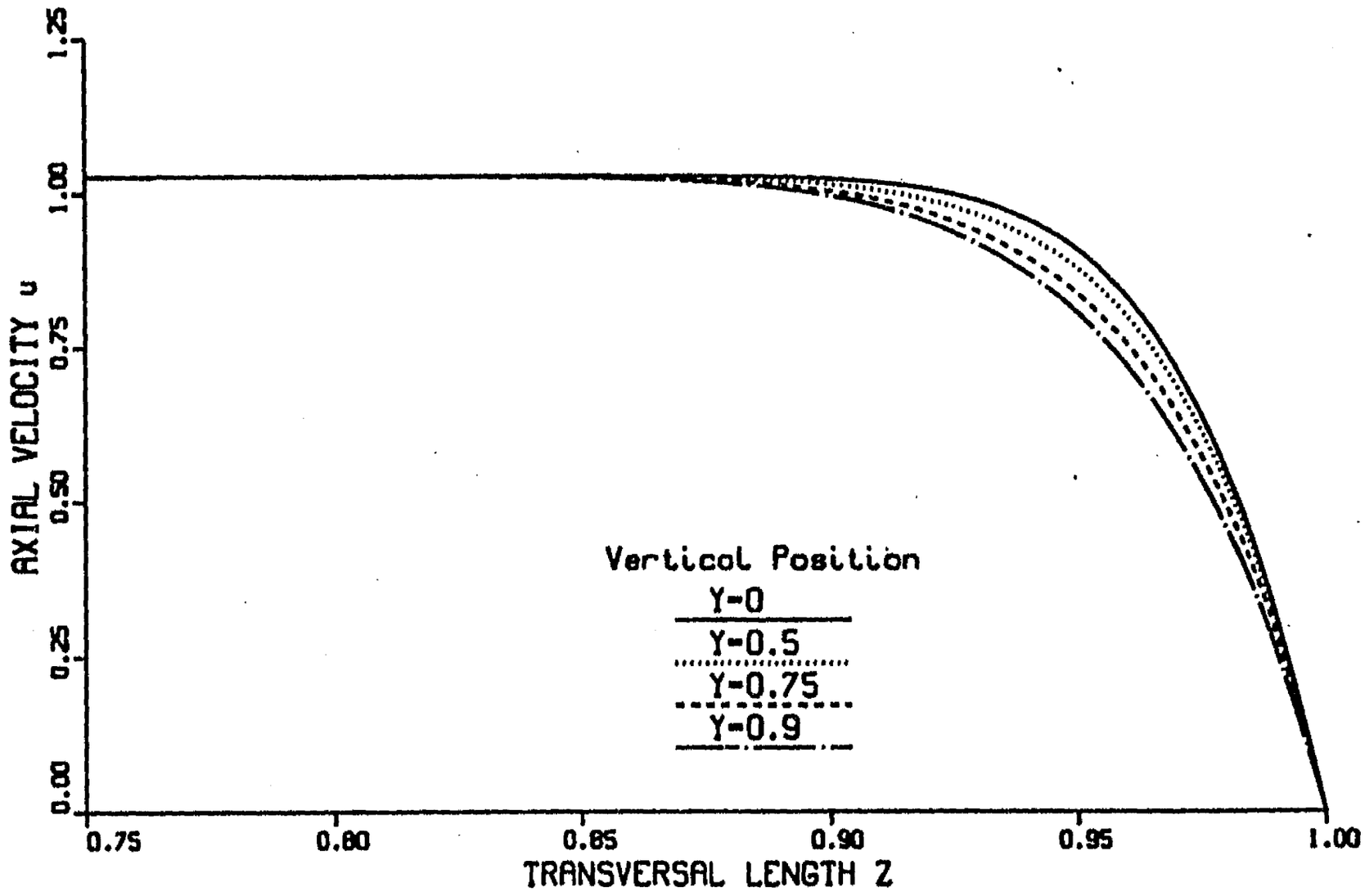

Figure 3.8: Laminar velocity vs. z in an insulating wall duct, for different y-positions. $M = 10^3$.

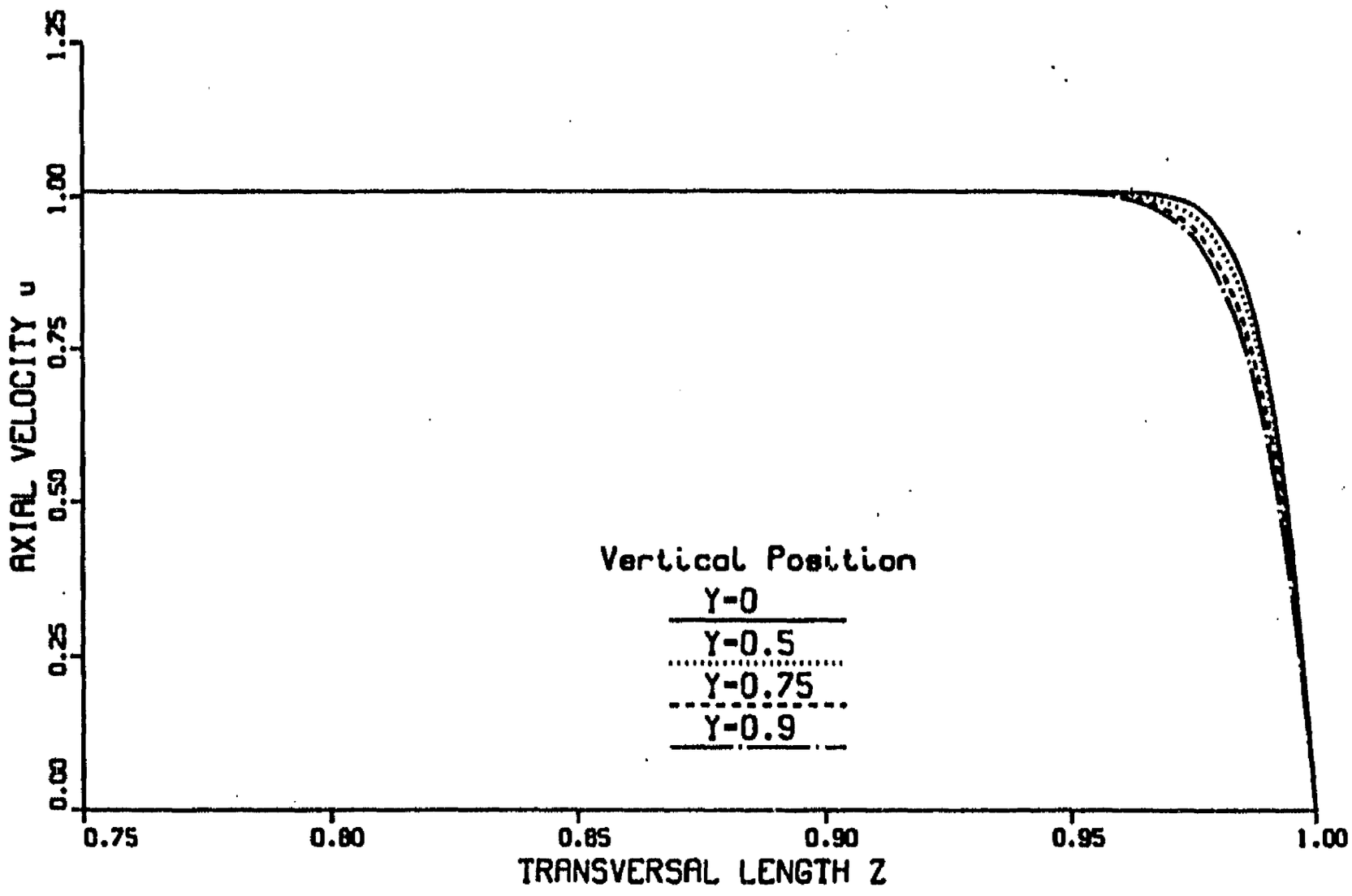

Figure 3.9: Laminar velocity vs. z in an insulating wall duct, for different y-positions. $M = 10^4$.

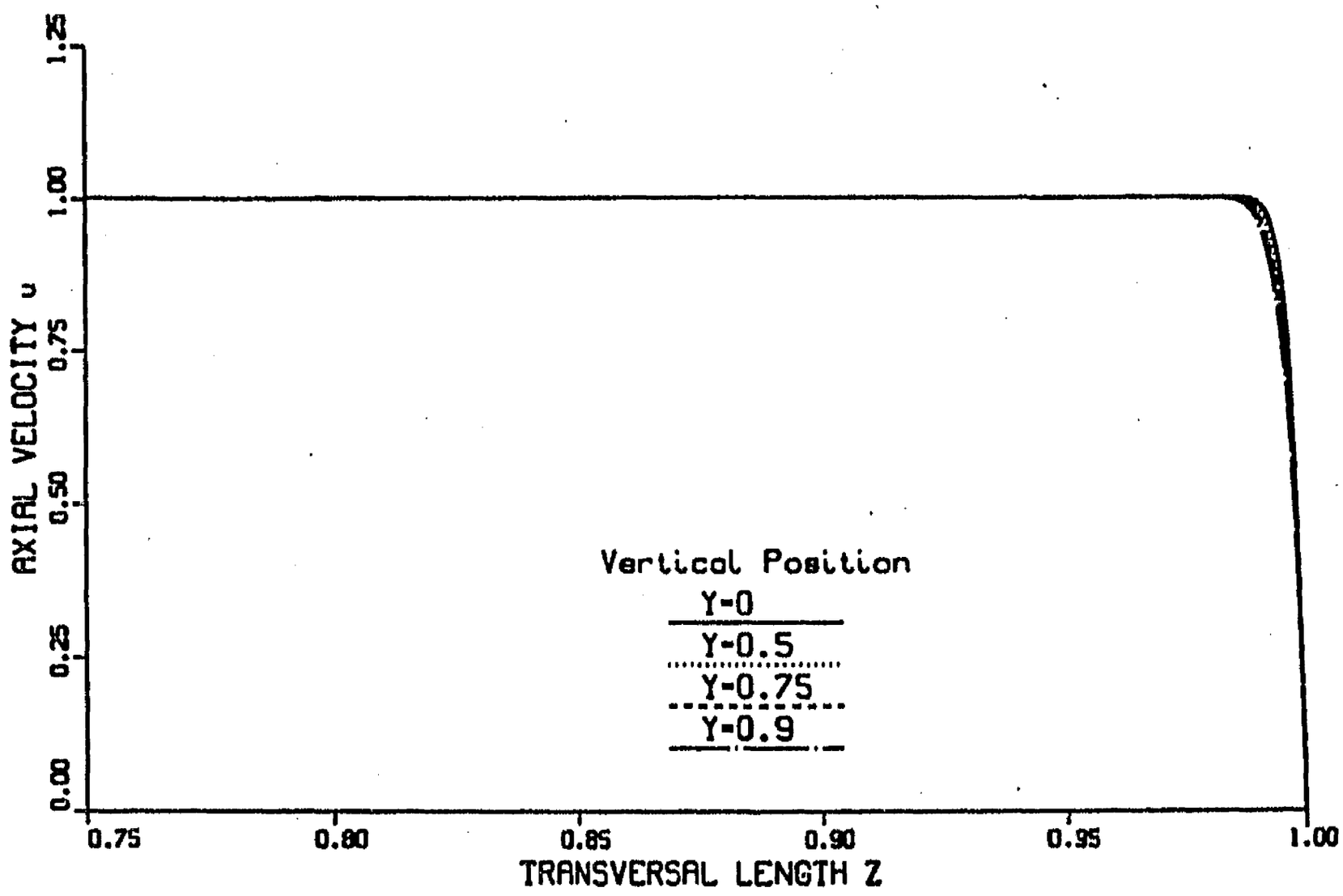

Figure 3.10: Laminar velocity vs. z in an insulating wall duct, for different y-positions. $M = 10^5$.

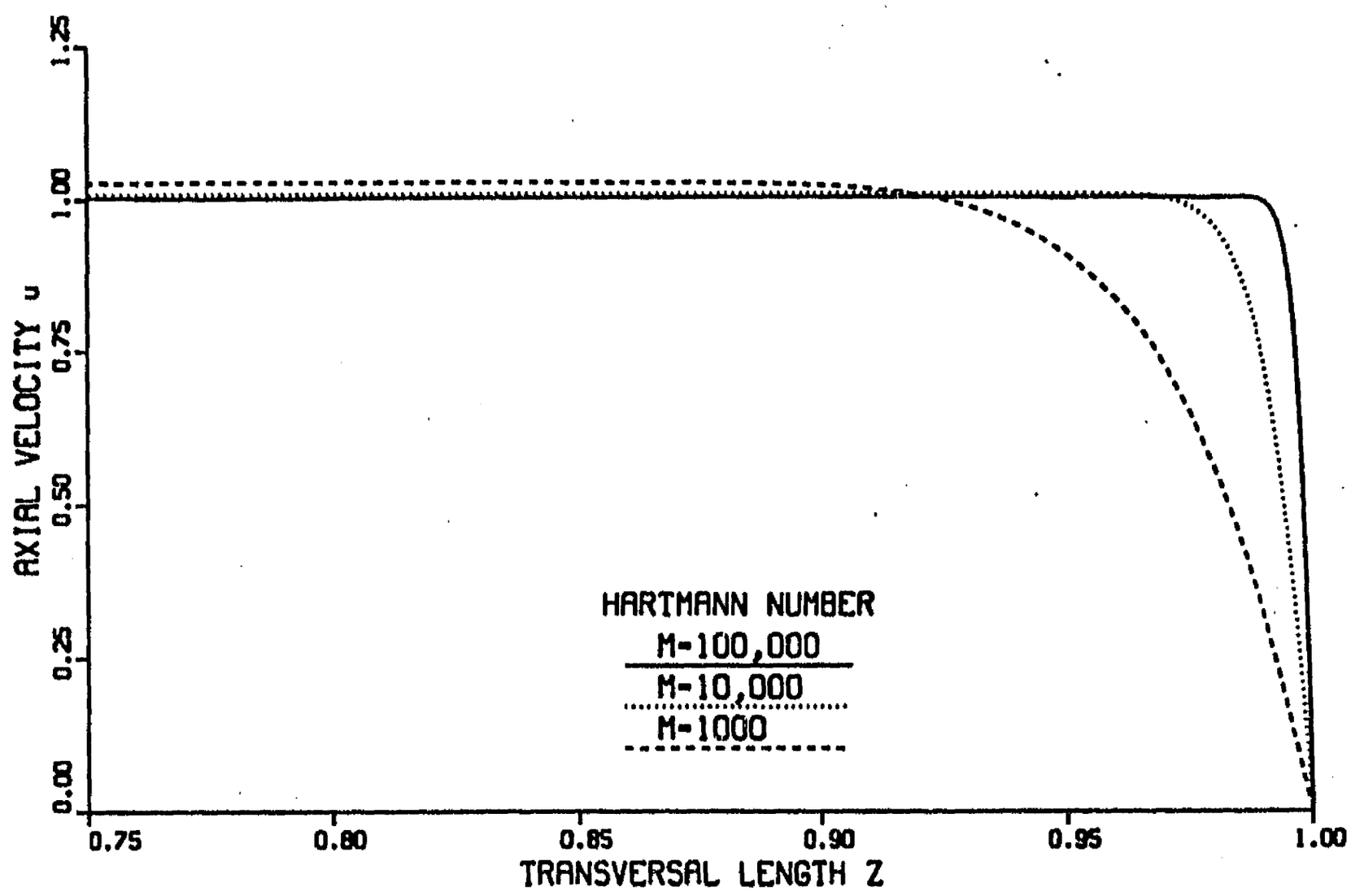

Figure 3.11: Laminar velocity vs. z in an insulating wall duct at $y = 0$, for different Hartmann numbers.

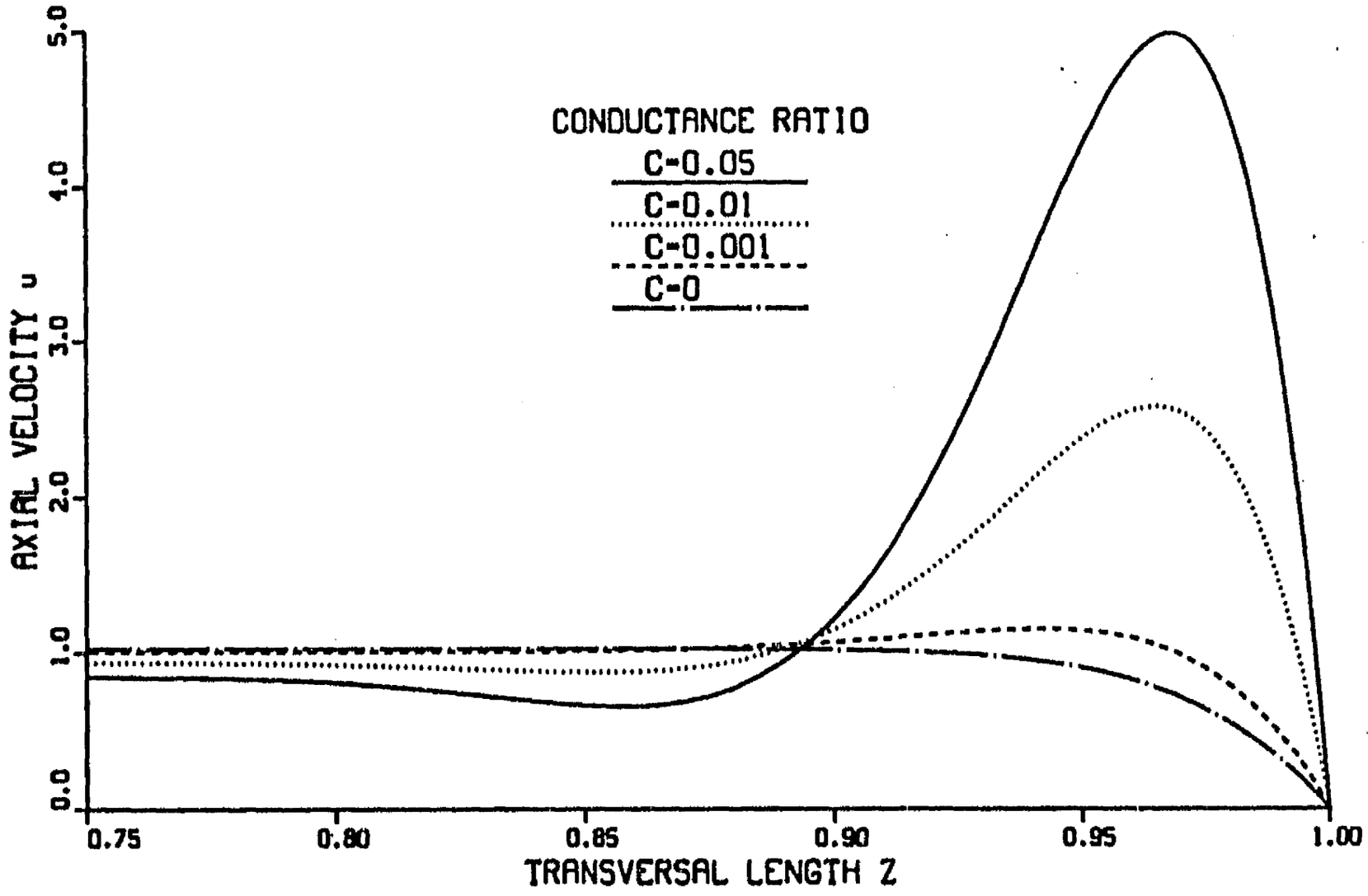

Figure 3.12: Laminar velocity vs. z at $y = 0$, for different wall conductances ratios. $M = 10^3$.

the velocity in the inner side layer is still $O(M^{\frac{1}{2}})$ and carries a constant fraction of the $O(1)$ volume flux given by $(1+3/a)^{-1}$ [Walker, 1981]. Since for the square duct $a = 1$, in this range each side layer carries one-eight of the total flow. Similar considerations can be addressed for $M = 10^5$ in figure 3.14. In this case the thin wall approximation is valid for $10^{-5} \ll c \ll 1$, hence, the values of c equal to 0.05, 0.01 and 0.001 are again within this range. A wall conductance ratio of 0.001 corresponds to the case $c \approx 3M^{-\frac{1}{2}}$ ($\alpha \approx 3$) while the values 0.05 and 0.01 lie in the range $M^{-\frac{1}{2}} \ll c \ll 1$, previously discussed.

3.3 Laminar MHD Heat Transfer in a Square Duct

In Chapter 1 we mentioned that a successful design of self-cooled liquid metal blankets relies on the knowledge of MHD thermal hydraulic effects. This, in turn, implies the understanding of the heat transfer processes within the blanket's cooling ducts, where the coolant removes energy either in the form of surface heat flux (mainly from the

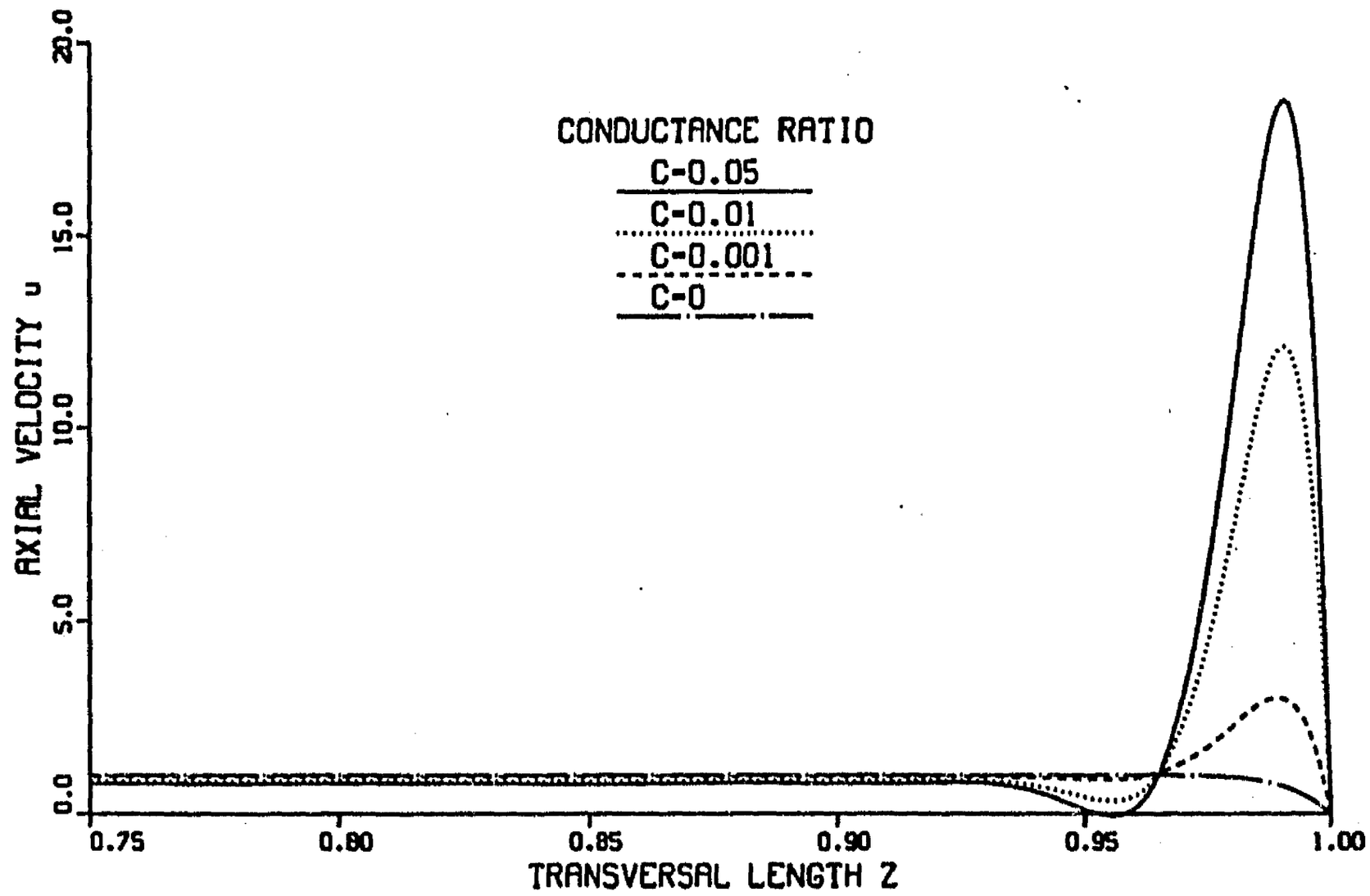

Figure 3.13: Laminar velocity vs. z at $y = 0$, for different wall conductances ratios. $M = 10^4$.

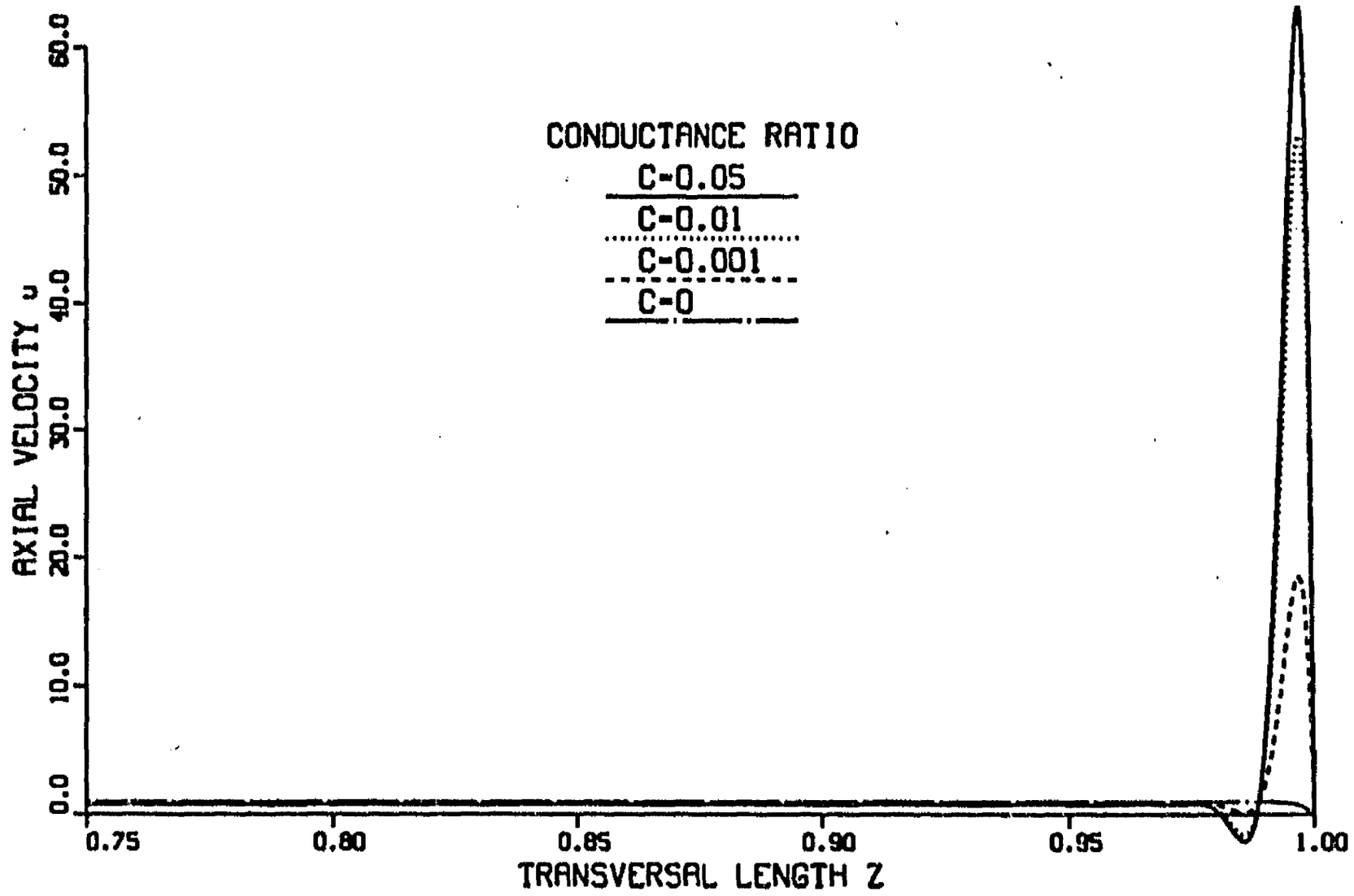

Figure 3.14: Laminar velocity vs. z at $y = 0$, for different wall conductances ratios. $M = 10^5$.

first wall) and volumetric energy deposition in the coolant itself. A first approach to the problem involves heat transfer calculations based on laminar forced convection. In order to accomplish this task, first, it is necessary to solve the MHD Navier-Stokes equations and obtain the velocity fields characteristic of flows in ducts with strong magnetic fields. This kind of flows were analyzed in the previous section. The second step involves the solution of the heat transfer equation with the previously calculated velocity fields. Evidently, the particular structure of these MHD flows will affect the heat transfer characteristics. As a matter of fact, since the MHD velocity fields present non-uniform flow distributions in the side layers, a three-dimensional heat transfer problem is originated. Hence, a suitable numerical method has to be provided for the solution of the heat transfer equation. In dimensional terms, the steady-state form of this equation in rectangular coordinates is

$$\rho c_p \left(u\frac{\partial T}{\partial x} + v\frac{\partial T}{\partial y} + w\frac{\partial T}{\partial z} \right) = \frac{\partial}{\partial x}\left(k_o \frac{\partial T}{\partial x} \right) + \frac{\partial}{\partial y}\left(k_o \frac{\partial T}{\partial y} \right) + \frac{\partial}{\partial z}\left(k_o \frac{\partial T}{\partial z} \right) + S, \tag{3.3}$$

where ρ, c_p and k_o are the density, specific heat and molecular thermal conductivity of the fluid, respectively; T is the temperature, u, v and w are the components of the velocity field $\mathbf{u}$, and S is a volumetric heat source. In a liquid-metal-cooled blanket, S represents the volumetric energy deposition due to neutron heating. Joule heating produced by induced electric currents circulating inside the liquid metal is also a heat source in the flow. However, it is negligible compared to neutron heating.

The heat transfer problem can be formulated as follows. Let us consider the steady-state laminar flow of a liquid metal inside a duct of constant rectangular cross-section immersed in an imposed transverse magnetic field. The physical properties of the fluid are assumed constant. In order to simulate heating of the first wall in a fusion blanket, a uniform surface heat flux is applied at the side wall at $z = 1$ from $x = 0$ to $x = x_h$, while the walls at $z = -1$ and at $y = \pm a$ remain adiabatic.[4] Figure 3.15 shows the schematic diagram of the problem.

The wall conductance ratio is the same for the four walls and ranges from 0.05 to 0, that is, from thin conducting to insulating walls. Since the flow is fully developed, $\mathbf{u} = (u(y,z),0,0)$. Hua and Picologlou [1989] presented two different methods of analysis for this MHD heat transfer problem, namely, the integral method and the explicit method. In the first one, the knowledge of the flow rate in the side layer is used to calculate the fraction of heat flux convected in this layer, the rest of the heat flux being conducted into the core across the layer/core interface. The boundary condition

[4]This is a restriction that can be easily removed. In general, we can consider a non-uniform surface heat flux depending on x and z.

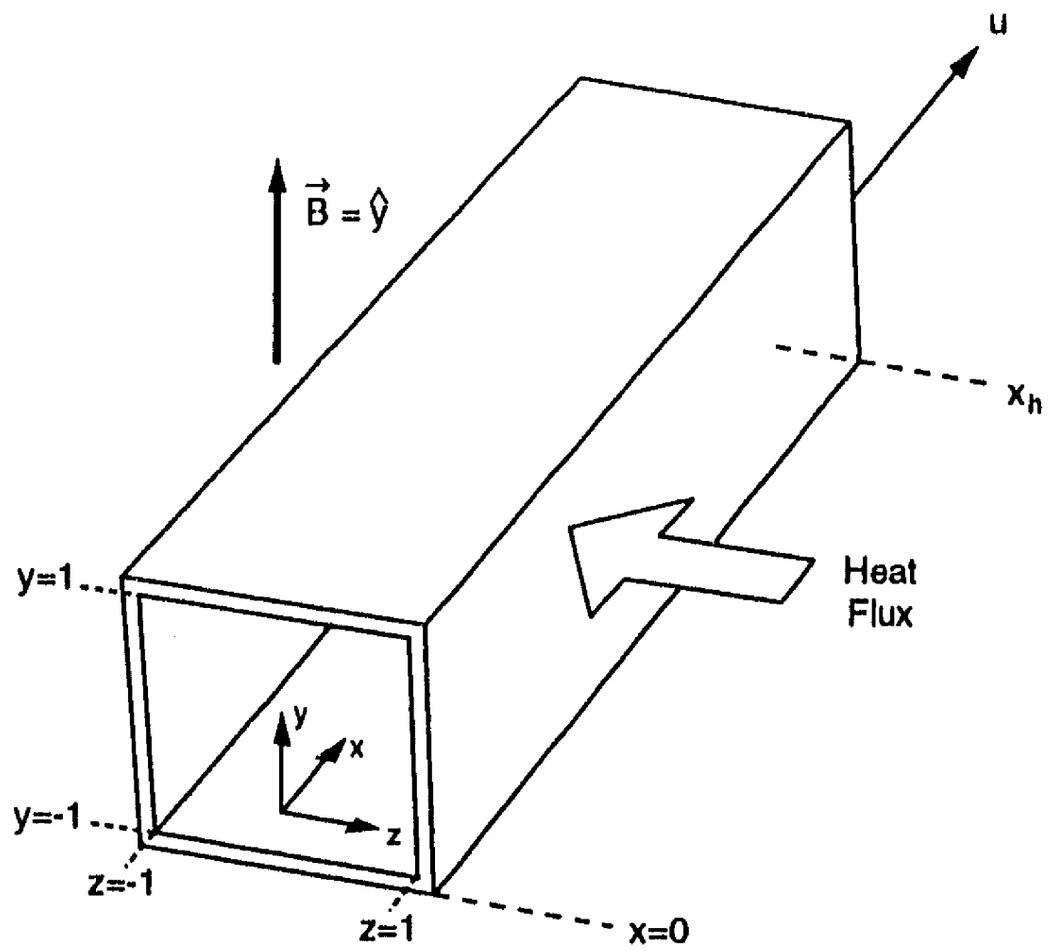

Figure 3.15: Schematic diagram of the heat transfer problem.

for the heated wall is derived from an energy balance across the side layer. This method can be applied when the volumetric flux and its distribution with y are known. However, with the integral method it is not possible to solve explicitly the conjugate problem which includes the temperature distribution inside the wall. On the other hand, as originally presented by Hua and Picologlou, the explicit method utilizes an analytical solution for the side layer flow and a solution for the inertialess, inviscid core. The boundary condition in the heated wall is simply expressed in a direct way. Since the formulation exposed in section 2.4 allows the calculation of a single core-side-layer solution, we will apply the explicit method and have the possibility of determining the temperature distribution at the wall. Nevertheless, in this work we assume an additional simplification, namely, the heated wall thickness is considered negligible for heat transfer purposes. So that, the temperature distribution inside this wall is not calculated and the (heated) wall temperature is considered to be the temperature at the boundary $z = 1$. For thin metal walls, this is a reasonable assumption. The calculation of the temperature distribution inside the wall is, actually, a straightforward generalization. In general terms, it can be said that the temperature distribution in the fluid and the wall will depend on the magnitude and distribution of the surface heat flux and volumetric energy deposition and on the value and structure of the velocity profile.

With the previous assumptions, the heat transfer equation and boundary conditions

of the problem, in dimensionless form, are[5]

$$Pe\ u\frac{\partial\Theta}{\partial x} = \frac{\partial^2\Theta}{\partial x^2} + \frac{\partial^2\Theta}{\partial y^2} + \frac{\partial^2\Theta}{\partial z^2} + S, \tag{3.4}$$

$$\frac{\partial\Theta}{\partial z} = 1 \quad z = 1, \quad -a \le y \le a, \quad 0 \le x \le x_h, \tag{3.5}$$

$$\frac{\partial\Theta}{\partial z} = 0 \quad z = -1, \quad -a \le y \le a, \quad 0 \le x \le x_h, \tag{3.6}$$

$$\frac{\partial\Theta}{\partial y} = 0 \quad y = \pm a, \quad -1 \le z \le 1, \quad 0 \le x \le x_h, \tag{3.7}$$

$$\Theta = 0 \quad x = 0, \quad -a \le y \le a, \quad -1 \le z \le 1, \tag{3.8}$$

where the dimensionless temperature Θ and the Péclet number Pe are defined as

$$\Theta = \frac{T - T_i}{q" L/k_o}, \quad Pe = \frac{\bar{U}L}{\alpha_o}. \tag{3.9}$$

respectively. The remaining variables are non-dimensionalized in the same way as in section 2.4. In equation (3.9), T_i is the fluid inlet temperature, $q"$ is the applied uniform surface heat flux and $\alpha_o = k_o/\rho c_p$ is the molecular thermal diffusivity. From its definition, we can see that Pe offers a relative measure of the effect of convection and diffusion transport mechanisms.

The system of equations (3.4)-(3.8) was solved using a finite difference method developed by Patankar [1980], with a power-law scheme to treat the convection-diffusion terms. Since the flow is symmetric with respect to the plane $y = 0$, we assumed that the heat transfer problem presents the same symmetry. Therefore, only the region $y \ge 0$ was considered in the computations. In order to perform the numerical calculations, the first step is the discretization of the three-dimensional domain into a non-uniform grid with finer meshes near the heated wall, to properly resolve the thermal boundary layer. The aforementioned system of partial differential equations is then transformed into an algebraic system of equations in the discretized variable Θ_i, where the subindex i denotes a certain grid point in a control volume. A three-dimensional finite difference algebraic equation is obtained by integration of equation (3.4) over a control volume centered at grid point P (see figure 3.16). The algebraic equation can be cast in the typical form

$$a_P\Theta_P = a_E\Theta_E + a_W\Theta_W + a_N\Theta_N + a_T\Theta_B + a_B\Theta_B + b. \tag{3.10}$$

[5]Here, again, we droped the $*$ in order to simplify the notation.

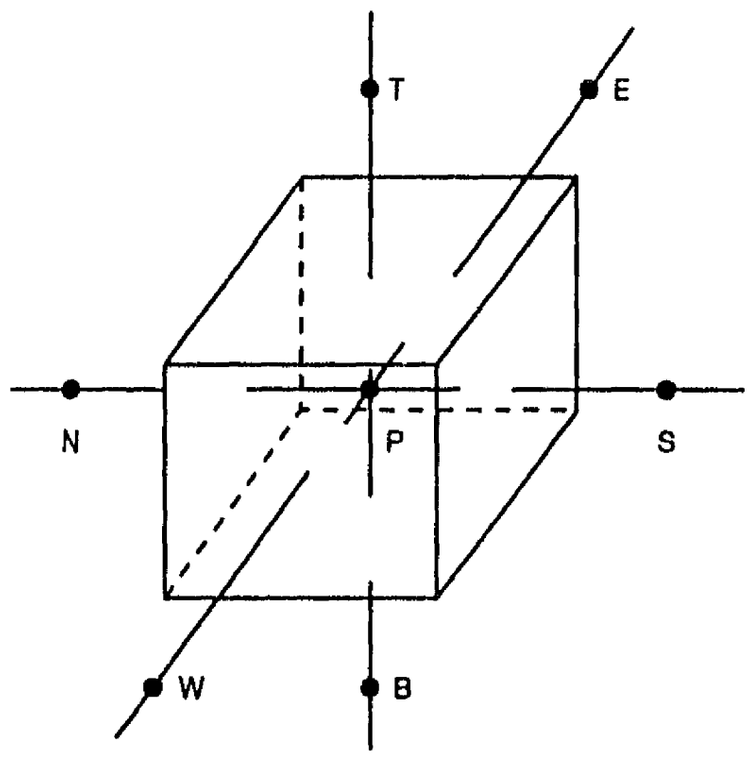

Figure 3.16: Three-dimensional control volume for finite difference integration.

The coefficients a_E, a_W, a_N, a_S, a_T and a_W, carry the information on the convection and conduction effects at the six faces of the control volume, while the term b represents the influence of the volumetric heat source.
Near the boundaries a half control volume is used, and boundary conditions provide additional information to get the required number of equations for the unknown temperatures. The solution of the algebraic system of equations was obtained through the Gauss-Seidel point-by-point method with over-relaxation In this very well known iterative method, starting from a guessed field Θ_i, the values of the variables are calculated by visiting each grid point in a certain order, altering the corresponding value of Θ in a prescribed way until convergence is reached [Patankar, 1980]. At the beginning of subsections 3.3.1 and 3.3.2, validation of the numerical method will be performed through comparison with analytical solutions for fully developed slug flow for square and cylindrical ducts, respectively.

3.3.1 Numerical Results

Carslaw and Jaeger [1959] obtained an analytical solution for the temperature distribution in a slab with prescribed uniform heat flux at its surface, in absence of volumetric heat sources. With a suitable variable transformation, this solution can be translated into the temperature distribution in a fluid with slug flow inside a rectangular duct with negligible wall thickness and prescribed uniform surface heat flux. Since, by definition, for slug flow the whole flow is in the core ($u = 1$, $v = w = 0$), the problem

becomes two-dimensional, disappearing the y-dependence. In addition, the Carslaw and Jaeger solution neglects axial heat conduction and assumes that the heat flux is applied at $z = 1$ from $x = 0$ to $x = x_h \to \infty$. In terms of our dimensionless variables, this solution can be expressed as

$$\begin{aligned}\Theta(x,z) &= 2\sqrt{\frac{x}{Pe}}\sum_{n=0}^{\infty}\left\{\frac{1}{\pi}\exp\left[-\frac{((2n+1)-z)^2}{4x/Pe}\right]\right. \\ &\quad -\frac{(2n+1)-z}{2\sqrt{x/Pe}}\mathrm{erfc}\frac{(2n+1)-z}{2\sqrt{x/Pe}} + \frac{1}{\pi}\exp\left[-\frac{((2n+1)+z)^2}{4x/Pe}\right] \\ &\quad \left. -\frac{(2n+1)+z}{2\sqrt{x/Pe}}\mathrm{erfc}\frac{(2n+1)+z}{2\sqrt{x/Pe}}\right\}. \qquad (3.11)\end{aligned}$$

At the heated wall $z = 1$, the first terms of the series expansion of equation (3.11) can be written as

$$\begin{aligned}\Theta(x,1) &= 2\left\{\sqrt{\frac{x}{\pi Pe}}\left[1 + 2\exp\left(-\frac{1}{x/Pe}\right) + \exp\left(-\frac{4}{x/Pe}\right) + \ldots\right]\right. \\ &\quad \left. + \left[2\mathrm{erfc}\frac{1}{\sqrt{x/Pe}} + 2\mathrm{erfc}\frac{2}{\sqrt{x/Pe}} + \ldots\right]\right\}. \qquad (3.12)\end{aligned}$$

Figure 3.17 presents the comparison of the wall temperature given by equation (3.12) against the finite difference solution of the system (3.4)-(3.8), properly modified by the simplifications already mentioned but including axial heat conduction. The former figure shows the comparison for three different Péclet numbers, namely, 250, 500 and 2500 and for $x_h = 50$. The numerical solution was obtained using a non-uniform mesh of 30×30 with finer meshes in the z-direction near the heated wall. The agreement between the numerical and analytical solutions is very good even though the numerical one includes axial conduction. This indicates that for slug flow with uniform surface heat flux, axial heat conduction has a negligible effect on the temperature distribution provided the Péclet number is high enough. In this as well as in all numerical calculations, the conservation of energy was verified.

In section 3.2 we showed that in the presence of strong magnetic fields, fully developed velocity profiles in square (rectangular) ducts tend to be very flat with very thin boundary layers.[6] This characteristic allows that, as a preliminary step, heat transfer calculations for liquid-metal-cooled blankets can be performed assuming slug flow. Evidently, this approach disregards the MHD boundary layers that, under certain conditions, can carry a significant fraction of the total flow and affect positively the

[6] Actually, this is also valid for ducts with circular cross-section.

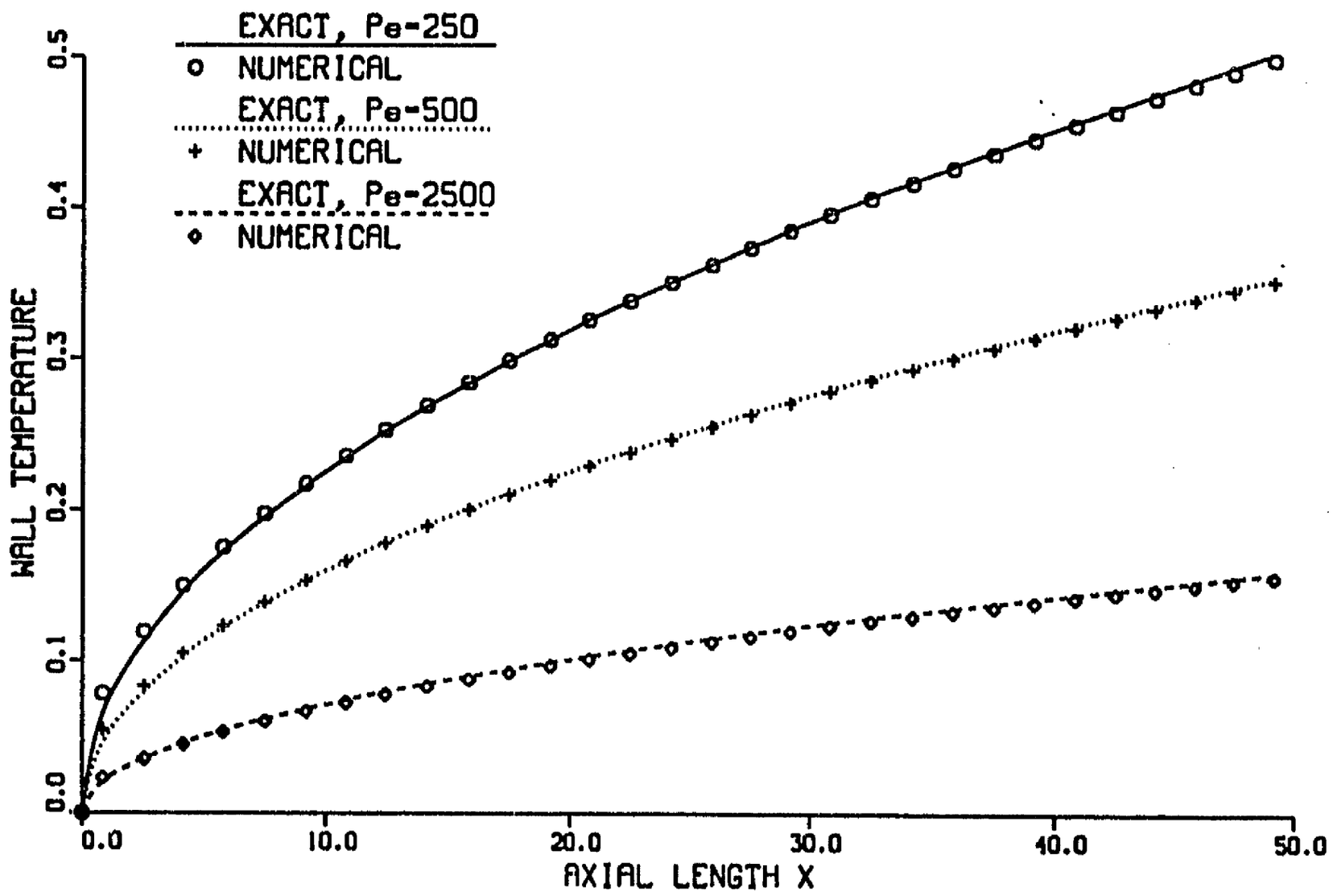

Figure 3.17: Comparison of finite differences and analytical wall temperature profiles with slug flow, for different Péclet numbers.

heat transfer process. However, even though the results obtained with slug flow may be conservative, they offer a reference point for the calculations performed with MHD velocity profiles and give a simple way of calculating some practical heat transfer parameters [Picologlou, 1992a]. In many of the figures that we will present below, results for slug flow are also shown for comparison purposes. The Péclet numbers used in the numerical calculations are 250, 500 and 2500, which correspond to average velocities of 0.1, 0.2 and 1.0 m/s, respectively, for the flow of liquid lithium in a duct with a characteristic length of 0.4 m. Actually, the Péclet number in a fusion reactor first wall coolant channel ranges typically from 10^2 to 10^3. The calculations presented here were performed in absence of volumetric heat sources but their inclusion is a straightforward extension that can be easily incorporated in the numerical code. Since the wall temperature is an important design parameter, special emphasis is given to its analysis in the results presented here.

Figure 3.18 shows the axial variation of the wall temperature at the plane $y = 0$, obtained with a thin-conducting wall duct velocity profile (that corresponding to fig. 3.4), where $M = 10^3$ and $c = 0.05$. The numerical calculations were accomplished for three different Péclet numbers using a three-dimensional non-uniform grid of $30 \times 30 \times 30$. In this figure, the effect of Pe on the wall temperature distribution resulting from the uniform surface heat flux is clearly shown. Evidently, for a given velocity profile, the larger the Péclet number, the more efficient the heat removal and the lower the wall temperature. The same results are shown in figure 3.19 but in a different useful form, namely, the local Nusselt number, Nu, as a function of the axial direction. Nu, also known as the local heat transfer coefficient, is defined here as

$$Nu = \frac{1}{\Theta_w - \Theta_B} \tag{3.13}$$

where Θ_w is the wall temperature and

$$\Theta_B(x) = \frac{\int_0^1 \int_{-1}^1 \Theta(x,y,z)u(y,z)dydz}{\int_0^1 \int_{-1}^1 u(y,z)dydz} \tag{3.14}$$

is the bulk temperature. In figure 3.19, the higher heat transfer coefficient corresponds to the higher Péclet number.

Figure 3.20 shows the wall temperature at different y-positions using the same velocity profile ($M = 10^3, c = 0.05$) with $Pe = 500$. The effect of the parabolic distribution of the side layer flow with the y-coordinate is clearly shown here. The temperature corresponding to the mid-plane $y = 0$, where the flow is more intense, is lower than the temperature corresponding to positions near the top wall, where the flow is substantially reduced. As we mentioned before, at the top wall $y = 1$ there is no flow in the side layer and, as a consequence, the wall temperature reaches its maximum. Since our core-side-layer solution does not satisfy the non-slip condition at $y = 1$, we can not calculate the (heated) wall temperature exactly at the top wall but we can

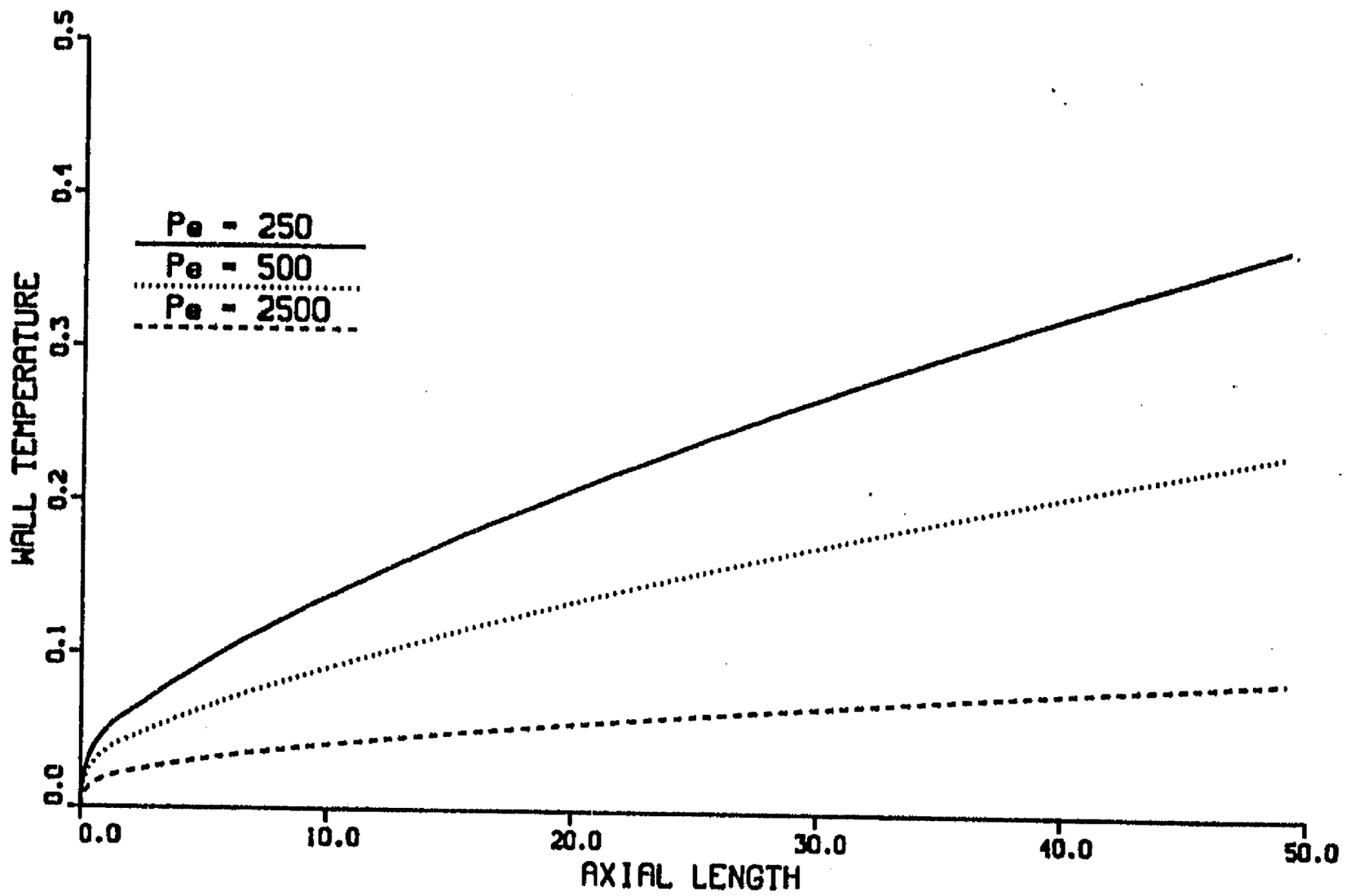

Figure 3.18: Wall temperature vs. x at $y = 0$, for different Péclet numbers. $M = 10^3$, $c = 0.05$.

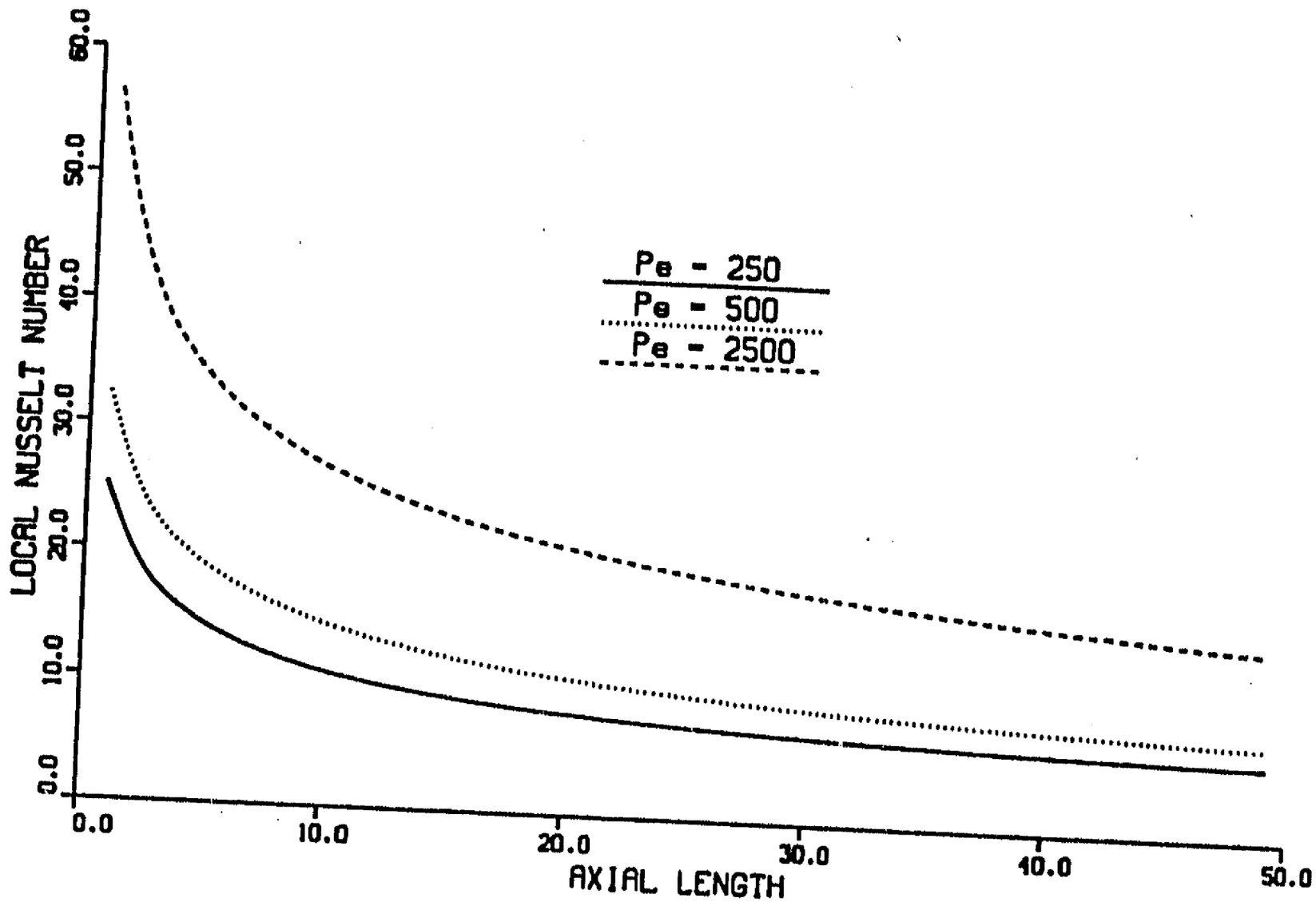

Figure 3.19: Local Nusselt number vs. x for different Péclet numbers. $M = 10^3$, $c = 0.05$.

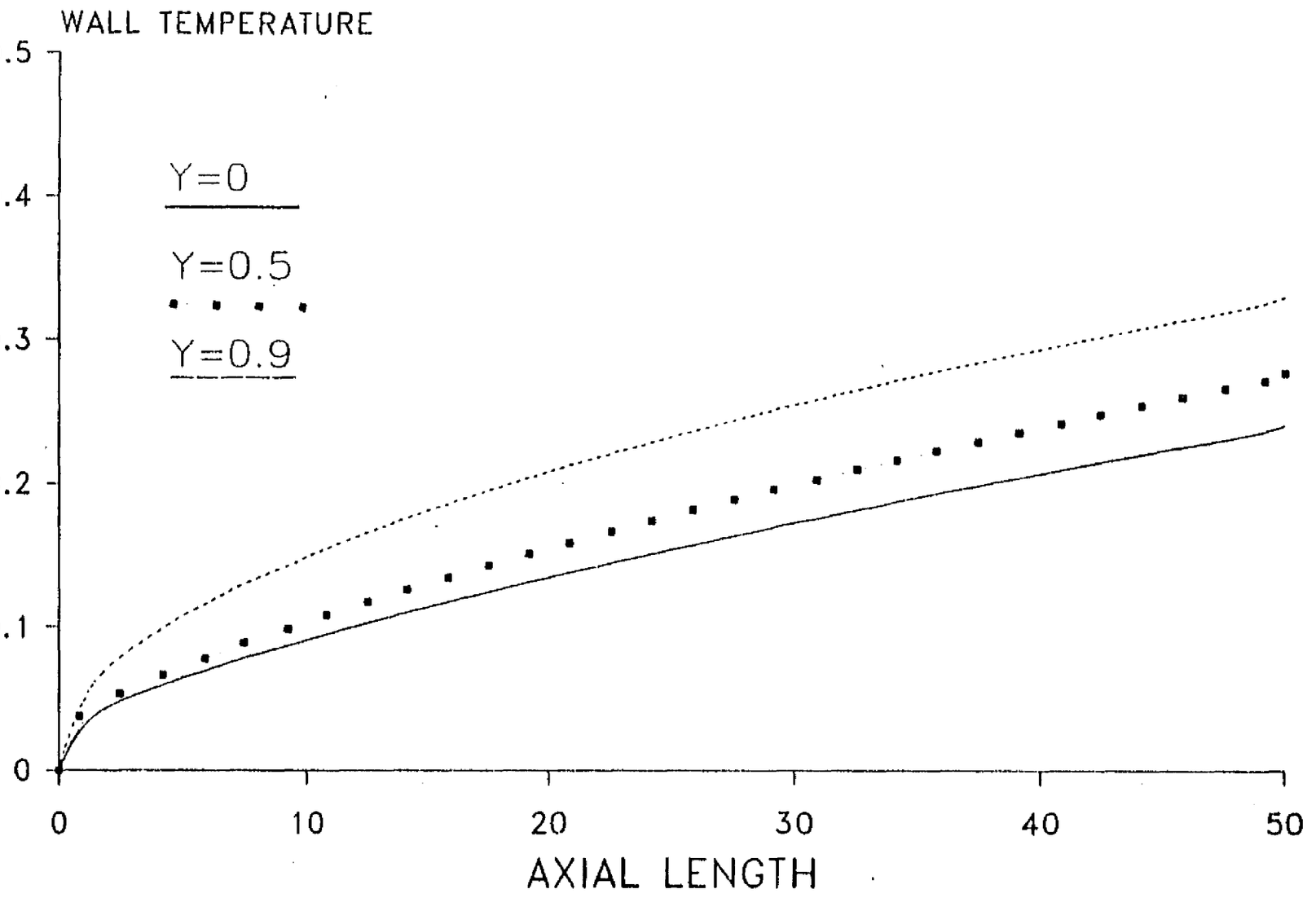

Figure 3.20: Wall temperature vs. x at different y-positions. $M = 10^3$, $c = 0.05$, $Pe = 500$.

get a very good estimate at positions very close to that wall ($> O(M^{-1})$). Figure 3.21 presents the temperature distribution in the mid-plane, as a function of the transversal z-coordinate at three different axial positions for $Pe = 500$, using the velocity profile shown in figure 3.4. In figure 3.21 we can appreciate the growth of the thermal boundary layer thickness in the downstream direction. At the three axial positions, $x = 10, 30, 50$, the dimensionless temperature decreases from its high value at the wall $z = 1$, to zero at the core, before reaching the plane $z = 0$. In other words, the thermal boundary layer thickness is less than the characteristic dimension of the channel and, therefore, the presence of the wall opposite to the heated wall is irrelevant. In cases where this occurs, it is only necessary to solve the heat transfer equation in a quarter-duct ($0 \leq y \leq 1$, $0 \leq z \leq 1$) which greatly simplifies the computational work. Estimations based on slug flow with uniform surface heat flux, indicate that this is the case for most cases of interest in liquid-metal blanket flows [Picologlou, 1992a].

Figure 3.22 and 3.23 are similar to figures 3.18 and 3.21 but were calculated with an insulating wall duct velocity profile, namely, for $c = 0$ and the same Hartmann number, $M = 10^3$. We observe that the wall temperatures for the insulating duct

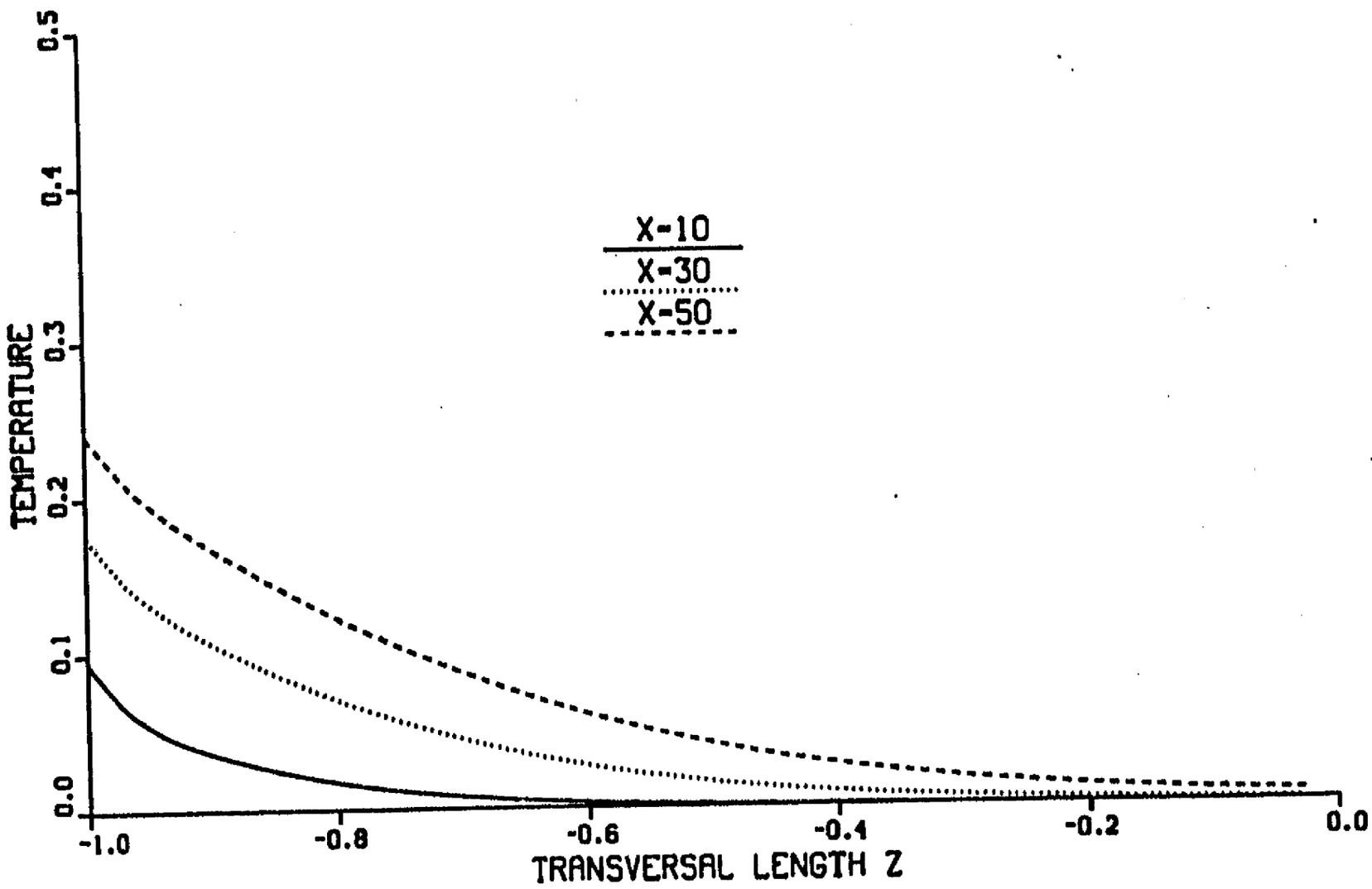

Figure 3.21: Temperature vs. z at $y = 0$, for different axial positions. $M = 10^3$, $c = 0.05$, $Pe = 500$.

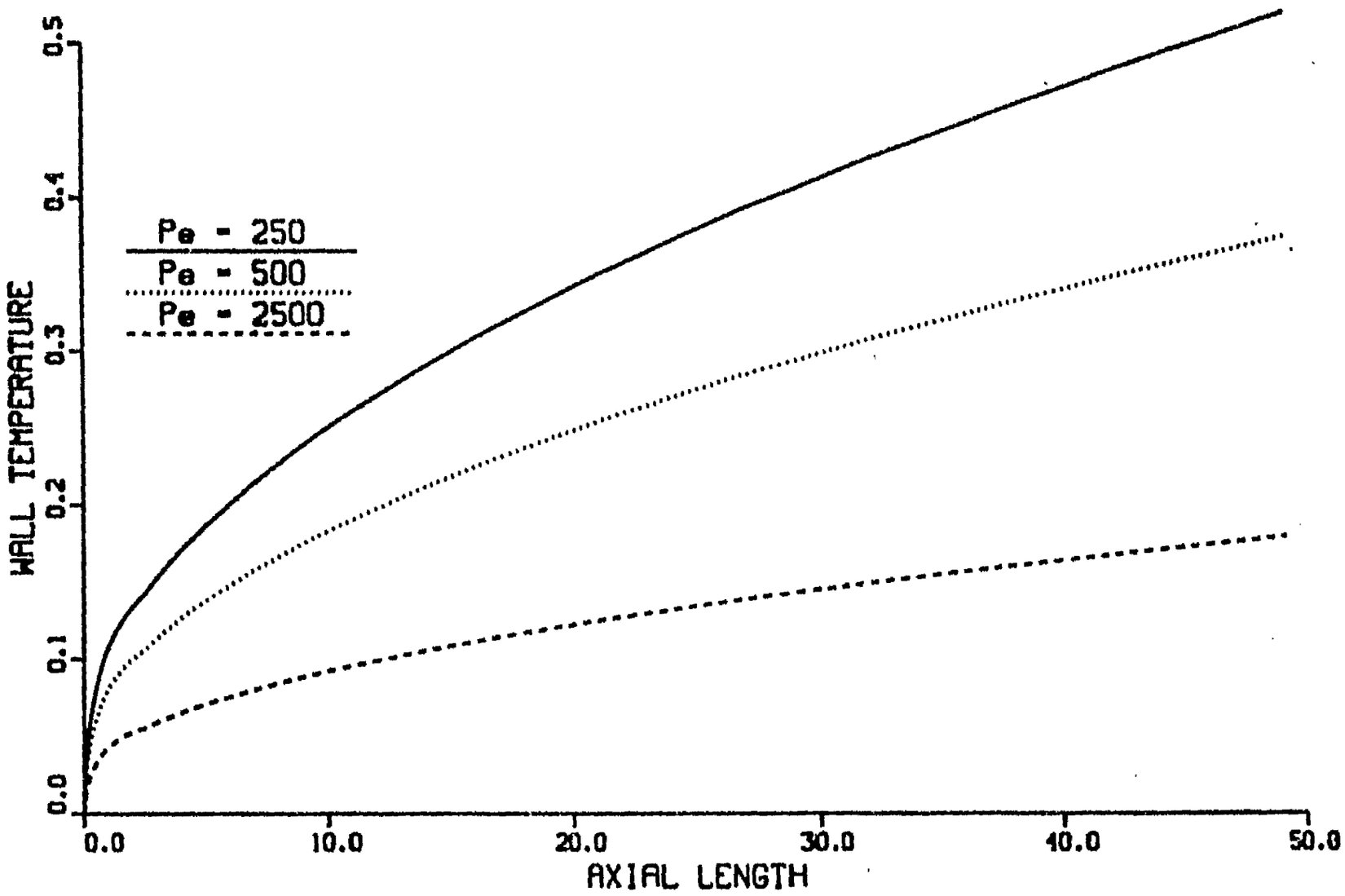

Figure 3.22: Wall temperature vs. x at $y = 0$, for different Péclet numbers. $M = 10^3$, $c = 0$, $Pe = 500$.

(figure 3.22) are higher than those for the thin-conducting wall duct (figure 3.18), for corresponding Péclet numbers. While in the insulating case the side layer velocity is $O(1)$, in the thin-conducting case the side layer velocity is $O(M^{\frac{1}{2}})$ and carries a fraction of the $O(1)$ volume flux. This characteristic allows a more efficient heat removal in the side layer and, as a consequence, a lower wall temperature. In figure 3.23, the thermal boundary layer for the insulating duct shows a similar behavior with respect to that of the thin-conducting wall duct (figure 3.21). In both cases, the thermal boundary layer does not cross the plane $z = 0$,[7] although in the insulating case, the wall temperature is higher and the temperature decrease is steeper than in the thin-conducting case.

The effect of the Hartmann number on the wall temperature in the mid-plane ($y = 0$) is presented in figures 3.24 and 3.25, for the thin conducting ($c = 0.05$) and insulating ($c = 0$) wall cases, respectively. Both cases correspond to $Pe = 500$; the wall

[7]At the end of the duct, $x = 50$, the temperature is slightly different from zero but for practical purposes, it can be considered that the temperature tends to zero inside the duct before reaching the plane $z = 0$.

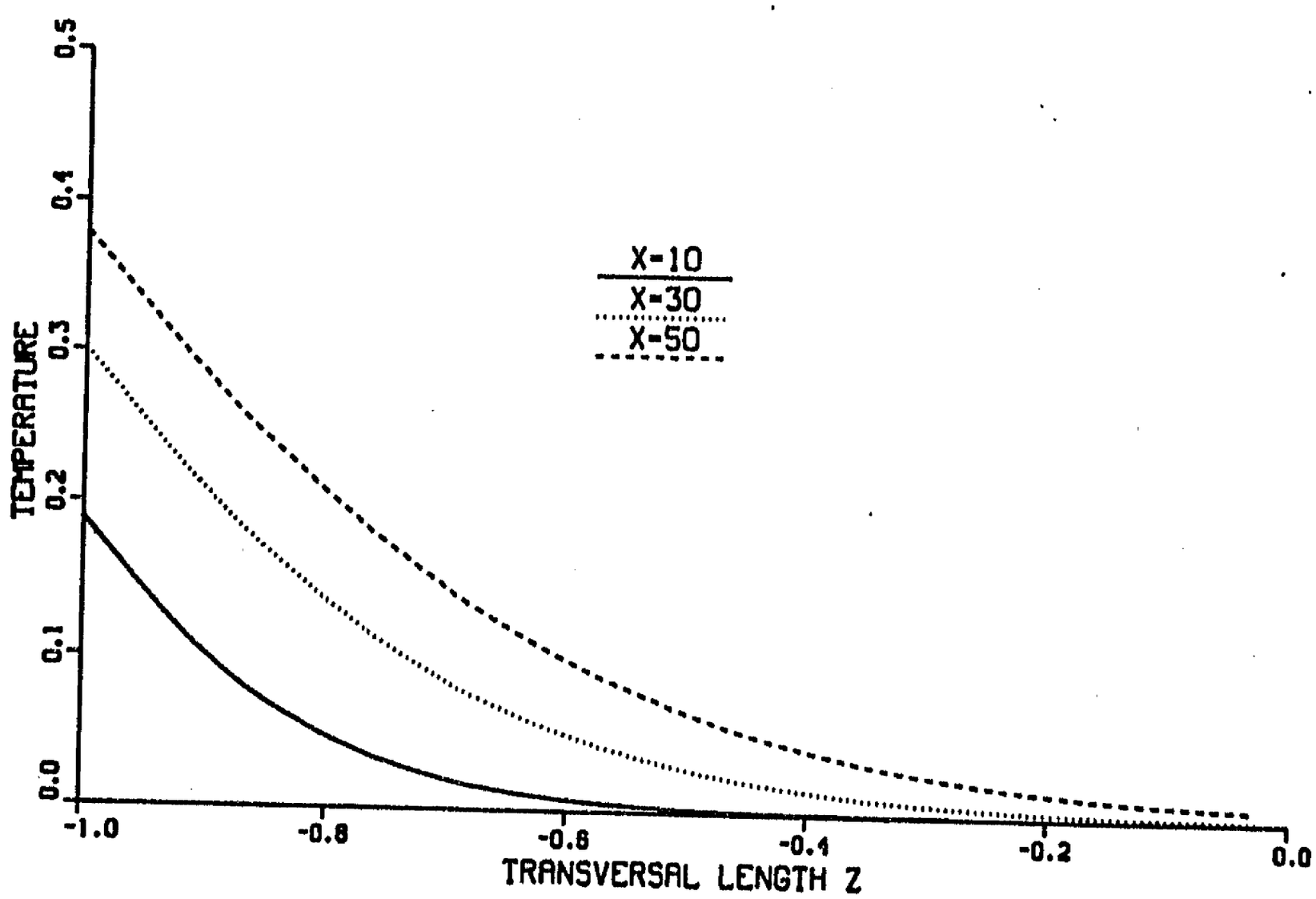

Figure 3.23: Temperature vs. z at $y = 0$, for different axial positions. $M = 10^3$, $c = 0$, $Pe = 500$.

temperature profile for slug flow is shown as a reference. In the thin conducting case, a drastic reduction in the wall temperature, relative to slug flow, is obtained with the MHD velocity profiles. For the three M values, the side layer carries a fraction of the $O(1)$ volume flux and the beneficial heat transfer effect of this property is clearly shown in figure 3.24. The higher the Hartmann number, the lower the wall temperature. The difference in wall temperatures for flows with $M = 10^3$ and $M = 10^5$ is marked, as it is the difference in their side layer velocities (see figure 3.7). By contrast, MHD wall temperature profiles shown in figure 3.25 for the insulating wall case present essentially no difference with respect to the wall temperature obtained with slug flow. Actually, the wall temperature profile for $M = 10^3$ is slightly higher than that of slug flow, while profiles for $M = 10^4$ and $M = 10^5$, remain close to it. As it was shown in figure 3.10, the velocity profile for an insulating duct for $M = 10^5$, approaches closely to slug flow. Figures 3.26 and 3.27 show basically the same results of figures 3.24 and 3.25 but for a higher Péclet number, namely, $Pe = 2500$. It can be observed that the trends remain the same, while there is a global decrease in wall temperatures as a result of the stronger forced convection mechanism.

Figures 3.28, 3.29 and 3.30 show the transition of the wall temperature from thin conducting to insulating wall duct case, for Hartmann numbers 10^3, 10^4 and 10^5, respectively. Temperature profiles correspond to $y = 0$ and the Péclet number is 500. Again, results for slug flow are shown for comparison purposes. The velocity profiles corresponding to the former temperature profiles were shown in figures 3.12, 3.13 and 3.14, respectively. The general trend shown in figures 3.28-3.30 is that an increase in the wall conductance ratio from the insulating value $c = 0$ to the thin conducting value $c = 0.05$, causes a reduction in the wall temperature, for a given Hartmann number. This is a consequence of the appearance of side wall jets in thin conducting wall ducts, which improves the heat transfer in the side layer. For $M = 10^3$ (figure 3.28), the wall temperature for $c = 0$ is even higher than that of slug flow. In other words, for this Hartmann number the heat removal is more efficient with slug flow than with the insulating velocity profile, which presents a defect flow in the side layer. The curve for $c = 0.001$ almost coincides with that for slug flow while thin conducting curves, $c = 0.01$ and $c = 0.05$, are considerably lower than the latter. For $M = 10^4$ (figure 3.29), the curves for the insulating case and slug flow come very close, and even the wall temperature profile for $c = 0.001$ remains below the slug flow profile. Remember that, for this M, the velocity profile for $c = 0.001$ presents an overshoot in the side layer (see figure 3.7), although the layer does not carry a fraction of the $O(1)$ volume flux. For the highest Hartmann number considered, $M = 10^5$ (see figure 3.30), the agreement of the insulating case with the slug flow case is almost perfect. The additional three curves correspond to thin conducting cases, and even for a wall conductance ratio as low as $c = 0.001$, there is a notorious decrease in the wall temperature with respect to the slug flow temperature. Also notice that there is only a slight difference between the curves $c = 0.01$ and $c = 0.05$.

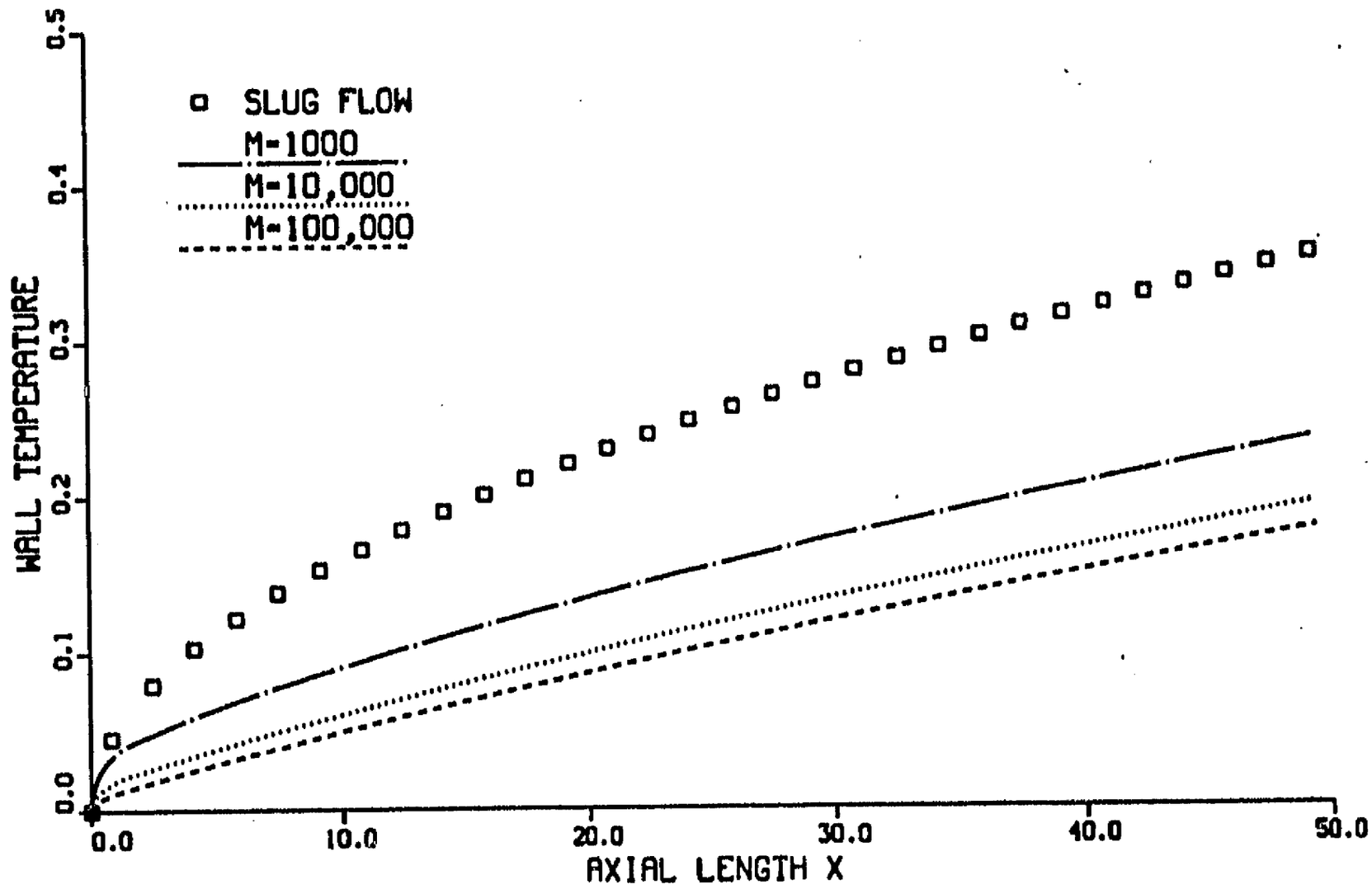

Figure 3.24: Wall temperature vs. x at $y = 0$, with slug and MHD flows for different Hartmann numbers. $c = 0.05$, $Pe = 500$.

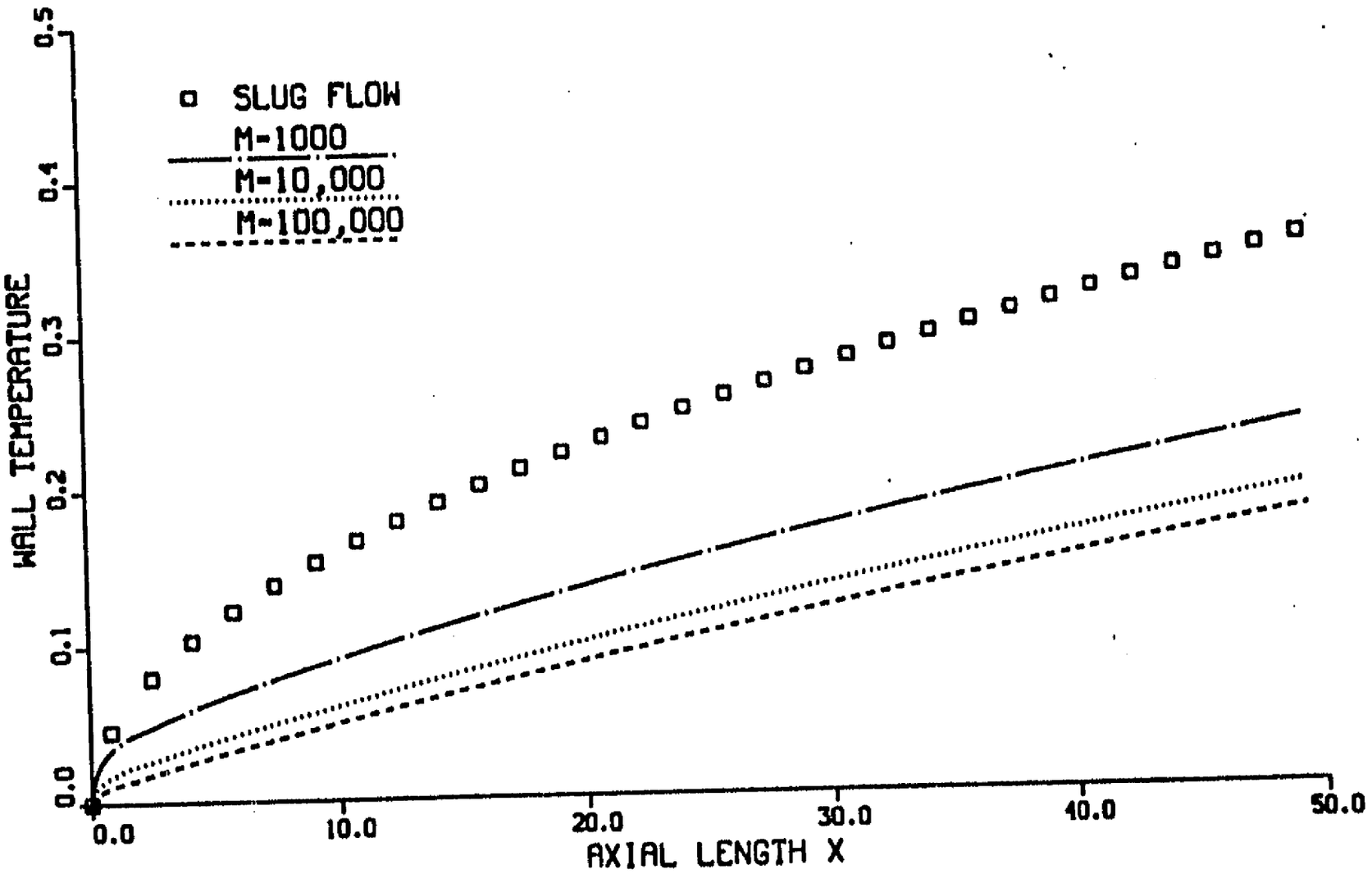

Figure 3.24: Wall temperature vs. x at $y = 0$, with slug and MHD flows for different Hartmann numbers. $c = 0.05$, $Pe = 500$.

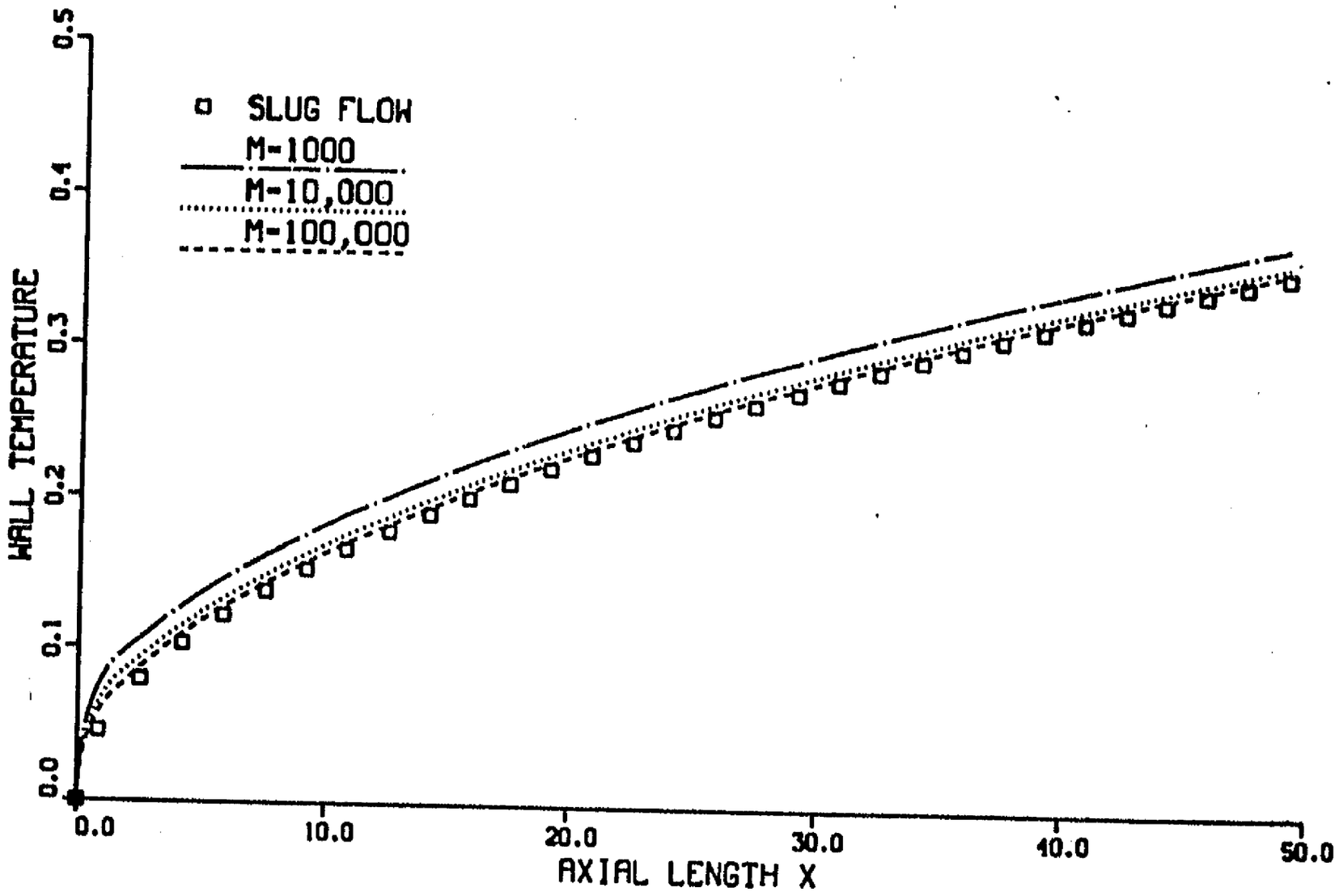

Figure 3.25: Wall temperature vs. x at $y = 0$, with slug and MHD flows for different Hartmann numbers. $c = 0$, $Pe = 500$.

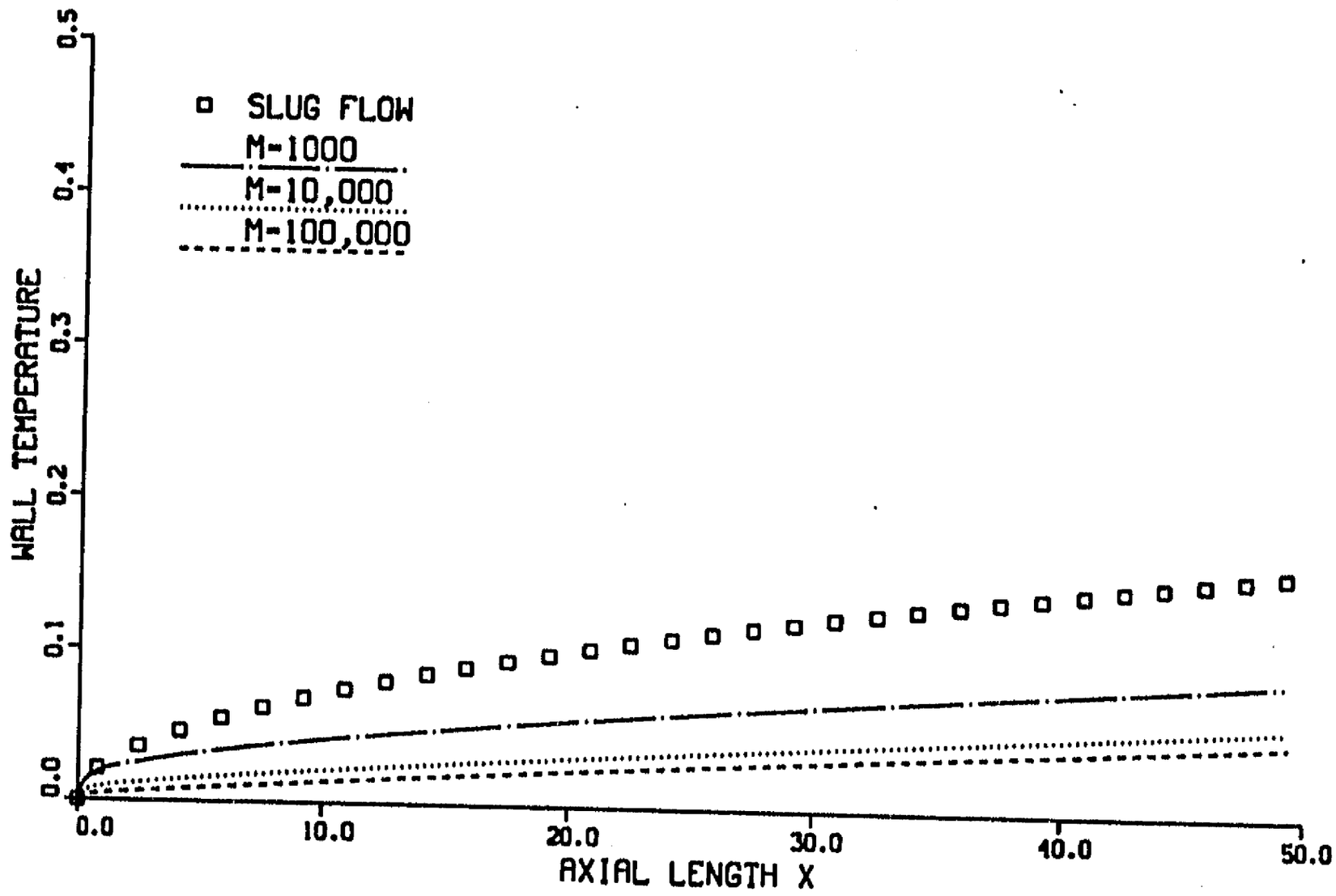

Figure 3.26: Wall temperature vs. x at $y = 0$, with slug and MHD flows for different Hartmann numbers. $c = 0.05$, $Pe = 2500$.

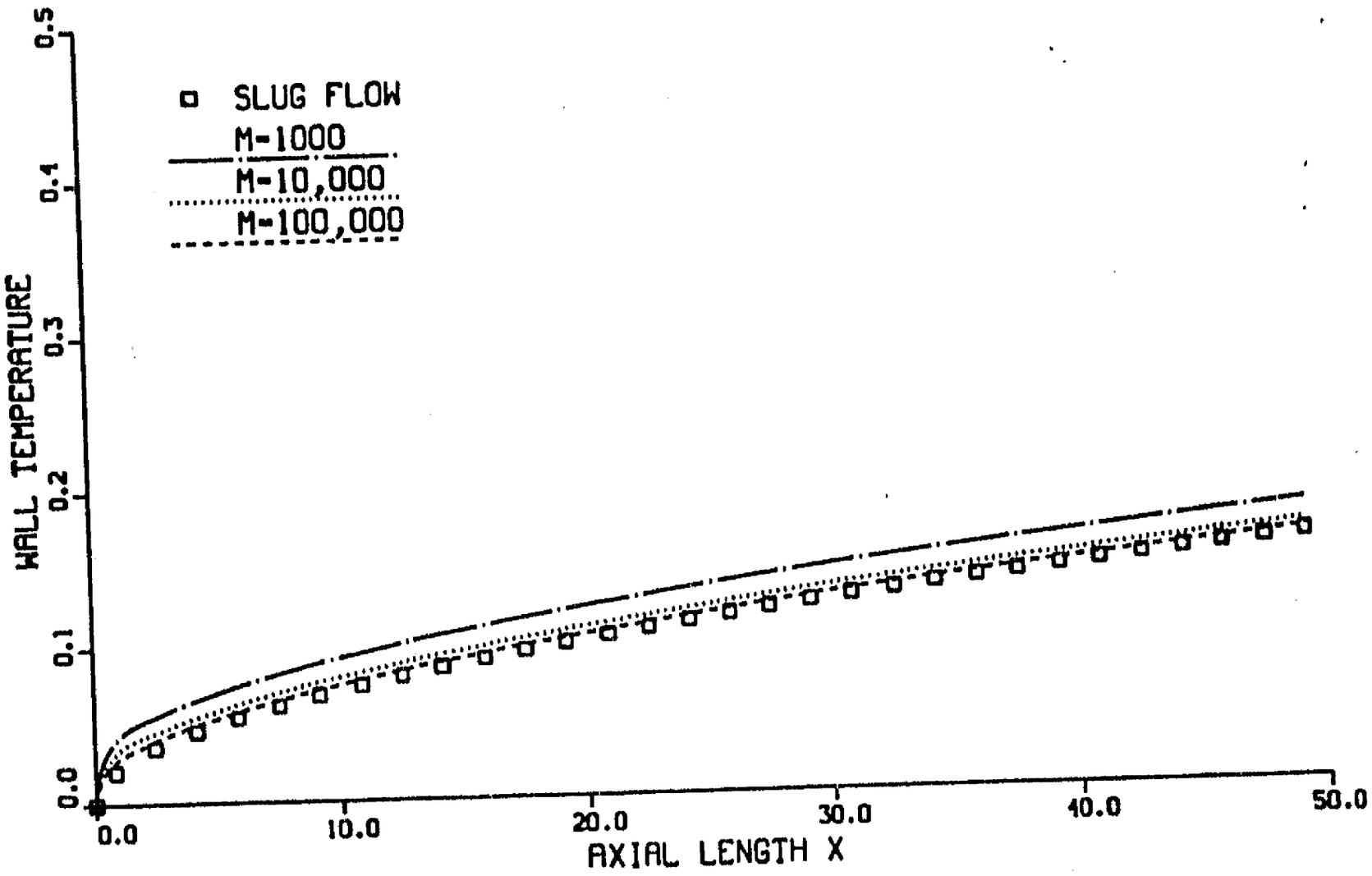

Figure 3.27: Wall temperature vs. x at $y = 0$, with slug and MHD flows for different Hartmann numbers. $c = 0$, $Pe = 2500$.

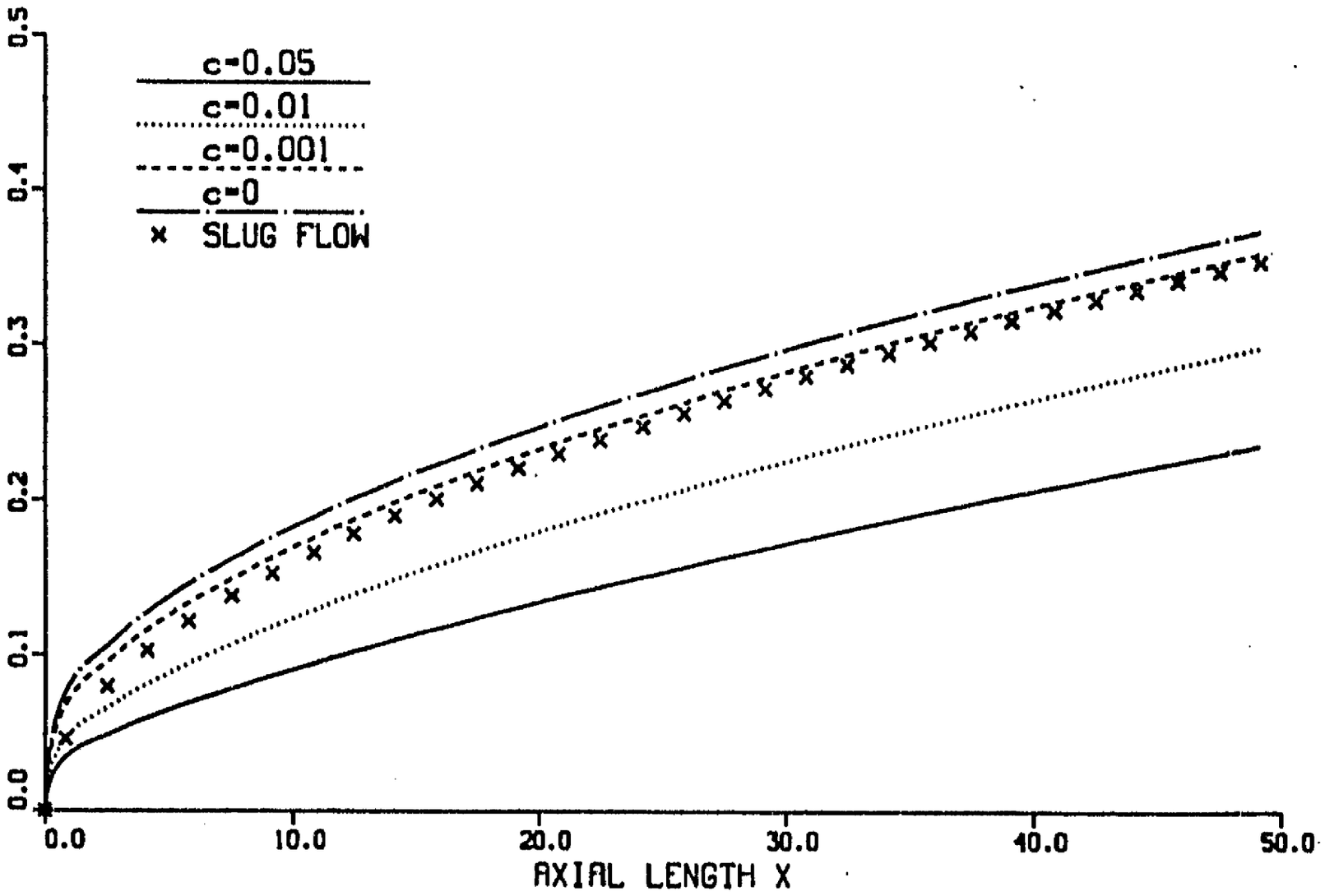

Figure 3.28: Wall temperature vs. x at $y = 0$, with slug and MHD flows for different wall conductance ratios. $M = 10^3$, $Pe = 500$.

Previous results reveal that, for insulating ducts, heat transfer analysis performed with slug flow can be considered a realistic approach at high Hartmann numbers. On the other hand, thin conducting cases where the side layer carries a fraction of the volume flux can considerably improve the heat transfer in the side layer and drastically reduce the wall temperature. For this latter cases, computations based on slug flow may overestimate the actual wall temperature.

3.4 Laminar Heat Transfer in a Cylindrical Duct

Among different fusion reactor liquid-metal-cooled blanket designs, the use of cylindrical cooling ducts has also been considered. From the mechanical stresses point of view, cylindrical ducts present a better option than rectangular ducts. In particular, electrically insulated cylindrical ducts present suitable characteristics. Hence, the heat transfer analysis of liquid metal flows in this kind of ducts is of practical interest. With this aim, the finite difference heat transfer code was extended to consider also

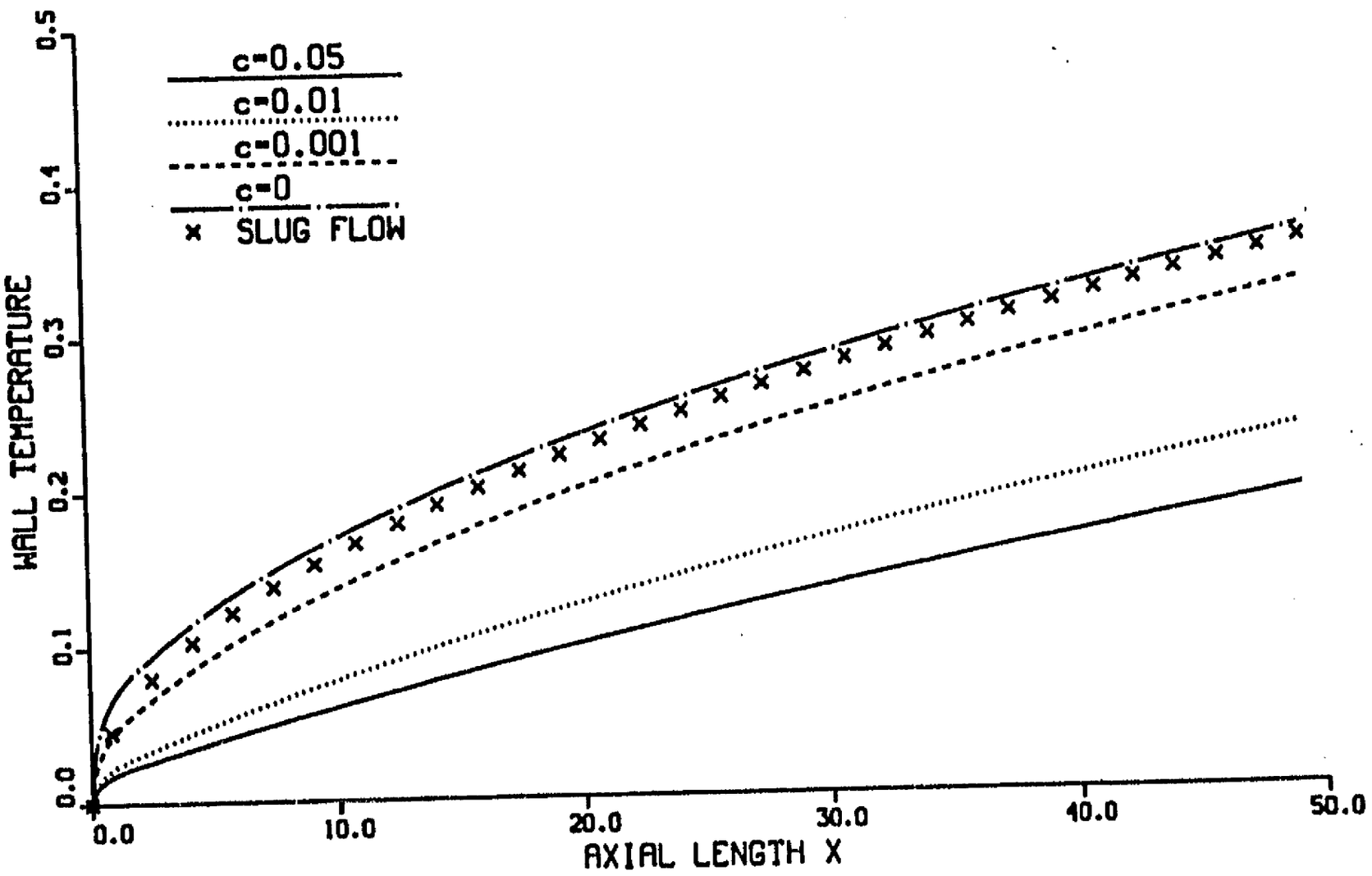

Figure 3.29: Wall temperature vs. x at $y = 0$, with slug and MHD flows for different wall conductance ratios. $M = 10^4$, $Pe = 500$.

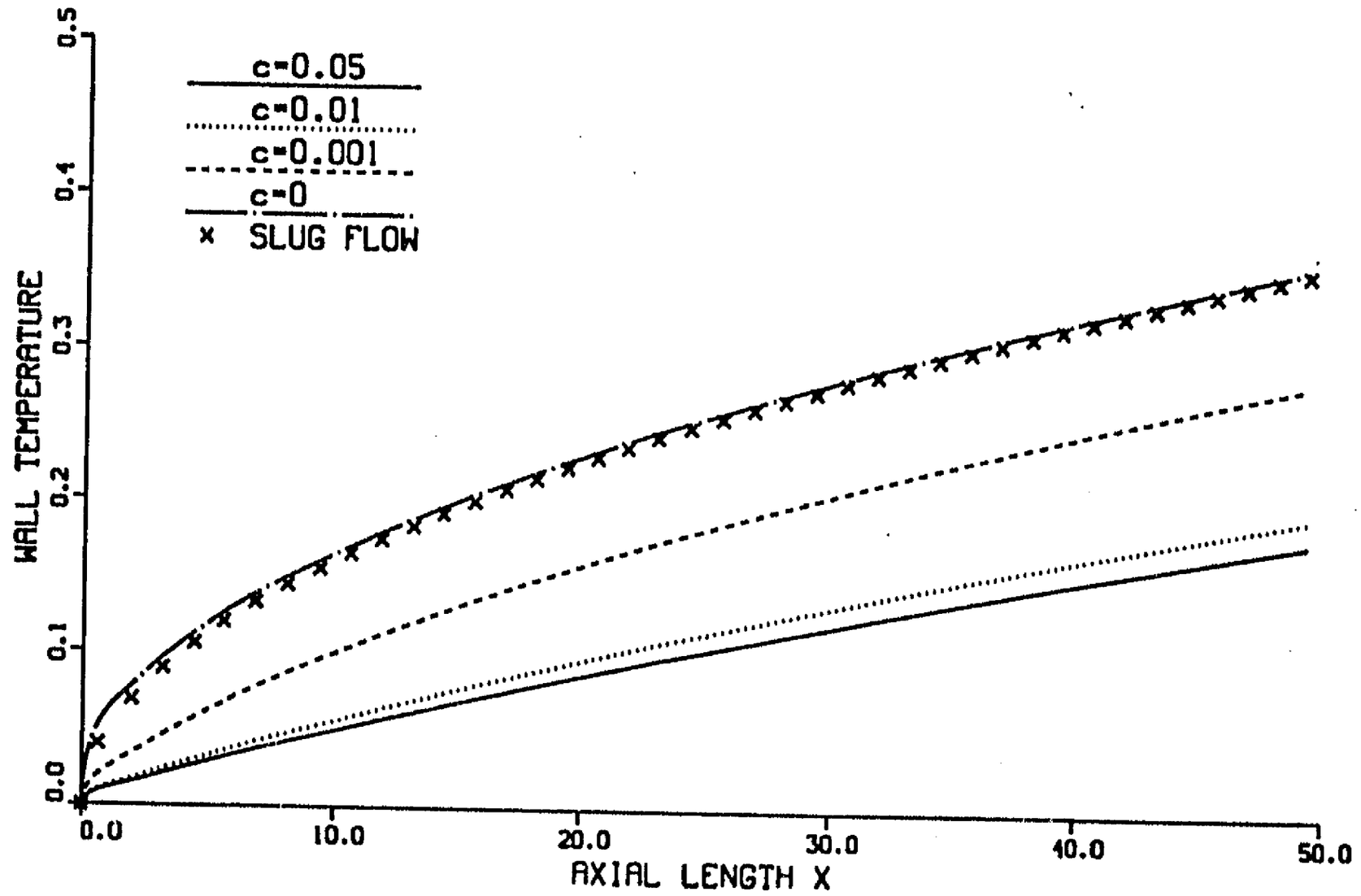

Figure 3.30: Wall temperature vs. x at $y = 0$, with slug and MHD flows for different wall conductance ratios. $M = 10^5$, $Pe = 500$.

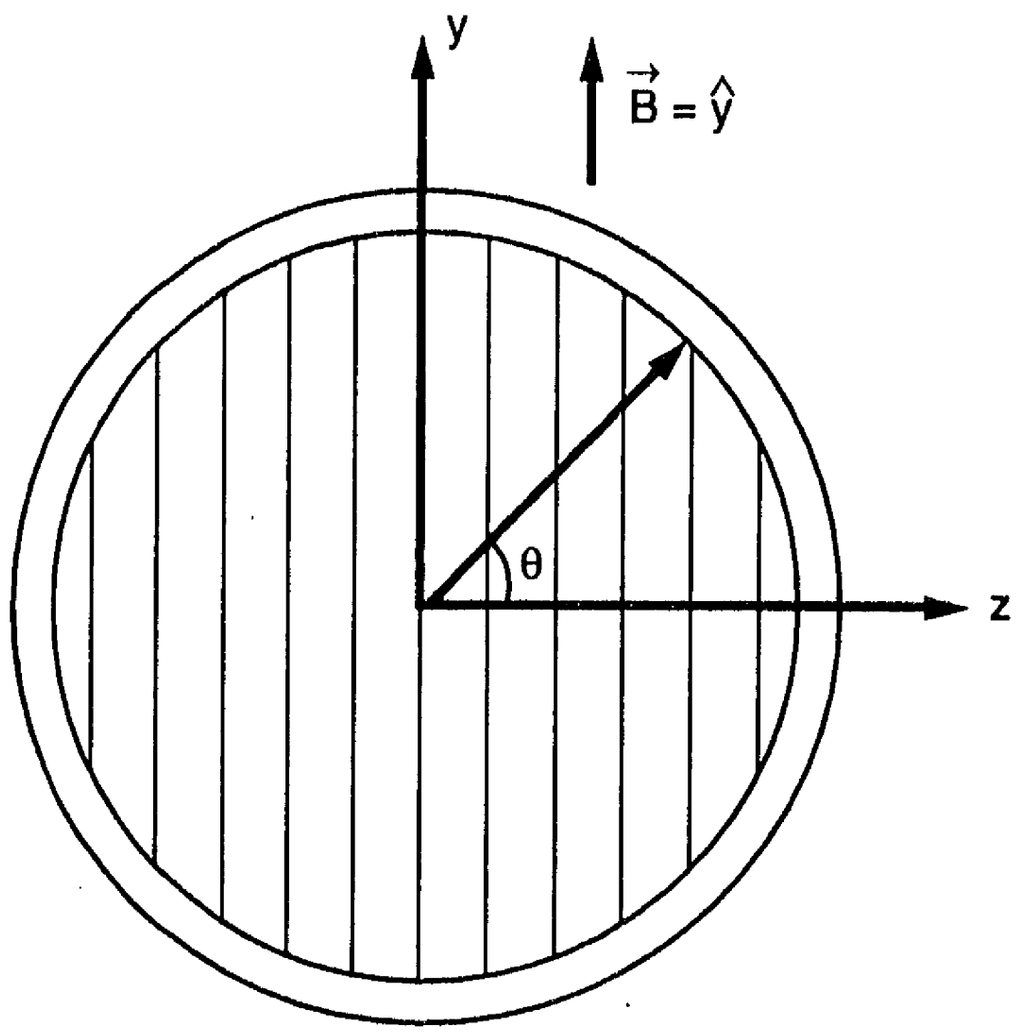

Figure 3.31: Stream lines in a cylindrical duct flow at $M \gg 1$.

cylindrical geometry.

As in the rectangular duct case, the velocity profile in cylindrical ducts is flattened under the action of a strong transverse magnetic field. Therefore, the use of slug flow in heat transfer calculations can also in this case be a reasonable approximation. Strictly, in fully developed flows, $\mathbf{u} = (u(r,\theta),0,0)$, and the degree of flattening presents an angular dependence. Gold [1962] obtained, analytically, the steady laminar velocity profile of a conducting fluid in an electrically insulated cylindrical duct immersed in transverse magnetic field. From this solution, it can be shown that, in the limit of very high Hartmann numbers, the stream lines aligned in the direction of the applied magnetic field (see figure 3.31), and the axial velocity component can be expressed in the following simplified form

$$u = u_{max} \sin\theta \tag{3.15}$$

where u_{max} represents the maximum velocity value and θ is the polar angle defined in figure 3.31.

In cylindrical coordinates, the dimensionless heat transfer equation without sources

for a fully developed flow reads

$$Pe\, u\frac{\partial\Theta}{\partial x} = \frac{1}{r}\frac{\partial}{\partial r}\left(r\frac{\partial\Theta}{\partial r}\right) + \frac{1}{r^2}\frac{\partial^2\Theta}{\partial\theta^2} + \frac{\partial^2\Theta}{\partial x^2}, \tag{3.16}$$

where the pipe radius R was used as the characteristic length for non-dimensionalization purposes. For the solution of equation (3.16), we consider two different boundary conditions, namely, a uniform radial surface heat flux and a non-uniform surface heat flux with an angular dependence. Figure 3.32 shows an schematic diagram of both boundary conditions. The first condition (fig. 3.32a) can be written in the form

$$\frac{\partial\Theta}{\partial r} = 1 \quad r = 1, \quad 0 \le \theta \le 2\pi, \quad 0 \le x \le x_h, \tag{3.17}$$

while the second (fig. 3.32b) is

$$\frac{\partial\Theta}{\partial r} = \cos\theta \quad r = 1, \quad 0 \le \theta \le 2\pi, \quad 0 \le x \le x_h, \tag{3.18}$$

In addition, for both cases we have to satisfy

$$\Theta = 0 \quad x = 0, \quad 0 \le \theta \le 2\pi, \quad 0 \le r \le 1, \tag{3.19}$$

As we assume a negligible wall thickness, the temperature inside the wall is not calculated. For liquid-metal-cooled blanket applications, boundary condition (3.18) is more realistic than (3.17), for the heating from the first wall reaches the cylindrical cooling ducts non-uniformly.

3.4.1 Numerical Results

The numerical solution of equation (3.16) was accomplished by the same finite difference method applied in the rectangular case. In order to validate the numerical method, comparison with an analytical solution was performed. Carslaw and Jaeger [1959] present the solution for the heat transfer problem of a solid circular cylinder with a uniform radial surface heat flux in absence of heat sources. As in the rectangular case, this problem can be translated into fluid flow terms, that is, a fluid with slug flow inside a cylinder with negligible wall thickness and uniform radial surface heat flux. This problem is defined by equation (3.16) with $u = 1$ and boundary conditions (3.17) and (3.19). With the previous conditions, the problem becomes axisymmetric, the θ -dependence disappearing. The analytical solution is then

$$\Theta(x,r) = \left\{\frac{2x}{Pe} + \frac{r^2}{2} - \frac{1}{4} - 2\sum_{s=1}^{\infty}\exp\left(-\frac{\alpha_s^2 x}{Pe}\right)\frac{J_o(\alpha_s r)}{\alpha_s^2 J_o(\alpha_s)}\right\}, \tag{3.20}$$

where J_o are the Bessel functions of zeroth order. Then, at the boundary $r = 1$ we have

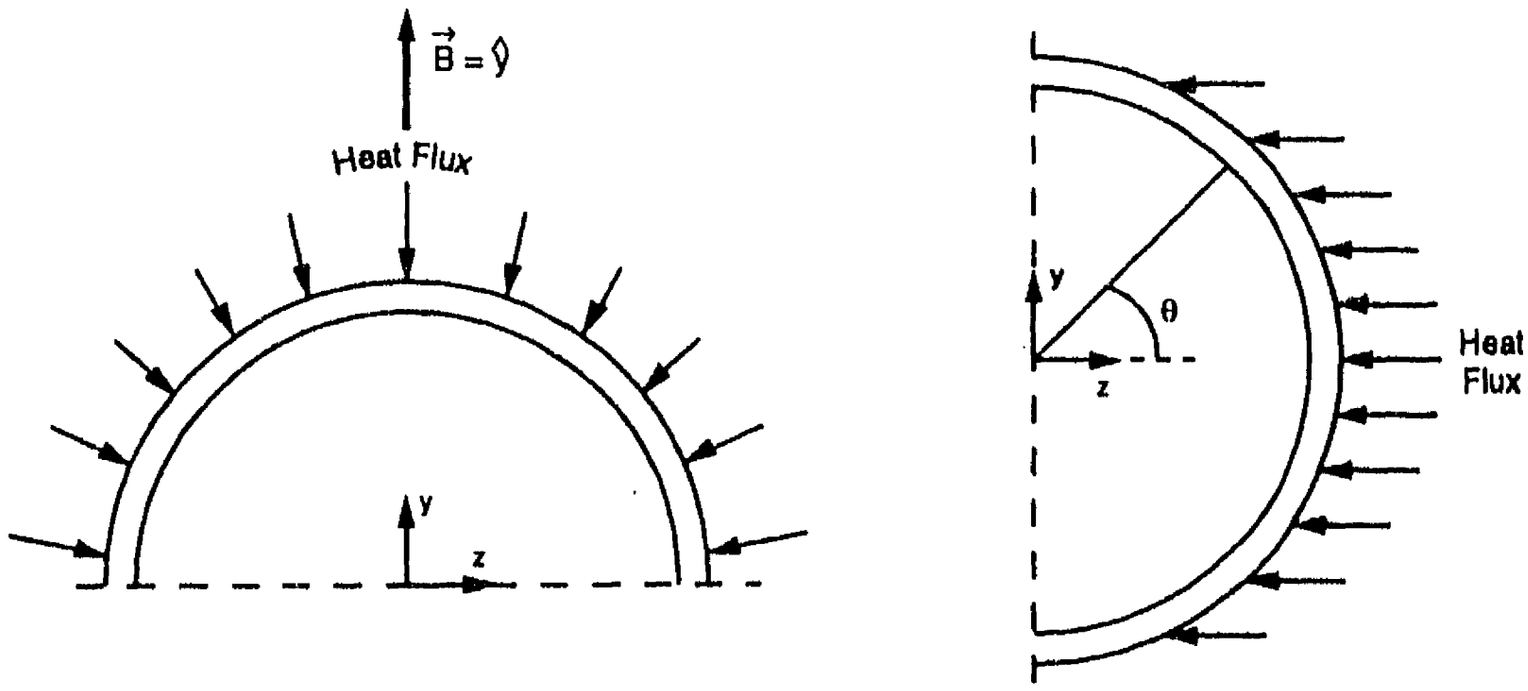

a) b), c)

Figure 3.32: Thermal boundary conditions in cylindrical duct flow. a) Uniform (radial) heat flux; b) Non-uniform heat flux.

$$\Theta(x,1) = \left\{ \frac{2x}{Pe} + \frac{1}{4} - 2\sum_{s=1}^{\infty} \exp\left(-\frac{\alpha_s^2 x}{Pe}\right) \frac{1}{\alpha_s^2} \right\}, \tag{3.21}$$

where the α_s are the positive roots of

$$J_1(\alpha) = 0.$$

Figure 3.33 shows the comparison of the wall temperature given by equation (3.21) against the finite difference solution, for three Péclet numbers, 250, 500 and 2500. It was found that, in order to get a good agreement with the analytical solution, much more control volumes in the direction of heat flux than in the rectangular case are required. Hence, a non-uniform radial grid with 70 control volumes, more densely distributed near the heated wall, was used. The axial grid consisted of 31 control volumes uniformly distributed. Although the agreement with the analytical solution is very good, there is a slight deviation in the region $x \leq 25$, more notorious for the lowest Péclet number. This is probably due to axial conduction effects present in the numerical calculations.

When the velocity profile and/or the boundary conditions present an angular dependence, the problem is evidently no longer axisymmetrical and a three-dimensional calculation has to be performed. Here, we analyze three different heat transfer cases:

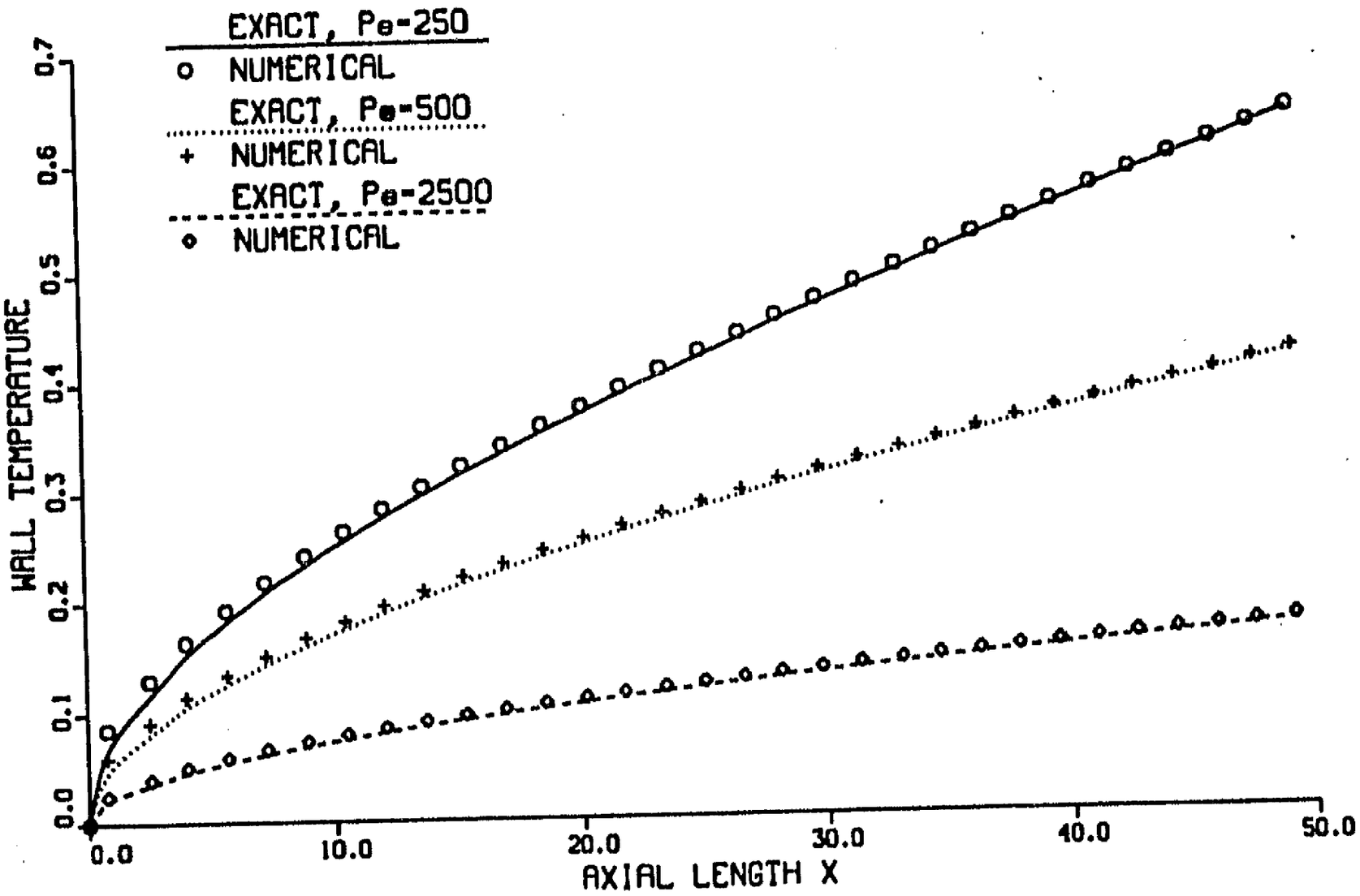

Figure 3.33: Comparison of finite differences and analytical wall temperature profiles with slug flow in a cylindrical duct, for different Péclet numbers.

i). Uniform radial heat flux (eq. (3.17)) with slug flow.
ii). Non-uniform heat flux (eq. (3.18)) with slug flow. Wall temperatures are computed for two different angles, $\theta = 0$ and $\theta = \pi/4$.
iii). Non-uniform heat flux (eq. (3.18)) with non-uniform flow (eq. (3.15)). Wall temperatures are computed for two different angles, $\theta = 0$ and $\theta = \pi/4$.

From figure 3.32b), it can be seen that for non-uniform z-heat flux, the maximum and minimum heat flux correspond to $\theta = 0$ and $\theta = \pi/2$, respectively. Figure 3.34 shows the wall temperature profile as a function of the axial coordinate for the axisymmetric case *i*), for different Péclet numbers. Comparing figure 3.34 with the similar square duct case shown in figure 3.22, we find a higher wall temperature in the cylindrical case. However, figure 3.22 should better be compared with figures 3.35 and 3.36, corresponding to non-uniform heat flux with slug flow (case *ii*)) at $\theta = 0$ and $\theta = \pi/4$, respectively. Figure 3.35 shows that the wall temperature profile for the maximum heat flux angle, is essentially the same that the one presented in figure 3.34 for case *i*). A significant reduction in wall temperature is obtained at the intermediate angle $\theta = \pi/4$ (see figure 3.36). While the wall temperature at $\theta = 0$ is higher than the corresponding square duct case (fig. 3.22) for a given Péclet number, at $\theta = \pi/4$ the cylindrical case presents a lower wall temperature than the square case. Figures 3.37 and 3.38 present the effect on wall temperature of both non-uniform heat flux and flow (case *iii*)) at the previous two angles, respectively. The increase in wall temperature due to the sine velocity distribution is rather high. At both angles, $\theta = 0$ and $\theta = \pi/4$, the wall temperature is about 40 % higher with non-uniform flow than with slug flow. Slug flow seems to remove wall heat more efficiently than the non-uniform flow given by equation (3.15), for the same Péclet number.

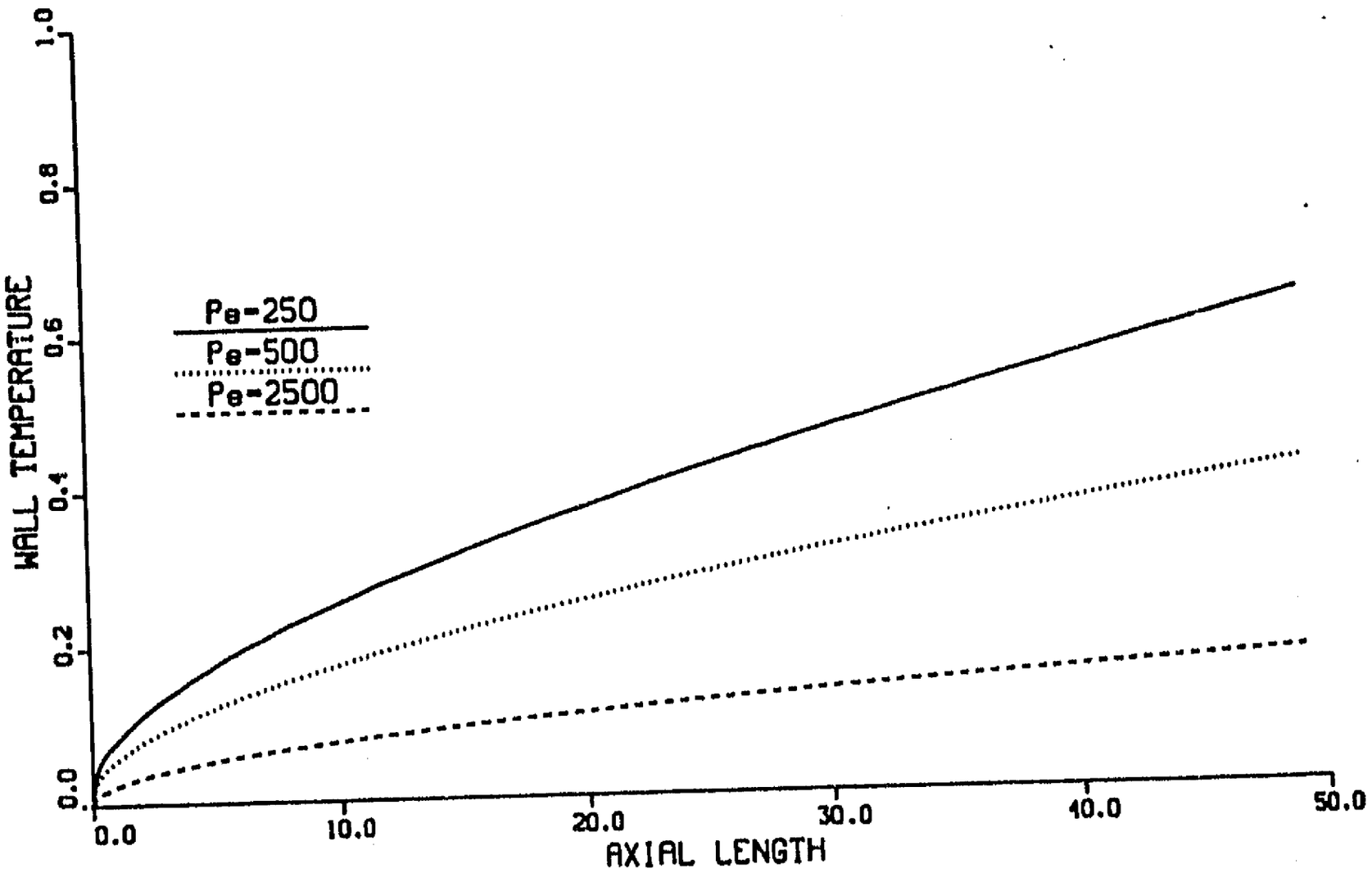

Figure 3.34: Wall temperature vs. x in slug flow in a cylindrical duct with uniform heat flux, for different Péclet numbers.

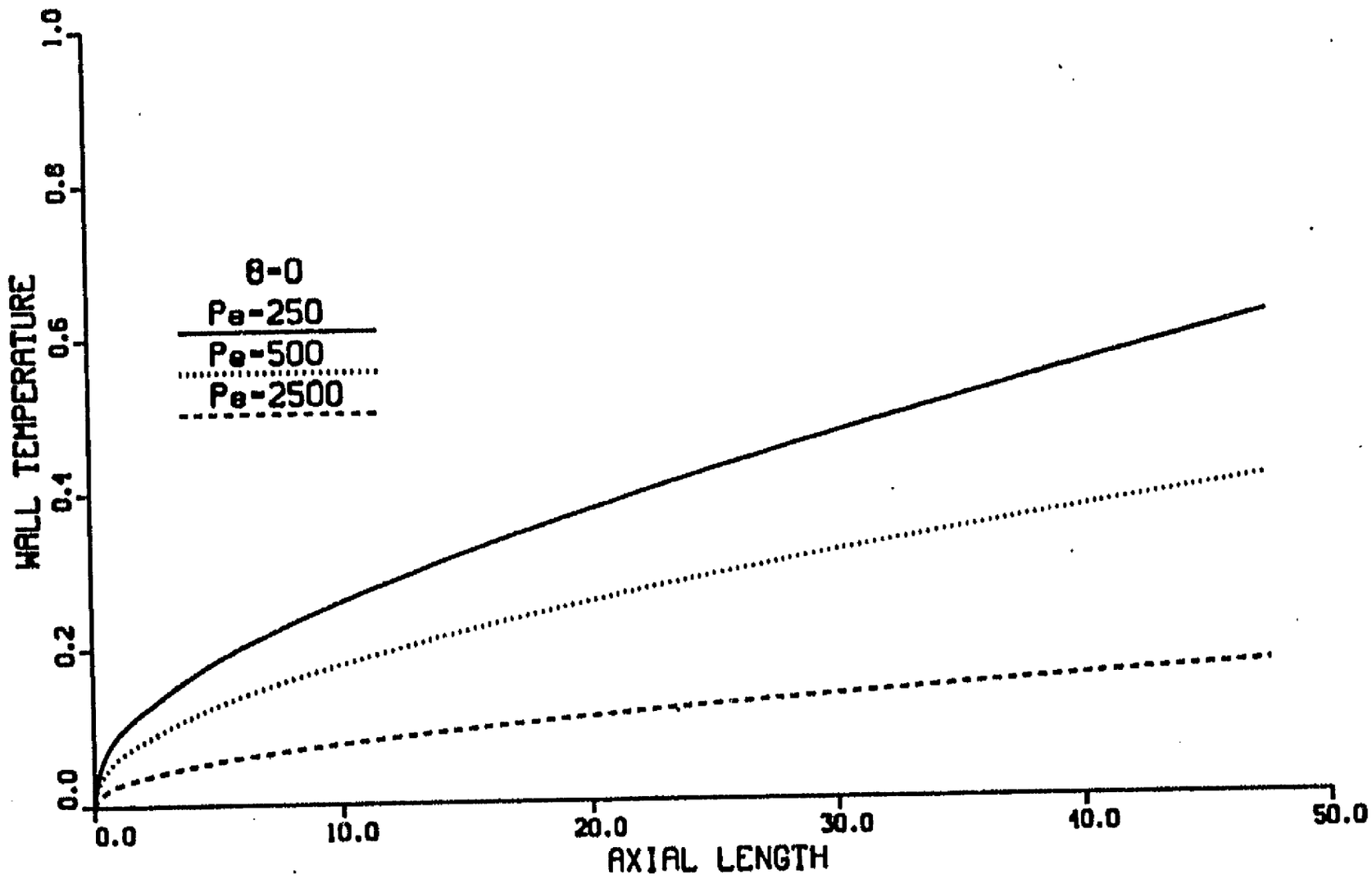

Figure 3.35: Wall temperature vs. x in slug flow in a cylindrical duct with non-uniform heat flux ($\theta = 0$), for different Péclet numbers.

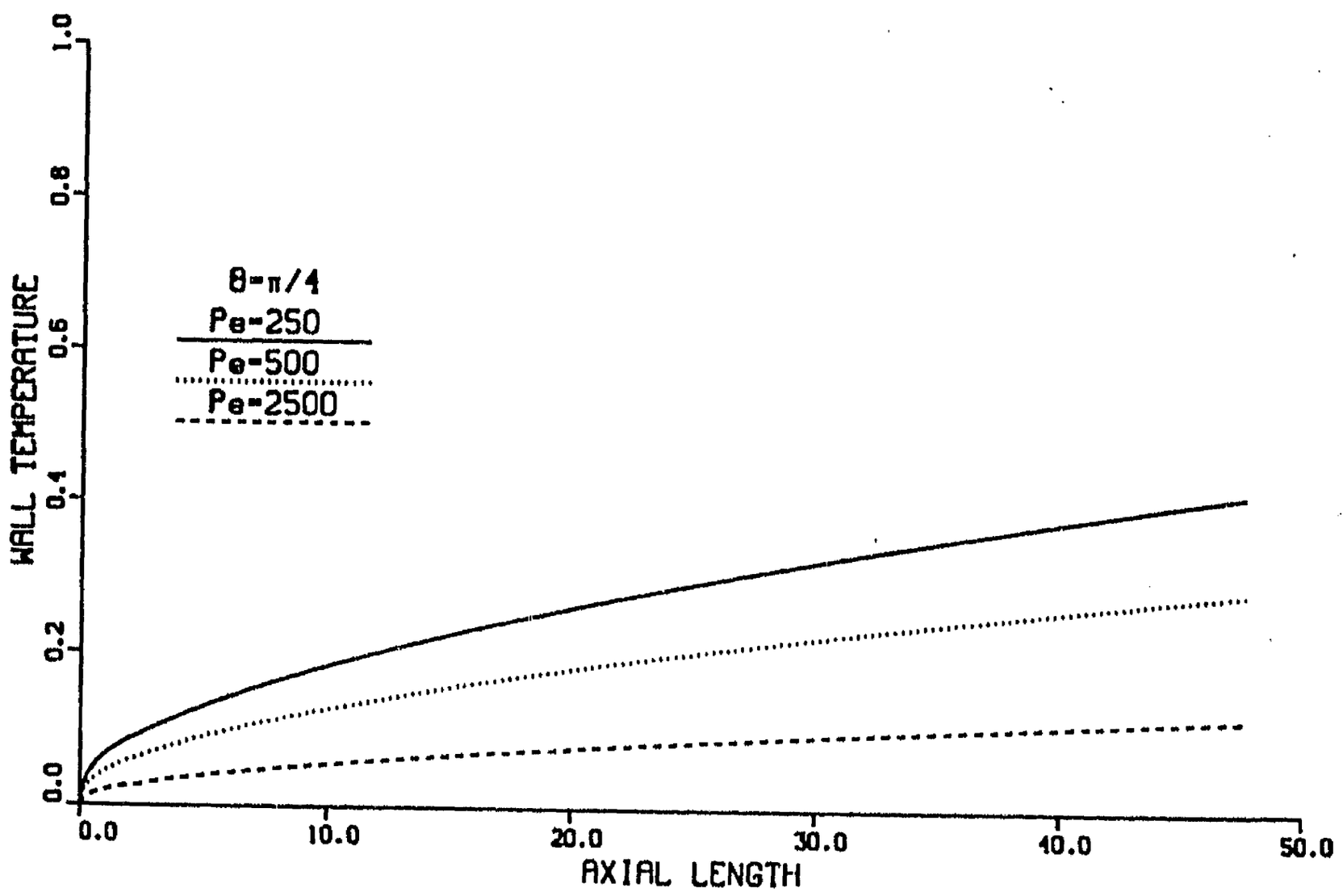

Figure 3.36: Wall temperature vs. x in slug flow in a cylindrical duct with non-uniform heat flux ($\theta = \pi/4$), for different Péclet numbers.

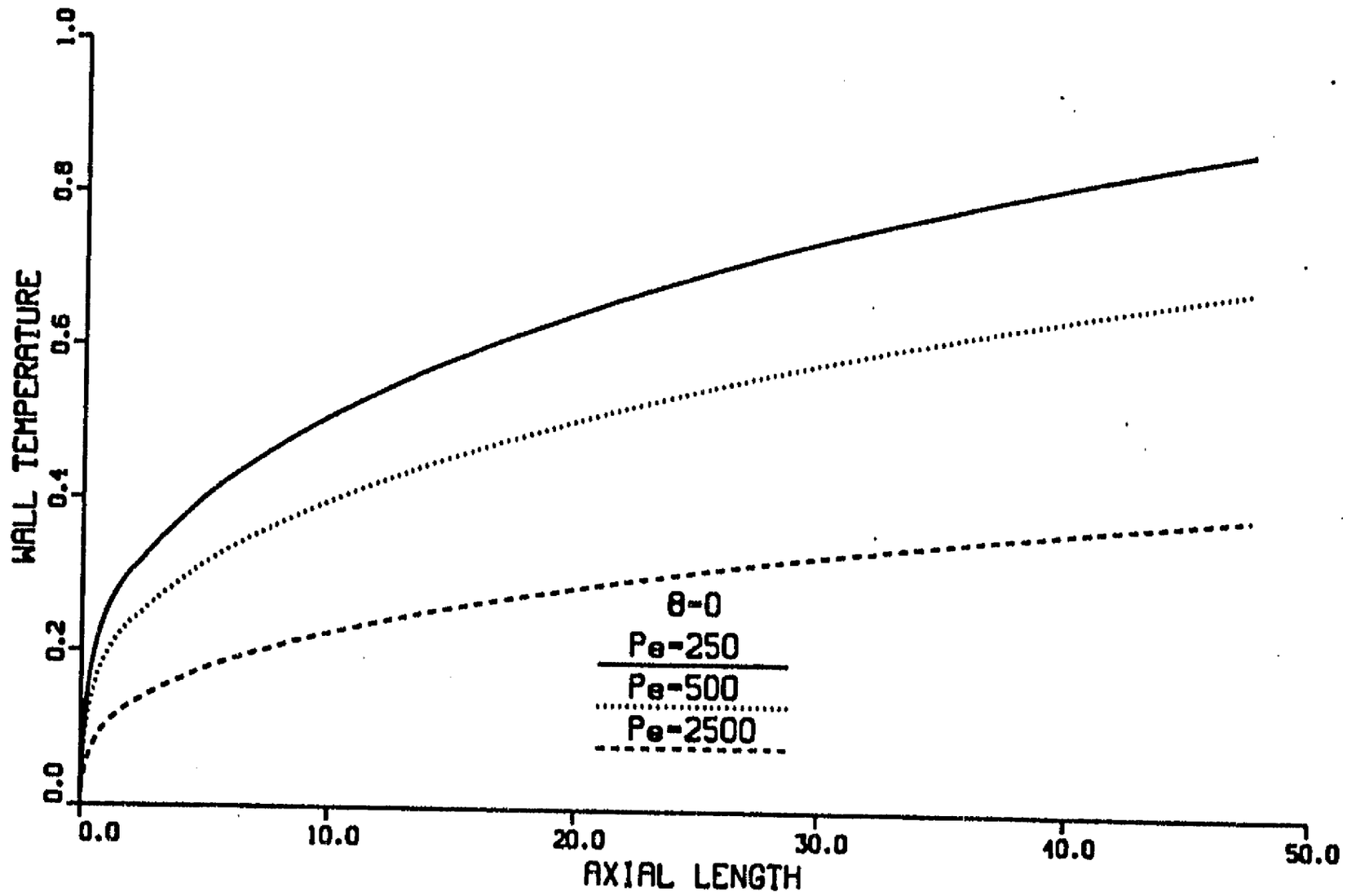

Figure 3.37: Wall temperature vs. x in non-uniform flow in a cylindrical duct with non-uniform heat flux ($\theta = 0$), for different Péclet numbers.

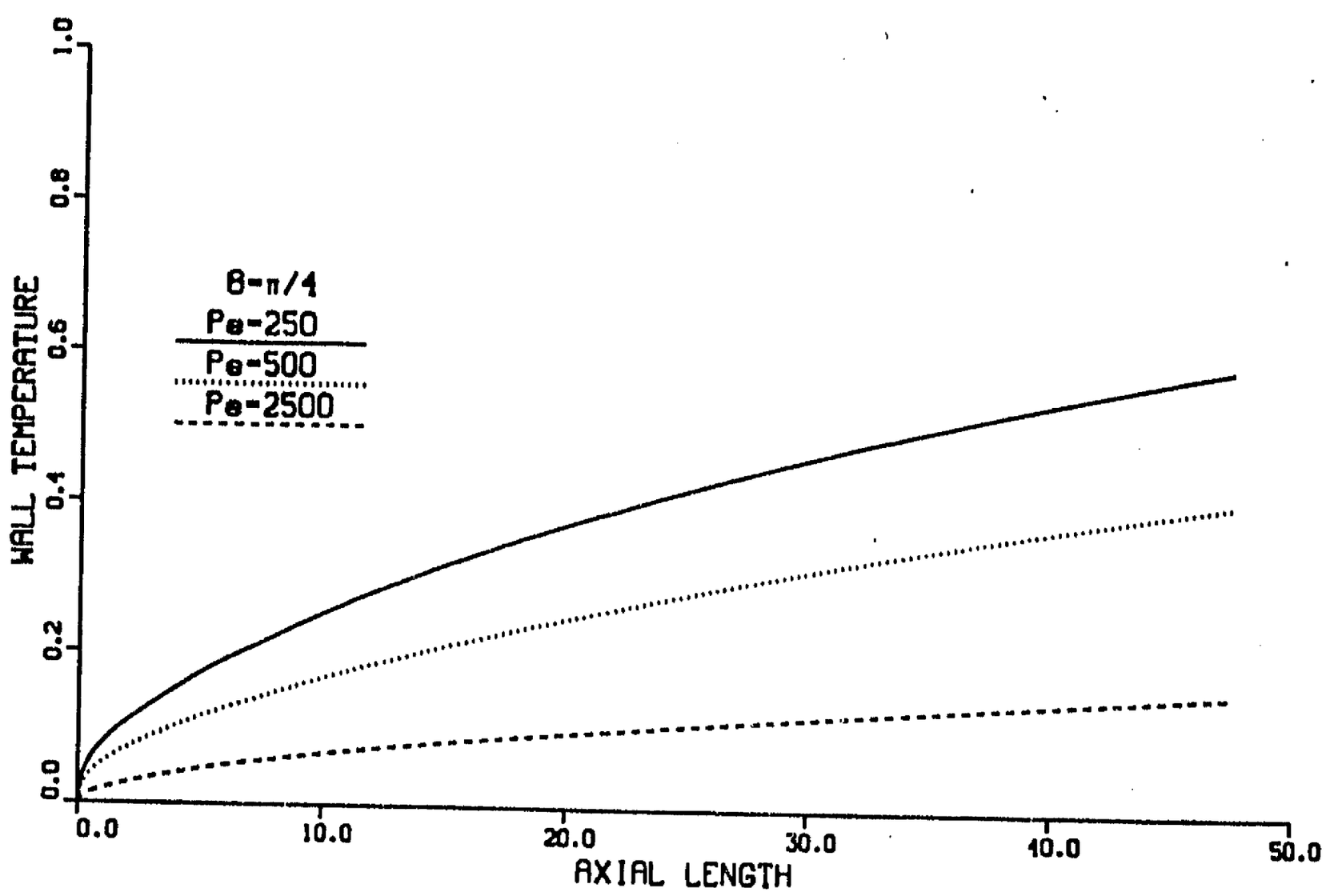

Figure 3.38: Wall temperature vs. x in non-uniform flow in a cylindrical duct with non-uniform heat flux ($\theta = \pi/4$), for different Péclet numbers.

Chapter 4

MHD Turbulence and Related Phenomena

4.1 Introduction

The purpose of this Chapter is to present a survey of some of the main concepts that sustain our understanding of turbulent phenomena, ordinary as well as MHD. Needless to say that this review is far from being complete. It only attempts to introduce, through a selective review, some basic ideas that may provide a background for the discussion of the model and results presented in Chapter 5, as well as clarify how the duct flow of liquid metals in the turbulent regime is affected by the action of strong magnetic fields . For instance, although the laminarization effect of a magnetic field is well known, there is some evidence that, under certain conditions, quasi-two-dimensional turbulence may persist even under the action of strong magnetic fields. Likewise, the existence of side layer instabilities in liquid metal flows in thin conducting ducts is also experimentally verified, though not satisfactorily explained. It is speculated that transport mechanisms similar to those present in MHD turbulence might be involved in the side layer instability, although the heat transfer effects have to be demonstrated. With the aim to provide a framework for a preliminary approach to these topics, some well known facts and concepts of MHD turbulence theory are exposed. We begin by stating the general characteristics of ordinary hydrodynamic (OHD) turbulence and its basic underlying concepts, and continue with an exposition of ordinary two-dimensional turbulence theory. Later, MHD turbulence is introduced and some works dealing with its different phases of evolution are discussed. The tendency of MHD turbulence towards two-dimensionality, including the formation and dissipation of elongated vortices in the direction of the magnetic field, is then considered and some explanations of this behavior are offered. We continue with the laminarization effects of a magnetic field and the observed residual turbulent disturbances. Finally, we present a review of the recent experimental evidence obtained at Beer-Sheva on strongly anisotropic turbulence with an inverse energy cascade and Argonne National Laboratory experiments on the side layer instability.

4.2 General Aspects of Ordinary Turbulence

The main characteristic of turbulent flows is their tendency to be highly irregular, dissipative and very diffusive. Their large diffusivity allows a high ability to mix properties efficiently, which from the practical point of view, is probably one of the most important features of turbulence. Evidently, turbulence is a property of the flow and not of the fluid. The presence of a wide range of interacting dynamic scales is the main problem in dealing with turbulent flows. Hence, any analytical or numerical approach aimed at describing these flows successfully, must take into account the continuous range of excited scales of motion. These scales range from the large ones, where the turbulence energy is input, to the small ones, where the effect of the molecular viscosity is dominant and dissipation into heat takes place. The lack of a clear separation between scales increases the complexity of turbulent flows, since they exhibit excitations from the largest scales down to the smallest.

Turbulence often occurs as a result of an instability of laminar flows when inertial nonlinear effects become dominant over viscous effects over most of the flow. The Reynolds number, previously defined, is often used to characterize turbulent flows. *Re* provides a (dimensionless) relative measure of the relevance of inertial over viscous effects. Hence, for small values of *Re*, inertial effects are negligible and the fluid shows a laminar behavior, with relatively regular and predictable development in space and time. As *Re* increases, inertial effects come into play and the flow experiences a series of instabilities and eventually becomes fully turbulent, with chaotic and unpredictable motions [Tennekes and Lumley, 1972]. The higher the Reynolds number the greater the number of excited scales of motion. The belief that irregularity and randomness are at the very heart of turbulent flows, has encouraged the idea that they might best be described in terms of their average, rather than their detailed properties. This has led to the development of the statistical theory of turbulence [Monin and Yaglom, 1975].

Turbulent motion can be thought of as the superposition of a large number of component motions of different size, called eddies, interacting and exchanging momentum and energy. Eddies make additive contributions to the total energy and interact with each other according to a certain non-linear dynamics prescribed by the equation of motion. Likewise, an eddy could be pictured as a disturbance containing waves of different wavenumbers. In this context, Fourier analysis is a very helpful tool in the description of turbulent flows since it offers a resolution into components of the motion of different linear size (different Fourier components being specified by their wave-lengths or wavenumbers). It also gives a definite meaning to the idea of the different degrees of freedom possessed by the fluid since it is possible to associate a specific wavenumber to each dynamic scale [Tennekes and Lumley, 1972]. In this form, we can define an energy spectrum $E(\mathbf{k}, t)$ which considers the contribution of all turbulent structures, taking into account the size of these structures and their orientations through a wave number vector $\mathbf{k}$.

Let us now expose other basic concepts underlying some classical approaches to turbulence theory.

Eddy Viscosity. A very useful phenomenological approach to turbulence theory is based in the concept of eddy viscosity. This concept has been widely used for visualizing and parametrizing the transport of turbulent energy both in space and between different scales of motion. For instance, eddy viscosity has been used to represent the effects of sub-grid-scale motions in large-scale computer simulation flows [Rogallo and Moin, 1984]. Many turbulent models are based on the concept of eddy viscosity. As a mater of fact, in section 2.4 we used this concept in order to close the system of equations for the mean variables. In Chapter 5, we will discuss the turbulence model used in this work and present the eddy viscosity formula for that model. In the eddy viscosity approach, originally formulated by Boussinesq, a relation between stress and rate of strain, that involves a *turbulence-generated viscosity*, is postulated. Eddy viscosity is assumed to play a role similar to molecular viscosity in laminar flows. Many important features of turbulence dynamics can be described in terms of eddy viscosity. The concept is based on an analogy with statistical mechanics and states that turbulent dynamics might be regarded in an analogous way to molecular motion, in the sense that small scale eddies are supposed to act on large scale eddies diffusively [Frisch and Orszag, 1990]. Hence, turbulent velocity fluctuations would transfer momentum in a similar way as molecular motions do. For instance, eddy viscosity is responsible for smoothing gradients in the mean velocity field and can also explain the enhancement of the diffusion rate in turbulent flows as well as the enhancement of kinetic energy dissipation. It is even possible to estimate these effects. The concept of eddy viscosity can be extended to the more general of eddy diffusivity to include the turbulent transfer of other quantities as heat [Bradshaw, 1976], as we do in Chapter 5. The fact that the eddy diffusivity is a property of the flow and not of the fluid could be inconvenient in certain cases but this inconvenience is overcome by the simplicity gained in the mathematical description of turbulence.

Cascade. In general, turbulent flows are dissipative. Since viscous shear stresses perform deformation work, kinetic energy is continuously dissipated into internal energy. Thus, in order to prevent the rapid decay of turbulence, energy has to be supplied almost continuously. The supply of energy for turbulent fluctuations will take place mostly through the direct transfer of energy from the mean flow or through an indirect transfer from large-scale eddies by a cascade process in which the energy is transferred progressively to smaller scale eddies [Hinze, 1975]. The concept of cascade is very common in turbulence theory and is based on the notion that turbulent flows are hierarchical and contain entities of varying sizes, the aforementioned eddies. The largest eddies present a size of the order of the characteristic dimension of the flow and are created by the forces driving the flow. These eddies are supposed to be unstable, pro-

ducing eddies of smaller size which, in turn, become unstable and generate even smaller eddies. This process is prolonged until, eventually, molecular viscosity becomes dominant and prevents further cascading [Frisch and Orszag, 1990]. At very small length scales, molecular viscosity induce the smoothing out of the velocity fluctuations. The generation of small scale fluctuations, due to inertial transfer, is represented by the nonlinear terms in the equation of motion, while the viscous term prevents the generation of infinitely small scales of motion by dissipating small scale energy into heat [Tennekes and Lumley, 1972].

Inertial Subrange and Kolmogorov's Law. The statement by Kolmogorov [1941] of a universal law governing the spectral density of energy in turbulent flow for a certain range of wavenumbers at high Reynolds numbers, known as the inertial subrange, is one of the cornerstones of turbulence theory. The existence of the inertial subrange can be understood by considering the transfer of energy from large scales, where the turbulence is originated, to small scales where turbulent energy tends to be dissipated by viscosity. Clear plausibility arguments for its existence are provided by Batchelor [1953]. The idea is that in a homogeneous and isotropic flow at very high Reynolds numbers, the wavenumber known as the viscous cutoff, k_{vis}, which marks the beginning of the range of wavenumbers affected considerably by the action of viscous forces, is also very large. Hence, for wavenumbers $k \ll k_{vis}$ viscous forces are considered negligible. On the other hand, it is assumed that the dependence on the external conditions which promotes the turbulence spread only at small wavenumbers (large scales) on which external forces act directly. Then there will be a range of wave-numbers which is not excited directly by the external large-scale forces which generate the motion, and which owes its excitation entirely to the energy transfer by inertia forces. The motion associated with sufficiently large wavenumbers (small scales) should be isotropic. The ranges of k which determine the injection and the dissipation of energy must be widely separated. This range of wave numbers (*i.e.* eddy sizes) which is not directly affected by the energy maintenance and dissipation mechanisms is called the inertial subrange. It is in this range where the assumptions of statistical equilibrium hold [Tennekes and Lumley, 1972]. Kolmogorov's hypothesis was that the small scale components of the turbulence are approximately in statistical equilibrium. These small components are created by non-linear interchange of energy between different wavenumber components, and Kolmogorov postulated that the equilibrium would be universal, apart from the effect of variation of two external parameters: the rate of removal and insertion of energy ϵ, and the molecular viscosity ν_o. Thus, when these two parameters are given, the complete statistical specification of the small scale components of the turbulence is determined, and many definite predictions may be made from dimensional analysis. Along with the basic invariance of the hydrodynamic equations which reflects the basic symmetries of Newtonian physics, the scale invariance reflects a new symmetry that arises macroscopically in the limit of infinite Reynolds number [Frisch and Orszag,

1990]. This fact is exploited in the Kolmogorov's theory of three-dimensional turbulence. One of the consequences of the Kolmogorov's theory is that the energy spectrum $E(k)$ satisfies the Kolmogorov's law [Batchelor, 1953]

$$E(k) = C_K \epsilon^{2/3} k^{-5/3}, \tag{4.1}$$

where C_K is the Kolmogorov constant. Scaling does not predict the value for this constant. Obviously, basic scaling symmetry, which is assumed to derive the above results, is broken at large and small scales, as we can conclude from the previous discussion. At large scales, the mechanisms producing the turbulence -v.g. boundaries or external forces- generally define a scale L. For Kolmogorov's scaling to hold at some scale l, it is therefore necessary that $l \ll L$. At small scales, molecular viscosity ν_o can be ignored only if the eddy viscosity at scale l, denoted by ν_l, satisfies $\nu_l \gg \nu_o$. Therefore, scaling requires that $l \gg l_d$ where $l_d \approx (\nu_o^3/\epsilon)^{1/4}$ is called the Kolomogorov dissipation scale ($l_d \approx 1/k_{vis}$). For $l \leq l_d$, molecular viscosity is important. It is at these scales that viscous dissipation occurs. Then, in terms of these length scales the (Kolmogorov) inertial range in which scaling arguments are valid is defined by $l_d \ll l \ll L$. It is expected that for all high Reynolds number flows, the predictions of the Kolmogorov theory hold universally in the inertial subrange [Frisch and Orszag, 1990].

4.2.1 Two-Dimensional Turbulence

Truly two-dimensional turbulence is never found in nature or the laboratory but only in computer simulations. Nevertheless, it provides a good starting point for modeling idealized geophysical phenomena in the atmosphere, oceans and magnetosphere and flows of conducting fluids in strong magnetic fields. The theory of two-dimensional turbulence has been developed mainly by R. Kraichnan and a good review of the principal achievements of the theory can be found in Kraichnan and Montgomery [1980]. This topic is of relevance in this work due to the observed tendency of MHD turbulence to become two-dimensional under certain circumstances, as will be discussed in section 4.3.

Strictly two-dimensional flow in a layer of fluid requires that the velocity vector everywhere lies in a given plane and that the variation of the velocity field perpendicular to that plane is inexistent. To obtain such a flow would require plane parallel, perfectly slippery boundary (horizontal) planes and a mechanism to inhibit vertical motion and variation. If the fluid layer is thin compared to its horizontal dimension, large-scale motions are necessarily horizontal, but this does not prevent vertical variation of the horizontal motion. The latter can be inhibited by a strong enough viscosity but also by either rotation about a vertical axis or the interaction with a vertical magnetic field. The first mechanism is evidently of great importance to geophysics and has been widely studied (v.g. [McWilliams, J. C., 1983]). The way in which a magnetic field

interacts with a conducting fluid to prevent the growth of vertical variations will be discussed in a subsequent section where a survey of experimental and theoretical results on MHD turbulence is performed. Here, we will restrict to mention some of the main characteristics of two-dimensional turbulence.

As we mentioned in the previous section, in three dimensional turbulence the energy cascade through the inertial range is from lower to higher wave-numbers, that is, from large to small scales. At high wavenumbers, turbulence intensity is suppressed by viscosity and it is natural to expect a net transfer towards these wavenumbers from the strongly excited low wavenumbers. In two dimensions this situation is drastically changed mainly because of the existence of two linearly independent quadratic constants of motion [Kraichnan, 1967]. While in three-dimensional inviscid flow, only the kinetic energy can be considered as an invariant, in two dimensions there is in addition a second invariant, namely the enstrophy which, by definition, is half the squared vorticity. In the viscous case, therefore, two kinds of dissipation may be considered fundamental: that of kinetic energy ϵ and that of enstrophy η. Kraichnan [1967] was the first one to notice that, correspondingly, two different kinds of inertial ranges could formally be defined: the Kolmogorov range for energy transfer through wave number space, and a new one in which enstrophy is similarly transferred. Similar results were conjectured by Batchelor [1969]. It was found that the vorticity constrain has profound effects on inertial energy transfer. In contrast to the predominantly one-way flow of energy familiar in three dimensions, transfer upward in wavenumber must be accompanied by comparable or greater downward transfer. Kraichnan was able to prove that if energy is injected in the fluid at a constant rate to a band of wave-numbers $\approx k_i$ and the Reynolds number is high, a quasi-steady state is developed in which energy is carried from higher to lower wavenumbers with a -5/3 range for $k \ll k_i$ while enstrophy is transferred from lower to higher wavenumbers with a -3 range for $k \gg k_i$, up to the viscous cutoff. Kraichnan also proved that these transfers are mutually exclusive; thus a $k^{-5/3}$ spectrum cannot transfer enstrophy up or down scale, and similarly energy cannot be propagated in wave space through a k^{-3} region. Kraichnan's hypothesis can be mathematically expressed as [Lilly, 1969]

$$E(k) = \alpha \epsilon^{2/3} k^{-5/3}, \qquad k_c < k < k_i \tag{4.2}$$

$$E(k) = \beta \eta^{2/3} k^{-3}, \qquad k_i < k < k_d \tag{4.3}$$

where k_i is the central wave-number of the forcing disturbance (injection) which continually produces kinetic energy and enstrophy within a viscous fluid at high Reynolds number; k_c and k_d are the low and high wave-number limits of the spectrum; and α and β are dimensionless constants. Incidentally, although equation (4.2) and (4.1) have the same form, constants α and C_K depend on the dimensionality. The meaning of equations (4.2) and (4.3) can be stated in the following way: In the high frequency spectrum, enstrophy is transferred to higher frequencies at the enstrophy dissipation rate

η, and k_d represents a dissipation length scale. Since kinetic energy cannot be transferred through this range, it is not dissipated provided that $k_i \ll k_d$. Kinetic energy is, however, transferred to larger scales through the $k^{-5/3}$ spectral region, and the lower limit k_c is necessarily a decreasing function of time. Eventually, when k_c reaches the scale limit of the physical system, energy must begin to pile up at the lowest available wavenumber [Lilly, 1969]. The transfer of energy from higher to lower wavenumbers (i.e. from small to large scales) is known as the *inverse cascade* and is one of the most characteristic features of two-dimensional turbulence. Some of the approaches dealing with two-dimensional turbulence involve the definition of a negative eddy viscosity. The negative eddy viscosity in two dimensions reflects the fact that energy flows to lower rather than to higher wavenumbers. Kraichnan's predictions have been widely confirmed through both numerical simulations and experimental investigations and a statistical theory of two-dimensional turbulence has also been developed [Kraichnan and Montgomery, 1980].

4.3 MHD Turbulence

A magnetic field can substantially affect the nature of turbulence. The field introduces a preferential direction in space and modifies the dynamics as well as the transport phenomena processes inside the flow. Laminarization effects are some of the features that, under certain conditions, can be obtained on a turbulent flow by the action of a magnetic field. In addition, there is a widespread belief that MHD turbulence at low magnetic Reynolds numbers presents a tendency towards two-dimensionality. Several experimental facts support this conclusion and in the last decades some theoretical explanations have been proposed to give account of the experimental results [Alemany et al., 1979, Sommeria and Moreau, 1982]. Two-dimensionality in MHD turbulence is seen more as an idealized limit than as a real physical state. Actually, although the tendency of MHD turbulence towards two-dimensionality is well established, there is no general agreement, at least in duct flows, if the final state reached in MHD turbulence presents all the characteristic features of two-dimensional turbulence. Motions that appear to present these features have been studied by Sommeria (v.g. [Sommeria et al., 1989]) in an electrically induced flow in a thin layer of mercury under a strong transverse magnetic field. In general, in spite of the recent advances, MHD turbulence (as well as OHD turbulence) is still a polemic and not thoroughly understood issue, without a generally accepted theoretical framework. The selective survey accomplished here attempts to offer an introductory approach to this topic.

MHD turbulence can be studied in different phases of evolution according to the time scales involved in the process. We can define three characteristic time scales: the eddy turnover time $\tau_{tu} = l/u$, where l and u are the characteristic length and velocity of energy containing eddies; the Joule time (or magnetic response time) $\tau_{Jo} = \rho/\sigma B^2$, where B is the magnetic field strength and ρ and σ are the density and electrical

conductivity of the fluid, respectively; and the viscous time $\tau_\nu = l^2/\nu_o$, where ν_o is the kinematic viscosity of the fluid. τ_{tu} represents the characteristic time of the eddy distortion process due to inertial effects, leading to the generation of small scale eddies. τ_{Jo} and τ_ν express the characteristic time for a fluctuation to substantially modify its structure by the action of Joule and viscous dissipation, respectively. In turbulent flows at high Reynolds numbers $\tau_\nu \gg \tau_{tu}$. It should be noted that although τ_{tu} and τ_ν depend on the fluctuation length scale l, the Joule time scale is independent of this length and can be modulated by changing the magnetic field strength. Then τ_{Jo} can be bigger or smaller than τ_{tu} depending on the field intensity. The ratio of these time scales is precisely the *local* interaction parameter $N_o = \tau_{tu}/\tau_{Jo} = \sigma B_o l/\rho u$ which measures the intensities of the Joule dissipation and the eddy distortion processes or, in other words, of the electromagnetic and the inertial interactions at eddy scale. When $N_o \ll 1$ ($\tau_{tu} \ll \tau_{Jo}$), the Lorentz force is small compared to the inertia force, and may be expected to have negligible effect on the turbulence. This means that a given turbulent fluctuation will break up before it experiences the action of the magnetic field. Therefore, interesting (and practical) cases of MHD turbulence are those in which $N_o > 1$ or $N_o \gg 1$. Moreau [1990] identifies three evolution phases in an initially isotropic turbulence submitted to the action of a magnetic field, namely, a linear and isotropic phase for times $t < \tau_{J_o}$, a linear and anisotropic phase for $\tau_{J_o} < t < \tau_{tu}$ and a non-linear and anisotropic phase for $t > \tau_{tu}$. Actually, a linear and isotropic phase can also be identified in the last stages of evolution of homogeneous decaying turbulence in the presence of a magnetic field.

The first studies on this field were engaged to clarify the influence of a magnetic field in two situations where the linear analysis can be applied: a homogeneous decaying turbulence under the action of a magnetic field and the initial response of an isotropic turbulent flow to the application of a strong magnetic field. In both situations, non-linear forces are negligible and the linearized MHD equations are valid. For instance, Lehnert [1955] considered the problem of decay of homogeneous turbulence in a conducting fluid subject to the action of an applied magnetic field, in conditions in which the velocity and magnetic fluctuations are sufficiently weak for non-linear effects to be permanently negligible. This would be the case if $Re \ll 1$ and $Rm \ll 1$. He found that if the kinematic viscosity of the fluid is small compared with its magnetic diffusivity, the field has a pronounced effect on the decay process, mainly manifested on the preferential suppression of those Fourier components of the velocity field whose wave vector k has a non-zero component in the direction of the applied field. The characteristic time of this preferential damping process is τ_{Jo}. Another pioneer studies analyzed situations restricted to the time interval $0 < t \ll \tau_{tu}$, in which the turbulence adjusts very fast to the new externally applied conditions. During this period of adjustment, non-linear effects are negligible. Nestlerode and Lumley [1963] carried out a first calculation of the initial response of turbulence to the application of a strong magnetic field, by means of a Taylor series in time. They found that the Fourier com-

ponents propagating in the cross-field directions are less attenuated than components propagating in the field-wise direction. Similarly, Moffatt [1967] analyzed the effect of sudden application (at $t = 0$) of a uniform magnetic field on initially isotropic turbulence. However, he extended his analysis to the linear and anisotropic phase. The problem is treated under the assumptions $Re \gg 1$, $Rm \ll 1$ and $N \gg 1$. Particularly, Moffatt was interested in determining the time dependence of quantities such as the kinetic and magnetic energy density during an interval defined by $\tau_{Jo} \ll t \ll \tau_{tu}$, when the turbulence has been considerably modified. He found a suppression of the intensity of the turbulence (preferential damping) as a result of the application of the field. For $t \gg \tau_{Jo}$ the bulk of the initial energy decays as $(\tau_{Jo}/t)^{1/2}$ and the motion tends to become independent of the coordinate in the direction of the field, reaching a state nearly two-dimensional in the sense that all correlations vary slowly in that direction compared with their variation perpendicular to the field. However, the velocity component in the field direction is not necessarily small. In Moffatt' study turbulence dynamics is dominated by the linear anisotropic Joule damping.

Moreau [1968] made some qualitative considerations to take into account the non-linear mechanisms of energy transfer. He found that in wavenumber space, three different regions can be established, namely, a viscous dissipation region, a Joule dissipation region and an inertial energy transfer region (see figure 4.1). Joule dissipation is concentrated in a cone whose axis is parallel to the applied magnetic field while viscous dissipation remains outside a sphere of radius $1/\eta$, where η is the Kolmogorov scale [Tennekes and Lumley, 1972]. He found that eddies with $\mathbf{k}$ inside the cone are damped more rapidly than those with $\mathbf{k}$ outside. However, only the part of this cone corresponding to wavenumbers characteristic of the energy carrying eddies contribute to Joulean dissipation. The small eddies induce an electric field $\mathbf{e}$ opposed to the field $\mathbf{u} \times \mathbf{B}$, and in this region the Joule dissipation is inhibited. During the non-linear phase, transfer from the energy to the Joule dissipation region is very important. For a strong magnetic field, only a small part of the turbulent energy can reach the zone of high wavenumbers and be dissipated by viscosity. Some of these effects will be discussed below.

Schumann [1976] performed a full nonlinear numerical simulation of the transition of isotropic three-dimensional to quasi-two-dimensional turbulence under a uniform magnetic field. He observed that, while the Lorentz force and the resultant Joule dissipation lead to an anisotropic effect and a tendency towards quasi-two-dimensionality, energy transfer due to inertial (non-linear) terms causes a return to the three-dimensional isotropic state. The non-linear terms produce an energy transfer from low to high wavenumbers, characteristic of three-dimensional turbulence. Nevertheless, for a strong enough magnetic field, the magnetic dissipation may cause the damping out of flow variations in the direction of the applied field and, therefore, a quasi-two-dimensional state. The simulation was performed for $Re = 60$ and a maximum interaction parameter of 50. However, for such small Reynolds number, the limited resolution in

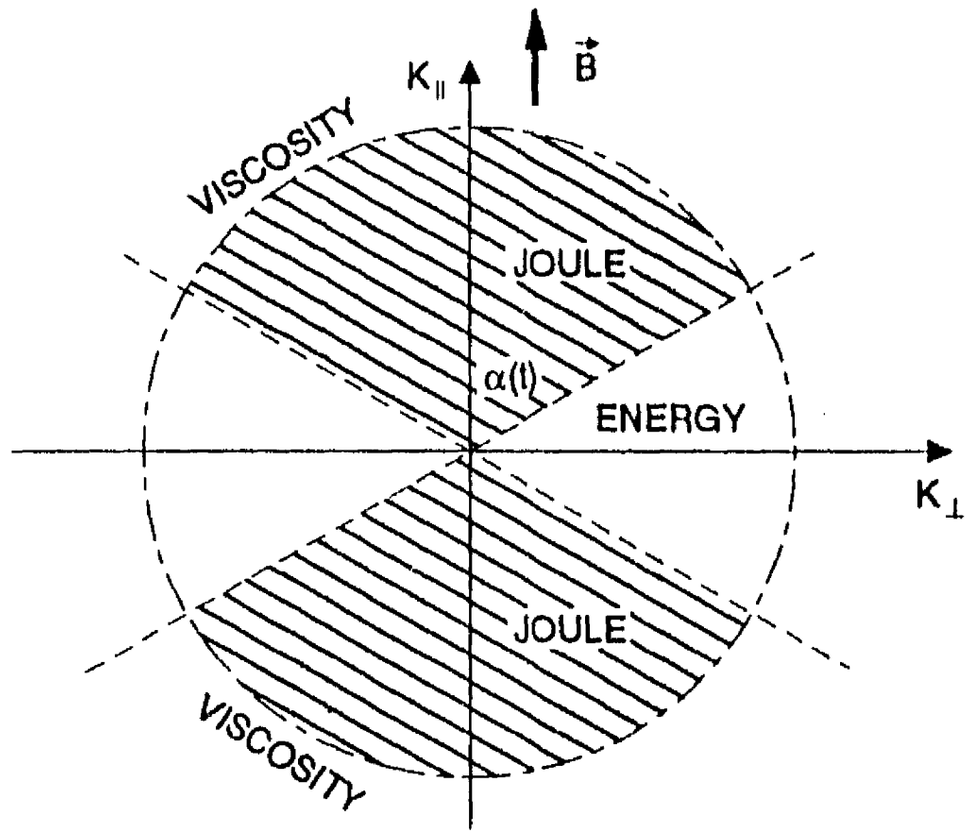

Figure 4.1: Organization of Fourier space into three separated regions in homogeneous MHD turbulence [Moreau, 1968; 1990].

wavenumber space prevents the nonlinear transport effects (that produce the restoration of isotropy at high wavenumbers) to manifest themselves clearly. In addition, the numerical integration spanned over a period of the order of one large eddy turnover time, but in order to produce sizable non-linear effects, longer integrations are needed [Alemany et al., 1979].

Alemany et al. [1979] performed a theoretical and experimental investigation on the influence of an external magnetic field on homogeneous MHD turbulence. The different phases of evolution, including the nonlinear phase, were considered. They found that for $Rm \ll 1$ with moderate or large interaction parameters, MHD turbulence evolves towards a state where Joule dissipation and inertial energy transfer are comparable, and their competition produces a quasi-steady equilibrium. For $t > \tau_{Jo}$, Joule dissipation begins to compete with inertial transfer and eventually produces an anisotropic state characterized by an elongation of energy containing eddies in the direction of the external field. Hence, the turbulence tends towards a two-dimensional configuration composed by elongated (and oscillating) eddies with parallel-to-the-field axes. The higher the interaction parameter, the more pronounced the two-dimensional tendency. Most of Joule dissipation occurs inside the cone previously defined by Moreau [1968] and, as the turbulence becomes more anisotropic, a significant part of the energy is transferred from the energy containing region to the dissipative cone (see figure 4.1). For $t > \tau_{tu}$, the energy is confined to nearly transverse wavevectors out of the cone.

However, Alemany et al. claim that, in spite of the quasi-two-dimensionality of the flow, its dynamics is not governed by the laws of two-dimensional turbulence. The energy spectra seem to follow a $\mathbf{k}^{-3}$ law, analogous to that of the enstrophy cascade of two-dimensional decaying turbulence, but it is interpreted in terms of the quasi-steady equilibrium between Joule dissipation and non-linear transfer. In this case, the energy of the eddies is dissipated by Joule effect instead of being transferred to larger scales. Actually, the action of Joule dissipation on the whole wavenumber range appears to prevent also, the establishment of the ordinary Kolmogorov energy cascade as soon as the interaction parameter becomes of order unity.

4.3.1 Two-dimensional Tendency of MHD Turbulence.

As we have seen, one of the most important features of MHD turbulence is its tendency towards two-dimensionality. This fact has been well established through a great experimental and theoretical effort. In general terms, we can state that body forces or boundary conditions are responsible of two-dimensional behavior by preventing the growth of three-dimensional disturbances. But let us try here to understand more deeply why MHD turbulence presents a tendency towards two-dimensionality.

In the MHD approximation, the magnetic field $\mathbf{B}$ immersed in a conducting fluid of electrical conductivity σ and moving with a velocity profile $\mathbf{u}$ satisfies the transport equation [Moreau, 1990]

$$\frac{\partial \mathbf{B}}{\partial t} = \nabla \times (\mathbf{u} \times \mathbf{B}) + \lambda \nabla^2 \mathbf{B}, \tag{4.4}$$

where $\lambda = 1/\mu_o \sigma$ is the magnetic diffusivity. This equation expresses the fact that the local rate of change of $\mathbf{B}$ (or, from a pictorial point of view, of the *magnetic lines of force*) results from the action of two effects, namely, a convective effect expressed by the first right-hand term and a diffusive effect given by the second term. The dominance of either convection or diffusion mechanisms depends on the value of the electrical conductivity of the fluid. A more precise measure of the relative importance of convection and diffusion is given by a dimensionless criterion based on the magnetic Reynolds number, $Rm = UL/\lambda$, previously defined. If Rm is large, convection dominates, and in the limit $Rm \rightarrow \infty$, i.e. if the conductivity of the fluid is infinite, the magnetic lines of force associated with currents within or external to the fluid are frozen in the fluid and move with it [Landau and Liftshitz, 1984]. The fluid acquires rigidity through the tension of the lines of force, giving rise to waves, similar to those in a tense string, which propagate along the lines of force. These waves are known as Alfvén waves. A finite conductivity of the fluid (*i.e.* a finite Rm) adds a diffusive effect to the lines of force and, consequently, a dissipation of energy. In general, exchange of kinetic and magnetic energy as well as dissipation by both viscosity and electrical resistance are present in a conducting fluid [Kraichnan and Montgomery, 1980]. In Chapter 1, we

mentioned that in flows of liquid metals inside strong magnetic fields in laboratory conditions, the magnetic Reynolds number is very small ($Rm \ll 1$) which means that diffusion of lines of force is dominant and any imposed magnetic field is hardly affected by the fluid motion. In other words, the magnetic field induced by the electric currents flowing in the fluid are negligible compared to the applied field.

In general, if the conducting fluid presents a motion either entirely parallel or entirely perpendicular to the lines of force in a uniform magnetic field, the motion is unaffected by the field. In both cases the lines of force are not distorted and equation (4.4) is trivially satisfied.[1] From a dynamic point of view, we can point out that in the parallel case, the Lorentz force is zero while in the perpendicular case, this force is irrotational. Therefore, in both cases the Lorentz force does not affect the original velocity distribution. If the fluid is confined by rigid parallel horizontal walls and the uniform field points vertically (as in duct flows previously considered), purely vertical motion is prevented by the boundaries and purely two-dimensional horizontal motion is unaffected by the magnetic field. Motions with vertical components and motions which are horizontal with vertical gradients distort the lines of force.[2] These motions are attenuated both by the resultant wave radiation and by Joule dissipation, as will be shown below. Thus, the uniform vertical magnetic field favours the pure two-dimensional motion [Kraichnan and Montgomery, 1980].

The description of MHD turbulence in Fourier space provided by Alemany et al. [1979] and by Moreau [1968 and 1990], also offers a very helpful picture of the tendency towards two-dimensionality. Let us consider that the magnetic field can be written as $\mathbf{B} = \mathbf{B}_o + \mathbf{b}$, where $\mathbf{B}_o$ is the applied magnetic field and $\mathbf{b}$ is the turbulent fluctuation of the field. The approximation $Rm \ll 1$ implies that the fluctuation $\mathbf{b}$ is very small compared to $\mathbf{B}_o$. Within this approximation, the governing equations are [Moreau, 1990]

$$\nabla \cdot \mathbf{u} = \nabla \cdot \mathbf{b} = 0, \tag{4.5}$$

$$\frac{\partial \mathbf{u}}{\partial t} + (\mathbf{u} \cdot \nabla)\mathbf{u} = -\frac{1}{\rho}\nabla p + \nu \nabla^2 \mathbf{u} + \frac{1}{\mu\rho}(\mathbf{B}_o \cdot \nabla)\mathbf{b}, \tag{4.6}$$

$$(\mathbf{B}_o \cdot \nabla)\mathbf{u} + \frac{1}{\mu\sigma}\nabla^2 \mathbf{b} = 0. \tag{4.7}$$

In equation (4.6) the irrotational part of the Lorentz force was included in the pressure term. The Fourier transform of the linearized form of the induction equation (4.7) leads to

[1] If the uniform field has the form $\mathbf{B} = B_o\hat{\mathbf{z}}$, an *entierly perpendicular* motion means that the velocity field satisfies $\mathbf{u} = u(x, y, t)\hat{\mathbf{x}} + v(x, y, t)\hat{\mathbf{y}}$.

[2] For instance, if the magnetic field points in the vertical z-direction and the horizontal velocity field is such that $\frac{\partial \mathbf{u}}{\partial z} \neq 0$, equation (4.4) can no longer be satisfied with a uniform field. This means that the magnetic lines of force must be necessarily modified.

$$\hat{\mathbf{b}} = i\mu\sigma \frac{\mathbf{k}\cdot\mathbf{B}_o}{k^2}\hat{\mathbf{u}}. \tag{4.8}$$

This can be used to obtain the Fourier transform of the electromagnetic forces, namely

$$\mathcal{F}\left\{\frac{1}{\mu\rho}(\mathbf{B}_o\cdot\nabla)\mathbf{b}\right\} = -\frac{\sigma(k\cdot\mathbf{B}_o)^2}{\rho k^2}\hat{\mathbf{u}} = -\frac{\sigma B_o^2}{\rho}\hat{\mathbf{u}}\cos^2\theta, \tag{4.9}$$

where θ is the angle formed by vectors $\mathbf{k}$ and $\mathbf{B}_o$. The importance of the factor $\cos^2\theta$ can be understood in relation with the dissipation process (Joule effect) carried out by the induced electrical currents flowing in the medium. Wave vectors located in the neighborhood of the plane $\theta = \pi/2$ (perpendicular to $\mathbf{B}_o$) are not affected by the Joule effect since they do not induce electric currents. This would correspond to a purely two-dimensional flow. In this case the term $\mathbf{u}\times\mathbf{B}$ is exactly balanced by potential gradients, so that the eddy currents vanish [Sommeria et al., 1989]. On the other hand, wave vectors laying in the vicinity of $\theta = 0$ are strongly affected by this kind of dissipation and they will lose their energy in a time scale of the order of τ_{Jo}, unless they receive a supply of energy by non-linear transfer mechanisms.

This discussion can also be addressed in terms of vorticity for $Rm \ll 1$. Turbulence always involves vorticity in all directions and in MHD, one fundamental issue is to determine how the Lorentz force can affect the vorticity field of the flow. This implies to know whether the force $\mathbf{j}\times\mathbf{B}$ is rotational or not, since only a rotational force is able to elude the opposition of the pressure and change the state of rotation of the fluid [Shercliff, 1965]. Obviously, the fact that the Lorentz force is rotational or irrotational depends on the particular situation. It has been long recognized that vorticity can be created or suppressed by the action of a magnetic field. Several interesting cases of this phenomenon have been treated by Shercliff [1965]. He stresses that in the $Rm \ll 1$ approximation the vorticity is only suppressed if it is perpendicular to the magnetic field, although some exceptions exist.[3] It can be shown that in a rectilinear, inviscid, incompressible, laminar shear flow normal to the magnetic field (such that all variables depend only in the coordinate in the B-field direction and time, as in Hartmann flow) the vorticity, transverse to the field, is suppressed exponentially with a characteristic time $\tau_{Jo} = \rho/\sigma B$ [Shercliff, 1965]. Here, the non-uniform Lorentz force suppresses the velocity differences from place to place, promoting uniformity. This can also be seen as the result of the damping of induced eddy currents by Joule dissipation. Similarly to the laminar case, in an MHD turbulent flow with $Rm \ll 1$, a preferential damping of the components of vorticity perpendicular to the field should be expected, despite of the natural tendency of turbulence towards isotropy. Therefore, initially homogeneous turbulence presents a tendency to become axisymmetric about the field direction and,

[3]For example, in a rectilinear shear flow parallel to a magnetic field, the magnetic forces do not affect the vorticity, even though it is perpendicular to the field, because the term $\mathbf{u}\times\mathbf{B}$ is zero.

eventually, decay into a two-dimensional eddying motion. Under the action of a uniform magnetic field perpendicular to the plane of the flow, the two-dimensional state tends to be preserved since the field can not modify the flow velocity distribution, as we previously observed. In this case, the vorticity is parallel to the field and the Lorentz force is irrotational (i.e. potential) and can be included in the pressure term of the equation of motion. So that, the motion (vorticity) is unaffected by the magnetic force provided the boundary conditions for the velocity field do not depend on the pressure [Branover, 1978].

4.3.2 The Mechanism of Formation of Quasi-two-dimensional Vortices

It has been mentioned that a uniform magnetic field transverse to the flow favours two-dimensional motion, first by dissipating the components of vorticity perpendicular to the field and second, by keeping unaffected pure two-dimensional motion in the plane normal to the field. The picture of fully developed MHD turbulence (at $Rm \ll 1$ and $N \gg 1$) as a collection of two-dimensional eddies with axes parallel to the magnetic field has been favored by many authors [Alemany et al., 1979; Sommeria and Moreau, 1982; Sukoriansky and Branover, 1987]. Sommeria and Moreau [1982] explained the formation of these elongated turbulent structures through the action of an electromagnetic diffusion along the field lines. In order to understand this diffusion mechanism, first notice that, if the applied magnetic field $\mathbf{B}_o$ points in the y-direction, the expression for the magnetic fluctuation $\mathbf{b}$ in terms of the velocity field $\mathbf{u}$, can be drawn from the induction equation (4.7) as [Moreau, 1990]

$$\mathbf{b} = -\mu\sigma B_o \nabla^{-1} \frac{\partial \mathbf{u}}{\partial y}, \tag{4.10}$$

where ∇^{-1} stands for the inverse of the Laplacian operator. Substituting $\mathbf{b}$ in the momentum balance equation (4.6) we get [Roberts, 1967]

$$\frac{D\mathbf{u}}{Dt} = -\frac{1}{\rho}\nabla p + \nu\nabla^2\mathbf{u} - \frac{\sigma B_o^2}{\rho}\nabla^{-1}\frac{\partial \mathbf{u}}{\partial y}. \tag{4.11}$$

Now, if we assume that the anisotropy in the field direction is strong enough the following approximations are valid

$$\frac{\partial}{\partial y} \ll \frac{\partial}{\partial x}, \frac{\partial}{\partial z} \quad u_y \leq u_x, u_z.$$

Then we can express equation (4.11) in the form

$$\frac{D\mathbf{u}}{Dt} = -\frac{1}{\rho}\nabla_\perp p + \nu\nabla_\perp^2\mathbf{u} - \frac{\sigma B_o^2}{\rho}\nabla_\perp^{-1}\frac{\partial \mathbf{u}}{\partial y}, \tag{4.12}$$

where $\nabla_\perp$, $\nabla_\perp^2$ and $\nabla_\perp^{-1}$ represent the gradient, the Laplacian and the inverse Laplacian operators in a transverse plane, respectively, and $D\mathbf{u}/Dt = \partial/\partial t + \mathbf{u}_\perp \cdot \nabla_\perp$. Taking the curl to equation (4.12) we find that the parallel component of vorticity ω_y (but not any other component) satisfies

$$\frac{D\omega_y}{Dt} = \nu\nabla_\perp^2\omega_y - \frac{\sigma B_o^2}{\rho}\nabla_\perp^{-1}\frac{\partial\omega_y}{\partial y}. \tag{4.13}$$

This equation shows that the interaction of different transverse planes is given through viscous and electromagnetic forces, though the former are much weaker in high Reynolds number flows. For a given eddy the application of the ∇^{-1} operator reduces to multiplication by $-l_\perp^2$. Hence the electromagnetic force drives a diffusion of vorticity in the $\mathbf{B}_o$-field direction with the diffusivity $\alpha = \sigma B_o^2 l_\perp^2/\rho$, dependent on the length scale $l_\perp$ of the given eddy. This unidirectional diffusion is a degenerate form of the propagation of the Alfvén waves when $Rm \ll 1$ [Roberts, 1967]. The effect of the diffusion mechanism is the suppression of velocity differences between transverse planes. The time required to establish a good correlation between two planes perpendicular to $\mathbf{B}_o$ and separated by a distance d, is

$$\tau_d = \frac{\rho}{\sigma B_o^2}\frac{d^2}{l_\perp^2}. \tag{4.14}$$

In homogeneous turbulence, the net result of this mechanism is manifested as dissipation by the Joule effect. In the non-magnetic case, a typical turbulent structure of length scale l, influenced by nonlinear transfer, will be rotated and broken up into smaller eddies in a turnover time τ_{tu}. In the magnetic case, on the other hand, during a turnover time $\tau_{tu} = l_\perp/u_\perp$), besides the nonlinear transfer the turbulent structure will experience the electromagnetic diffusion mechanism that promotes the propagation of vorticity in the $\mathbf{B}_o$-direction. Hence, all transverse planes for which the separation is less than

$$\sqrt{\alpha\tau_{tu}} \approx l_\perp\sqrt{\frac{\sigma B_o^2 l_\perp}{\rho u_\perp}} = l_\perp\sqrt{N_o}$$

will be correlated, where N_o is the local interaction parameter based on the eddy transverse length scale $l_\perp$. In other words, the correlation reaches all the planes along a cylinder of characteristic length $\sqrt{\alpha\tau_{tu}} = l_\parallel \approx l_\perp\sqrt{N_o}$. This gives, as a consequence, the inhibition of energy transfer towards small scales, some slight increase of the eddy transverse size and the formation (after a transient phase) of an anisotropic state characterized by the condition $l_\parallel/l_\perp \approx \sqrt{N_o}$ for each turbulent structure [Sommeria and Moreau, 1982]. This last conclusion is valid only for eddies for which $l_\perp\sqrt{N_o}$ is smaller than the gap of the walls normal to the field. Experimental evidence of this behavior has been provided through the measurements of the correlations of fluctuations in the longitudinal flow velocity at two points of the cross-section of a rectangular duct

[Platnieks and Freibergs, 1972]. When these points lie on a magnetic line of force, the correlations become close to unity, while for points located on a straight line perpendicular to the field, the correlation is slightly modified by the field. Sommeria [1983] also verified experimentally the two-dimensional tendency of fully developed MHD turbulence and the formation of elongated structures in insulated ducts. He found a relatively slow decay of turbulence energy in strong magnetic fields with a k^{-3} spectra, characteristic of MHD turbulence in a uniform field. He interprets this spectra as an indication that the inertial transfer towards small scales is inhibited, which is partly indicative of an enstrophy cascade. Measurements of turbulent heat diffusion along two perpendicular directions demonstrated the two-dimensionality of large eddies. His experiments support the idea that this sort of turbulence should be described as a mixture of two-kinds of interacting eddies, namely, large two-dimensional eddies slightly affected by the magnetic field, according to the model of Sommeria and Moreau, and small three-dimensional eddies involving strong Joule dissipation.

Even though the mechanism that creates the elongated structures in the field direction is present in both conducting and insulating ducts, the kind of walls perpendicular to the field is of fundamental importance for the behavior of the turbulence. Sommeria and Moreau [1982] stressed that the presence of insulating walls perpendicular to the magnetic field is a necessary condition for the persistence of turbulence and eventually to the development of two-dimensional behavior.[4] This conclusion is based on some experimental results [Platnieks and Freibergs, 1972] that showed the complete damping of turbulence in channels with conducting walls when the parameter M/Re exceeds a certain critical value. On the other hand, in insulated ducts the turbulence persists even when $M/Re > (M/Re)_{crit}$. These results are related with the fact that the rate of decay of vortex elongated in the direction of the magnetic field is much lower in insulated channels than in conducting ones, as we will show later. While the currents induced by a vortex perpendicular to an insulated wall are dissipated through Hartmann layers, in the presence of a conducting wall currents are allowed to go through the wall, where the electrical resistance is much lower than in the Hartmann layers and dissipation is completed faster. Sommeria and Moreau also showed that the Hartmann layers in insulating channels have a decisive influence on the turbulence. They found that because of the interaction of the bulk of the flow with the Hartmann layers, the axes of quasi-two-dimensional eddies have their ends perpendicular to the walls to a good approximation, although they could bend away. Furthermore, the presence of insulating walls perpendicular to the field separated by a certain distance, leads to a kind of *quantization* of the portion of Fourier space which carries the energy.

[4] However, some recent experiments reviewed in sections 4.5 and 4.6 appear to contradict this conclusion.

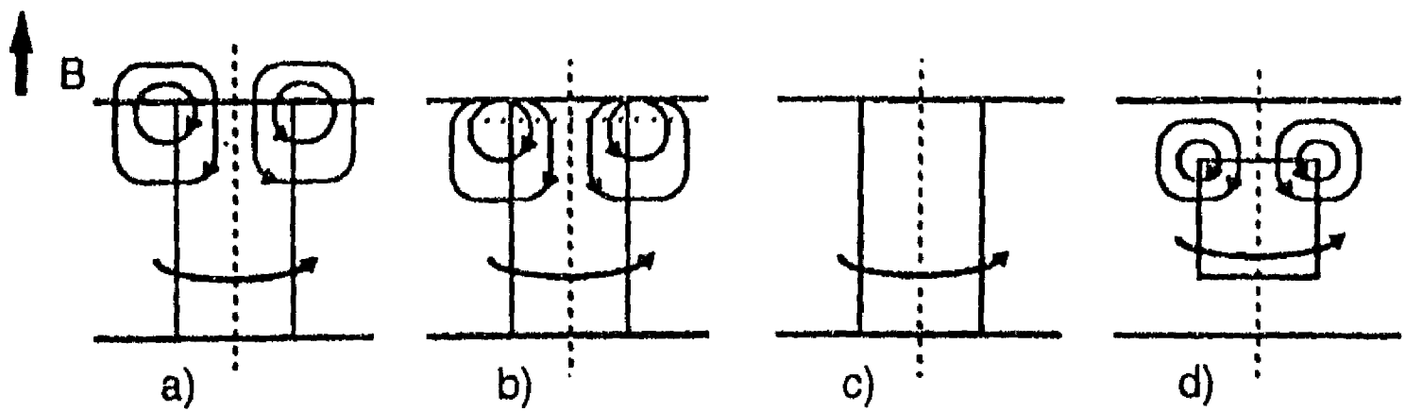

Figure 4.2: A vortex aligned with a uniform magnetic field confined between: a) conducting walls; b) insulating walls; c) two free surfaces and d) liquid-metal surfaces [Sommeria *et al.*, 1989].

4.3.3 Dissipation of elongated vortices

In order to understand the mechanism of electromagnetic dissipation in a simplified way and to assess the role of the walls perpendicular to the magnetic field, let us consider a vortex aligned with a uniform field B_o [Sommeria *et al.*, 1989]. In this configuration the vortex acts as an electric dynamo that produces a voltage of the order of $U B_o L$, where U and L are the characteristic velocity and transverse dimension of the vortex. When the vortex is confined between conducting walls, spanning the whole gap, a strong current circulates through the highly conducting walls, and the kinetic energy of the vortex is transformed into electric energy and dissipated by Joule effect in a characteristic time τ_c (fig. 4.2.a). If the walls are insulating the currents will circulate only through the poorly conducting Hartmann layers (fig. 4.2.b), and the characteristic dissipation time τ_{nc} will be much longer than τ_c. In saying highly and poorly conducting here, we are comparing the high resistance $1/\sigma\delta_{Ha}$ of the boundary layer, where δ_{Ha} is the thickness of this layer (Hartmann layer), with the low resistance $1/\sigma_w t_w$ of the wall, where t_w is the thickness of the solid wall. In the ideal case of a vortex spanning the whole gap between two free surfaces, the dynamo would be in an open circuit and dissipation would be absent (fig. 4.2.c). On the other hand, a vortex that does not span the whole width, which represents a flow dependent on the coordinate in the direction of the **B**-field (i.e. a three-dimensional flow), is damped in a similar way as with a conducting wall (fig. 4.2.d).

In a real flow an elongated vortex can be broken both by inertial effects or Joule dissipation. In addition, it was previously shown (see eq. (4.14)) that the time required to establish a good correlation between two planes perpendicular to $\mathbf{B_o}$ and separated by a distance d is

$$\tau_d = \frac{\rho}{\sigma B_o^2}\frac{d^2}{l_\perp^2} = \frac{1}{N_o}\frac{d^2}{l_\perp^2}\tau_{tu}. \tag{4.15}$$

It appears that in many laboratory experiments τ_d is much smaller than τ_{tu}. Then it is possible to establish a good correlation between parallel planes perpendicular to $\mathbf{B}_o$ (i.e. quasi two-dimensionality) before the elongated eddy breaks due to inertial transfer. Let us now see how τ_d compares with the dissipation times τ_{nc} and τ_c. It can be shown [Picologlou, 1992b] that an elongated vortex $U_\theta(r,t)$ aligned with the magnetic field and confined between insulating walls will decay according to

$$U_0(r,t) = U_0(r,0)exp\left[-\frac{N}{M}t\right]$$

where all the variables are expressed in dimensionless terms. Then the characteristic time of decay in dimensional units is

$$\tau_{nc} = \frac{M}{N}\frac{d/2}{\bar{U}}$$

where M and N are the global Hartmann number and the interaction parameter and $\bar{U}$ is a mean characteristic velocity. The correlation time τ_d (eq. (4.15)) can also be expressed as

$$\tau_d = \frac{\rho\bar{U}}{\sigma B_o d/2}\frac{d^2}{l_\perp^2}\frac{d/2}{\bar{U}} = \frac{1}{N}\frac{d^2}{l_\perp^2}\frac{d/2}{\bar{U}},$$

and then we get

$$\frac{\tau_d}{\tau_{nc}} = \frac{1}{M}\frac{d^2}{l_\perp^2}.$$

In the case of thin conducting walls, the characteristic time of vortex decay is [Picologlou, 1992b]

$$\tau_c = \frac{1}{Nc}\frac{d/2}{\bar{U}}$$

where $c = \sigma_w t_w/\sigma(d/2)$ is the conductance ratio. So we have

$$\frac{\tau_d}{\tau_c} = c\frac{d^2}{l_\perp^2}.$$

Taking some experimental values for the flow of NaK in a square duct with $d/2 = 0.439m$, $c = 0.07$, $M = 5300$ and $N = 2900$ [Reed and Picologlou, 1989] we can obtain a quantitative idea of how these times are compared:

$$\frac{\tau_d}{\tau_{nc}} \approx \frac{10^{-2}}{l_\perp^2}$$

$$\frac{\tau_d}{\tau_c} \approx \frac{10}{l_\perp^2}.$$

Since the vortex transverse characteristic dimension $l_\perp$ is small ($l_\perp \ll d$)[5] we have

$$\tau_d < \tau_{nc}, \qquad \tau_d > \tau_c.$$

This means that in insulating wall ducts a good correlation is established before the vortex decay, while in conducting walls the decay arrives before the correlation is established. Nevertheless, even with conducting walls a certain degree of correlation is expected to be reached, which is enhanced with smaller conductance ratios.

4.4 Laminarization and Residual Turbulent Disturbances.

A magnetic field affects the stability of a conducting fluid by interacting on the turbulent fluctuations and on the mean stationary flow. In addition to viscous dissipation, in a magnetic field energy is also dissipated by Joule effect which causes a faster damping of perturbations than in non-MHD flows. Hence, the magnetic field will enhance the decay of turbulence through Joule dissipation.

Many experimental investigations have confirmed the *suppression* of turbulence in the presence of a transverse magnetic field both in conducting and nonconducting channels. An extensive review of these works can be found in Branover [1978] and Branover and Gershon [1979]. Most of the studies reveal that, exceeding a critical value of the parameter M/Re, the duct flow obeys the laminar theory according to friction measurements. However, some unexpected results have also been found. Although the friction factor follows a laminar law, the turbulence level still remains quite significant. In some cases, an increase in the magnetic field strength provokes a decrease in the turbulence level and then it starts increasing again, while the friction remains in the laminar level. Experiments also show an abrupt reduction of turbulence intensity at the entry of the flow into the magnetic field, nevertheless, the intensity along the remaining part of the flow stays almost unchanged. Hence, experimental results appear to support the idea that, in the presence of a strong transverse magnetic field, a flow may present a laminar behavior according to its integral characteristics but still contain strong velocity fluctuations [Branover, 1978].

The laminar behavior of the friction factor once M/Re reaches its critical value suggests that, for $M/Re \geq (M/Re)_{cr}$, there is virtually no generation of turbulence.

[5] Assuming the $l_\perp$ is meassured in meters.

Therefore, convection of fluctuations should be the cause of the velocity fluctuations observed at large distances from the entrance of the flow in the magnetic field. The persistence of low-frequency velocity fluctuations (with very slight damping) even in strong magnetic fields implies that they should present a quasi-two-dimensional structure in the plane perpendicular to the field. In such a case, Joule dissipation is reduced to a minimum (as it was discussed in subsection 4.3.1) and the maintenance of a high turbulence level does not require the generation of additional turbulence [Branover, 1978]. The transition from three-dimensional isotropic turbulence to quasi-two-dimensional turbulence under a uniform magnetic field, could then be considered as a process where the flow is *laminarized* by the field while quasi-two-dimensional *turbulent* disturbances still persist. The origin of this *residual* turbulence was addressed by Branover and Gershon [1979]. They claim that these disturbances are mainly generated at the entry of the flow into the magnetic field region, as a result of an strong instability of the M-shaped mean velocity profile. Turbulent structures conveyed by the flow upstream from the entrance to the magnetic field appear to have little influence.

4.5 Beer-Sheva Experiments

Experimental results obtained at the University of Beer-Sheva, Israel, point to the existence of an inverse energy cascade along with an enstrophy cascade in liquid-metal flows in non-conducting channels [Sukoriansky *et al.*, 1986; Branover *et al.*, 1988; Sukoriansky and Branover, 1988]. This conclusion is supported through energy spectra measurements that show a $k^{-5/3}$ spectra in the low wavenumber region (characteristic of inverse cascade) along with a k^{-3} spectra in the high wavenumber region (characteristic of enstrophy cascade). An increase of energy of low frequency disturbances was detected. The aim of the experiments was to clarify how this two-dimensional turbulent situation is established. Although these experiments were performed far from fusion reactor relevant conditions, it is expected that they may clarify some fundamental phenomena and have some relevance to fusion technology.

Turbulent mercury flows in a rectangular cross-section duct subjected to a transverse magnetic field were investigated. Conducting and non-conducting wall ducts were analyzed. In non-conducting wall ducts, a source of forced turbulence was placed either inside the magnetic field or upstream from the magnet. Turbulence forcing was realized using grids with either cross bars or with parallel bars of different orientation relative to the magnetic field direction [Sukoriansky, *et al.*, 1986]. It is argued that a strong enough magnetic field originates a directional redistribution of turbulent energy which leads to a strong anisotropy of turbulence. When turbulence becomes highly anisotropic, the energy transfer mechanism is modified and, in the case of turbulence with permanent forcing, the normal direct energy cascade is inversed. Experiments in nonconducting channels showed that when energy is injected to the flow outside the magnetic field, turbulent energy decreases at all wavenumber values with an increase of

the magnetic field strength. On the contrary, when energy is injected within the magnetic field, after an initial decrease, turbulent energy increases in the low wavenumber region. The fact that the increase of turbulent energy is observed at wavenumbers that are one or two orders of magnitude smaller than the wavenumbers where the energy injection occurs, suggests that the energy is transferred from the high k-region into the low k-region. It is speculated that this inversion of the spectral energy transfer takes place when the (local) interaction parameter $N_o = \sigma B^2 l/\rho u_l$, based on eddy characteristic velocity and length scale, approaches unity. Or, in other words, when the Joule time becomes of the same order as the eddy turnover time. The inversion of the energy transfer was also observed when vortices parallel to the magnetic field lines were created by a grid. However, when the grid produced vortices perpendicular to the field, no inverse energy transfer was detected. In such a case, vortices were quickly damped by Joule dissipation. An inverse energy transfer inhibits the energy flux toward small-scale regions where viscous dissipation occurs and leads to the persistence of large scale strongly anisotropic (quasi-two-dimensional) turbulent structures with a very low dissipation rate. It is claimed that such structures dramatically enhance the heat transfer in the direction perpendicular to the magnetic field [Sukoriansky, *et al.*, 1988].

Measurements carried out in channels with electrically conducting walls also reveal heat transfer enhancement. Even though previous experimental evidence indicates a rapid damping of turbulence in channels with conducting walls, The Beer-Sheva experiments show the persistence of turbulence in these channels in conditions where the flow should be 'laminarized'. It appears that the magnetic field suppresses the turbulence only in the core of the flow whereas significantly enhances the turbulence intensity in the vicinity of the channel walls without the need of external flow perturbing means. Experiments indicate that the turbulence in conducting channels is continuously created along the channel, probably due to steep velocity gradients associated with M-shaped velocity profiles. The continuous excitation of eddies might lead to the establishment of a significant level of quasi-two-dimensional turbulence and to the enhancement of heat transfer [Branover *et al.*, 1986].

4.6 Argonne National Laboratory Side Wall Instability Experiments

Experiments carried out at Argonne National Laboratory demonstrated the existence of a flow instability in a rectangular thin conducting wall duct near fusion reactor relevant conditions [Reed and Picologlou, 1989]. The instability developed in a side layer jet attached to a side wall parallel to the magnetic field and presented a very strong periodicity and lack of small scale structure. It is speculated that this instability may have beneficial effects on the thermo-hydraulic performance of the blanket through an

enhancement of heat transfer from the first wall. Hence, one of the most important points that remain to be determined is the possibility of reaching and maintaining such instability at the actual conditions that prevail in the first wall coolant channels of lithium-cooled blankets.

Experiments were carried out in the ALEX facility designed to the study of liquid-metal MHD flows of relevance to fusion reactor blankets. The flow of a liquid metal (NaK) in a thin conducting wall duct ($c = 0.07$) of square cross section ($L = 0.439m$), under the action of a strong transverse magnetic field generated by an electromagnet was analyzed. Referring to the same coordinate system as in figure 3.15 where the magnetic field points in the z-direction, measurements were performed in the mid-plane of the duct ($y = 0$) and extended, in the axial direction, from near the inlet to the magnet to near the exit of the flow from the magnetic field. Likewise, in the transverse to the field z-direction, measurements were obtained in the region $0.95 > z \geq 0.60$. For $z < 0.60$, the velocity is uniform. The quantitative information about the evolution and spreading of the instability was obtained by power spectral density (PSD) plots[6] and velocity time histories (oscilloscope traces), as well as mean velocity measurements and pressure distributions. The range of Hartmann numbers and interaction parameters explored was $2900 < M < 5800$ and $540 < N < 1.26 \times 10^4$, respectively. Whenever the instability is formed, it always appears well within the region of homogeneous magnetic field, downstream of the inlet fringing field region. Figure 4.3, obtained as a superposition of measurements taken at different axial positions, shows qualitatively the physical extent of the instability in the axial and transverse directions and its relative position with respect to the magnetic field distribution. The normalized magnetic field distribution with respect to the dimensionless axial coordinate is shown near the top of the figure. This distribution is uniform in the z-direction. Figure 4.3 corresponds to the case $M = 5300$ and $N = 2900$. Many characteristic features of the phenomena are reflected in this picture.

After the onset of the instability, it quickly expands to occupy a region of the flow which extends more than 20 characteristic lengths of the duct in the x-direction within the uniform region of the field; its width is approximately constant in the z-direction, namely, $0.70 < z < 1.0$. The instability begins as a harmonic oscillation in the mean velocity. It appears that there is movement of energy out of the low frequencies as the flow proceeds downstream, even though the physical size of the region of the instability remains constant. Actually, after a few characteristic lengths, the instability reaches a somewhat stable size that maintains with slow changes over many characteristic lengths in the axial direction. Reed and Picologlou noted two striking features of the axial distribution of velocity time histories near the wall: the large amplitude of the instability oscillations with respect to the mean velocity, and the strongly periodic character of the velocity signals as the flow proceeds downstream. This fact indicates the well organized structure of the instability in the near-the-wall region, reaching a

[6]PSD plots give a measurement of the energy content of the perturbations.

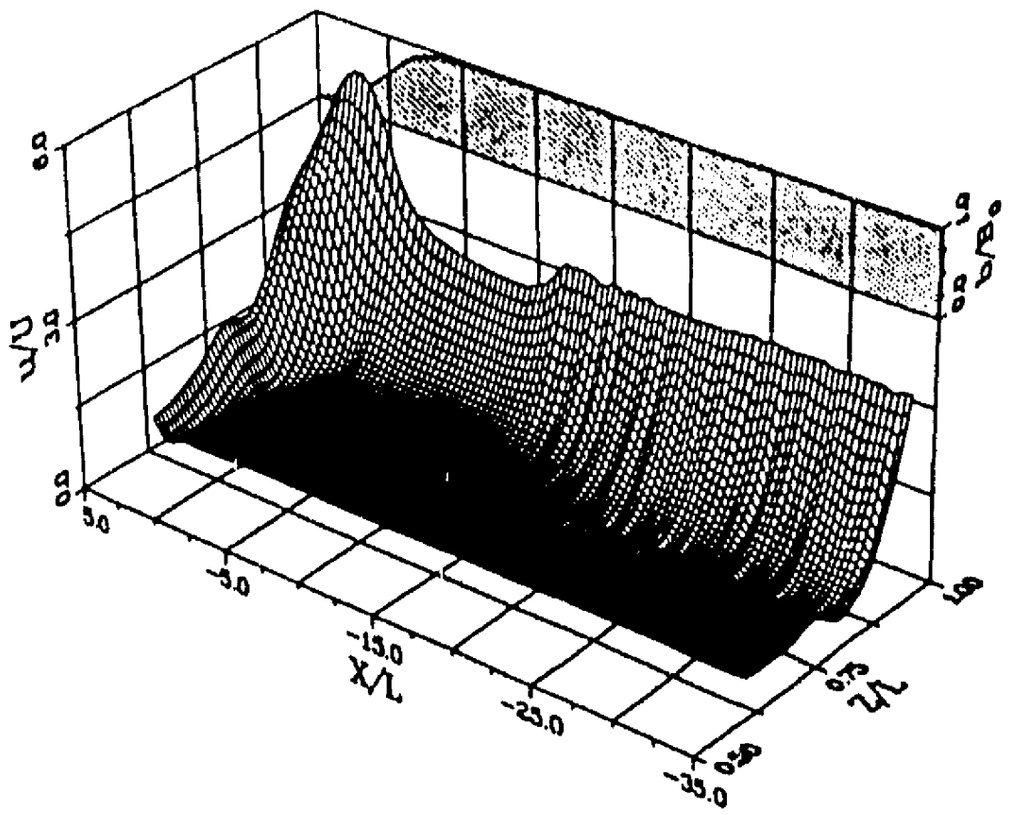

Figure 4.3: Two-dimensional velocity distribution surface in a thin conducting wall rectangular duct showing the wall-jet instability region. $M = 5300$, $N = 2900$, $c = 0.07$. [Reed and Picologlou, 1989].

higher degree of coherence as the flow travels in the downstream direction. Although oscillations at $z = 0.95$ are of large amplitude, coherent and well defined, they present a fast decrease with distance from the wall and, at $z = 0.75$, disappear almost completely (see figure 4.4). In general, the whole spectrum increases in energy content as the wall is approached (the frequency content of the spectra including higher and higher frequencies). In the region of uniform field, a smooth and monotonic growth of spectral energy content is found as one approaches the wall region but with a dramatic increase in the energy content of the perturbations as one moves from $z = 0.60$ to $z = 0.95$. One of the main effects of the presence of the instability on the mean velocity distributions is the apparent thickening of the wall jet layer.

Additional measurements showed the progressive suppression of the instability as the interaction parameter was increased. As a matter of fact, for the same Hartmann number ($M = 5300$) but an interaction parameter of 11,000, the instability is still present but has a minimum influence on the behavior of the flow. Measurements indicate a negligible increase in the intensity of the fluctuations as one moves downstream. For this high N, the effects of the instability are more closely confined to the near wall region than in the low interaction parameter case. For positions $z < 0.75$ there is virtually no presence of the instability. Increase in the interaction parameter from 2900 to 11,000 leads to a very rapid suppression of the instability and for the highest

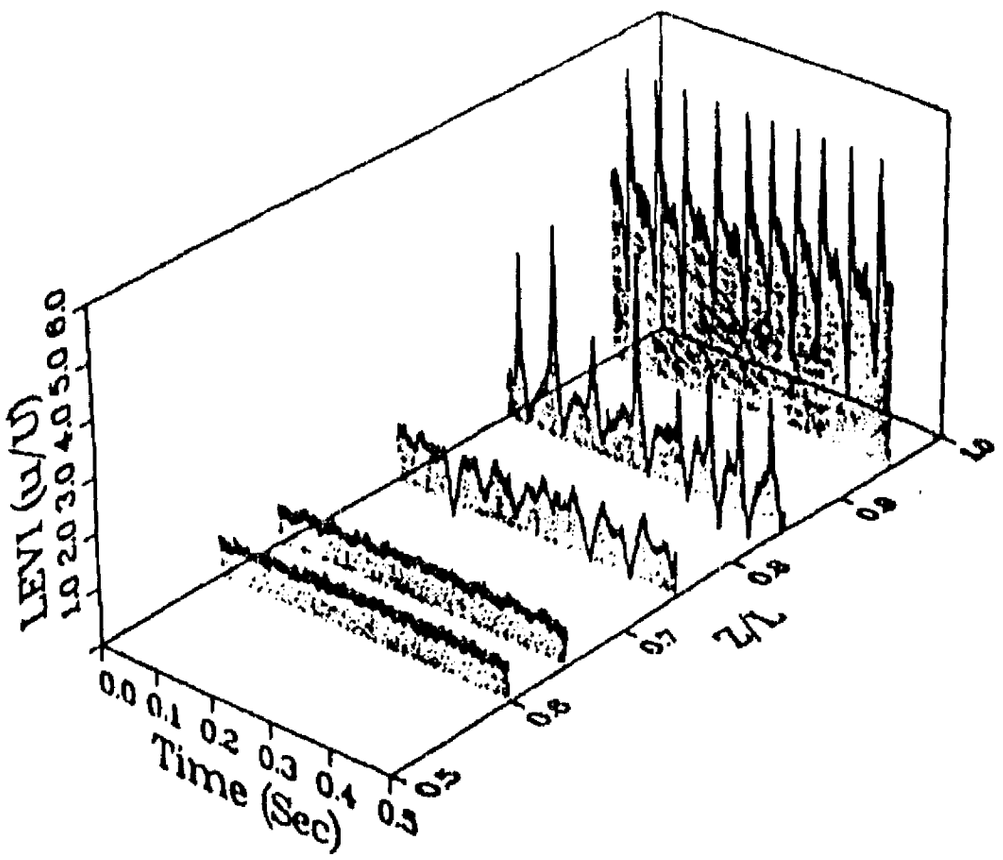

Figure 4.4: Transverse distribution of velocity time histories in a thin conducting wall rectangular duct: $X/L = -36$, $M = 5300$, $N = 2900$, $c = 0.07$. [Reed and Picologlou, 1989].

experimental value of $N = 48,000$ it can be considered completely non-existent.

The influence of the Hartmann number was also explored. It was found that as long as the Hartmann number is large enough, it has a negligible importance on the onset of the instability. This was concluded after noting that three spectra obtained for different Hartmann numbers in conditions near the onset of the instability, collapse on each other after scaling the spectral frequencies with $N^{-1/3}$. The insensitivity of the onset of the instability on M implies that the stability of the wall jet is not, to a first order, affected by the magnitude of the magnetic field. Nevertheless, the evolution and final state of the instability as well as its heat and mass transfer properties present a very strong dependence on M. Over the ranges of M and N examined, the onset of the instability depends primarily on the Reynolds number. It was concluded that the critical Reynolds number lies in the range $2650 < Re_{cr} < 5100$ and is independent of M in the range $2700 < M < 5400$.

A preliminary linear stability analysis of the side layer instability flow indicates that the steady flow in the core is unconditionally stable and is never perturbed by any fluctuations in the side layers [Ting, *et al.*, 1991]. This analysis also shows that the instability involves only motions in planes perpendicular to the magnetic field. Significant values of the component of the velocity in the direction of the field for all wave lengths and all values of the Reynolds number do not seem to affect the stability

of the high velocity side layers. The transverse disturbance velocity is of the same order of magnitude of the axial disturbance velocity which, in turn, coincides with the observed experimental fluctuations. The instability of the side layers involves a disturbance vorticity parallel to the magnetic field which is confined to the layer and which has an axial scale comparable to its transverse $O(M^{-1/2})$ scale.[7] The analysis presents some limitations due to its linear nature, and this is partly reflected in the predicted critical Reynolds number of the instability which is one order of magnitude less than the experimental value. Although the instability found in the experiments probably contains high nonlinear ingredients, the former linear analysis implies the existence of large, periodic fluctuations inside the high-velocity side layer which will produce an excellent mixing in this region and strongly enhance the heat transfer from the first wall.

[7] A propagation of vorticity in the field direction as a result of an electromagnetic diffusion mechanism similar to the one proposed by Sommeria and Moreau [1982] could be expected.

Chapter 5

Turbulent Flow and Heat Transfer Analysis

5.1 Introduction

This Chapter is devoted to the analysis of turbulent liquid-metal flow and heat transfer in square ducts with walls ranging from thin conducting to insulating, under strong transverse magnetic fields. The analysis is motivated by experimental results obtained at Argonne National Laboratory and Beer-Sheva, which were reviewed in Chapter 4. The ANL experiments demonstrated the existence of a flow instability in the layers attached to the side walls (parallel to the magnetic field) near to fusion reactor relevant conditions. Experimental results showed high-energy periodic fluctuations in the side layer that can not be classified as turbulent, although it is speculated that they will originate an excellent mixing and will enhance the heat transfer in that region. Likewise, the Beer-Sheva experiments at different conditions, found the enhancement of turbulent intensity in the vicinity of the walls, even in conducting channels. The beneficial implications for the heat transfer were also verified. However, a deeper insight into the mechanisms producing and controlling these phenomena is required for practical applications. For instance, the present understanding of the side layer instability phenomena does not allow the implementation of a numerical or analytical model to reproduce the experimentally observed results. In order to explore duct flows beyond laminar conditions, imaginative theoretical approaches should be devised. Here, we address the problem assuming a fully developed turbulent flow though, evidently, results differ from the ANL experimental situation. However, this work represents a first step towards the modeling of the side wall boundary layer phenomena beyond the laminar regime. In addition, as the introduction of turbulent effects in this kind of flows has not been previously considered, it becomes an interesting theoretical problem. We extend the core-side-layer solution to include turbulent effects through an eddy viscosity model from the Renormalization Group (RNG) theory of turbulence. Although this is an ordinary (non-MHD) turbulence model, it draws some features that make physical sense in the MHD situation. The RNG turbulent model is not an *ad hoc* model but it is easily implemented and has been previously used in some MHD problems with

positive results. On the other hand, there is no abundance of MHD turbulence models available for this problem. The spectral code developed for the turbulent regime allows the introduction of models that can be expressed through an eddy viscous diffusivity. A future task will be the implementation of additional models.

We first introduce the basic ideas behind the RNG theory of turbulence and present the eddy viscosity model as it was originally formulated, together with the concept of integral length. Afterwards, a second version of the RNG eddy viscosity with an integral length scale model that considers boundary layer characteristics is exposed. Validation of the model for an OHD flow is performed through comparison of friction factor values calculated with the model against empirical correlations. We also compare results obtained with both models for the MHD problem and select the original version as the one that makes more physical sense for our problem. Later, we carry out a parametric study of the influence of conductance ratio and Hartmann and Reynolds numbers on the structure of both mean velocity and total viscosity profiles. The heat transfer analysis is then addressed using as an input the turbulent profiles and the RNG effective thermal diffusivity formula for the case of liquid lithium. The influence of c, M and Re on mean temperature profiles and local Nusselt numbers is also analyzed and some observations regarding the effect of turbulence on heat transfer in thin conducting and insulating wall ducts are performed.

5.2 Renormalization Group (RNG) Theory of Turbulence

In the numerical simulation of turbulent flows, a large number of excited scales of motion must be resolved. However, practical considerations regarding computing storage and capacity prevent from a full direct numerical simulation for high-Reynolds-number flows. Even for moderately high Reynolds numbers (100-1000), direct simulation becomes a difficult task. Large Eddy Simulation (LES) provides an alternative approach. In the LES approach only large scale motions, which are directly affected by the boundary conditions and the forces driving the flow, are explicitly computed while small (sub-grid) scale motion, which is assumed to be nearly universal, is modeled. Another alternative involves the classical approaches of Reynolds and Boussinesq, in which only mean values are calculated while fluctuations are modeled through an eddy viscosity. This is the approach we follow in the present work. It is expected that the eddy viscosity contains information about the motion of different scales that are not explicitly resolved. The eddy viscosity used here comes from the Renormalization Group (RNG) theory of turbulence developed by Yakhot and Orszag [1986]. This theory has received much attention in recent years [Kraichnan, 1987; Smith and Reynolds, 1992; Lam, 1992] and has been applied to a number of MHD and non-MHD problems with relative success [Yakhot *et al.*, 1987; Sukoriansky *et al.*, 1992; Talmage *et al.*, 1991b;

Talmage, 1993; Yakhot *et al.*, 1992]. Extension of this theory to Plasma MHD has also been carried out [Langcope and Sudan, 1991; Camargo and Tasso, 1992]. Actually, the Yakhot and Orszag RNG theory provides information for closing LES and two-equation $K-\epsilon$ models. Also, this theory gives an algebraic eddy viscosity expression in which there is a length scale that must be specified outside the theory. This last option, a *zero-equation turbulent model*, is chosen in this work.

Renormalization theory was mainly developed in the physics of phase transitions based on the idea of self-similarity, that is, the tendency of identical mathematical structure to recur on many levels. This idea was exported to turbulence theory noticing that the classical picture of a turbulent *cascade* involves precisely this structure. In addition, the transition to turbulence can also be interpreted as a kind of *phase* transition in a fluid, namely, a transition in flow-pattern. The basic idea behind the RNG theory of turbulence is the elimination of the smaller-scale modes and the inclusion of their influence in an effective (renormalized) viscosity, so that only the largest scales remain.[1] In this way, it is expected that the effect of small and fast eddies on large and slow turbulent eddies can be assessed.

The RNG procedure involves dynamic scaling and invariance along with iterative perturbation methods. It allows the systematic elimination of small scale isotropic disturbances by considering their averaged influence on large scales, and the calculation of renormalized transport coefficients. The elimination of all fluctuating isotropic scales takes place, essentially, in the inertial range. Hence, it is assumed that the Reynolds number is sufficiently large for such a range to exist. During the scale elimination procedure, the dissipation cut-off is moved from k_{vis} to a new cut-off at smaller wavenumber k_f and once the whole inertial range is eliminated, k_f is related to the integral length scale of the system. Hence, the integral length corresponds to the smallest fluctuating scale retained in the system after the RNG procedure of scale elimination is completed. As a result of the scale elimination process, a renormalized equation of motion together with an expression for the total viscosity are obtained. In this way, the viscosity increases from the molecular value ν_o to an effective value ν_t, which depends on the local rate of strain. The elimination of only small isotropic scales is justified by Yakhot and Orszag by arguing that not all turbulent eddies interact with the mean flow and, consequently, not all eddies contribute to turbulent viscosity. The laminarization effect of a magnetic field appears to support this conclusion. As we mentioned in Chapter 4, a large enough magnetic field originates a strong anisotropy in turbulent channel flow; the velocity and friction factor approach those of laminar flow while the total turbulent intensity remains quite high. It appears that strongly anisotropic fluctuations of the velocity field may not interact with the mean flow and do not contribute to turbulent diffusivity. Yakhot and Orszag also claim that a sufficiently anisotropic small-scale flow, either decouples from the large-scale flow or gives its energy to the large eddies. Only when small scales are sufficiently isotropic they do increase the dissipation of

[1] In the case of Plasma MHD, simultaneous renormalization of viscosity and resistivity is required.

large scales and thus give rise to a positive turbulent viscosity. The renormalization procedure has also been applied to the heat transfer equation, obtaining as a result an effective thermal diffusivity [Yakhot and Orszag, 1986] that will be presented in section 5.4 where the turbulent heat transfer problem is addressed.

5.2.1 RNG Eddy Viscosity Model: First Version

Due to the anisotropic effect of the magnetic field, in Chapter 2 we distinguished two different total viscosities in each direction, namely, ν_{ty} and ν_{tz}. However, in the core-side-layer flow we want to consider, the principal viscous effects come from the side wall, for Hartmann layers are neglected. Therefore, the relevant viscosity is ν_{tz}. In what follows, we assume that $\nu_{ty} = 1$ and $\nu_t = \nu_{tz}$.

In dimensional terms, the total viscous diffusivity (molecular + turbulent) given by the RNG model of Yakhot and Orszag [1986] is

$$\nu_t = \nu_o \left[1 + H\left(\frac{C_1 \bar{\epsilon} l_o^4}{\nu_o^3} - C_2\right)\right]^{1/3}, \tag{5.1}$$

where the Heaviside function $H(x)$ is defined as $H(x) = x$ when $x > 0$ and $H(x) = 0$ when $x < 0$; $C_1 \approx 0.12$ and $C_2 = O(100)$ are constants of the model, l_o is the integral length scale and $\bar{\epsilon}$ is the local (large-scale) rate of strain (or mean dissipation rate) which is given by

$$\bar{\epsilon} = \frac{\nu_t}{2}(\nabla \bar{u})^2. \tag{5.2}$$

Since the steepest velocity gradients are in the z-direction (perpendicular to the wall), we can neglect gradients in the y-direction and assume

$$|\nabla \bar{u}| \approx \frac{d\bar{u}}{dz}. \tag{5.3}$$

Introducing equations (5.2) and (5.3) into equation (5.1) and using the following dimensionless variables

$$\nu_t^* = \frac{\nu_t}{\nu_o}, \quad l_o^* = \frac{l_o}{L},$$

$$\bar{u}^* = \frac{\bar{u}}{\bar{U}}, \quad z^* = \frac{z}{L},$$

equation (5.1) can be expressed in dimensionless terms:

$$\nu_t = \left[1 + H\left(C_1 Re^2 \nu_t \left(\frac{d\bar{u}}{dz}\right)^2 l_o^4 - C_2\right)\right]^{1/3}, \tag{5.4}$$

where the $*$ was dropped for simplicity and the constant C_1 was rescaled by a factor of 2. The Reynolds number is based on the molecular viscosity and the average flow velocity, that is, $Re = \bar{U}L/\nu_o$. The integral length l_o can also be considered as the maximum eddy size that plays a role in turbulent viscosity. Actually, in equation (5.4), l_o is a free parameter and must be specified outside the theory. It should be calculated taking into account the effect of all surfaces and the magnetic field. In principle, if we only want to consider the influence of all surfaces in channel flow, we can take into account the effect of the four walls in the following way [Talmage *et al.*, 1990]

$$\frac{1}{l_o} = \frac{1}{l_1} + \frac{1}{l_2} + \frac{1}{l_3} + \frac{1}{l_4},$$

where l_i is the distance from each wall to the point of interest. So, we get

$$\frac{1}{l_o} = \frac{2a}{a^2 - y^2} + \frac{2}{1 - z^2}. \tag{5.5}$$

The effect of the magnetic field must be superimposed to that of the walls. Sukoriansky and Branover [1987] derived a modification of the integral length that accounts for the diffusive action of the magnetic field. The modification affects only the coordinate in the field direction, therefore, in equation (5.5) only the first right-hand term is altered while the second remains the same. The effect of the field is introduced through a factor proportional to $1/\sqrt{N_o(l_o)}$, where N_o is the local interaction parameter, therefore, the contribution of the first term of equation (5.5) to l_o will be small for strong magnetic fields. Since we deal with cases where $N_o \gg 1$, the latter contribution to l_o can be neglected. In addition, we are mainly interested in the phenomena occurring in the side boundary layers and the most important effects come from the side wall. Hence, as a first approximation, l_o can be taken as the distance to the wall in question, disregarding the dependence on the vertical coordinate. Later, we will show a definition of l_o that takes into account the structure of the boundary layer.

Very near the wall, the argument of $H(x)$ in equation (5.4) is negative since l_o is very small. This leads to $\nu_t = 1$, that is, the total viscosity reduces to the molecular value. Therefore, equation (5.4) reproduces the behavior of the laminar sublayer found in turbulent boundary layers. Evidently, for sufficiently low Re (laminar flow), $\nu_t = 1$ everywhere. When the argument of $H(x)$ is positive ($C_1 Re^2 \nu_t (d\bar{u}/dz)^2 l_o^4 > C_2$), equation (5.4) reduces to a cubic equation for ν_t at each space point, namely,

$$\nu_t^3 - C_1 Re^2 \left(\frac{d\bar{u}}{dz}\right)^2 l_o^4 \nu_t + C_2 - 1 = 0. \tag{5.6}$$

Talmage [1989] and Lund [1990] found that this cubic equation leads to oscillations of the eddy viscosity as a consequence of a jump-discontinuity that appears at the point where the turbulent viscosity turns on ($C_1 Re^2 \nu_t (d\bar{u}/dz)^2 l_o^4 = C_2$), that is, at the point of the laminar-turbulent transition. Talmage overcame this problem by replacing the

turbulent viscosity that appears on the right hand side of equation (5.4) by $(\nu_{told})^2/\nu_{tnew}$ and the turbulent viscosity that appears on the left-hand side by ν_{tnew}. In this way, a quartic equation for ν_{tnew} is obtained, namely,

$$\nu_{tnew}^4 + (C_2 - 1)\nu_{tnew} - C_1 Re^2 \left(\frac{d\bar{u}}{dz}\right)^2 l_o^4 \nu_{told}^2 = 0, \tag{5.7}$$

where ν_{told} represents the local value of ν_t at the previous iteration which was used to calculate the current value of $d\bar{u}/dz$ and ν_{tnew} is the turbulent viscosity at the current iteration. When $\nu_{tnew} = \nu_{told}$, equation (5.4) is satisfied. Equation (5.7) has only one physically realistic root and does not present discontinuities about the point where the turbulent viscosity is activated.

5.2.2 RNG Eddy Viscosity Model: Second Version

In order to overcome the oscillating viscosity problem posed by the cubic algebraic equation for ν_t, Yakhot *et al.* [1992] used a different expression for the mean dissipation rate, $\bar{\epsilon}$. The change leads to an algebraic quartic equation for the eddy viscosity. They also proposed a new length scale model based on boundary layer characteristics. The length scale model is specially suitable for wall-bounded turbulent flows and turbulent boundary layers. In turbulent boundary layers there are three fairly distinct regions that are easily recognized [Schlichting, 1979]. First, there is the laminar sublayer which is typically 0.01 to 0.001 of the total thickness of the layer, δ. Beyond this sublayer, there is a turbulent region which extends 0.1 to 0.2 of δ and comprises the inner part of the layer. Finally, there is the outer 0.8 to 0.9 of the layer where the eddies are limited in lateral extent only by the confines of the layer and mixing is relatively free.

Yakhot et al. [1992] claim that the expression (5.2) for the mean dissipation rate is correct if the equilibrium assumption (production balancing dissipation) is valid and $\nu_t \gg \nu_o$ ($\nu_t \approx \nu_{turb}$). It appears that these conditions are not guaranteed in near-the-wall turbulence and an alternative approach may be required. Instead of equation (5.2), they expressed $\bar{\epsilon}$ using a well-known form in $K - \epsilon$ transport models, namely,

$$\bar{\epsilon} = C_\mu \frac{K^2}{\nu_t}, \qquad C_\mu \approx 0.09, \tag{5.8}$$

where K is the turbulent energy. In addition, they noticed that for turbulent flows in boundary layers, channels and pipes, the velocity within the inner region is governed by

$$\nu_t \frac{du}{dz} = u_*^2, \tag{5.9}$$

where $u_* = (\tau_w/\rho)^{1/2}$ is the wall-shear velocity and τ_w is the wall-shear stress. Assuming that equilibrium between production and dissipation occurs when

$$\bar{\epsilon} = \nu_t \left(\frac{du}{dz}\right)^2, \tag{5.10}$$

and substituting (5.10) and (5.9) into (5.8), they obtain

$$K \approx C_\mu^{-1/2} u_*^2. \tag{5.11}$$

Finally, substituting (5.8) and (5.11) into (5.1), the total viscosity is given by

$$\nu_t = \nu_o \left[1 + H\left(\frac{C_1 u_*^4 l_o^4}{\nu_t \nu_o^3} - C_2\right)\right]^{1/3}. \tag{5.12}$$

The additional requirement that $\nu_t = \kappa u_* z$, as used in mixing length theory, leads to the selection of constant C_1 equal to κ^4, where $\kappa \approx 0.4$ is the von Kármán constant. Substituting the definition of the wall-shear stress

$$\tau_w = \rho \nu_o \left(\frac{du}{dz}\right)_{z=z_w},$$

(where z_w denotes the position at the wall) into u_* and using the non-dimensional variables, equation (5.12) can be expressed as

$$\nu_t = \left[1 + H\left(C_1 Re^2 \left(\frac{du}{dz}\right)^2_{z=1} \frac{l_o^4}{\nu_t} - C_2\right)\right]^{1/3}, \tag{5.13}$$

where the $*$ has been dropped again. When $H(x) = x$, equation (5.13) leads to the following algebraic quartic equation for ν_t at every point in space:

$$\nu_t^4 + (C_2 - 1)\nu_t - C_1 Re^2 \left(\frac{du}{dz}\right)^2_{z=1} l_o^4 = 0. \tag{5.14}$$

Notice that the velocity gradient is evaluated at the wall. The solution of (5.14) is governed by the independent term, which depends on the integral length l_o. Yakhot et al. noticed that in the outer region of turbulent boundary layers, the eddy viscosity may be approximated as

$$\nu_t^{(outer)} = \alpha U_o \delta_*,$$

where α is an experimental constant, U_o is a free stream velocity, and δ_* is the displacement thickness. Hence, they assume the following definition of the integral length scale:

$$l_o = min(z, \gamma \delta_*), \tag{5.15}$$

where γ is given by

$$\gamma = \gamma_o(1 - \mathcal{H}^{-1})^{-1}. \tag{5.16}$$

In equation 5.16, γ_o is a constant and $\mathcal{H}^{-1} = \theta/\delta_*$ is a shape factor, where δ_* and θ are the displacement and momentum-loss thicknesses, respectively, defined by [Schlichting, 1979]

$$\delta_* = \int_0^\infty \left(1 - \frac{u}{U_o}\right) dz, \tag{5.17}$$

$$\theta = \int_0^\infty \frac{u}{U_o}\left(1 - \frac{u}{U_o}\right) dz. \tag{5.18}$$

The estimated value of the constant γ_o in two limiting non-MHD cases of fully turbulent and transitional boundary layer over a flat plate was 0.3. For a duct flow, using definitions (5.15)-(5.18), the outer integral length scale can be written as

$$l_o^{(outer)} = \gamma_o(1 - \mathcal{H}^{-1})^{-1} = \gamma_o \frac{[\int_0^\infty (U_o - u)dz]^2}{\int_0^\infty (U_o - u)^2 dz}. \tag{5.19}$$

It is expected that the introduction of boundary layer characteristics in the definition of the integral length provides a better assessment of the factors influencing the turbulent flow. Numerical calculations based on equations (5.15)-(5.19) showed that l_o corresponds to z only very near the wall while in the remaining region takes the value $\gamma\delta_*$. As a matter of fact, this is an important issue for the convergence of the numerical scheme. Because of these reasons, we decided to apply the previous integral length model defined by equations (5.15)-(5.19) in both the first and second versions of the RNG total viscosity model. Under this approach, the magnetic effect is taken into account via the velocity distribution.

5.3 Turbulent MHD Flow in a Square Duct

The numerical iterative scheme used to get the turbulent solution of the governing equations was sketched at the end of Chapter 2. In short, the iteration procedure begins with the calculation of the coefficients corresponding to a laminar profile ($\nu_t = 1$, $\partial\nu_t/\partial z = 0$) for a given conductance ratio, Hartmann number and pressure gradient. The linear algebraic system is solved and the laminar velocity profile is obtained. Velocity gradients and the integral length are then computed and introduced, along with the given Reynolds number, in the eddy viscosity formula. The quartic algebraic equation for ν_t is solved at each point and viscosity gradients are calculated. The new value of ν_t and their gradients are introduced in the matrix elements and, once the linear algebraic system of equations is solved, a modified velocity profile is obtained. The procedure continues until convergence is reached and, finally, the Reynolds number and the pressure gradient are rescaled. The solution of the quartic equation for ν_t, given

by either (5.7) or (5.14), was carried out through a numerical subroutine [Press *et al.*, 1992] and it was verified with an analytical solution. Likewise, the calculation of the viscosity gradients was performed using a spline method [Press *et al.*, 1992].

5.3.1 Selection and Validation of the Turbulence Model

Before addressing the validation and selection of the most suitable model for the derivation of turbulent results, some comments about the model constants are necessary. In both first and second versions of RNG total viscosity models, three constants are required. Two of them, C_1 and C_2, appear in equations (5.4) and (5.13) (depending on the model), while the third constant, γ_o, occurs in the definition of the integral length model, equation (5.19). The interpretation of these constants is not straightforward as they do not influence the behavior of the model independently, but act together. Roughly, C_1 affects in some way the intensity of the turbulence; the larger C_1, the stronger the turbulent effects. C_2 is related to the point of the laminar-turbulent transition: the greater C_2, the larger the Reynolds number required to activate the turbulent viscosity for a given du/dz, l_o and C_1. γ_o represents a kind of *penetration depth* factor, in the sense that an increase in γ_o leads to an increase in $l_o^{(outer)}$ and, consequently, the turbulent effects go deeper into the boundary layer.

There is not a clear way how to evaluate these constants for a particular flow situation. Yakhot *et al.* [1992] assigned some values and orders of magnitude to the constants, based on RNG theory and estimations performed on particular OHD flows. As we mentioned, the assigned values were $C_1 = (0.4)^4 = 0.0256$, $C_2 = O(100)$ and $\gamma_o = 0.3$. However, these values do not hold a universal character. Actually, a proper calibration of the model for a particular situation should be carried out on an experimental basis but, evidently, this is a very restrictive approach. An alternative would be the variation of constants and comparison with empirical correlations though, this is limited to a number of cases where empirical correlations exist. This is the approach we followed in the OHD case. In order to validate the turbulence models, we carried out a comparison of friction factor values obtained through the model for an OHD turbulent flow, against empirical correlations. We selected the turbulent flow of an incompressible fluid in a parallel plates duct as a good candidate to perform the comparison. Such flow can be obtained as a limit case of our MHD problem by ignoring derivatives in the y-direction and assuming electrically insulating walls ($c = 0$) and negligible magnetic interaction ($M = 1$). In dimensional terms, the Fanning friction factor is given by

$$\lambda_f = -\frac{D_h}{2\rho\bar{u}^2}\frac{dP}{dx}, \tag{5.20}$$

where D_h is the hydraulic diameter which, for a flat duct with walls separated by a distance $2b$, is equal to $4b$.

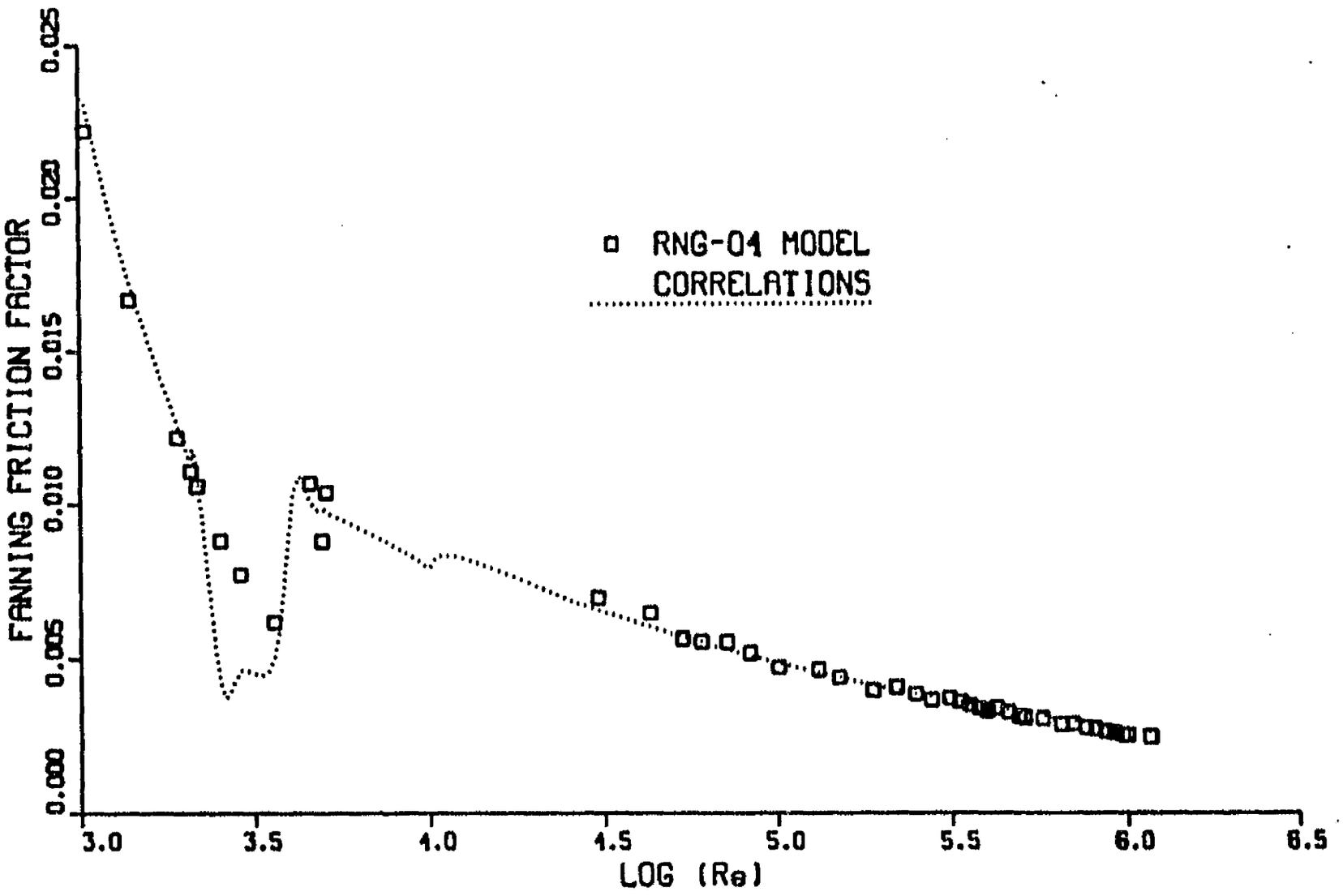

Figure 5.1: Comparison of RNG model results and empirical correlations for the Fanning friction factor of an OHD turbulent flow in a flat duct.

To begin with, we chose the set of constants proposed by Yakhot et al. and compared the rescaled value of λ_f given by both versions of the RNG eddy viscosity model, against empirical correlations for the turbulent flow in a flat duct, provided by Bhatti and Shah [1987]. The agreement with empirical values was rather bad and, in some cases, convergence was difficult to obtain. A variation of constants C_2 and γ_o was carried out, keeping C_1 fixed to 0.0256 since it is related to the von Kármán constant. After many tries, a set of constants for the second version model which reproduces reasonably well the empirical friction factor values was found, namely, $C_1 = 0.0256$, $C_2 = 200$ and $\gamma = 0.1$. The comparison of the model against the correlations is shown in figure (5.1), where the Fanning friction factor was plotted as a function of the logarithm of Re.

The agreement is very good in the laminar region ($Re < 2.2 \times 10^3$) as well as for $Re > 3{\times}10^4$. However, results found with the model in the range $Re \approx 5.6{\times}10^3 - 3{\times}10^4$ do not agree with correlations and are not shown in figure 5.1. Actually, in this region some convergence problems appeared. The laminar-turbulent transition region presents also some disagreement but in this region even correlations are not very reliable. We

used the same set of constants for the first version model but it was not possible to find a good agreement with correlations even though velocity profiles look very close to those of the turbulent regime. Variation of constants was carried out unsuccessfully since for this OHD case, the first version model is very sensitive to changes in the value of the constants and even a slight variation may lead to situations where the scheme does not converge. A partial validation of this model was accomplished indirectly by comparing MHD turbulent velocity profiles for both models and finding a good agreement between them, as it will be shown later.

For MHD turbulent flows, a comparison with empirical correlations is not possible since correlations are inexistent for the case we are interested in, namely, the fully developed turbulent liquid-metal flow in a square duct (with walls ranging from thin conducting to insulating), under a transverse magnetic field. Therefore, we decided to apply the constants used by Talmage [1989] for the MHD flow in homopolar devices, namely, $C_1 = 0.0256$ and $C_2 = 110$. In addition, constant γ_o was set equal to 0.4. For the former value of γ_o, it was found that the range where the total viscosity is different from the laminar value, approximately agrees with the experimental range where the instability takes place, for the corresponding Hartmann number and wall conductance ratio. Reasonable results, in terms of convergence and spreading of turbulent effects into the boundary layer, were found in the range $0.3 \leq \gamma_o \leq 0.5$. Values of γ_o less than 0.3 were too small for the turbulent effects to be notorious. Actually, γ_o is the constant that influences the most the behavior of the model. Variation of C_1 and C_2 led only to slight changes in the turbulent profiles. Due to the lack of calibration of the model against empirical values, numerical results can be considered only for a qualitative description.

The first and second versions of the RNG effective viscosity model, with the integral length of Yakhot *et al.* [1992], were applied to the MHD channel flow problem. We found that MHD turbulent velocity profiles obtained through both versions of the model are very similar though total viscosity profiles are radically different. Figures 5.2 and 5.3 show the mean axial velocity and total viscosity profiles, respectively, as a function of the z-coordinate for different vertical positions using the first version model (with Talmage's procedure [1989] to get the quartic equation). Results correspond to the case $M = 10^4$, $c = 0.05$ and $Re = 5 \times 10^4$.

Similarly, figures 5.4 and 5.5 are the corresponding profiles obtained with the second version model. Comparison of figures 5.2 and 5.4 reveals a close similitude between turbulent velocity profiles obtained with both models although, the first version model presents smoother curves. In both cases, as a result of turbulent effects, the mean axial velocity profiles spread out further from the wall, that is, boundary layer gets thicker and, in addition, the velocity in this region decreases with respect to laminar flow (see figure 3.5). On the other hand, the first and second version models predict a completely different behavior of the total viscosity, as can be seen from figures 5.3 and 5.5, respectively. While the first version model presents a high total viscosity in

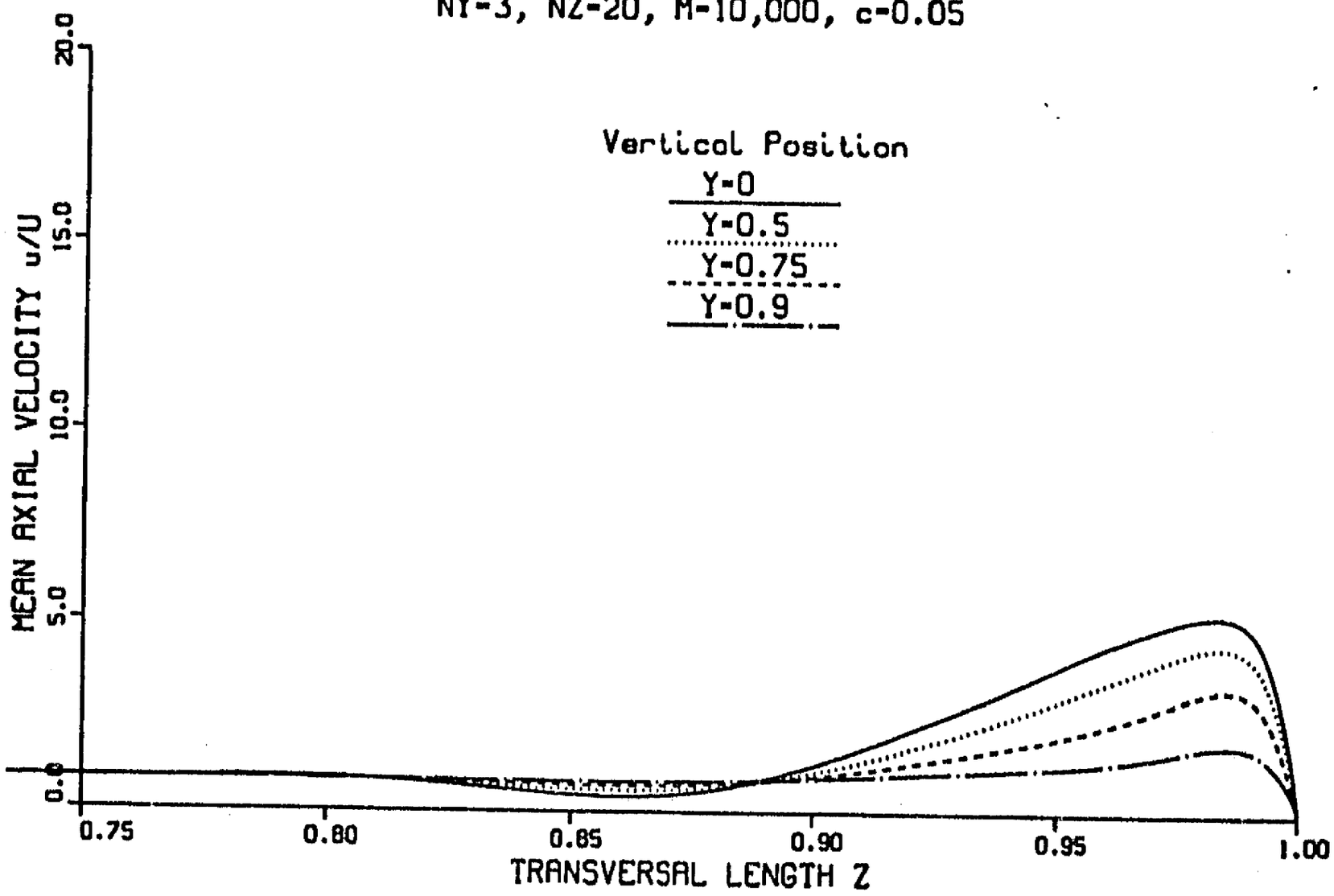

Figure 5.2: Mean axial velocity vs. z for different y positions, calculated with the first version model. $M = 10^4$, $c = 0.05$ and $Re = 5 \times 10^4$.

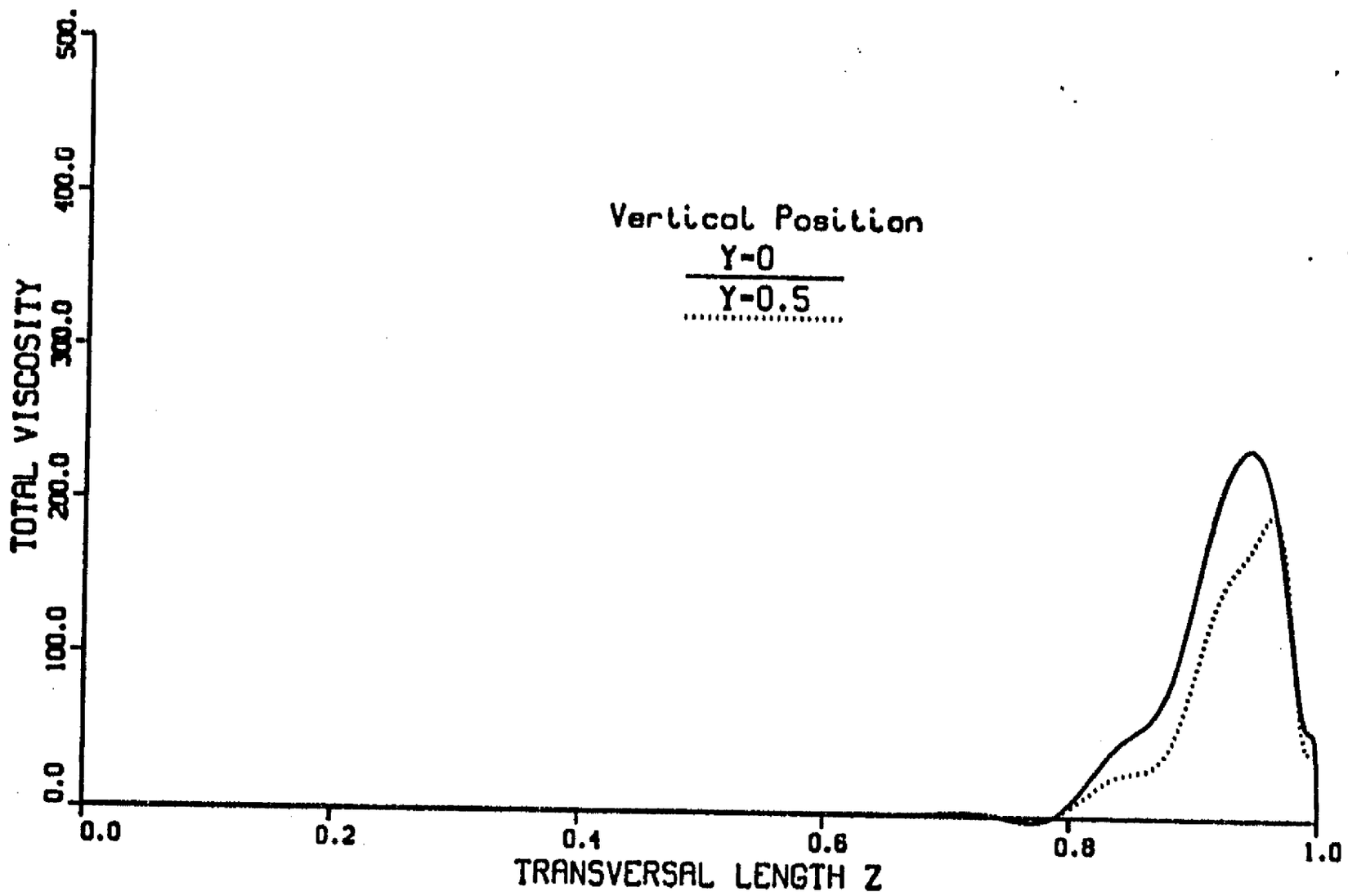

Figure 5.3: Total viscosity vs. z for different y positions, calculated with the first version model. $M = 10^4$, $c = 0.05$ and $Re = 5 \times 10^4$.

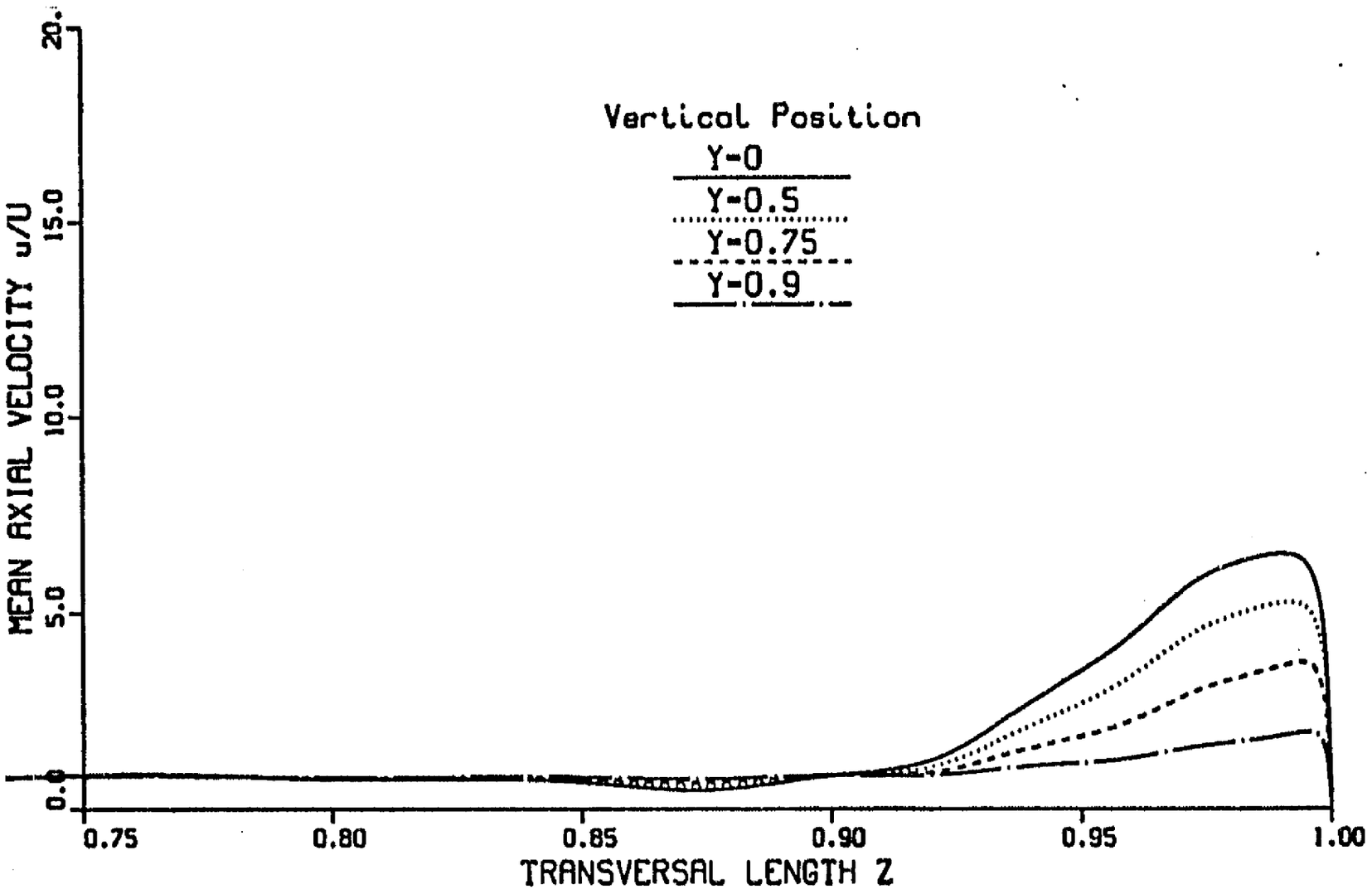

Figure 5.4: Mean axial velocity vs. z for different y positions, calculated with the second version model. $M = 10^4$, $c = 0.05$ and $Re = 5 \times 10^4$.

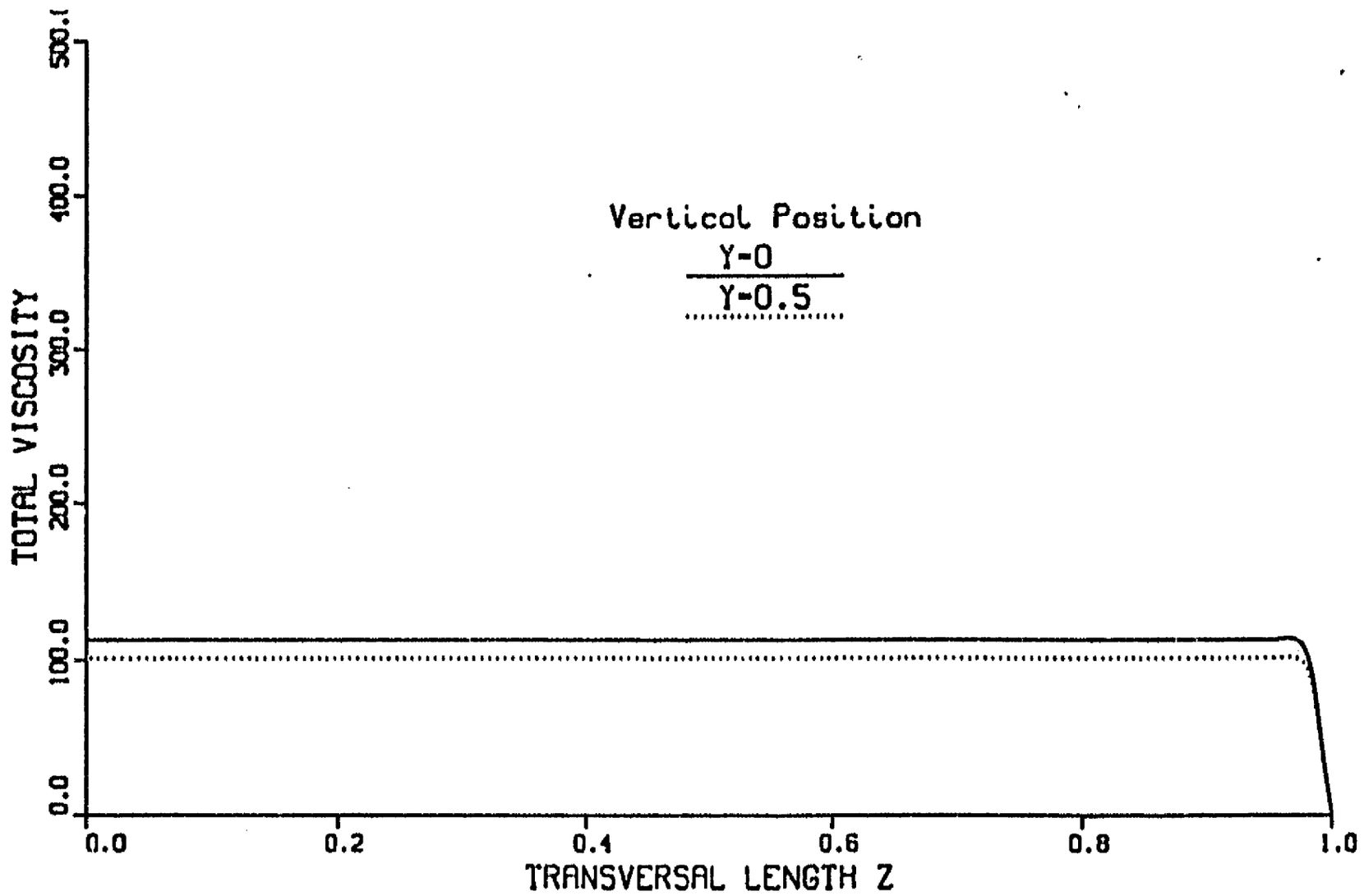

Figure 5.5: Total viscosity vs. z for different y positions, calculated with the second version model. $M = 10^4$, $c = 0.05$ and $Re = 5 \times 10^4$.

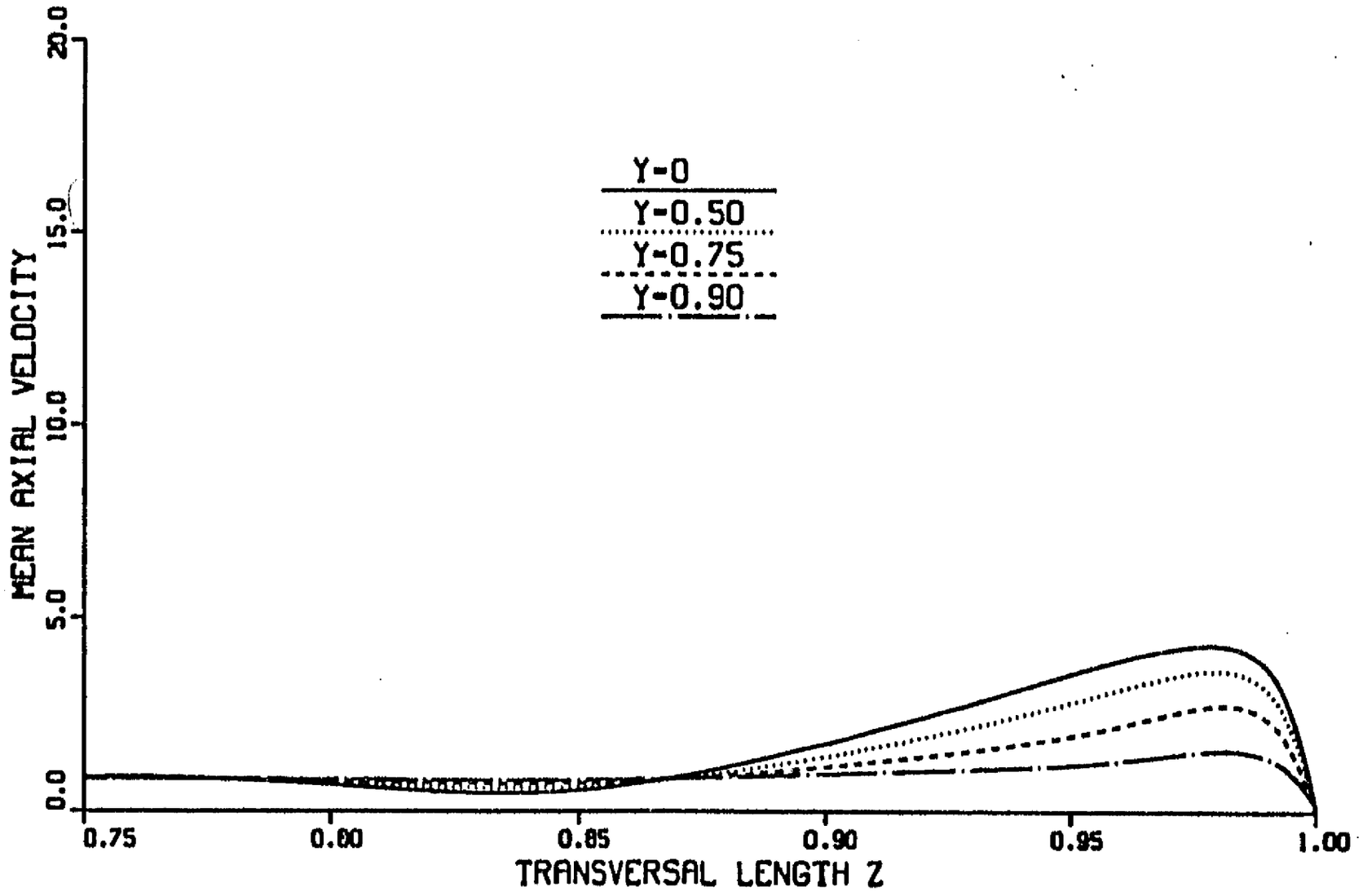

Figure 5.6: Mean axial velocity vs. z for different y positions, calculated with the first version model. $M = 10^4$, $c = 0.05$ and $Re = 10^5$.

the extended boundary layer region that decreases to the laminar value as one travels into the core of the flow, the second version model shows a linear increase in the near-the-wall region and then a constant value over the whole core-side-layer region. The explanation of former results is found in the definition of each model. Equation (5.7) shows that in the first version model the velocity gradients are calculated in the whole flow region. Therefore, gradients are high in the boundary layer region due to velocity overshoots and zero in the core where a slug-like flow exists. This leads to high viscosity values in the boundary layer and laminar values in the core. On the other hand, in the second version model governed by equation (5.14), the value of the gradient at the wall (which is very high due to velocity overshoots) is kept in the independent term of the quartic equation for any flow position. As a consequence, the total viscosity takes high values even at points far away from the wall. Figures 5.6 and 5.7 show mean velocity and total viscosity profiles for the first version model with a higher Reynolds number, namely, $Re = 10^5$; figures 5.8 and 5.9 present the corresponding results using the second version model.

With the increase in Re, turbulent effects are more pronounced, that is, velocity

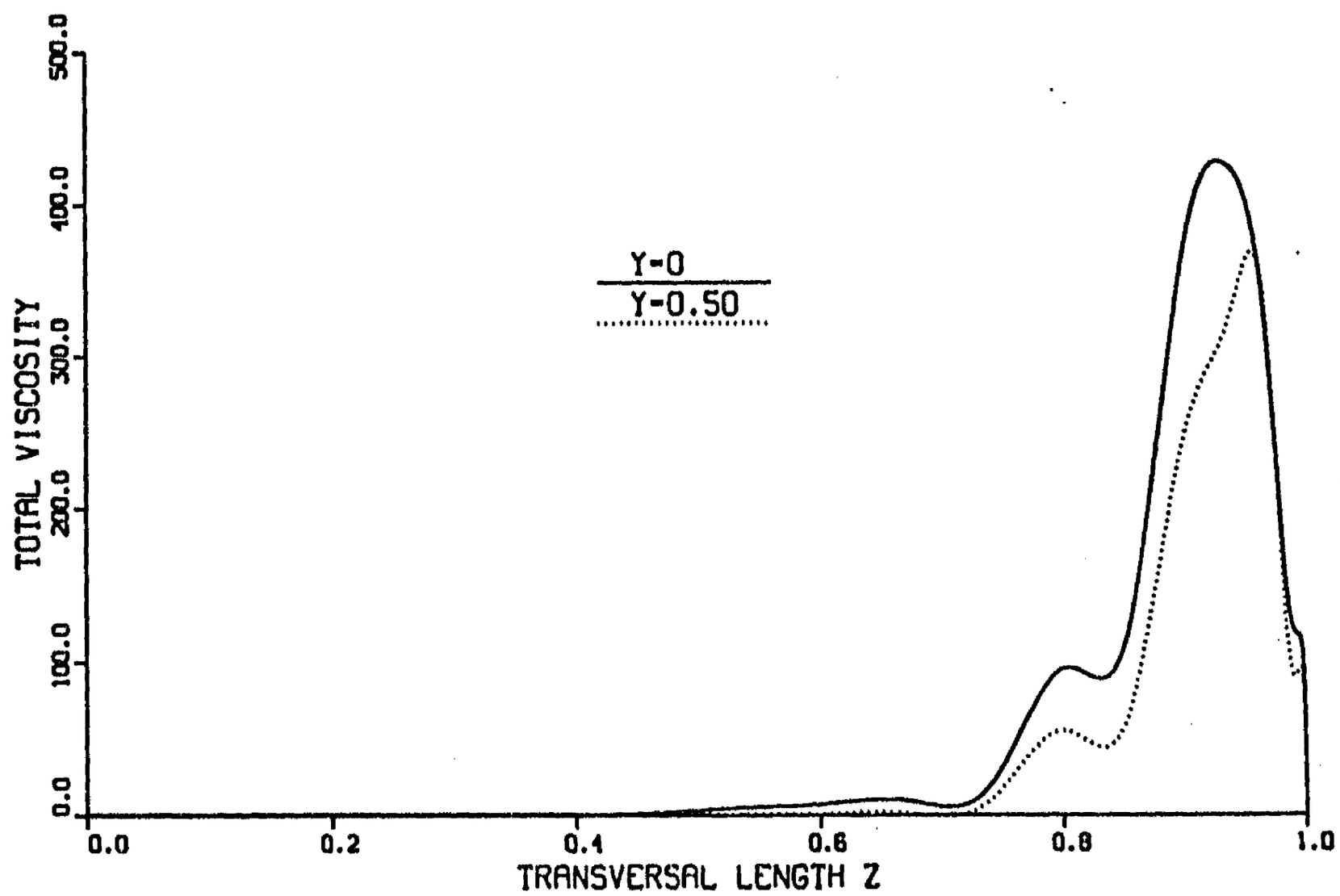

Figure 5.7: Total viscosity vs. z for different y positions, calculated with the first version model. $M = 10^4$, $c = 0.05$ and $Re = 10^5$.

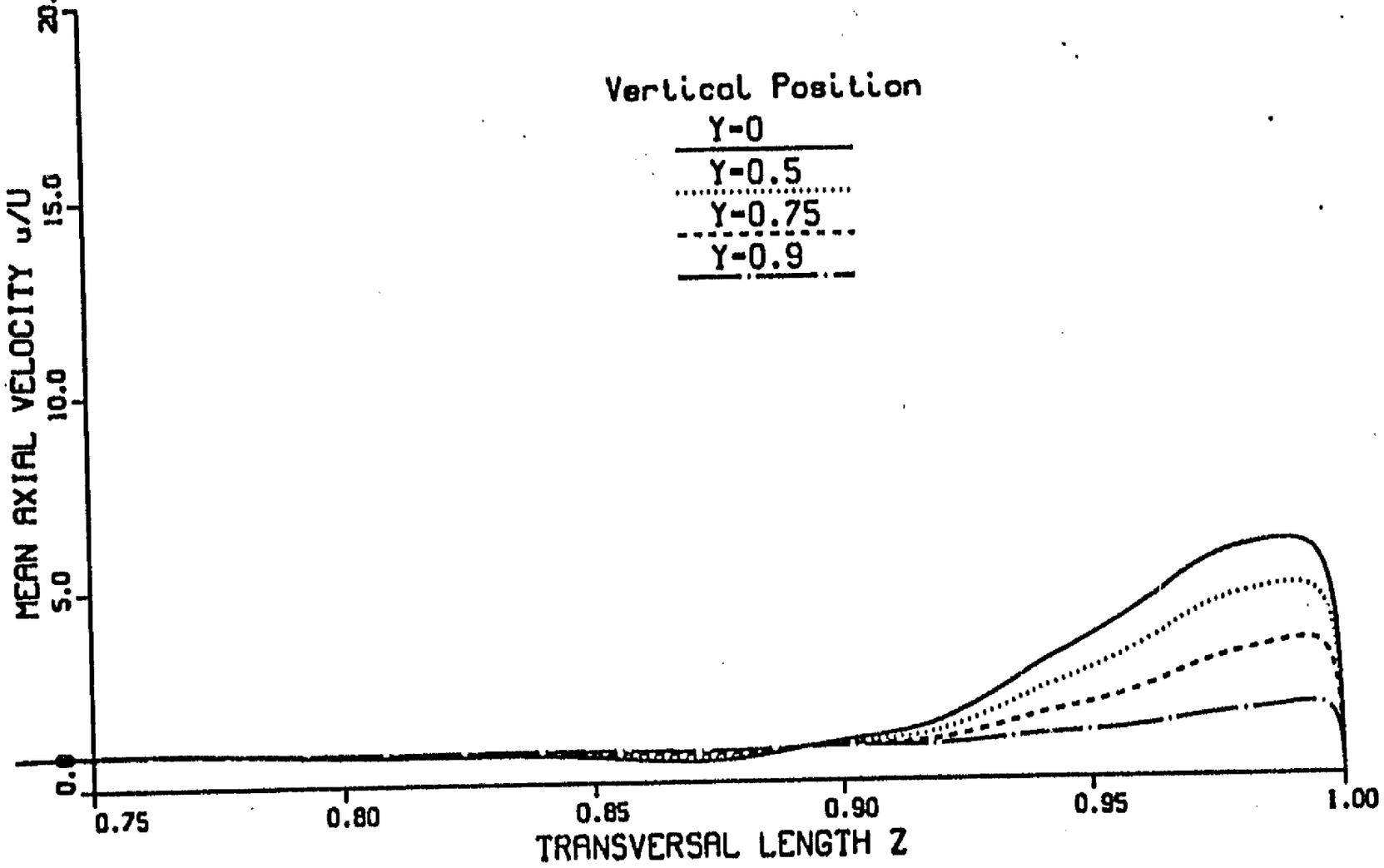

Figure 5.8: Mean axial velocity vs. z for different y positions, calculated with the second version model. $M = 10^4$, $c = 0.05$ and $Re = 10^5$.

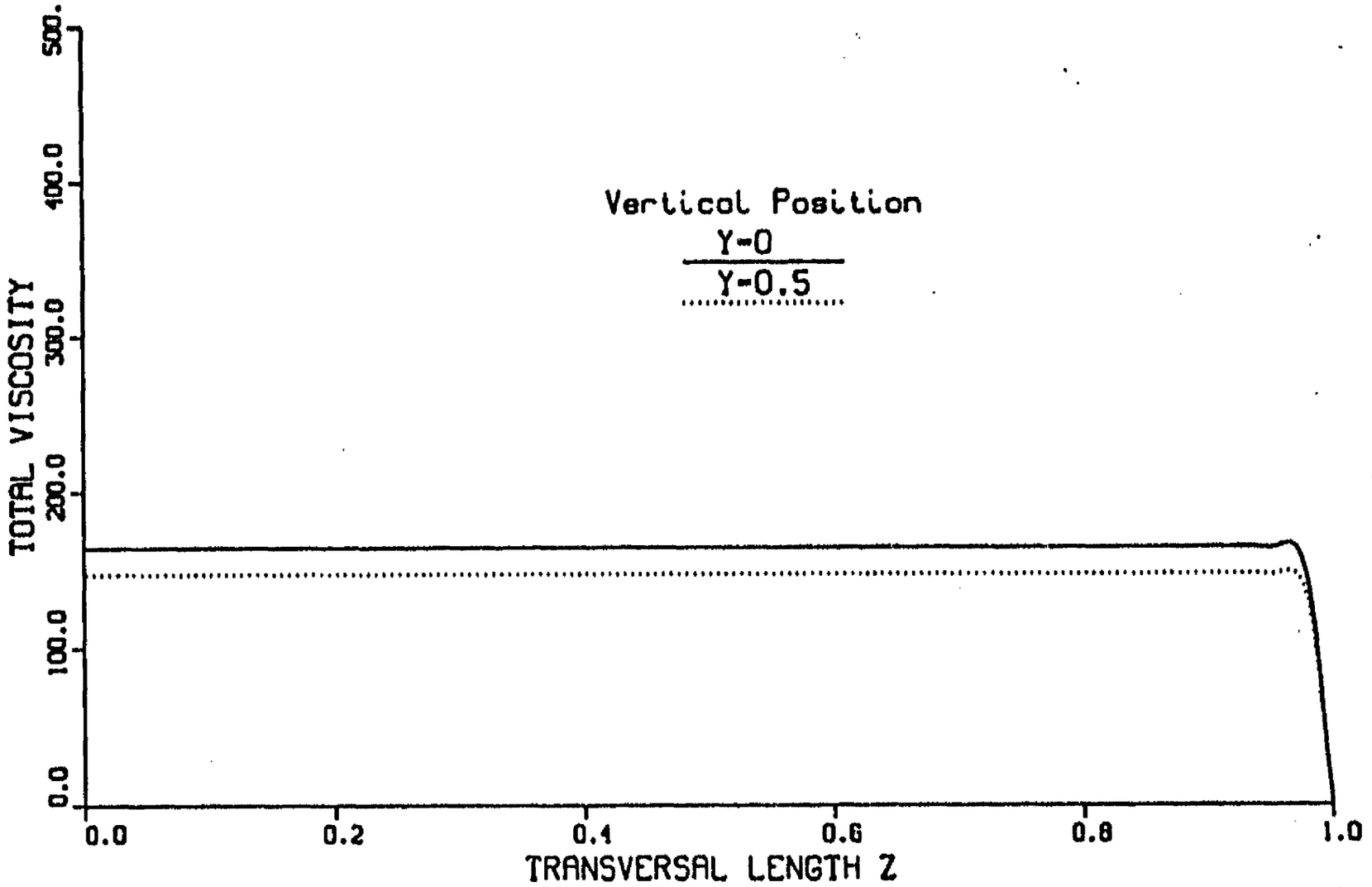

Figure 5.9: Total viscosity vs. z for different y positions, calculated with the second version model. $M = 10^4$, $c = 0.05$ and $Re = 10^5$.

profiles become flatter, boundary layers get thicker and total viscosity takes higher values. However, the overall behavior of the total viscosity profiles for each model remains the same. The no monotonic behavior of the total viscosity in figure 5.7, displays a problem of numerical interpolation and resolution rather than a particular physical effect. With a higher number of collocation points, the *humps* get smoother although such number must be carefully selected in order to guarantee the convergence.

From the previous results, it is possible to select, on a physical basis, the first version model as the one that yields better results for the problem under consideration. In a qualitative picture of the transition from a laminar flow with high-velocity side wall jets to a fully developed turbulent flow, we could expect that perturbations in the jets may originate instabilities leading to the formation of vortices in the boundary layer, the core flow remaining stable with respect those perturbations. These vortices would increase the boundary layer thickness and the total effective viscosity in this layer, leading to an enhancement of the mixing in that zone while the mean side layer velocity would be reduced. This kind of behavior is reproduced by the first version model (see figs. 5.3 and 5.7). Although initially the produced vortices would be three-dimensional, the magnetic diffusion mechanism described in Chapter 4 may enter into play, favoring a two-dimensional tendency through the alignment of the vortices in the field direction. Since the side wall jets are originally located in a very thin boundary layer with thickness $O(M^{-\frac{1}{2}})$, it would be rather unlikely that, even at high Re, the created vortices would spread throughout the core. While generation of vortices would take place near the wall due to the side-wall-jet instability, dissipation of vortices would occur either in Hartamnn layers (for insulating wall ducts) or in top/bottom wall (for conducting wall ducts), in the way described in Section 4.5. Near the side wall, there would be a continuous promotion of vortex formation that compete with dissipation in top/bottom wall region. Hence, dissipation of vortices would be more effective the largest the distance from that side wall, which would prevent the penetration of vortices into the core of the flow. For a high enough interaction parameter,[2] the instability would disappear, vortex generation would be completely suppressed and laminar flow would be recovered. In general terms, this qualitative picture agrees with side-wall-jet instability experiments and the linear stability analysis though, differences in physical conditions must be borne in mind. Evidently, we could not expect the RNG turbulence model to introduce neither two-dimensional behavior nor turbulent suppression effects, due to magnetic field interactions. However, the general physical behavior of the first version model can be considered suitable for the problem at hand. The introduction of the specific structure of the MHD boundary layer through the integral length model is a convenient way of considering, at least in part, MHD effects.

[2]If magnetic intensity is maintained constant, increasing N would imply decreasing Re.

5.3.2 Numerical Results

The laminar steady-state duct flow problem analyzed in Chapter 3 is independent of the Reynolds number, the relevant parameters being the Hartmann number and the wall conductance ratio. However, the stability of the flow as well as its turbulent behavior depend also on the Reynolds number. Therefore, in addition to exploring the effects of the intensity of the magnetic field and the electrical conductivity of the walls through variation of the Hartmann number and the wall conductance ratio, respectively, inertial effects are investigated by means of the Reynolds number. In the present study, we considered the same range of Hartmann numbers and wall conductance ratios as in the laminar case, that is, $M = 10^3$, 10^4, 10^5 and $c = 0.05, 0.01, 0.001, 0$. In turn, three Reynolds numbers were analyzed: 5×10^4, 10^5, and 5×10^5. Since we do not have information about the laminar-turbulent transition, to begin with, we guessed the existence of a fully developed turbulent regime for the former Reynolds numbers.

The number of collocation points required to obtain smooth turbulent profiles was less than in the laminar case, for corresponding Hartmann numbers. For $M = 10^5$, the number of collocation points varied from 27 to 32; for $M = 10^4$, from 18 to 20 and for $M = 10^3$, from 10 to 15, depending on the Reynolds number. Recall that in the laminar case, the number of collocation points for $M = 10^5$, $M = 10^4$ and $M = 10^3$ was 45, 25 and 15, respectively. The decrease in the required number of collocation points may be due to the fact that turbulent boundary layers are thicker (and more easily resolved) than the laminar ones.

In order to contrast the introduced turbulent effects, figure 5.10 compares the laminar velocity profile at $y = 0$ as a function of the transverse z-coordinate for the case $M = 10^5$ and $c = 0.05$, against the corresponding mean velocity profiles for the three different Reynolds numbers, 5×10^4, 10^5 and 5×10^5.

Two main effects are clearly noticed in the turbulent cases with respect to the laminar one: a dramatic decrease of the side layer velocity and the thickening of the boundary layer. Both effects are more pronounced the higher the Reynolds number and are a consequence of momentum transfer due to turbulence. For $Re = 5 \times 10^5$, the maximum side layer velocity is about one-sixth of the maximum laminar velocity while the turbulent boundary layer thickness is about five times the thickness of the laminar layer. Figure 5.11 shows the corresponding total viscosity profiles at $y = 0$ in a quarter duct for the former Reynolds numbers.

Notice that turbulent effects bring about a marked increase in total viscosity in the extended boundary layer region: the higher Re, the higher the total viscosity. While in the core the viscosity holds its laminar value $\nu_t = 1$, in the boundary layer it takes values from $O(10^2)$ for $Re = 5 \times 10^4$ to $O(10^3)$ for $Re = 5 \times 10^5$, for the given M and c. Figures 5.12 and 5.13 show similar mean velocity and total viscosity profiles for the same Hartmann number but for a lower wall conductance ratio, $c = 0.01$. The overall behavior of both profiles is the same as in the previous case although, turbulent effects

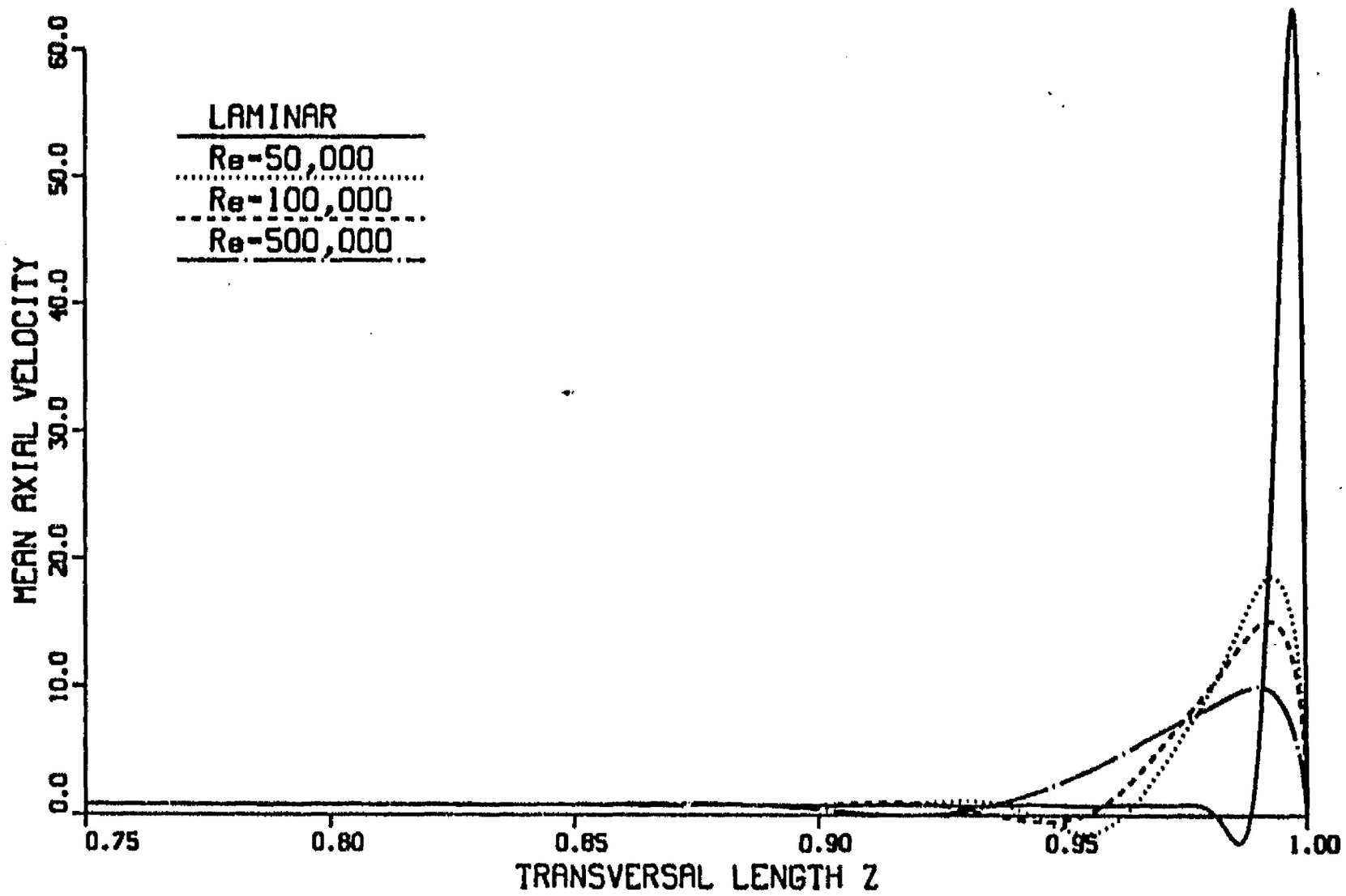

Figure 5.10: Laminar and mean axial velocities vs. z at $y = 0$ for different Re. $M = 10^5$ and $c = 0.05$.

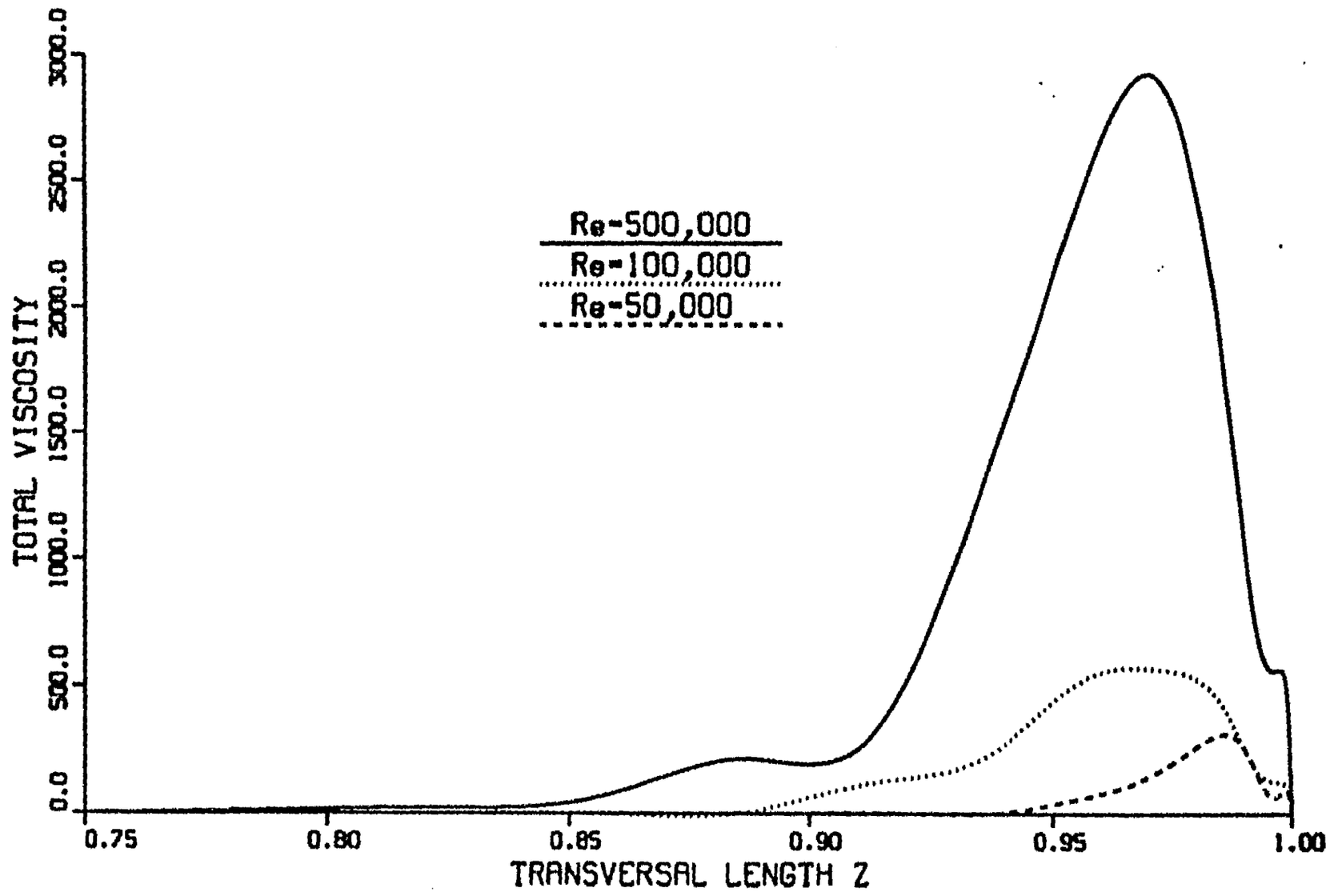

Figure 5.11: Total viscosities vs. z at $y = 0$ for different Re. $M = 10^5$ and $c = 0.05$.

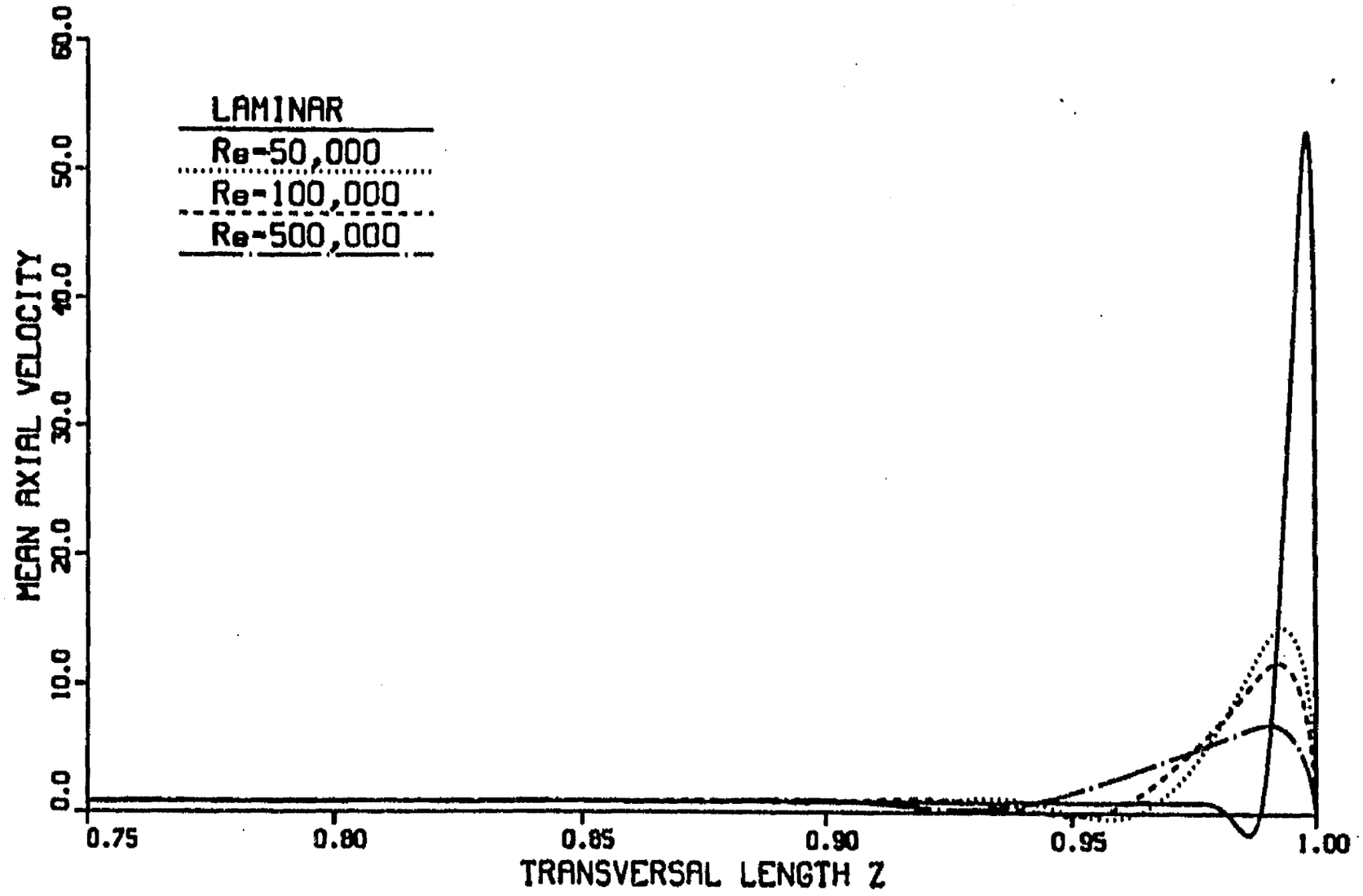

Figure 5.12: Laminar and mean axial velocities vs. z at $y = 0$ for different Re. $M = 10^5$ and $c = 0.01$.

are less notorious. That is, with respect to the case $c = 0.05$, the turbulent boundary layer thickness is thinner and total viscosity values are lower. This tendency persists while decreasing even more the wall conductance ratio, as it is shown in figures 5.14 and 5.15, where velocity and viscosity profiles are presented for the case $c = 0.001$, respectively. Total viscosity values are considerably lower than in previous cases and turbulent effects are restricted to a narrower region near the side wall.

Finally, figure 5.16 presents the velocity profiles for $c = 0$. In this case, the model predicts a laminar viscosity for the three Reynolds numbers, that is, laminar behavior is maintained even for high Reynolds numbers. It is necessary to point out that convergence of the iterative scheme was difficult to reach when $c = 0$. As a consequence, mean velocity profiles are not very smooth and, for Re equal to 5×10^4 and 10^5, small oscillations appeared near the wall (see fig. 5.16). A total coincidence with the laminar profile should be expected in a well converged solution.

Notice that in all previous (and well converged) cases ($c = 0.05, 0.01, 0.001$) the thin wall approximation, $M^{-1} \ll c \ll M^{-\frac{1}{2}}$, holds. The general trend shown in the previous results for fixed Hartmann and Reynolds numbers, seems to indicate that

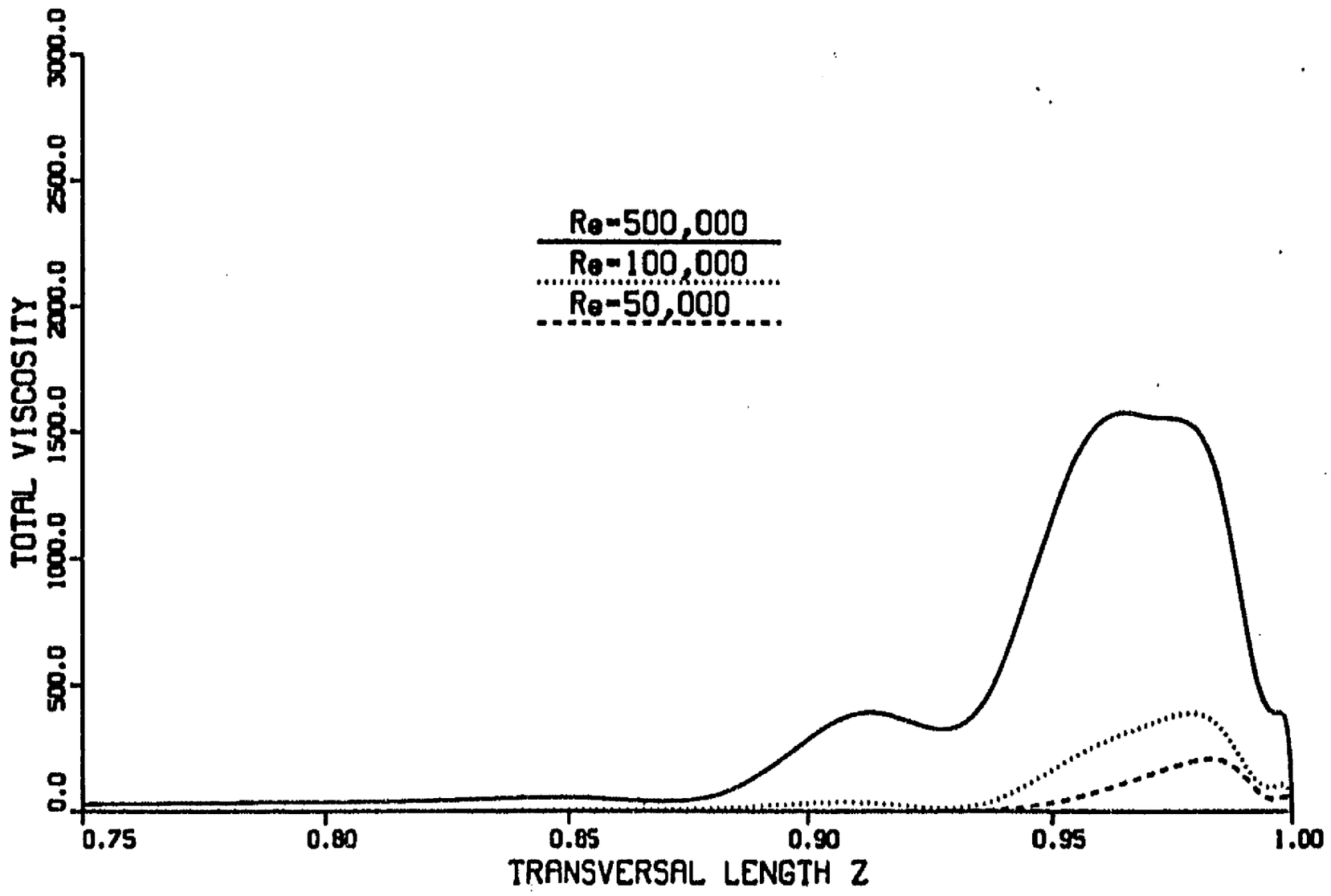

Figure 5.13: Total viscosities vs. z at $y = 0$ for different Re. $M = 10^5$ and $c = 0.01$.

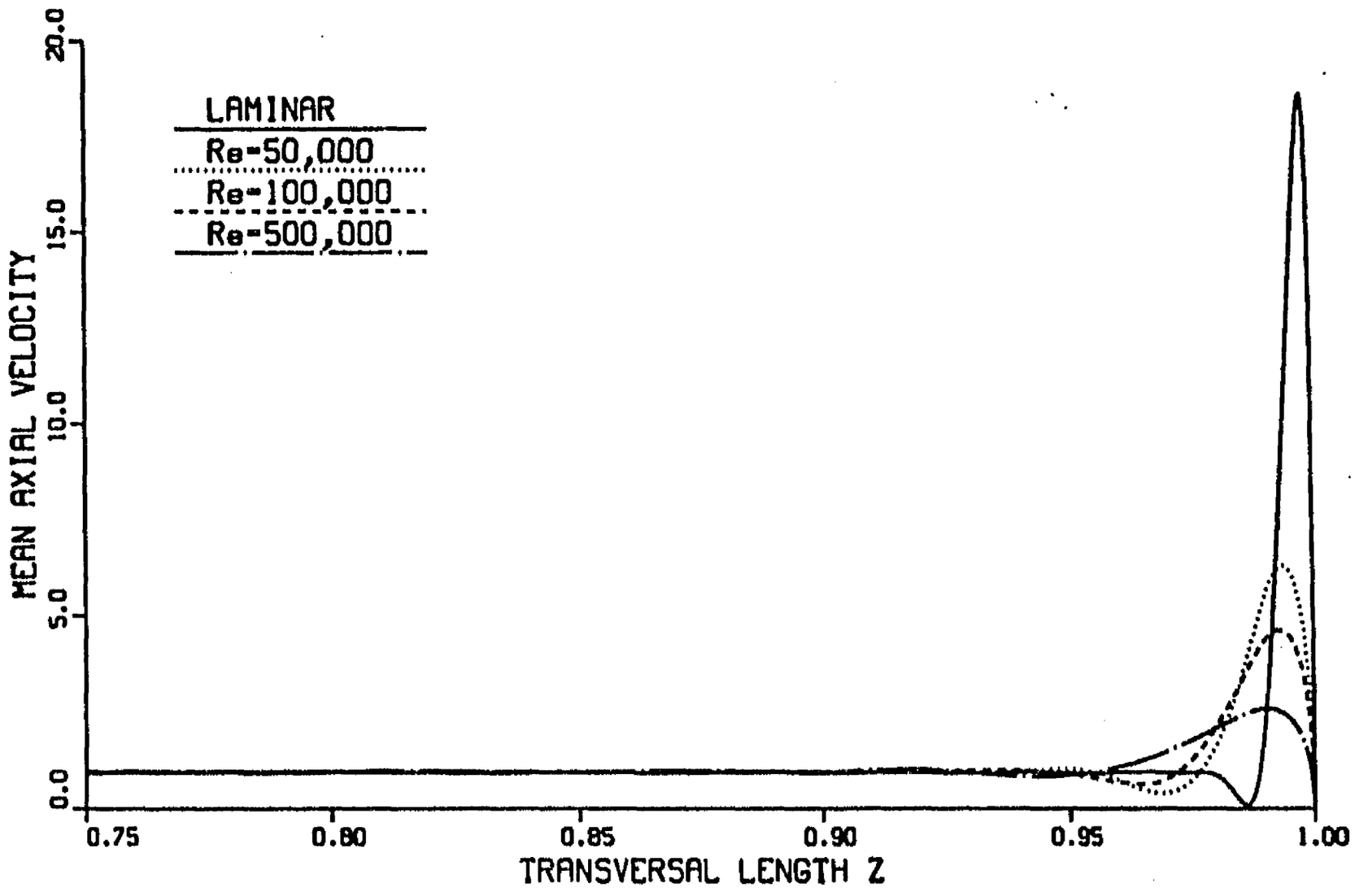

Figure 5.14: Laminar and mean axial velocities vs. z at $y = 0$ for different Re. $M = 10^5$ and $c = 0.001$.

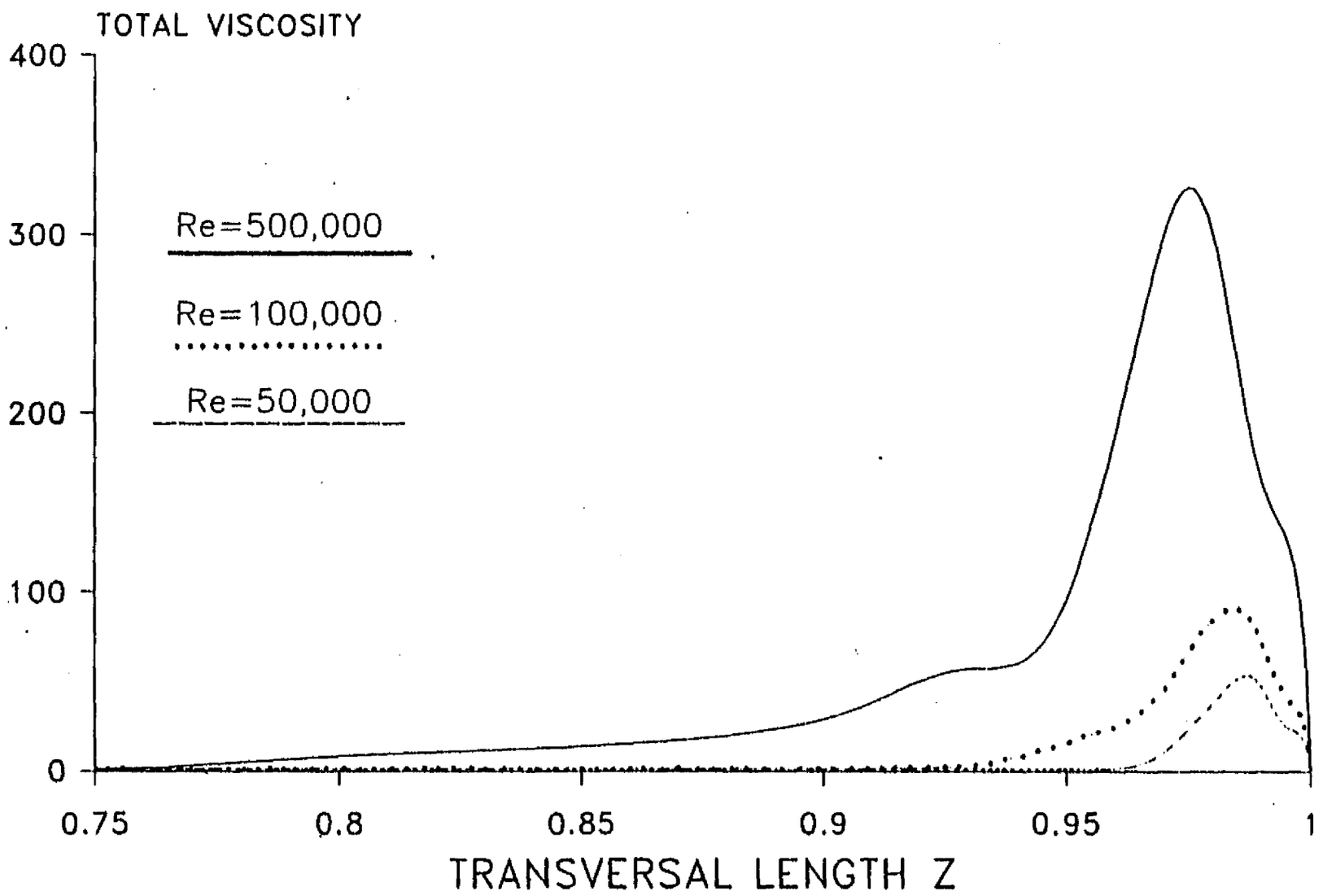

Figure 5.15: Total viscosities vs. z at $y = 0$ for different Re. $M = 10^5$ and $c = 0.001$.

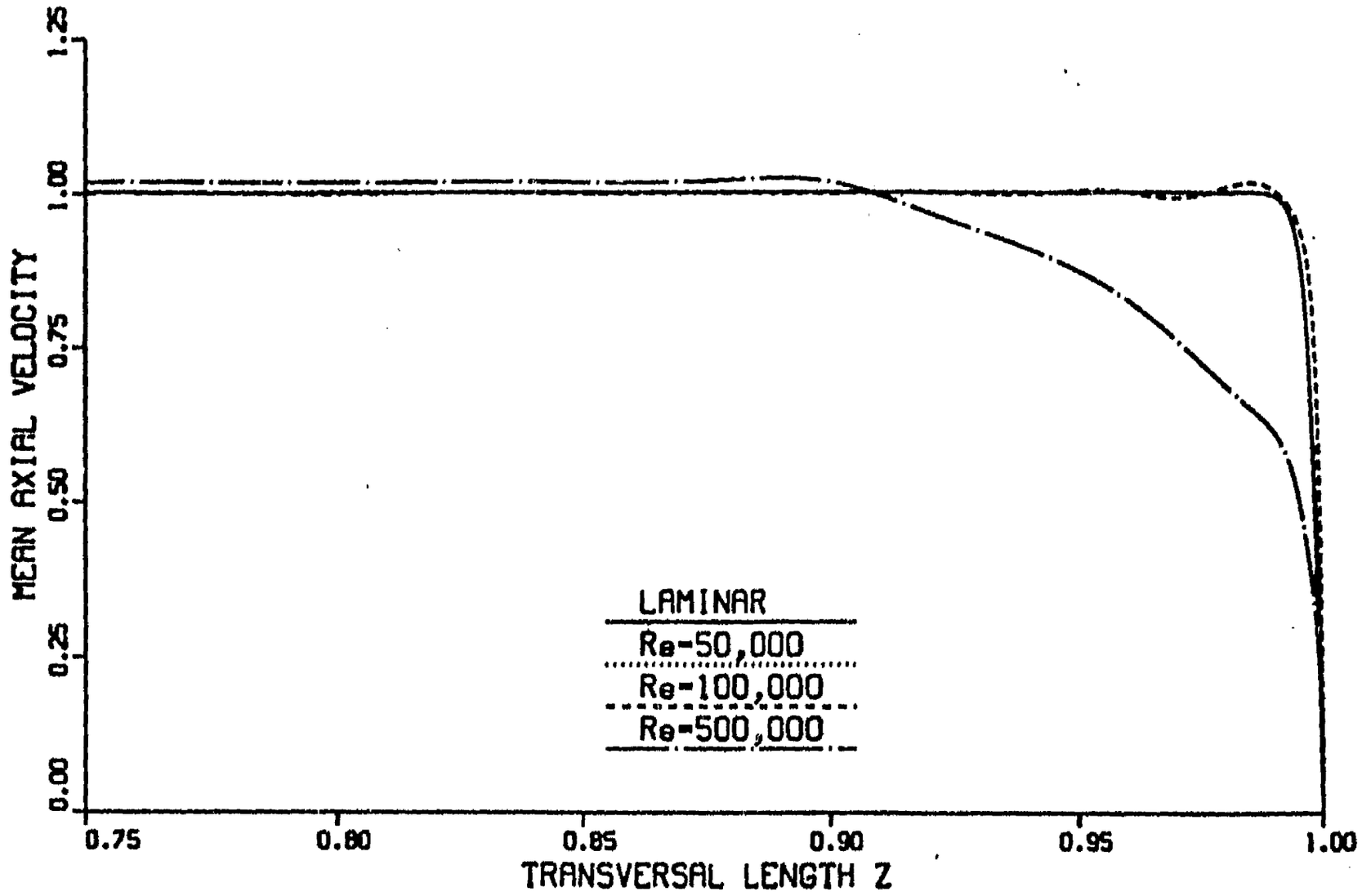

Figure 5.16: Laminar and mean axial velocities vs. z at $y = 0$ for different Re. $M = 10^5$ and $c = 0$.

decreasing the wall conductance ratio tends to suppress the turbulence: the smaller the wall conductance ratio the less pronounced the turbulent effects. Hence, we could state that a reduction in c tends to stabilize the flow. Evidently, this behavior has to do with the fact that, for a given M, a reduction in c implies a decrease in the velocity overshoots in the side layer[3] which are the main source of instability. The slug-like flow in an insulating duct at very high M will be hardly destabilized even with a strong perturbation. This conclusion agrees with the qualitative analysis performed by Hunt [1965]. He pointed out that in an insulating duct at $M \gg 1$, the velocity profile in the side wall boundary layers has no point of inflexion and the magnetic field presents a stabilizing effect on the flow. Coincidently with our results, he remarked that "*uniformly lowering the conductivity of the walls will tend to stabilize the flow in the boundary layers*".

Figures 5.17-5.20 show the laminar and turbulent velocity profiles for $M = 10^4$ and c equal to 0.05, 0.01, 0.001 and 0, respectively. Essentially, profiles present the same tendencies that in the case $M = 10^5$ but turbulent effects are less pronounced. Although total viscosity profiles are not shown here, it was found that their values in the boundary layer are lower than in the previous case for corresponding Reynolds numbers. Nevertheless, turbulent effects are still clearly observed. For instance, in figures 5.17, 5.18 and 5.19, the mean velocity profile for $Re = 5 \times 10^5$ becomes rather flat, disappearing almost completely the velocity overshoot in the side layer. Convergence problems appeared as the wall conductance ratio decreased from 0.01 to 0.001 and were even stronger for $c = 0$, where laminar behavior was again predicted. The non-smooth and oscillating mean velocity profiles obtained for $c = 0$ are shown in figure 5.20. For this M also the first three values of the wall conductance ratio are within the thin conducting wall approximation.

Figures 5.21 and 5.22 show the velocity profiles for $M = 10^3$ and c equal to 0.05 and 0.01, respectively. For the cases $c = 0.001$ and $c = 0$, which, incidentally, lie outside the thin conducting wall approximation, it was not possible to find a converged solution with our iterative scheme. Again, a decrease in the Hartmann number implied weaker turbulent effects with respect to the cases $M = 10^5$ and $M = 10^4$ for corresponding c and Re. The lack of convergence as c is lowered may be due to oscillations in the laminar-turbulent transition region as the velocity gradients (velocity overshoots) in the boundary layer disappear and the flow becomes more stable. A deeper insight is necessary to clarify this point.

In general terms, we can state that provided the thin conducting wall approximation holds, decreasing the Hartmann number reduces the turbulence of the flow for a given Re: the lower the Hartmann number, the weaker the turbulent effects. In more physical terms, the former statement implies that the higher and thinner the side-wall-jets, the more suitable the boundary layer flow to promote a high level of turbulence. We can also assert that in order to reach a certain level of turbulent viscosity near the wall (for

[3]This effect was clearly stated in Chapter 3.

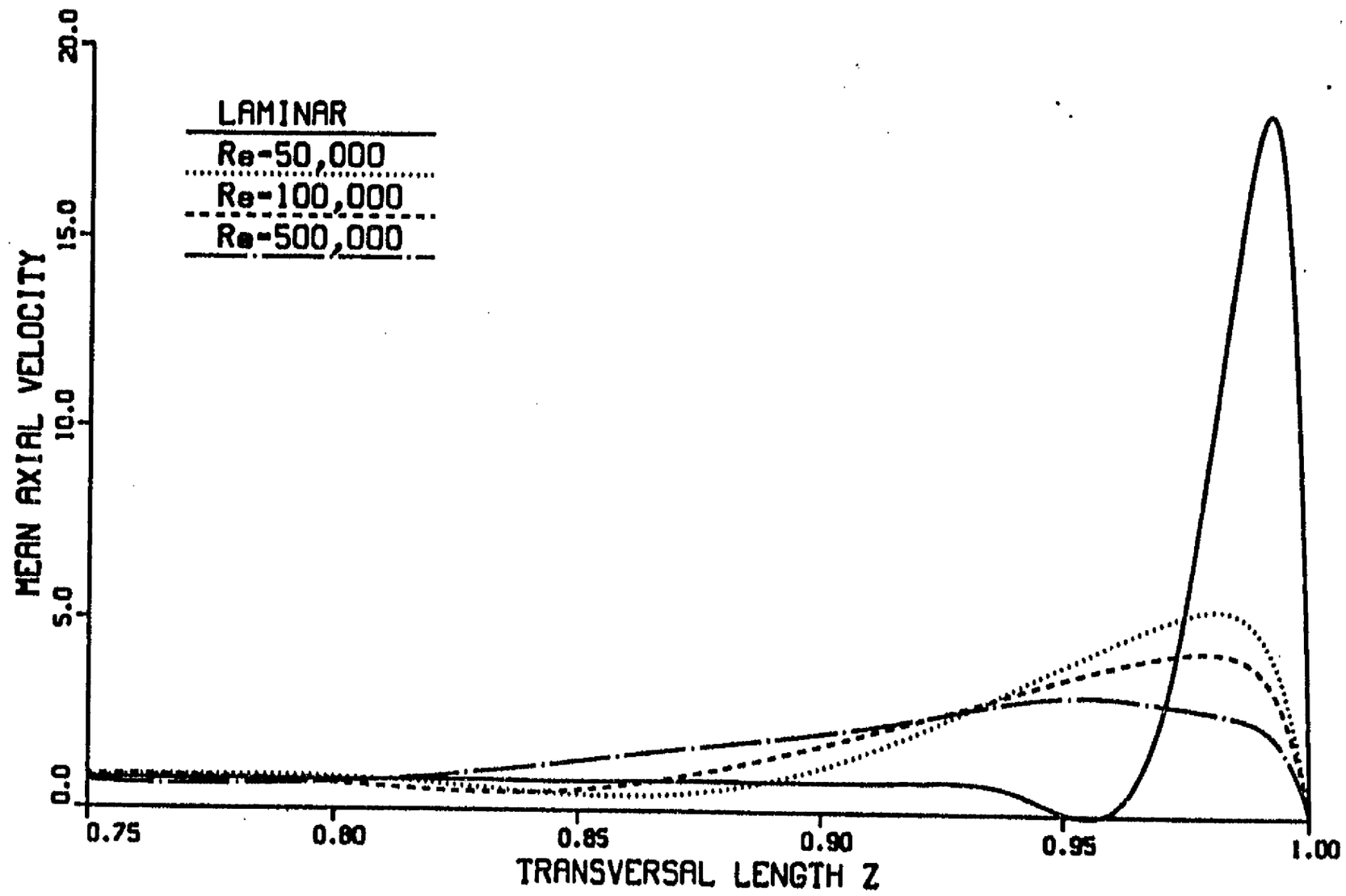

Figure 5.17: Laminar and mean axial velocities vs. z at $y = 0$ for different Re. $M = 10^4$ and $c = 0.05$.

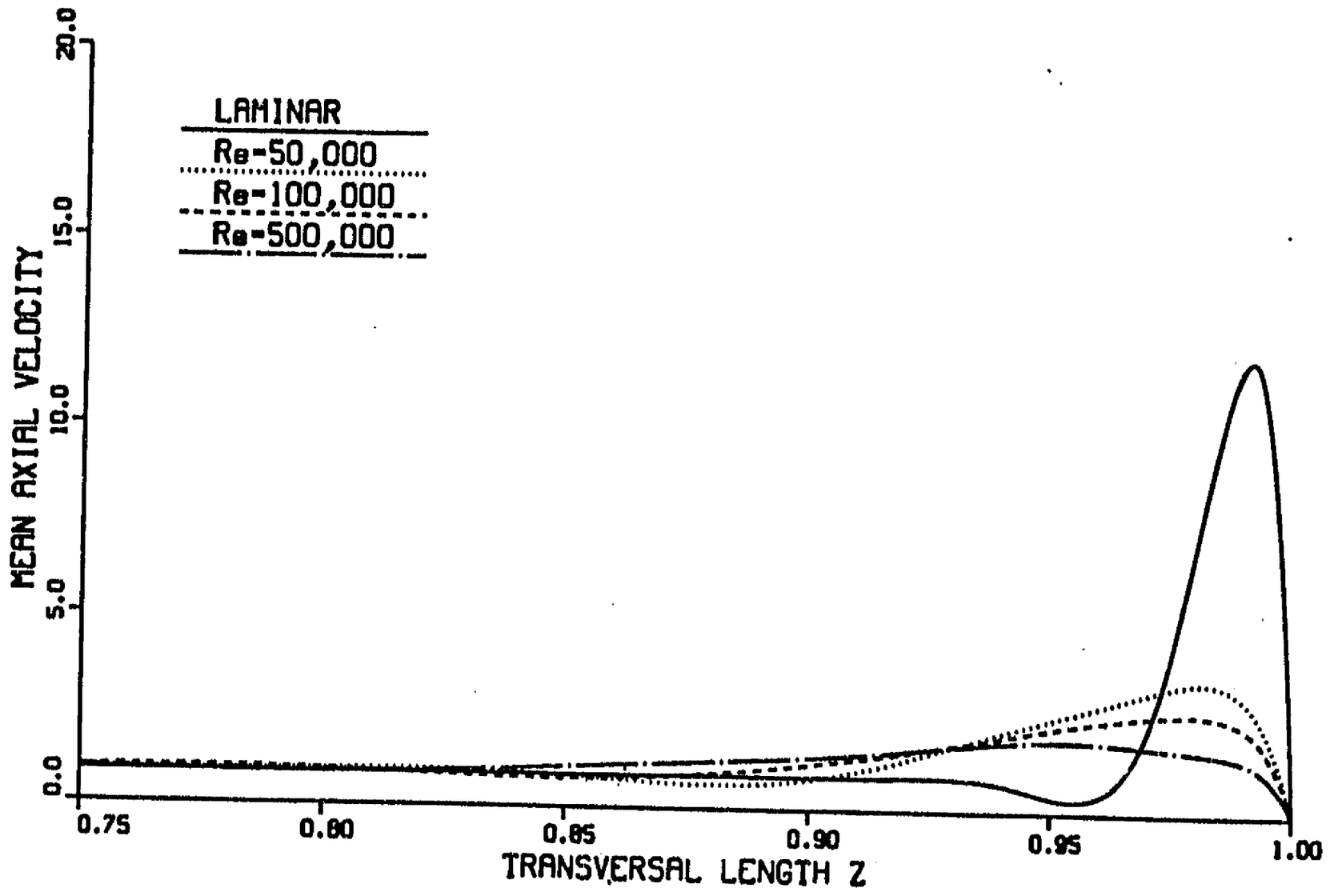

Figure 5.18: Laminar and mean axial velocities vs. z at $y = 0$ for different Re. $M = 10^4$ and $c = 0.01$.

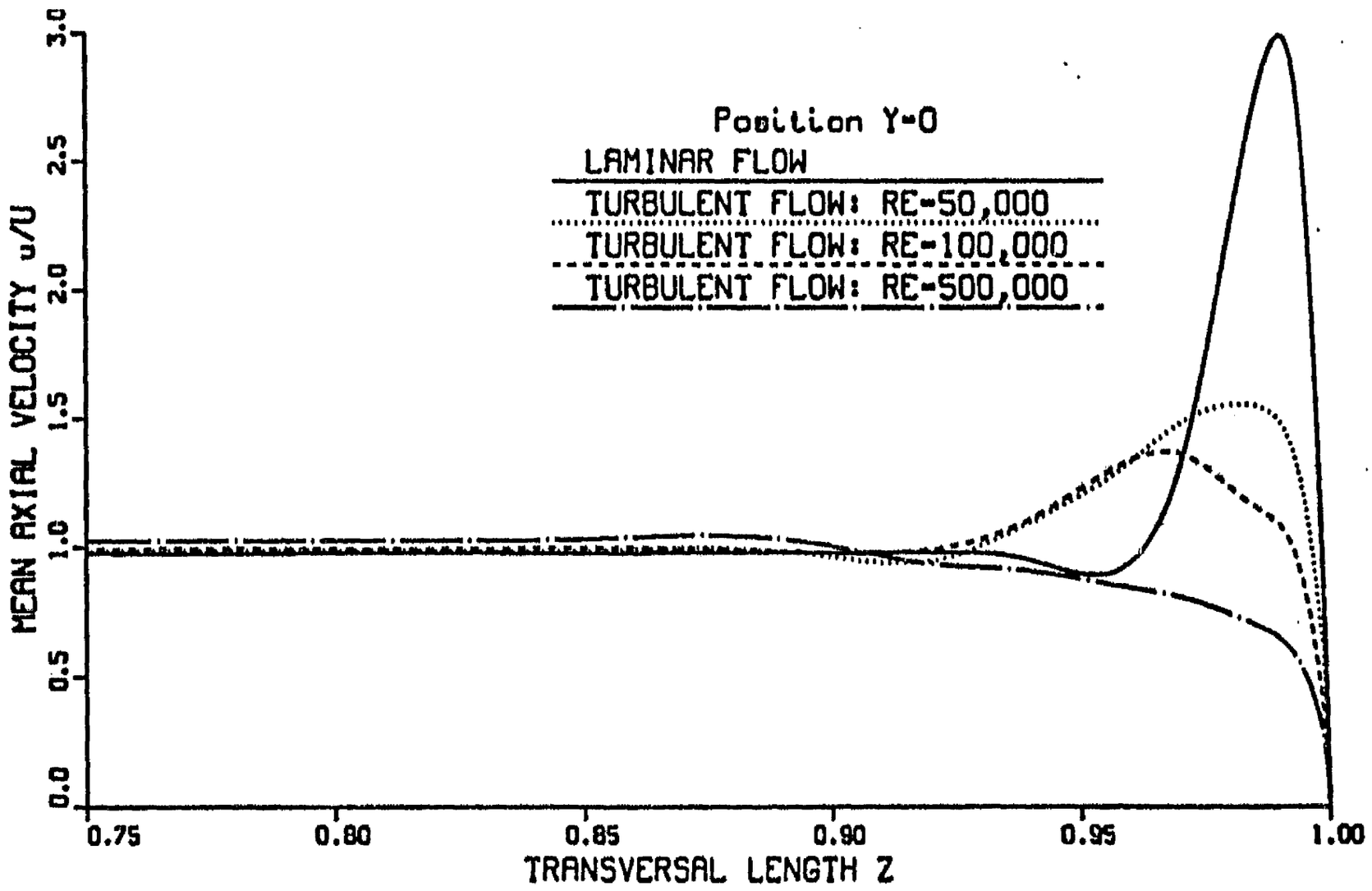

Figure 5.19: Laminar and mean axial velocities vs. z at $y = 0$ for different Re. $M = 10^4$ and $c = 0.001$.

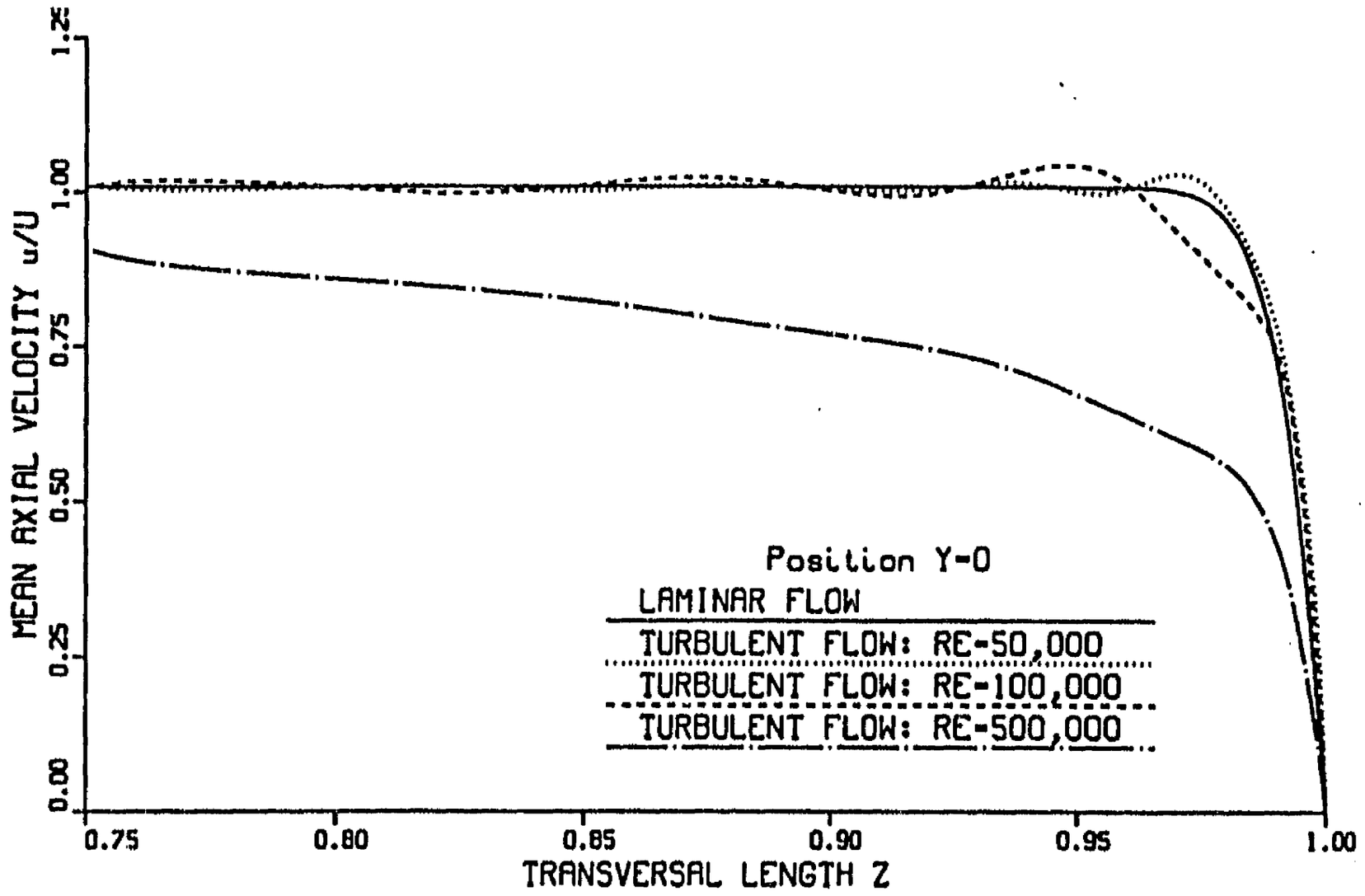

Figure 5.20: Laminar and mean axial velocities vs. z at $y = 0$ for different Re. $M = 10^4$ and $c = 0$.

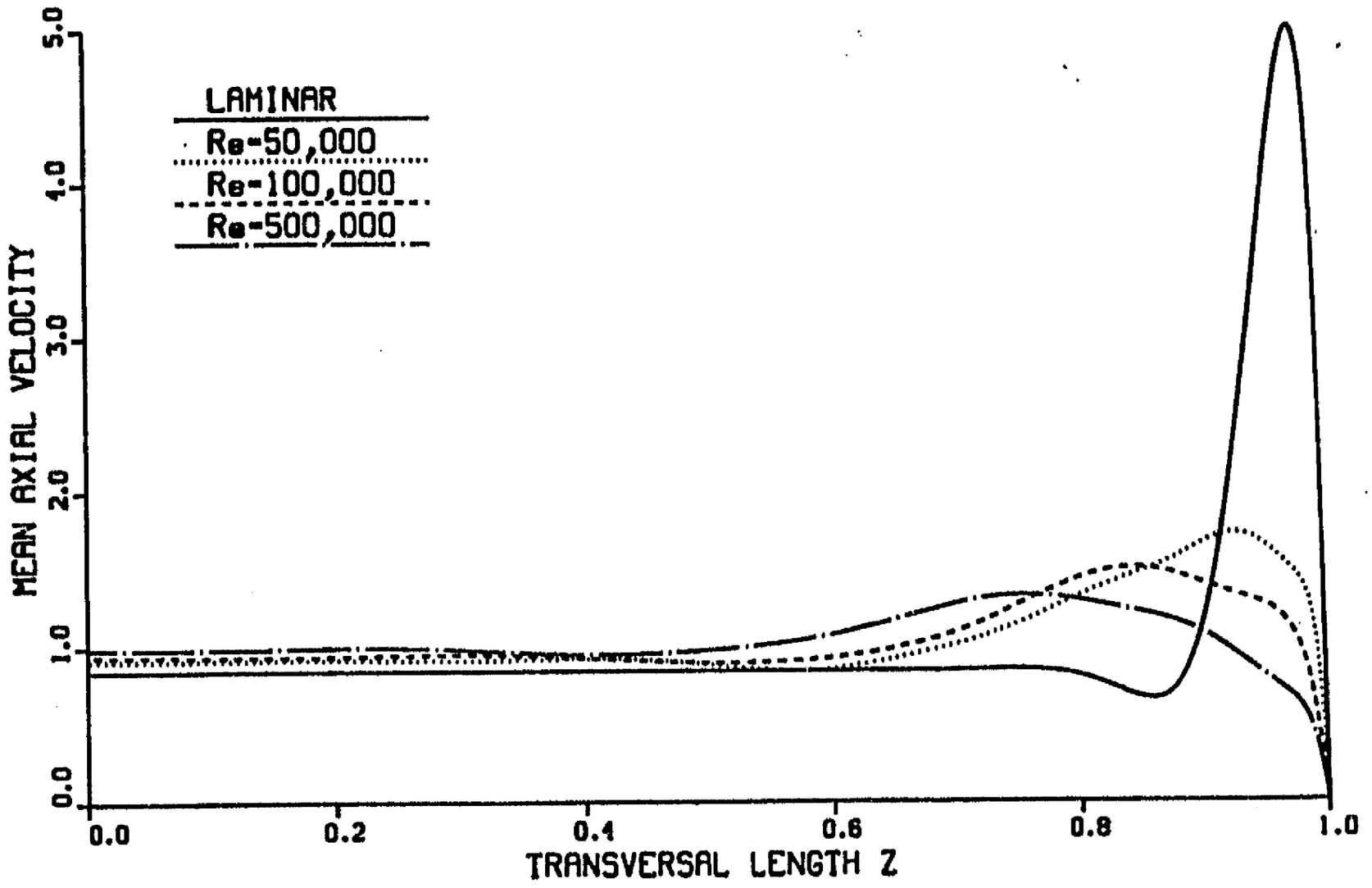

Figure 5.21: Laminar and mean axial velocities vs. z at $y = 0$ for different Re. $M = 10^3$ and $c = 0.05$.

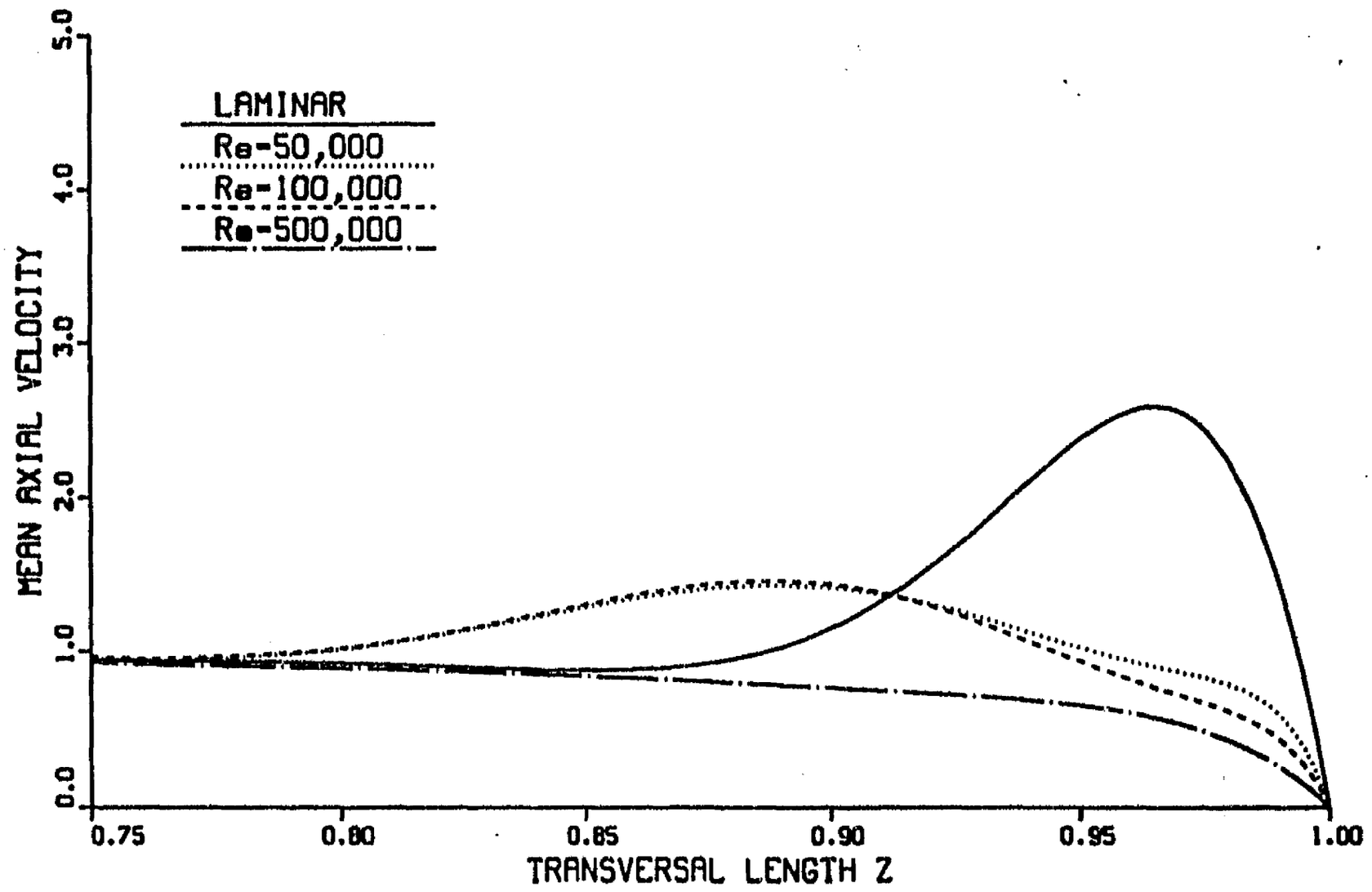

Figure 5.22: Laminar and mean axial velocities vs. z at $y = 0$ for different Re. $M = 10^3$ and $c = 0.01$.

c such that $M^{-1} \ll c \ll M^{-\frac{1}{2}}$), a lower Re is required, the higher M. In this sense, for thin conducting wall ducts at $M \gg 1$, an increase of the magnetic field may become a destabilizing factor. A similar statement was drawn by Hunt [1965] as a tentative conclusion from his qualitative analysis though he only considered ducts whose walls are either perfect conductors or insulators. He observed that for flow in a rectangular duct with conducting walls, the value of the Reynolds number at which the side wall boundary layers become unstable decreases as the Hartmann number increases. He also remarked that this may be contrasted to the case of flow in a plane channel where the stabilizing effect of the magnetic field has been shown, both theoretically and experimentally. As a matter of fact, the duct's aspect ratio is an additional factor that influences the stability of the flow. Since we only considered the square duct case, the effects of variation of aspect ratio were not explored but may be interesting for a future analysis.

Hunt also made the important observation that it is incorrect to assume that the side wall boundary layers are always unstable as $M \to \infty$, since for small enough Re, the boundary layer flow should be stable whatever the value of M (and c). In terms of the interaction parameter $N = M^2/Re$, we can expect a stable laminar flow at sufficiently high N. Incidentally, at small enough Re, the RNG turbulence model allows us to recover the laminar velocity profiles for given M and c. On the other hand, recall that the model should predict a turbulence suppression effect at sufficiently high M, for given Re and c. This effect is not present in the RNG turbulence model but it may be included by introducing a damping factor of the form $\exp(-Nct)$ for the thin conducting wall case. Such factor, presented in section 4.5, would introduce the dissipation, at the top/bottom conducting walls, of the elongated vortices that we may assume to exist in a turbulent MHD flow, as it was discussed in Chapter 4. The dimensionless time t can be assessed in terms of a suitable characteristic length and velocity of the flow. This extension of the model will be addressed in a future investigation.

The main conclusions of the previous analysis can be summarized as follows:

- In thin conducting wall ducts, for a given M, the introduction of turbulence brings about a dramatic decrease of the side layer velocity, the thickening of the boundary layer and a marked increase in the total viscosity in the extended boundary layer region. The former turbulent effects are stronger, the higher Re.

- Turbulent effects are restricted to the boundary layer while the core remains unperturbed.

- Insulating and nearly-insulating wall cases seem to preserve the laminar behavior, even at high Re. The magnetic field prevents the appearance of turbulence in the flow in insulating ducts at $M \gg 1$.

- Given M and Re, the smaller c, the less pronounced the turbulent effects. A reduction in c tends to reduce the level of turbulence in the flow.
- For a given Re, provided the thin conducting wall approximation holds, the lower M, the weaker the turbulent effects. In thin conducting wall ducts at $M \gg 1$, an increase of the magnetic field may promote the appearance of turbulence.

5.4 Turbulent MHD Heat Transfer in a Square Duct

In this section, the consequences of turbulent effects on heat transfer are explored. There are several issues affecting the heat transfer in turbulent liquid-metal flows in magnetic fields. Firstly, the anisotropy introduced in the flow distribution by the magnetic field, promotes a non-homogeneous energy transfer process, characterized by a preferential heat transfer direction. For the side-wall-jet instability, the experimental evidence and the linear stability analysis confirmed that the strongest velocity fluctuations are localized in planes perpendicular to the magnetic field. Hence, the largest contribution to the heat transfer in the near wall region comes from velocity fluctuations in the z-direction, i.e. in the direction perpendicular to the side wall, that is considered to be the heated wall. Similarly, in the turbulent case it is also expected that the mixing in the side layer will be mainly increased due to velocity fluctuations perpendicular to the side wall. These fluctuations may be considered as a manifestation of the elongated vortices created in the side wall boundary layer. Although our turbulent solution does not include z-velocity components explicitly, their effects are modeled through the total viscosity which, in turn, influences the heat transfer process. Once turbulence suppression effects by the magnetic field are manifested, the turbulent convection transfer mechanism is inhibited by the damping of velocity fluctuations. Under such conditions, heat transfer occurs through turbulent diffusion. The mean flow distribution itself determines to a great extent the specific heat transfer characteristics and plays a fundamental role in the calculation of the temperature distribution. The fact that liquid metals have a low molecular Prandtl number also influences the heat transfer, as we will discuss below.

Similarly to the dynamic problem, a straightforward way of introducing the effect of turbulent fluctuations on heat transfer is through an effective or eddy thermal diffusivity, in the sense of the Boussinesq approach. First, we can write the heat transfer equation in a typical form for turbulent flows

$$\rho c_p \bar{u}_i \frac{\partial \bar{T}}{\partial x_i} = \frac{\partial}{\partial x_i}\left(k_o \frac{\partial \bar{T}}{\partial x_i} - \rho c_p \overline{u_i' T'}\right) + \bar{S}, \qquad i = 1,2,3 \tag{5.21}$$

where x_i, $i = 1,2,3$, correspond to coordinates x, y and z, respectively. $\bar{T}$ is the

mean temperature and $\bar{u}$ is the mean component of the velocity field in the i-direction. Finally, T' and u_i' are the temperature and velocity fluctuations, respectively and $\bar{S}$ is a volumetric heat source. As we mentioned in Chapter 3, in liquid-metal-cooled blankets $\bar{S}$ represents the neutron heating. Joule heating due to both mean flow and pulsant currents produced by velocity fluctuations is negligible. The term $\rho c_p \bar{u}$ represents the x_i-directional mean energy flux due to turbulent effects. We can put equation (5.21) in the form for laminar flow by introducing an analog of the Fourier law in the form of the Boussinesq relationship, that is,

$$(q)_i = -k_o \frac{\partial \bar{T}}{\partial x_i} + \rho c_p \overline{u_i' T'} = \rho c_p (\alpha_o + \alpha_e) \frac{\partial \bar{T}}{\partial x_i}, \tag{5.22}$$

where $\alpha_o = k_o/\rho c_p$ is the molecular thermal diffusivity and α_e is the eddy thermal diffusivity. The total thermal diffusivity (molecular + turbulent) is then given by

$$\alpha_t = \alpha_o + \alpha_e. \tag{5.23}$$

While using the Boussinesq eddy diffusivity approach, we have to take into account that the assumed transport mechanism is a gradient type diffusion by small-scale eddies. Hence, the convective action of large scale motion (big eddies) is not properly modeled.

Since we are interested in fully developed channel flow, the only non-zero mean velocity is in the axial direction. With this assumption, substituting equations (5.22) and (5.23) into (5.21), we get the turbulent heat transfer equation for the mean temperature:

$$\rho c_p \bar{u} \frac{\partial \bar{T}}{\partial x} = \frac{\partial}{\partial x}\left(\alpha_t \frac{\partial \bar{T}}{\partial x}\right) + \frac{\partial}{\partial y}\left(\alpha_t \frac{\partial \bar{T}}{\partial y}\right) + \frac{\partial}{\partial z}\left(\alpha_t \frac{\partial \bar{T}}{\partial z}\right) + \bar{S}, \tag{5.24}$$

where the turbulent effects are introduced through the non-uniform thermal diffusivity α_t. In dimensionless terms, equation (5.24) can be written as

$$Pe \bar{u} \frac{\partial \bar{\Theta}}{\partial x} = \frac{\partial}{\partial x}\left(\alpha_t \frac{\partial \bar{\Theta}}{\partial x}\right) + \frac{\partial}{\partial y}\left(\alpha_t \frac{\partial \bar{\Theta}}{\partial y}\right) + \frac{\partial}{\partial z}\left(\alpha_t \frac{\partial \bar{\Theta}}{\partial z}\right) + \bar{S}, \tag{5.25}$$

where dimensionless variables have been defined in an analogous way as in Chapter 3 and the $*$ has been dropped. In addition, boundary conditions for the mean fields are the same as in the laminar problem:

$$\frac{\partial \bar{\Theta}}{\partial z} = 1 \quad z = 1, \quad -a \le y \le a, \quad 0 \le x \le x_h, \tag{5.26}$$

$$\frac{\partial \bar{\Theta}}{\partial z} = 0 \quad z = -1, \quad -a \le y \le a, \quad 0 \le x \le x_h, \tag{5.27}$$

$$\frac{\partial \bar{\Theta}}{\partial y} = 0 \quad y = \pm a, \quad -1 \le z \le 1, \quad 0 \le x \le x_h, \tag{5.28}$$

$$\bar{\Theta} = 0 \qquad x = 0 \qquad -a \leq y \leq a, \quad -1 \leq z \leq 1. \tag{5.29}$$

The main issue here is to find an adequate expression for either the total thermal diffusivity or the eddy diffusivity, that models the average effect of the turbulent fluctuations. Probably, the most common approach is provided by the *mixing length* theory which, by analogy with kinetic theory, assumes that the eddy diffusivity can be modeled as

$$\alpha_e = u_e L_e, \tag{5.30}$$

where u_e and L_e are the characteristic velocity and length scales of the 'mixing process', respectively. L_e is known as the mixing length. The problem turns into finding suitable means for evaluating u_e and L_e. Prandtl's approach assumes that the mixing length is proportional to the width of the mixing zone in the case of free turbulence or proportional to the distance from the wall, in the case of wall turbulence.

In the present problem, we follow the RNG approach [Yakhot and Orszag, 1986], and assume that, in dimensional terms, the total thermal diffusivity α_t is given by

$$\alpha_t = \frac{\nu_t}{Pr_t}, \tag{5.31}$$

where the total (dimensional) viscosity ν_t is given by equation (5.1) and the total Prandtl number Pr_t (molecular + turbulent) is obtained from the following RNG equation:

$$\left(\frac{Pr_t^{-1} - b}{Pr_o^{-1} - b}\right)^{\xi} \left(\frac{Pr_t^{-1} + d}{Pr_o^{-1} + d}\right)^{1-\xi} = \frac{\nu_o}{\nu_t}. \tag{5.32}$$

$Pr_o = \nu_o/\alpha_o$ is the molecular Prandtl number and $b = 1.3929$, $d = 2.3929$ and $\xi = 0.65$ are model constants. If we define

$$\alpha_t^* = \frac{\alpha_t}{\alpha_o}, \quad \nu_t^* = \frac{\nu_t}{\nu_o}, \quad Pr_t^* = \frac{Pr_t}{Pr_o},$$

equation (5.32) can be rewritten in dimensionless terms as

$$\left(\frac{\mathrm{Pr}_t^{-1} - Pr_o b}{1 - Pr_o b}\right)^{\xi} \left(\frac{\mathrm{Pr}_t^{-1} + Pr_o d}{1 + Pr_o d}\right)^{1-\xi} = \frac{1}{\nu_t}, \tag{5.33}$$

where the $*$ has been dropped for simplicity and dimensionless ν_t is given by equation (5.4). In heat transfer problems, in addition to the dimensionless numbers characterizing the dynamic problem, we have to include another dimensionless criterion, namely, the Prandtl number. Due to their high thermal conductivities, liquid metals are characterized by a low molecular Prandtl number. This dimensionless criterion determines

the relative importance between convective and molecular heat transfer in the boundary layer. When $Pr_o \ll 1$, transport processes in laminar flows are mainly determined by molecular transfer. Similarly, turbulent Prandtl number measures the contribution of the turbulent convective transfer relative to the turbulent transfer by diffusive means.

The RNG total thermal diffusivity model defined by equation (5.33) was obtained by applying the renormalization procedure to the energy balance equation [Yakhot and Orszag, 1986]. The RNG model has been used to describe the heat transfer process in OHD turbulent flow pipe, finding a good agreement with experimental data [Yakhot, *et al.*, 1987]. The model has also been applied for some MHD cases [Sukoriansky, *et al.*, 1987; Talmage, 1993], though comparison with experimental data was not available. In the present investigation, the RNG total thermal diffusivity model was applied in its original form, that is, the same model constants obtained by Yakhot and Orszag were used. In an analogous way to the total viscosity model, a calibration against empirical results for the MHD flow problem we are considering may become necessary. However, the lack of heat transfer experimental data for this problem prevents from such calibration. Under these circumstances, as in the dynamic problem, turbulent heat transfer results should be considered only for a qualitative description. The necessity of calibration arise from the expectation that the magnetic field affects to some extent the turbulent Prandtl number. However, some authors claim that empirical correlations show a very slight deviation of Pr_t under applied magnetic fields, from its value in the absence of fields [Blùms *et al.*, 1987]. Therefore, it appears that a reasonable assumption is that the magnetic field does not affect the turbulent Prandtl number. Under such approximation, the specific heat transfer characteristics are mainly determined by the hydrodynamic peculiarities of MHD flows.

5.4.1 Numerical Results

In order to get the turbulent heat transfer results, equation (5.25) without heat sources and with boundary conditions (5.26)-(5.29) was solved using the finite difference method described in Section 3.3. The wall thickness was considered negligible, so that the wall temperature distribution was not computed. The solution requires as an input the previously calculated mean velocity profiles along with the non-uniform total thermal diffusivity. In turn, the calculation of the total diffusivity requires to determine, at each point, the total Prandtl number from the RNG formula (5.33), for a given Pr_o and the corresponding total viscosity distribution. Finally, the total thermal diffusivity $\alpha_t(y,z)$ is obtained from equation (5.31).

Since we are interested in liquid-metal-cooled blanket flows, lithium, which molecular Prandtl number is 0.005, was chosen as the working fluid for heat transfer numerical calculations. Péclet and Reynolds numbers are related through the equation $Pe = RePr_o$. Therefore, for the former Prandtl number, the three analyzed Reynolds

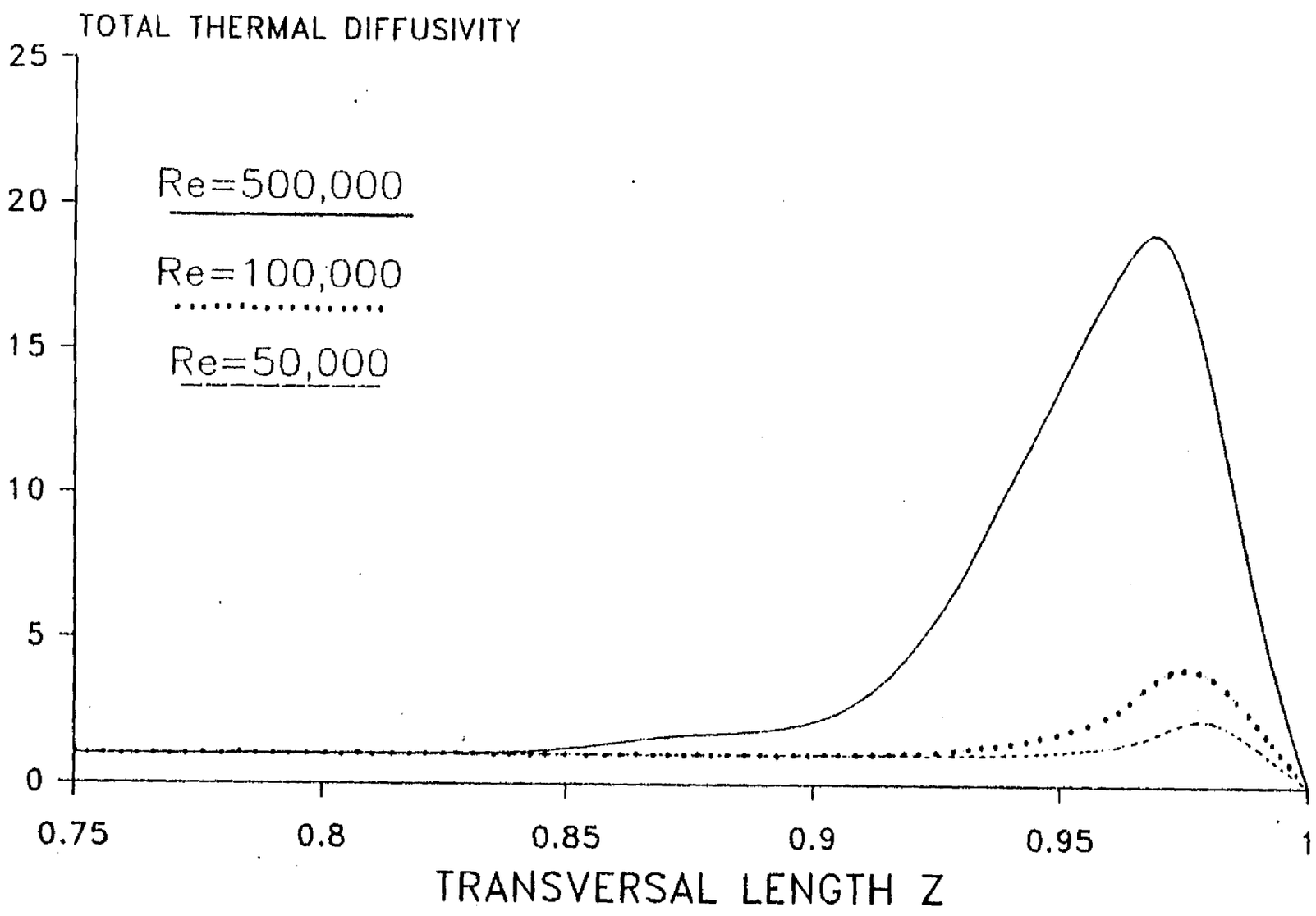

Figure 5.23: Total thermal diffusivity vs z at $y = 0$ for different Reynolds numbers. $M = 10^5$, $c = 0.05$.

numbers 5×10^4, 10^5 and 5×10^5 correspond to the Péclet numbers 250, 500 and 2500, respectively. Hence, once the Prandtl number is specified, the heat transfer analysis can be equivalently carried out in terms of either Re or Pe. Here we show the results in terms of Pe (except in figure 5.23) for correspondence with the laminar analysis. Recall that Re, and consequently Pe, are based on the average velocity.

The numerical results obtained with the RNG model predict that the appearance of turbulence affects more strongly the dynamic than the thermal behavior. In other words, despite the fact that the total viscous diffusivity is strongly increased by turbulence in the boundary layer[4], for a low-Prandtl-number fluid as lithium the total thermal diffusivity is not increased in the same proportion. This can be shown by contrasting figures 5.11 and 5.23. In figure 5.11, the total viscous diffusivity in the central plane ($y = 0$) is plotted as a function of the z-coordinate for the three different Reynolds numbers, and for $M = 10^5$ and $c = 0.05$. In figure 5.23, on the other hand, the total thermal diffusivity is plotted for the same M, c and Re's (*i.e.* Pe's). Notice

[4]Strictly, the increase of viscous diffusivity was observed for thin conducting wall ducts.

that the physical behavior of viscous and thermal diffusivities is very similar, that is, they markedly increase in the boundary layer region and decrease as the core of the flow is approached, until the laminar (molecular) value is reached. However, while the total viscosity for the highest Reynolds number, $Re = 5 \times 10^5$ (*i.e.* $Pe = 2500$), is about $O(10^3)$ (≈ 3000), the corresponding total thermal diffusivity is not higher than $O(10)$ (≈ 20). Actually, this behavior is not surprising once we analyze the behavior of the RNG formula (5.33) in the limit $Pr_o \rightarrow 0$. In such limit, we find that $Pr_t^{-1} \approx 1/\nu_t$. In other words, using equation (5.31), we have that

$$\alpha_t = \frac{\nu_t}{Pr_t} \approx 1.$$

In dimensional terms, the former limit implies that the total thermal diffusivity is of the same order than the molecular thermal diffusivity. Evidently, this tendency will be reflected in the heat transfer calculations performed with low-Prandtl-number fluids, as it is shown below. It was also numerically confirmed that a higher Pr_o leads to a lower Pr_t and, as a consequence, to a higher total thermal diffusivity, α_t. It may be interesting to analyze other working fluids with possibilities for fusion applications, as lithium-lead.

Let us now analyze the effect of the mean velocity profiles and the non-uniform total thermal diffusivity on the mean wall temperature in the thin conducting and insulating wall duct cases. Figure 5.24 shows the mean wall temperature as a function of the axial coordinate for $M = 10^5$ and $c = 0.05$ and for the three different Péclet numbers. The effect of increasing the Péclet number (*i.e.* the Reynolds number) for a given M and c, is obviously the same as in the laminar case, namely, the higher the Péclet number, the stronger the convective effects and the lower the wall temperature. Or, in other words, for larger Re (Pe), turbulent effects in the boundary layer are stronger, therefore, more energy is convected away from the wall and the wall temperature decreases.

The mean wall temperature versus the axial coordinate for $Pe = 500$, $M = 10^5$ and $c = 0.05$ is shown in figure 5.25, where wall temperature profiles obtained with slug and laminar MHD flows are also shown for comparison. Contrary to the result we could expect, the turbulent wall temperature is slightly higher than the laminar one: turbulence seems not to improve the heat transfer in the boundary layer. Notice that the (mean) side layer velocity in the turbulent case is considerably smaller than its laminar counterpart (see fig. 5.10). The joint effect of the mean velocity profile and the non-uniform total thermal diffusivity does not lead to an improvement in the heat transfer in the near-the-wall region despite the fact that the total viscosity is very large in that region (see fig. 5.11). With a lower Péclet number (250) the same trend is maintained. Figure 5.26 displays the same results as in figure 5.25 but in different form, namely, the local Nusselt number is plotted as a function of the axial coordinate for slug, laminar and turbulent flow cases. The highest values of the local Nusselt number correspond to the laminar flow. Figure 5.27 shows the mean temperature profiles in

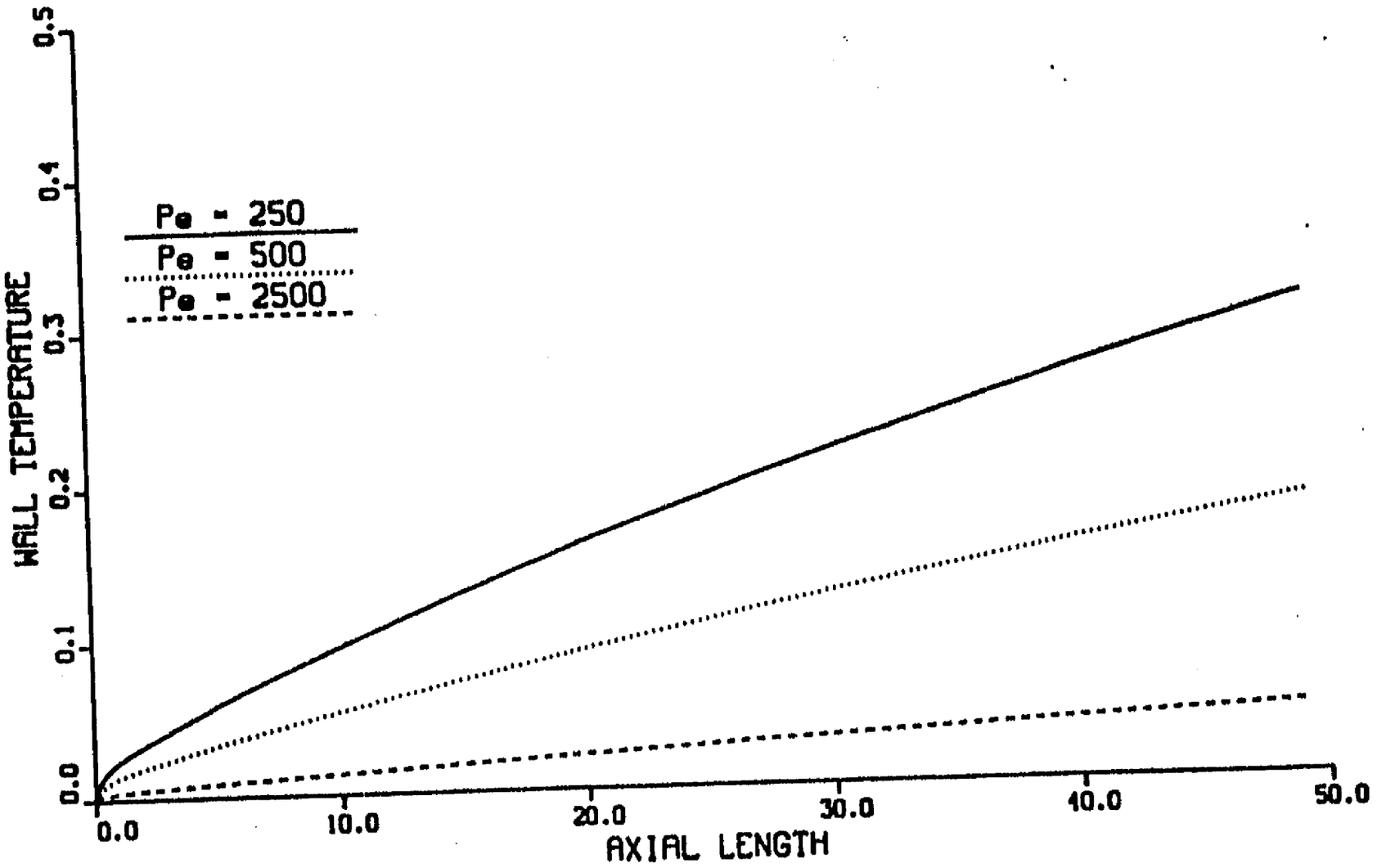

Figure 5.24: Mean wall temperature vs x at $y = 0$ for different Péclet numbers. $M = 10^5$, $c = 0.05$.

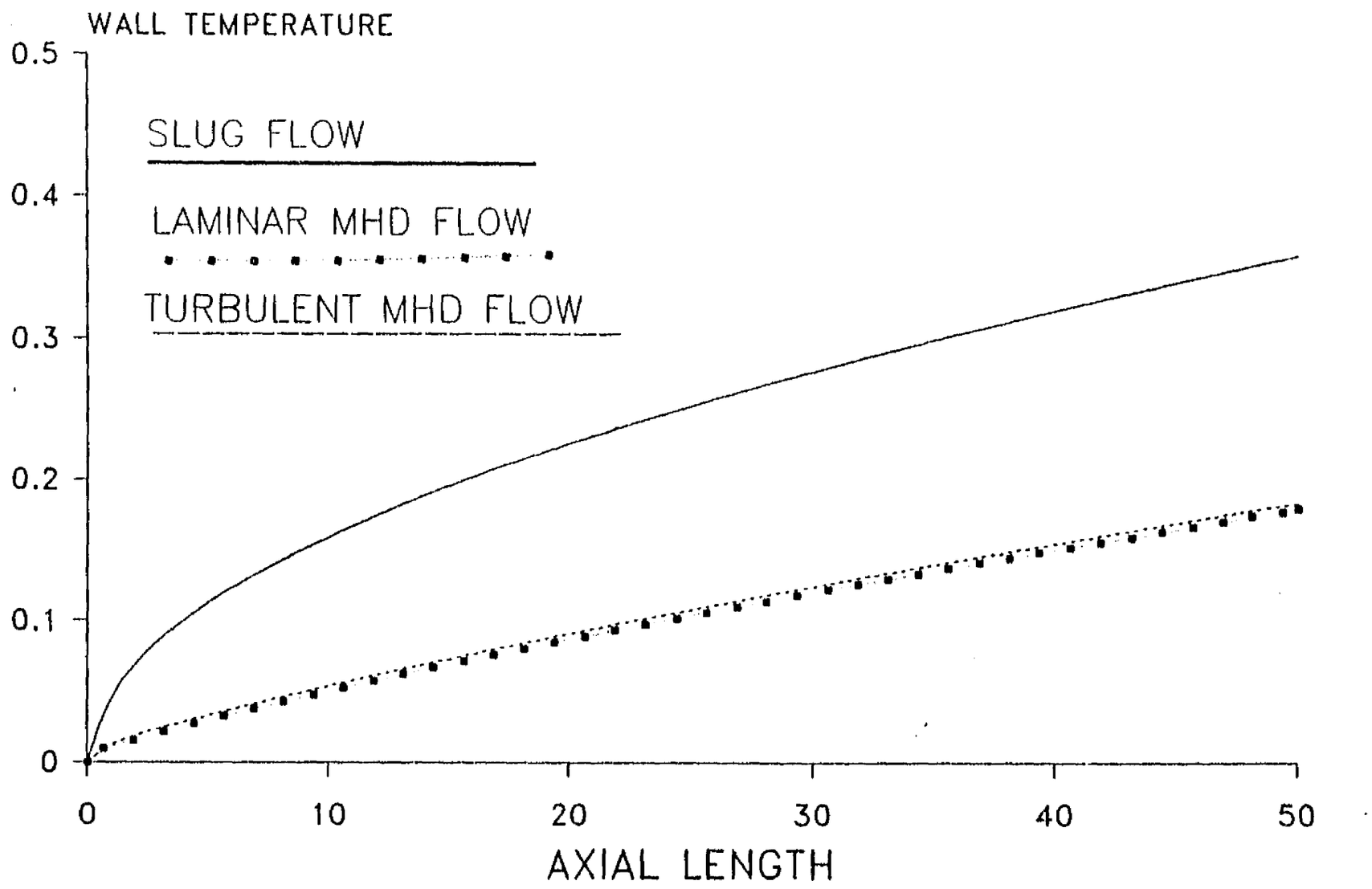

Figure 5.25: Slug, laminar and mean wall temperature vs x at $y = 0$. $M = 10^5$, $c = 0.05$, $Pe = 500$.

the mid-plane as a function of the z-coordinate at three different axial locations for the previous case ($M = 10^5$, $c = 0.05$ and $Pe = 500$). At the three axial positions, the mean temperature decreases to zero before reaching the plane $z = 0$. As in the laminar case, the thermal boundary layer thickness is less than the characteristic length of the channel and, therefore, the presence of the opposite wall does not have any relevance to the heat transfer problem.

Figures 5.28 and 5.29 present the wall temperature profiles and the local Nusselt numbers, respectively, for the previous Hartmann number and conductance ratio ($M = 10^5$, $c = 0.05$) but a higher Péclet number, namely, $Pe = 2500$. In this case, the turbulent wall temperature is slightly lower than the laminar one and, correspondingly, the local Nusselt number for turbulent flow is higher than laminar and slug flows. With the increase in Pe, the presence of turbulence brings about a strong enough mixing in the boundary layer which improves the heat transfer rate in that zone with respect to the laminar case.

Figures 5.30 and 5.31 show the wall temperature and local Nusselt number for the same Hartmann and Péclet numbers as in figs. 5.26 and 5.27 ($M = 10^5$, $Pe = 500$) but

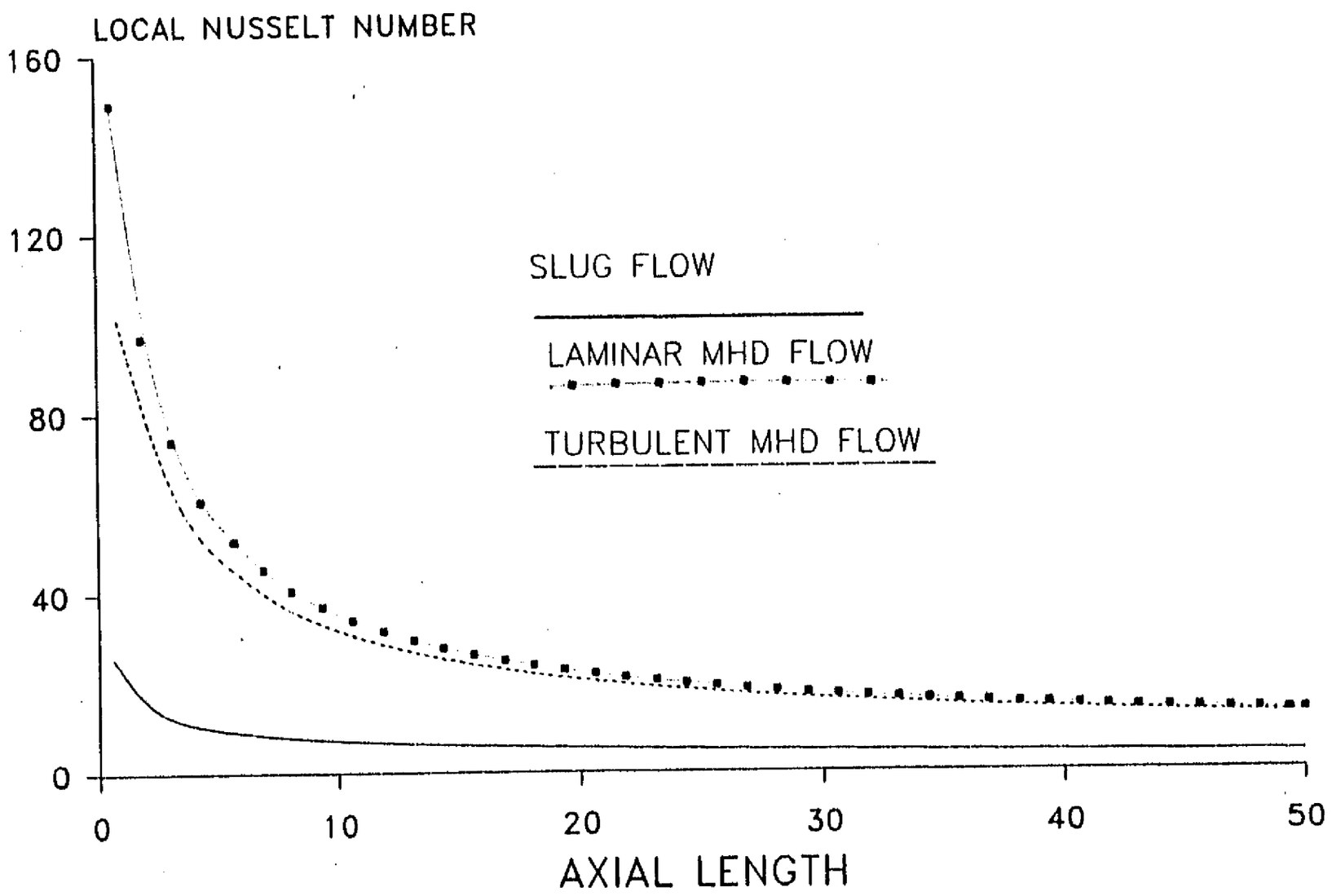

Figure 5.26: Local Nusselt number vs x at for slug, laminar and turbulent flows. $M = 10^5$, $c = 0.05$, $Pe = 500$.

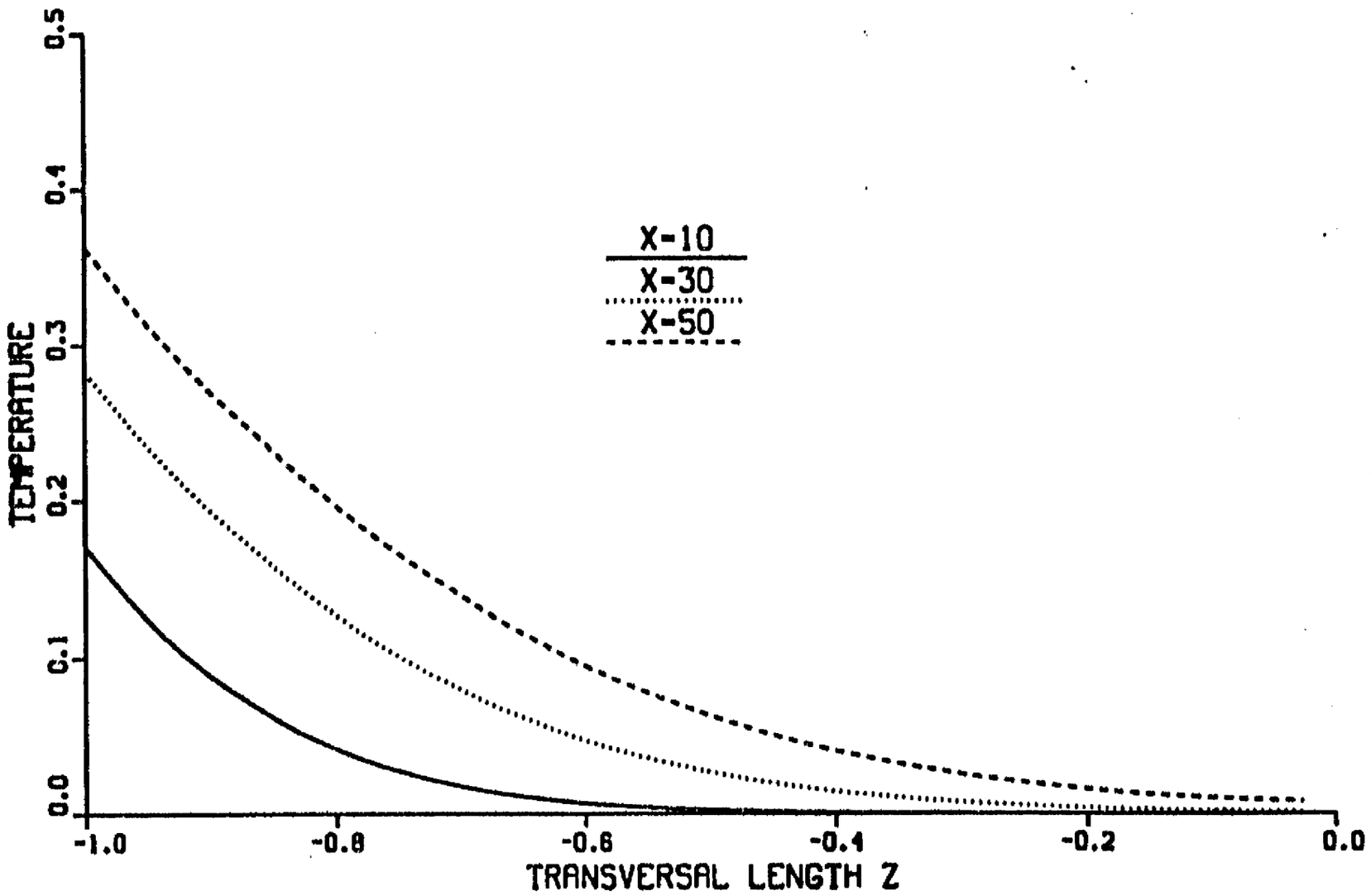

Figure 5.27: Mean temperature vs z at $y = 0$ at different axial positions. $M = 10^5$, $c = 0.05$, $Pe = 500$.

a smaller wall conductance ratio, $c = 0.01$. For this c, the turbulent wall temperature profile is also higher than the laminar profile although the reduction in c leads to a larger separation between both profiles. Figures 5.32 and 5.33 show that for $M = 10^5$ and $c = 0.01$, the improvement in the turbulent heat transfer obtained by increasing the Péclet number to 2500, is not enough to do better than the laminar flow. Comparing the corresponding mean velocity profiles ($Re = 10^5$) for $c = 0.05$ and $c = 0.01$ shown in figures 5.10 and 5.12, respectively, we observe that both profiles are not dramatically different. However, the reduction in the total viscosity when the wall conductance ratio goes form $c = 0.05$ (fig. 5.11) to $c = 0.01$ (fig. 5.13) is rather marked. This indicates that the mixing in the boundary layer for $c = 0.01$ is less pronounced and, as a consequence, the total thermal diffusivity decreases. This originates an increase in the turbulent wall temperature higher than the one obtained with the laminar flow. In other words, laminar flow seems to remove heat more efficiently than the turbulent flow: the increase in the total thermal diffusivity in the boundary layer produced by turbulence does not compensate the reduction in the mean side layer velocity. This tendency continues as the wall conductance ratio is reduced even more, independently of the Péclet number. This is shown in figures 5.34 and 5.35 where the wall temperature profiles for $Pe = 500$ and $Pe = 2500$, respectively, are displayed for the previous Hartmann number but a lower wall conductance ratio, $c = 0.001$.

Wall temperature profiles for the insulating wall duct, $c = 0$, are shown in figures 5.36 and 5.37 for $Pe = 500$ and $Pe = 2500$, respectively. For $Pe = 500$ (fig. 5.36), laminar and turbulent profiles overlap and, as a matter of fact, in heat transfer terms, slug flow presents a better performance. This result is not surprising. In the previous section we found that for $c = 0$, the turbulence model predicts a laminar behavior whatever the Reynolds number. Therefore, turbulent and laminar velocity profiles coincide and the total thermal diffusivity takes the molecular value everywhere. Since flows in insulating ducts have not velocity overshoots in the side layer, slug flow conveys the heat in the boundary layer slightly more efficiently than MHD flows. Nevertheless, for $Pe = 2500$, the turbulent wall temperature profile overlaps the slug profile while the laminar profile is slightly higher. For practical purposes, for $c = 0$, heat transfer calculations carried out with laminar and turbulent flows may be considered equivalent to those performed with slug flow.

From the previous results we can clearly separate the thermal behavior of the thin conducting wall cases ($c = 0.05$, 0.01, 0.001) from the insulating wall case. For both laminar and turbulent flows, as the wall conductance ratio decreases, the wall temperature increases. This effect is related to the velocity profile. As the wall conductance ratio decreases, the peak axial velocity decreases and the axial velocity profile narrows (see figs. 5.10, 5.12, 5.14 and 5.16). Therefore, the convective effects are lessened and the wall temperature rises. Notice, however, that c influences the laminar velocity profile to a greater degree than it does the mean turbulent velocity profile: as c decreases, the peak axial velocity undergoes a more significant decrease for the laminar than for

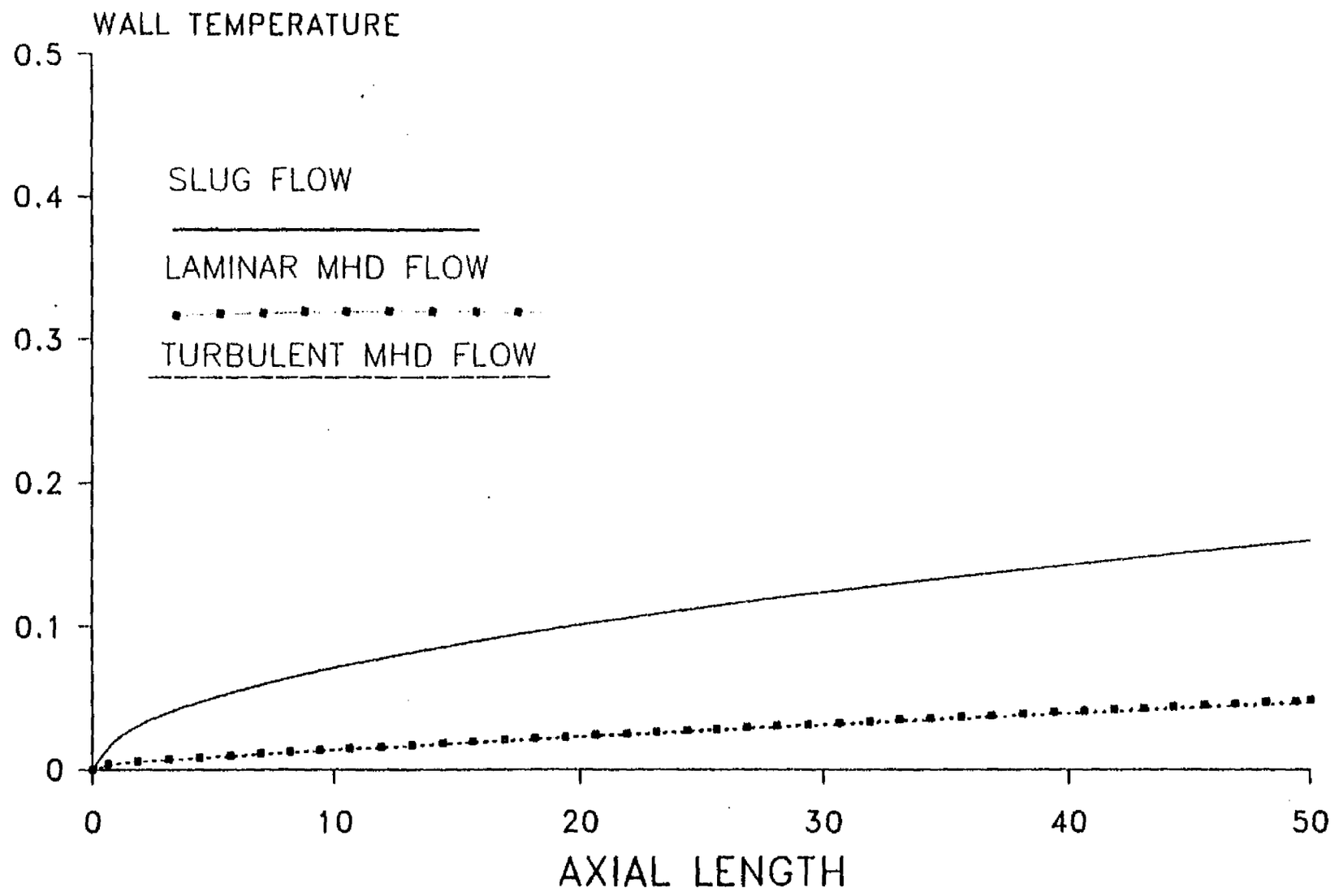

Figure 5.28: Slug, laminar and mean wall temperature vs x at $y = 0$. $M = 10^5$, $c = 0.05$, $Pe = 2500$.

the turbulent flow.

Figures 5.38 - 5.41 show the wall temperature profiles for $M = 10^4$ and $Pe = 500$, and for wall conductance ratios equal to 0.05, 0.01, 0.001 and 0, respectively. With the reduction in the Hartmann number, the essential trends with respect to variations in c and Pe remain unchanged and, in this case as well, turbulence does not seem to produce beneficial heat transfer effects: the RNG turbulence model predicts higher turbulent wall temperatures than in the laminar case. For $c = 0.05$ (fig. 5.38), the turbulent profile is very close to the laminar one, although the former is higher. Reducing the wall conductance ratio to 0.01 (fig. 5.39), this tendency persists but the difference between the wall temperature values calculated with laminar and turbulent flows becomes even larger. For $c = 0.001$ (fig. 5.40), the turbulent profile gets very close to the slug flow profile, while the laminar profile remains below. Finally, the insulating case (fig. 5.41) shows the same behavior as for $M = 10^5$, that is, laminar and turbulent profiles overlap, while the profile calculated with a slug flow shows lower wall temperatures. For $Pe = 2500$, a global decrease in the wall temperature is observed but the general trends remain practically unchanged. Results for $M = 10^3$ present essentially the

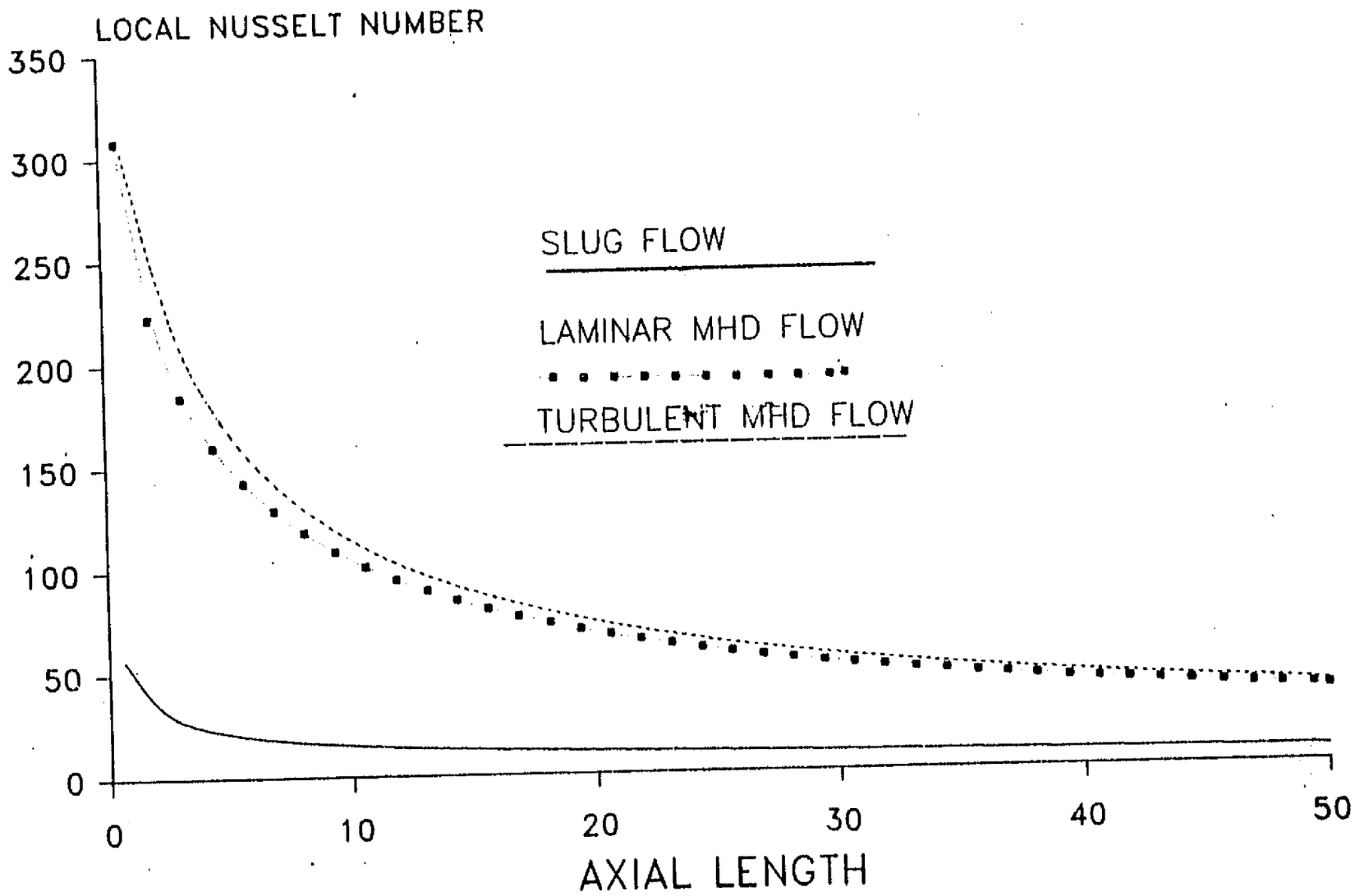

Figure 5.29: Local Nusselt number vs x at for slug, laminar and turbulent flows. $M = 10^5$, $c = 0.05$, $Pe = 2500$.

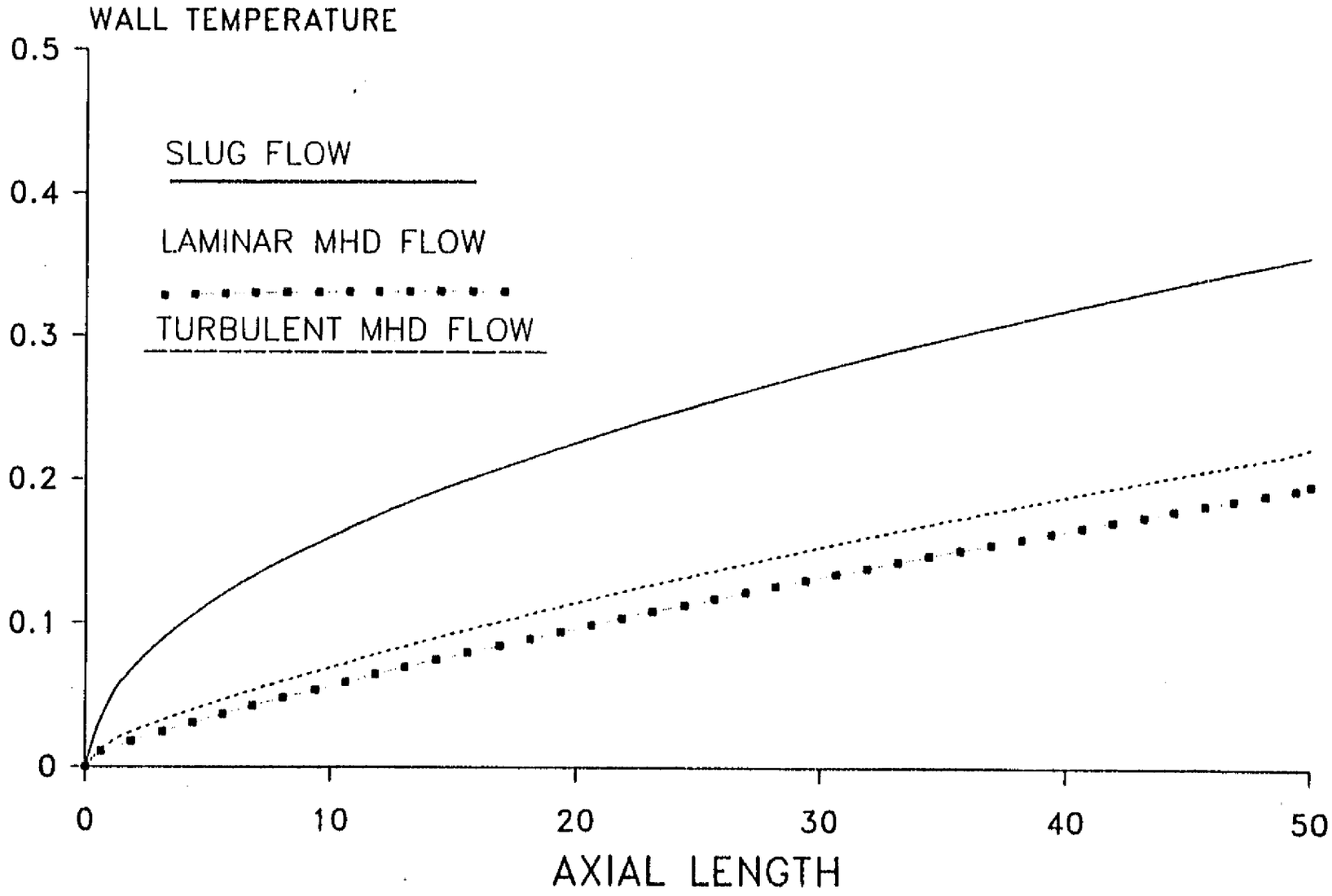

Figure 5.30: Slug, laminar and mean wall temperature vs x at $y = 0$. $M = 10^5$, $c = 0.01$, $Pe = 500$.

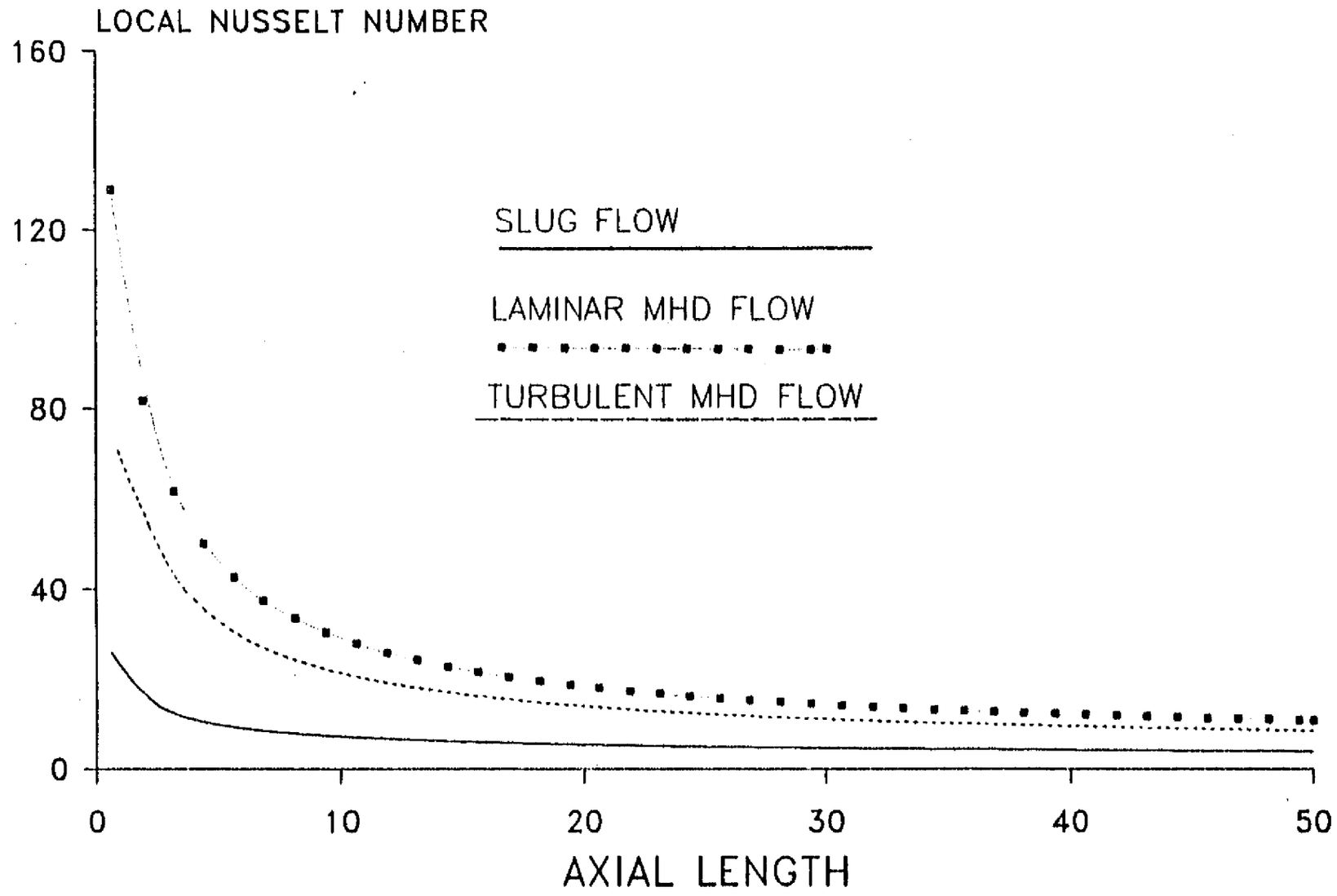

Figure 5.31: Local Nusselt number vs x at for slug, laminar and turbulent flows. $M = 10^5$, $c = 0.01$, $Pe = 500$.

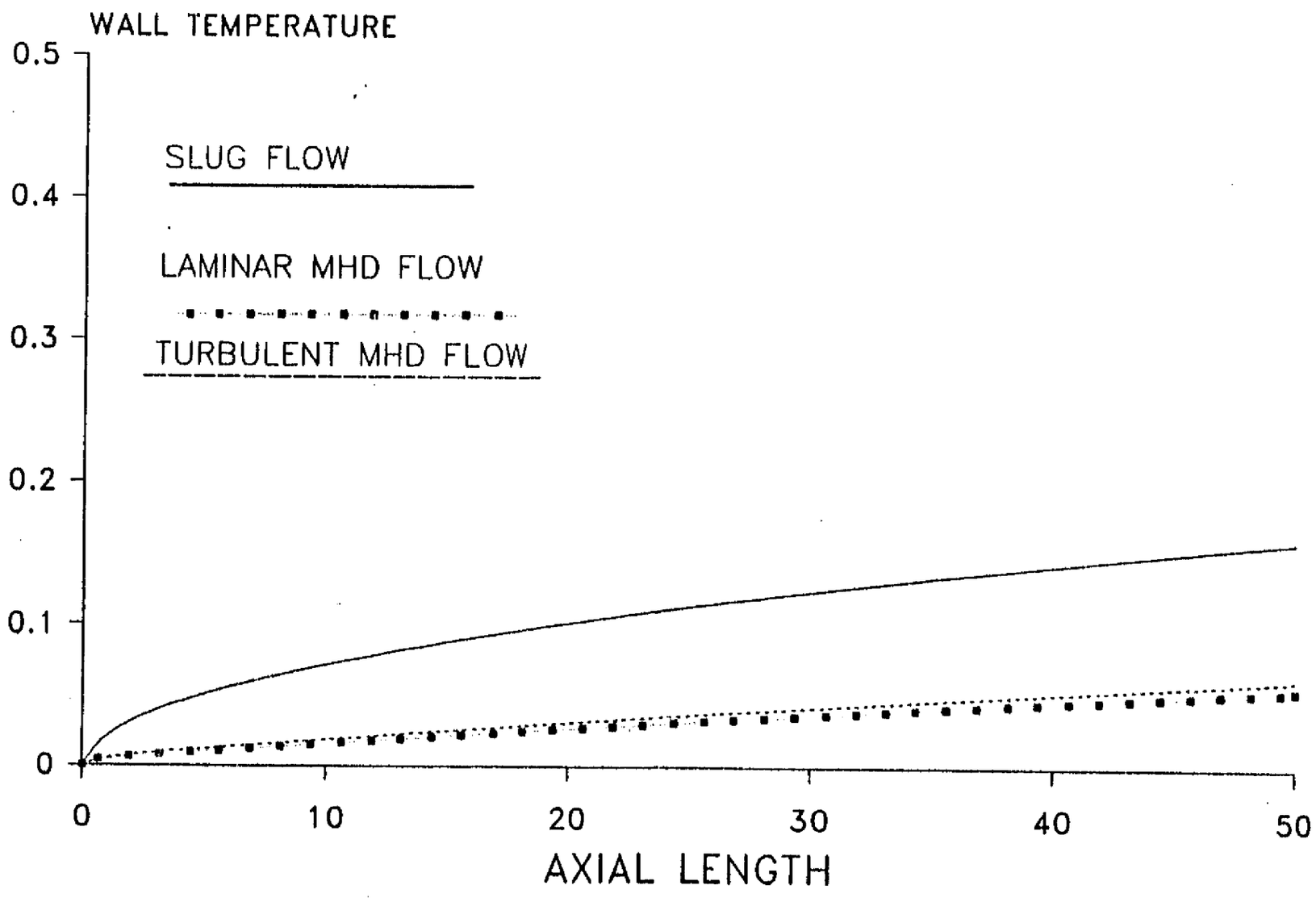

Figure 5.32: Slug, laminar and mean wall temperature vs x at $y = 0$. $M = 10^5$, $c = 0.01$, $Pe = 2500$.

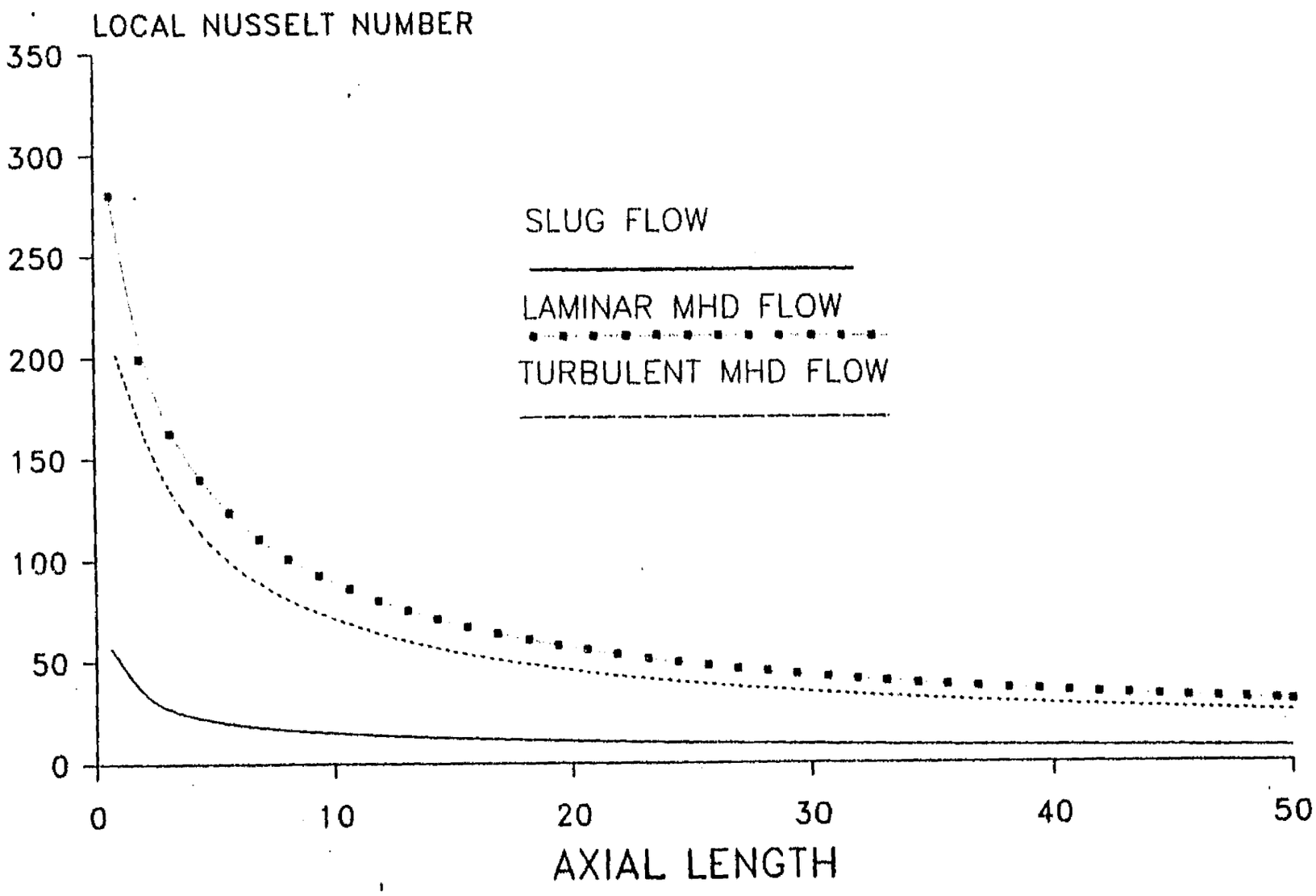

Figure 5.33: Local Nusselt number vs x at for slug, laminar and turbulent flows. $M = 10^5$, $c = 0.01$, $Pe = 2500$.

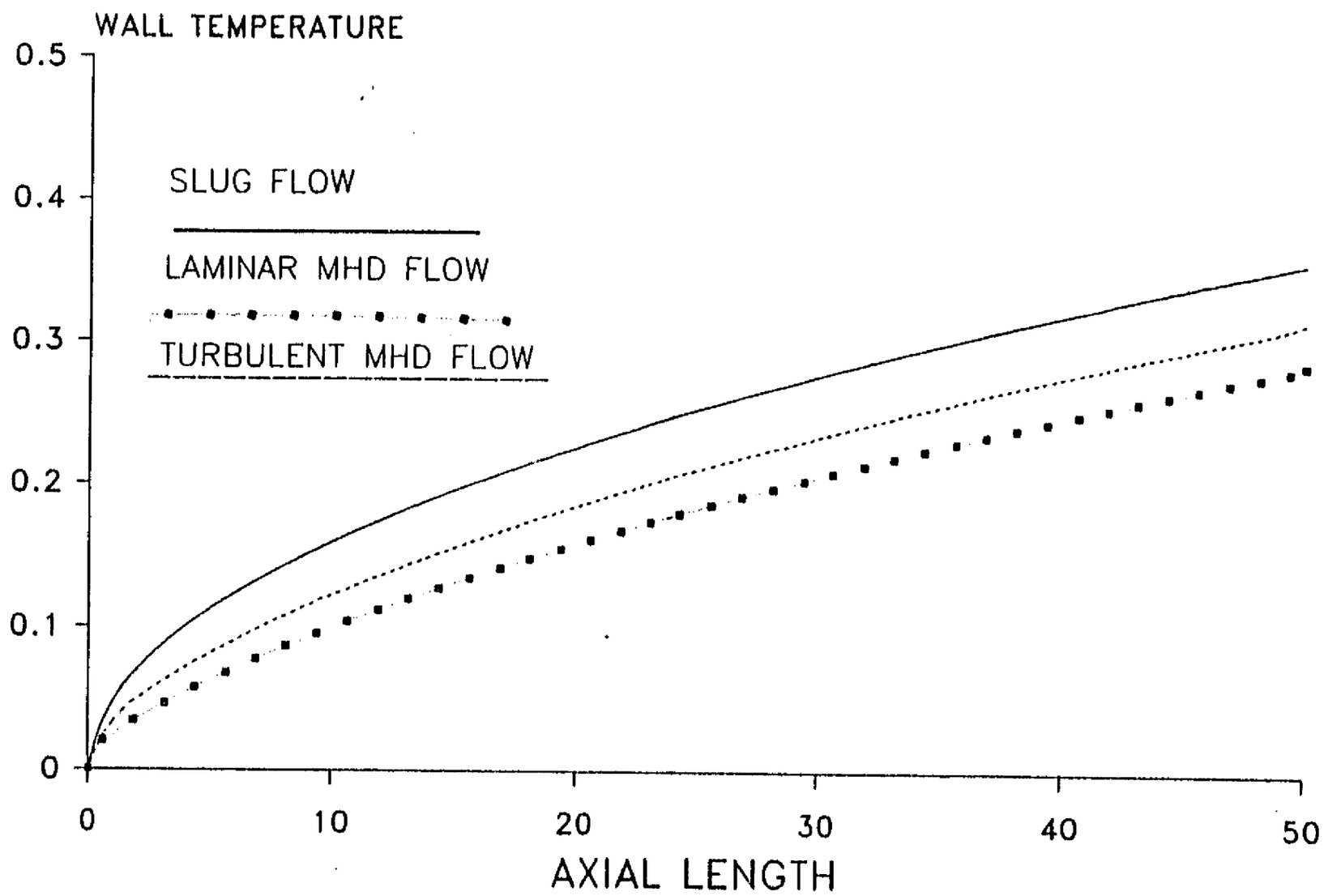

Figure 5.34: Slug, laminar and mean wall temperature vs x at $y = 0$. $M = 10^5$, $c = 0.001$, $Pe = 500$.

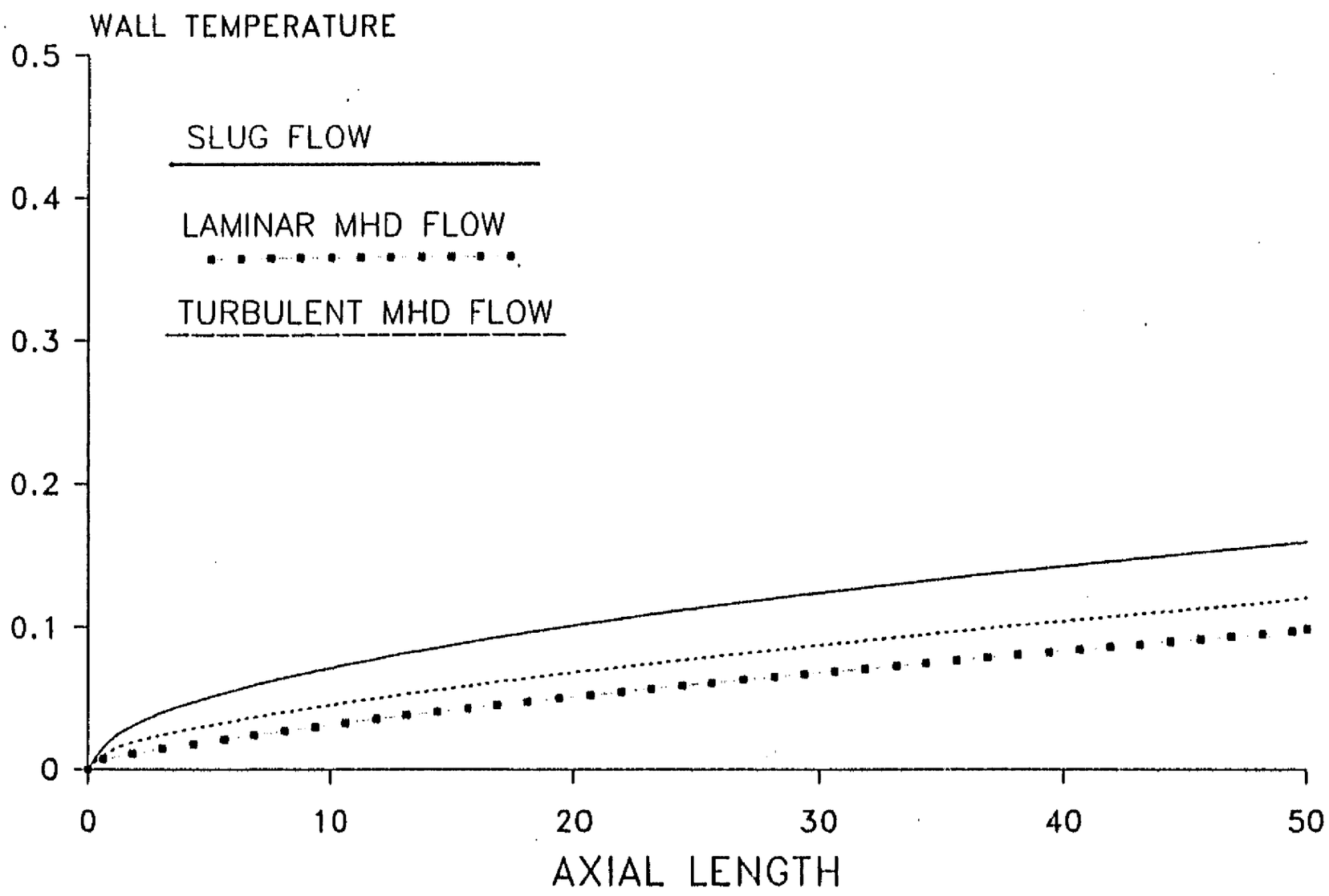

Figure 5.35: Slug, laminar and mean wall temperature vs x at $y = 0$. $M = 10^5$, $c = 0.001$, $Pe = 2500$.

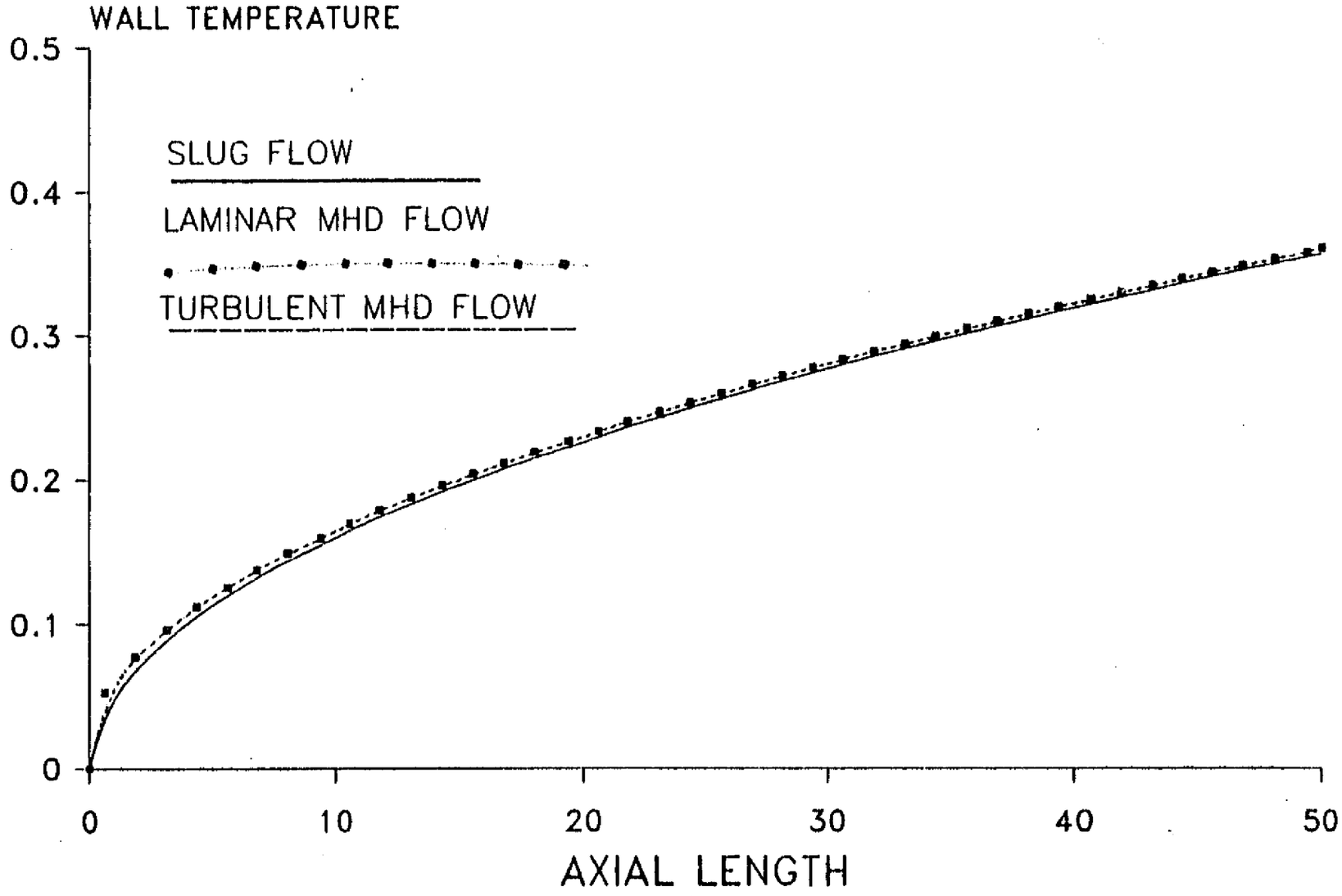

Figure 5.36: Slug, laminar and mean wall temperature vs x at $y = 0$. $M = 10^5$, $c = 0$, $Pe = 500$.

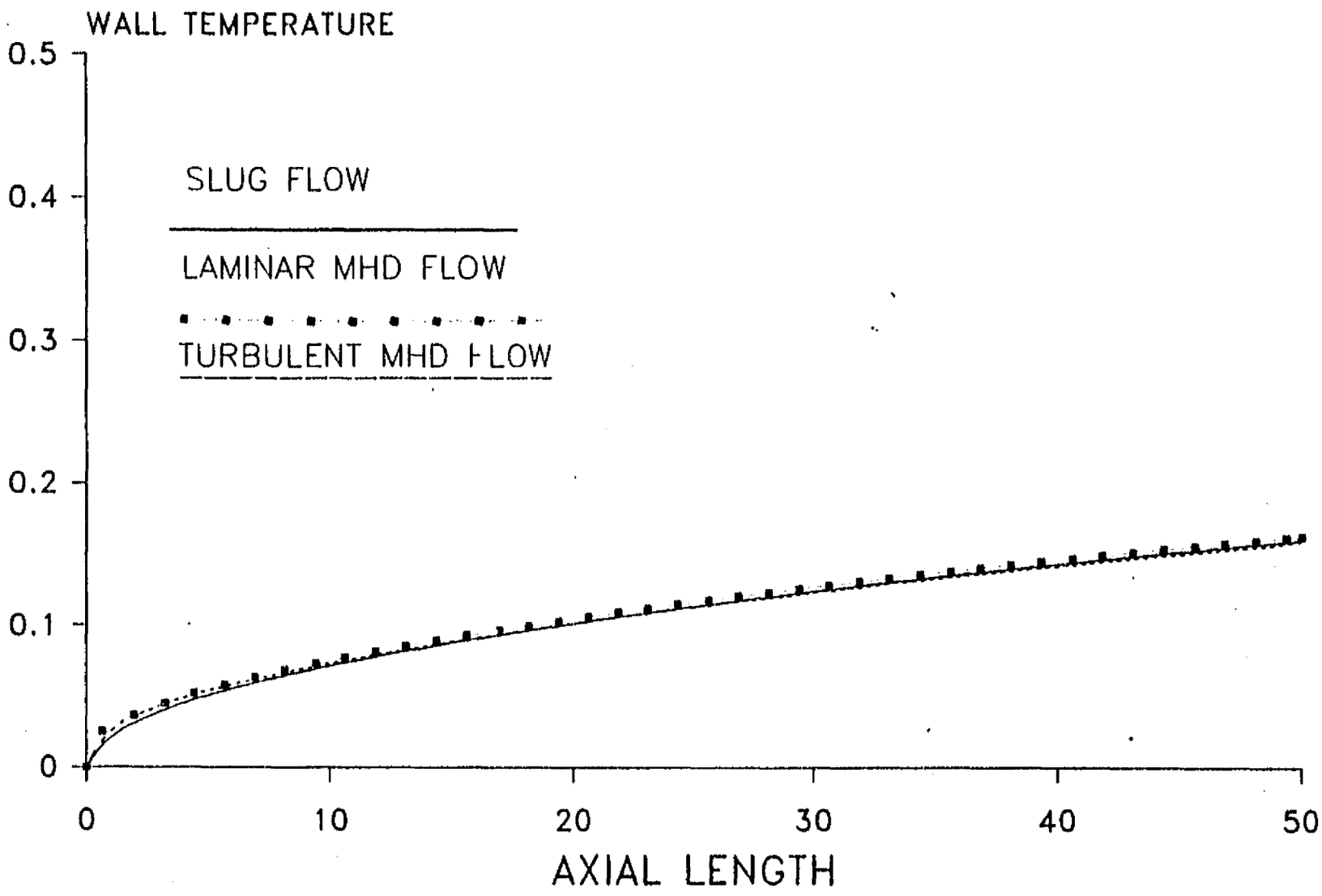

Figure 5.37: Slug, laminar and mean wall temperature vs x at $y = 0$. $M = 10^5$, $c = 0$, $Pe = 2500$.

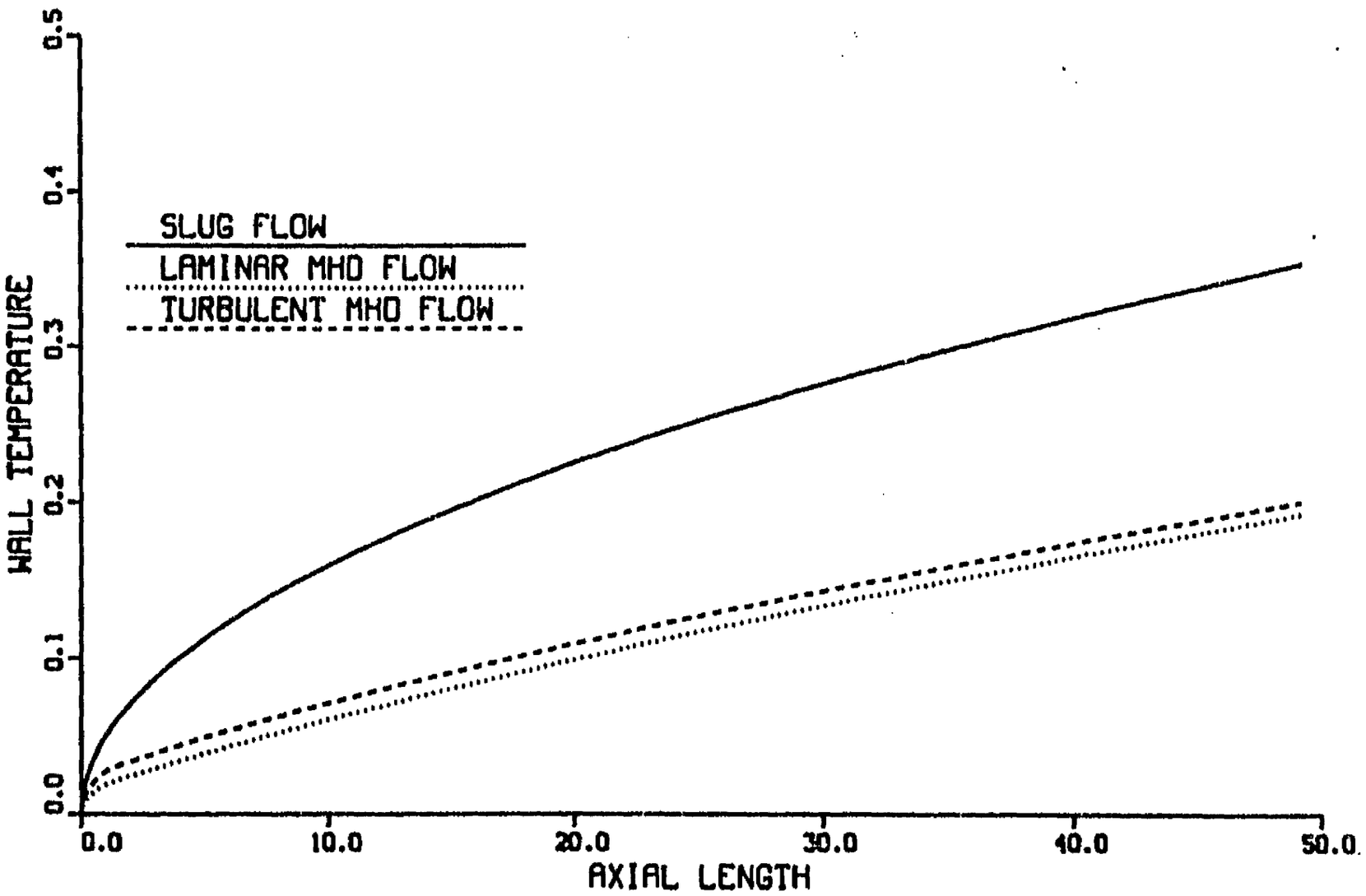

Figure 5.38: Slug, laminar and mean wall temperature vs x at $y = 0$. $M = 10^4$, $c = 0.05$, $Pe = 500$.

same trends as for $M = 10^4$ and are not shown here. In this case as well, profiles calculated with a thin conducting turbulent flow give higher wall temperatures than the corresponding laminar MHD profiles. For laminar as well as turbulent flows, a reduction in the Hartmann number leads to higher wall temperatures, whatever the values of c and Pe. This fact is explained through the changes in the (mean) velocity profiles.

We would have expected that, for thin conducting wall ducts, the turbulent wall temperature would have been lower than the laminar case, independently of the Hartmann and Péclet numbers, instead of the reversed behavior predicted by the model. For the analyzed Hartmann numbers, the joint effect of the mean velocity profile and the non-uniform total thermal diffusivity does not improve the heat transfer in the near-the-wall region with respect to the laminar cases. This indicates that the heat removal mechanism by turbulent mixing in the boundary layer is not as efficient as the laminar side-wall-jets.

We can summarize the main conclusions of the turbulent heat transfer analysis, for the considered range of parameters, in the following form:

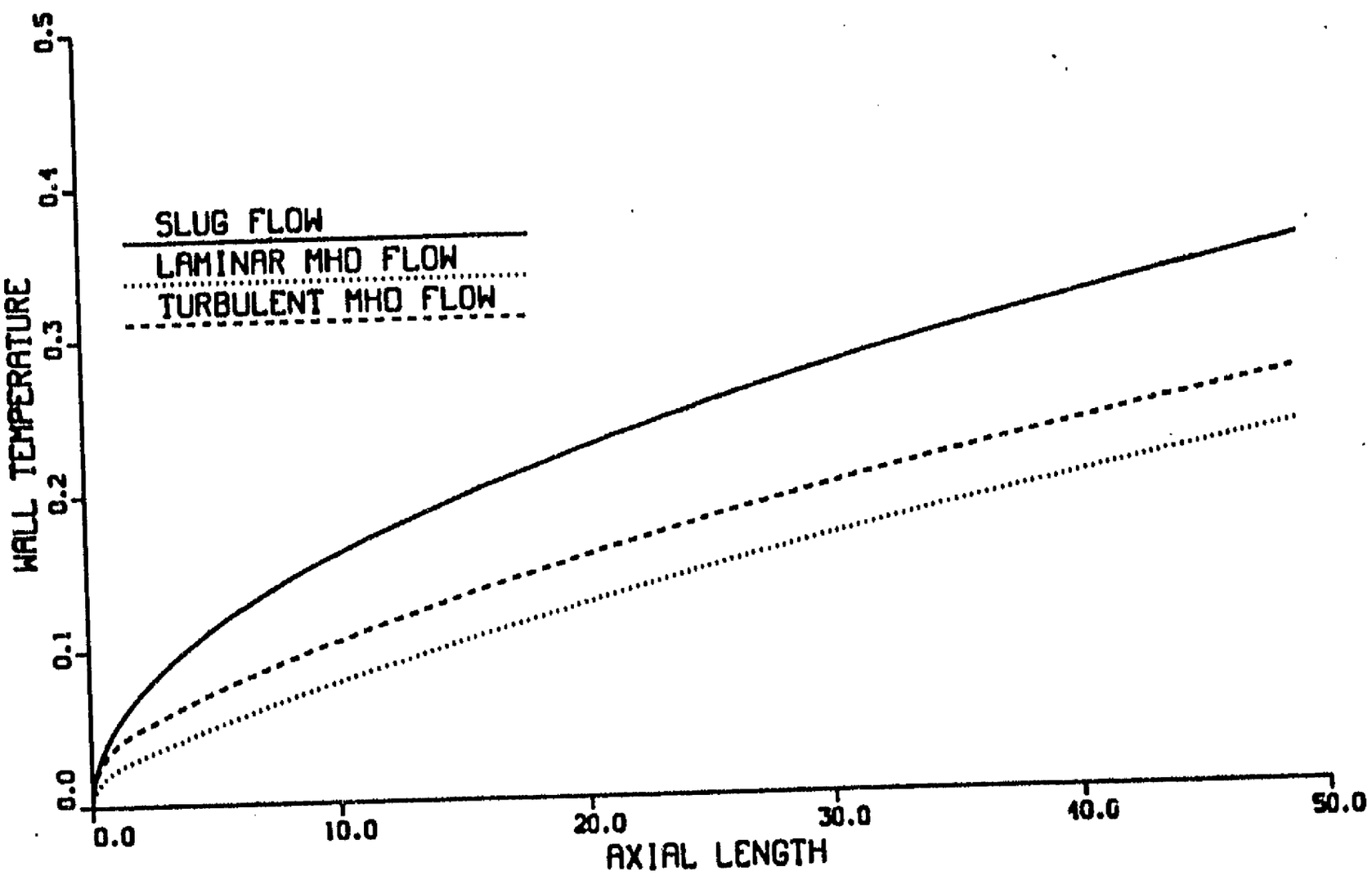

Figure 5.39: Slug, laminar and mean wall temperature vs x at $y = 0$. $M = 10^4$, $c = 0.01$, $Pe = 500$.

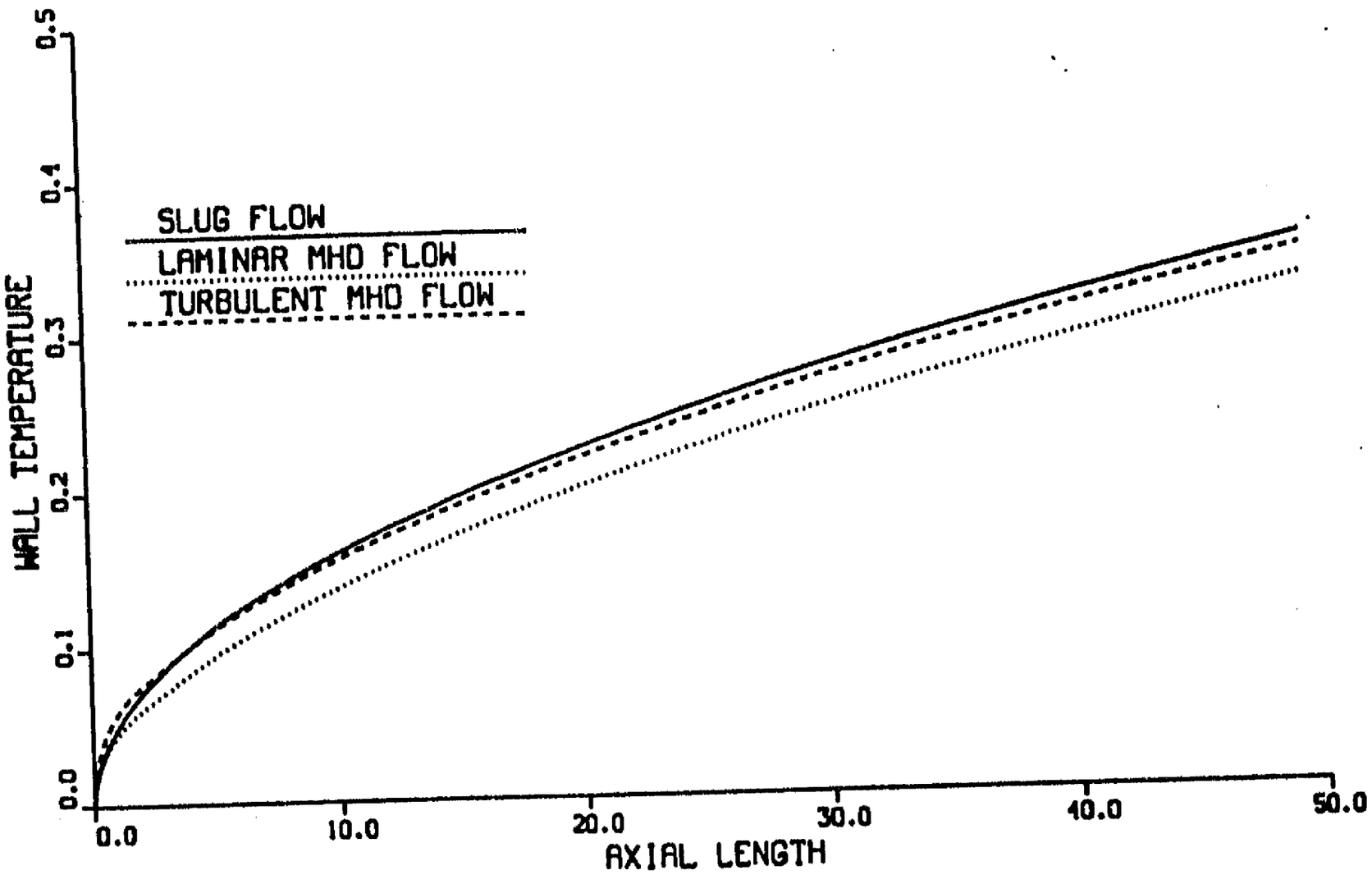

Figure 5.40: Slug, laminar and mean wall temperature vs x at $y = 0$. $M = 10^4$, $c = 0.001$, $Pe = 500$.

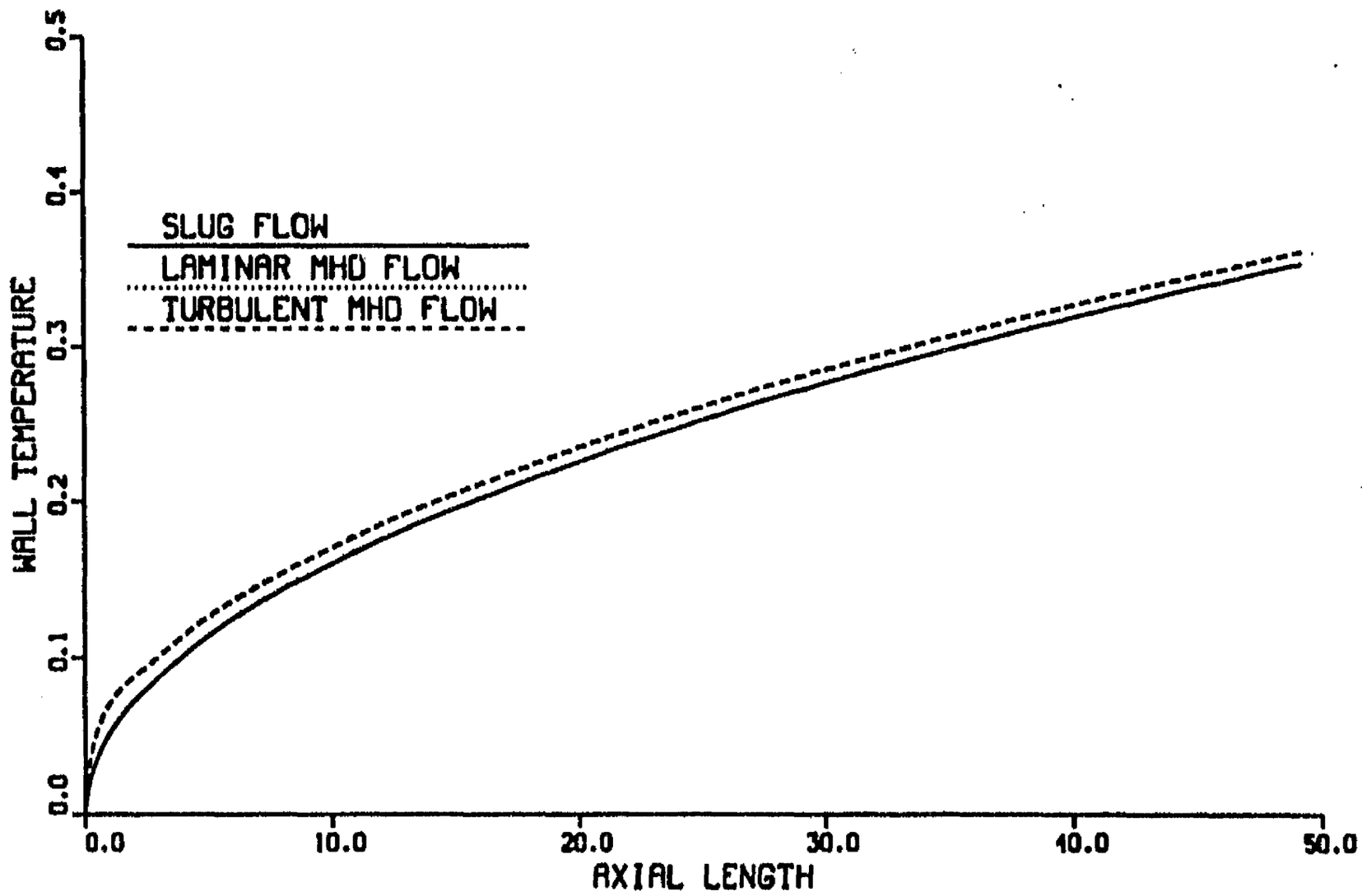

Figure 5.41: Slug, laminar and mean wall temperature vs x at $y = 0$. $M = 10^4$, $c = 0$, $Pe = 500$.

- Turbulent effects on the heat transfer are not as strong as on the flow dynamics, leading to more dramatic changes in the mean velocity profiles than in the mean temperature distributions, with respect to laminar cases. Viscous and thermal total diffusivities display similar behavior although the former is several orders of magnitude larger than the latter.

- For both laminar and turbulent flows, the higher Pe, the stronger the convective effects and the lower the wall temperature, whatever the value of M and c.

- For both laminar and turbulent flows, as c decreases, the wall temperature increases, whatever the value of M and Pe.

- For both laminar as well as turbulent flows, a reduction in M leads to higher wall temperatures, whatever the values of c and Pe.

- The laminar MHD heat transfer mechanism in thin conducting wall ducts is more efficient than the turbulent for most of the studied cases. The increase in the total thermal diffusivity in the boundary layer produced by turbulence does not compensate the reduction in the mean side layer velocity. In general, turbulent mixing in the boundary layer is not strong enough to reduce the mean wall temperature to lower levels than those obtained with the laminar MHD flow, characterized by high-velocity side-wall-jets.

- For a given M and large Pe, laminar, *turbulent* and slug flows in insulating wall ducts are equivalent in the heat transfer problem. For low Pe ($\leq$ 500), heat removal by slug flow is more efficient than MHD flows.

Chapter 6

Conclusions

The fully developed flow of a liquid-metal in a square duct in the presence of a strong transverse magnetic field was investigated. A spectral collocation solution for the composite core-side-layer flow, which offers the possibility of considering thin conducting as well as insulating wall duct flows, was found for both laminar and turbulent regimes. Therefore, the range of interest of wall conductance ratios for fusion blanket technology (0.05-0) was explored. In addition, very high Hartmann numbers characteristics of fusion applications were also considered ($10^3 - 10^5$). A very good agreement of the laminar velocity profiles calculated with the spectral collocation method and the available analytical solutions was found. The core-side-layer spectral collocation solution allowed the successful resolution of the side layers in a very efficient computing way, even for Hartmann numbers as high as 10^5, contrasting with finite difference approaches which prove inefficient even for $M \leq 10^3$. The transition from a thin conducting to an insulating wall duct clearly reveals the dramatic change in the flow structure, from a flow with high velocity side-wall-jets to a slug-like flow. An increase in the Hartmann number leads to higher side layer velocity values for thin conducting wall cases and to flatter profiles for insulating wall cases. The flow stability problem has not been explored in this work. A careful stability analysis extending the results obtained by Ting *et al.* [1991], is among the relevant tasks for a future investigation. The influence of the laminar velocity profiles on the heat transfer was studied by solving, by a finite differences method, the heat transfer equation in a square duct with one uniformly heated side wall and three insulating walls. Numerical results confirmed the beneficial heat transfer effects of the thin conducting wall duct flows where the side layer velocity is $O(M^{\frac{1}{2}})$ and carries a fraction of the $O(1)$ volume flux, with respect to calculations performed with slug flow, in the range of analyzed Hartmann numbers. The effects are larger in the mid-plane where the side-wall-jets reach their peak velocity. On the other hand, for insulating wall duct flows where the side layer velocity is $O(1)$, slug and MHD flows presented a quite similar heat transfer performance. The wall temperature profiles for a given M and different c's, clearly display the transition from thin conducting to insulating wall duct cases.

Turbulent effects were introduced in the core-side-layer solution through an eddy viscosity model from the Renormalization Group (RNG) theory of turbulence. Al-

though there is no experimental evidence that a fully developed turbulent regime can be reached under fusion reactor relevant conditions, and more studies are necessary to establish if the side layer instability may, under certain conditions, evolve into a fully developed turbulent flow, the approach we followed offers the possibility of exploring the flow behavior beyond the laminar regime. Intrinsic limitations of the model for MHD flows prevented a full quantitative description. Nevertheless, turbulent results showed physically reasonable trends. As a matter of fact, the presence of turbulence in thin conducting wall duct flows was manifested by a marked decrease of the side layer velocity, a thickening of the boundary layer and a notorious increase of the total viscosity. While the former effects were amplified as the Reynolds number increased, turbulence only affected the boundary layer region, the core remaining unperturbed. A reduction in the wall conductance ratio brought about a *laminarization* effect, in the sense that turbulent effects were lessened for a given M and Re. This is a clear consequence of the reduction of the side-wall-jets, which are the main source of turbulence phenomena. In the limit of insulating wall ducts, where the side-wall-jets have disappeared, the turbulence model predicted a laminar flow behavior whatever the Reynolds number, in the studied range. On the other hand, for thin conducting wall duct flows at $M \gg 1$, the magnetic field may play a turbulence promoting role in the sense that an increase in M led to stronger turbulent effects for a given Re. This, in turn, reveals the fact that the higher the side-wall-jets, the more susceptible of becoming turbulent and the higher the generated level of turbulence. The trends presented by turbulent results agreed, in general terms, with the qualitative stability analysis performed by Hunt [1965], though he only considered flows in either insulating or perfectly conducting wall ducts. Some resemblance of turbulent results with the overall behavior of the side-wall-jet instability experiments can be glimpsed although, due to differences in physical conditions, extrapolations would be tenuous. Nevertheless, we consider the present investigation as a first step towards the modeling of liquid-metal duct flows in strong magnetic fields beyond the laminar regime. The introduction of a turbulence magnetic suppression mechanism in the RNG model by dissipation of elongated vortices and the study of additional turbulence models are among the future tasks that we foresee.

Heat transfer results obtained with turbulent velocity and viscosity profiles and the RNG total thermal diffusivity formula showed that the heat transfer characteristics are less affected by turbulence than the flow dynamics. Although both viscous and thermal total diffusivities presented a notorious increase in the boundary layer region, the former is several orders of magnitude larger than the latter. This behavior is predicted by the RNG model when using low-Prandtl-number fluids. Some global physically reasonable trends of wall temperature profiles with variations of wall conductance ratio and Hartmann and Péclet numbers, for both laminar and turbulent MHD flows, were observed. Likewise, as a direct consequence of turbulent flow results, the heat transfer in insulating wall duct flows is the same for laminar and turbulent regimes and the wall

temperature profiles are practically the same for slug and MHD flows. Turbulent heat transfer results obtained with the RNG model for the thin conducting wall cases are not encouraging since a clear improvement in the heat transfer rates was only found for $M = 10^5$, $c = 0.05$ and $Pe = 2500$. In most of the analyzed cases, the laminar MHD heat transfer mechanism, characterized by high-velocity side-wall-jets, is more efficient than the turbulent mixing in the boundary layer. We would have expected that, in most of the cases, the turbulent mixing, reflected as a marked increase of the total viscosity in the boundary layer, would have led to lower wall temperatures than with laminar flows for thin conducting wall ducts. However, the results predict, in general, the opposite behavior. Here we face the question about the validity of the used model. In this study we have offered a consistent physical interpretation of the results thrown by the RNG model and, under these circumstances, no major objections have been found. However, the possibility that the RNG model is not suitable for the problem investigated here is still present. To discern about this point requires more theoretical and experimental work. Since we are exporting the RNG turbulence model from OHD to MHD flows, heat transfer results may be pointing to the necessity of scaling the RNG formula for MHD flows or introducing modifications in the model that account for the magnetic field effects on the heat transfer. Changes should be devised on an experimental basis. A phenomenological effective thermal diffusivity based on the experimental side-wall-jet instability results using, for instance, the mixing length theory, may provide an alternative approach for the assessment of the influence of side-layer velocity fluctuations on the heat transfer.

Bibliography

- Alemany, A., Moreau, R., Sulem, P.L. and Frisch, U. (1979) "*Influence of an External Magnetic Field on Homogeneous MHD Turbulence*", J. de Mécanique, **18**(2), pp. 277-313

- Batchelor, G.K. (1953) "*The Theory of Homogeneous Turbulence*", Cambridge University Press, Great Britain

- Batchelor, G.K. (1969) "*Computation of the Energy Spectrum in Homogeneous Two-Dimensional Turbulence*", Phys. Fluids Supplement II, pp. II-233239

- Bhatti, M.S. and Shah, R.K. (1987) "*Turbulent and Transition Flow Convective Heat Transfer in Ducts*", Handbook of Single-Phase Convective Heat Transfer, Kakac, S., Shah, R.K. and Aung (eds), Wiley, New York, pp. 4.59-63

- Blúms, E., Mikhailov, Yu.A. and Ozols, R. (1987) "*Heat and Mass Transfer in MHD Flows*", World Scientific, Singapur

- Bradshaw, H. (1976) "*Turbulence: Topics in Applied Physics*", vol. 12, Springer-Verlag, Berlin

- Branover, H. (1978) "*Magnetohydrodynamic Flow in Ducts*", Halstead Press, New York.

- Branover, H. and Gershon, P. (1979) "*Experimental Investigation of the Origin of Residual Disturbances in Turbulent MHD Flows After Laminarization*", J. Fluid Mech., **94**, pp. 629-647

- Branover, H., Sukoriansky, S., Talmage, G. and Greenspan, E. (1986) "*Turbulence and the Feasibility of Self-Cooled Liquid-Metal Blankets for Fusion Reactors*", Proc. American Nuclear Soc. Meeting, Reno, Nevada, June 15-19

- Branover, H. Greenspan, E. and Sukoriansky, S. (1988) "*Liquid Metal Turbulent Flow Phenomena and Their Implications on Fusion Reactor Blankets Design*", ITUAM Symp. on Liquid Metal MHD, Riga, Salaspils, USSR, May 16-20

- Camargo, S.J. and Tasso, H. (1992) "*Renormalization Group in Magnetohydrodynamic Turbulence*", Phys. Fluids B, **4**, pp. 1199-1212

- Canuto, C., Hussani, M.Y., Quarteroni, A. and Zang, T.A. (1987) "*Spectral Methods in Fluid Dynamics*", Springer-Verlg, New York.

- Carslaw, H.S. and Jaeger, J.C. (1959) "*Conduction of Heat in Solids*", Oxford University Press, Oxford.

- Conn, R.W., Chuyanov, V.A., Inoue, N. and Sweeetman, D.R. (1992) "*The International Thermonuclear Experimental Reactor*", Sci. American, April, pp. 103-110

- Cordey, J.G., Goldston, R.J. and Parker, R.R. (1992) "*Progress Toward a Tokamak Fusion Reactor*", Phys. Today, January, pp. 22-30

- Cuevas, S. and Ramos, E. (1991) "*Heat Transfer in an MHD Channel Flow with Boundary Conditions of the Third Kind*", Appl. Sci. Res., **48**, pp. 11-33

- Cuevas, S. and Ramos, E. (1993) "*Heat Transfer in an MHD Flow inside a Channel with Walls of Finite Thickness.*", Progress in Astronautics and Aeronautics AIAA, **148**, pp. 566-579

- Frisch, U. and Orszag, S. (1990) "*Turbulence: Challenges for Theory and Experiment*", Phys. Today, January, pp. 24-32

- Gold, R.R. (1962) "*Magnetohydrodynamic Pipe Flow. Part 1*", J. Fluid Mech., **13**, pp. 505-512

- Hinze, J.O. (1975) "*Turbulence*", 2nd ed. Mc Graw-Hill, New York

- Hua, T.Q., Walker, J.S., Picologlou, B.F. and Reed, C.B. (1988) "*Three-Dimensional Magnetohydrodynamic Flows in Rectangular Ducts of Liquid-Metal-Cooled Blankets*", Fusion Technology, **14**, pp. 1389-1398

- Hua, T.Q. and Picologlou, B.F. (1989) "*Heat Transfer in Rectangular First Wall Coolant Channels of Liquid-Metal-Cooled Blankets*", Fusion Technology, **15**, pp. 1174-1179

- Hua, T.Q. and Picologlou, B.F. (1991) "*Magnetohydrodynamic Flow in a Manifold and Multiple Rectangular Coolant Ducts of Self-Cooled Blankets*", Fusion Technology, **19**, pp. 102-112

- Hughes, W.F. and Young, F.J. (1989) "*The Electromagnetodynamics of Fluids*", Krieger Pub. Co., Malabar, Florida

- Hunt, J.C.R. (1965) "*Magnetohydrodynamic Flows in Rectangular Ducts*", J. Fluid Mech., **21**, pp. 577-590

- Hunt, J.C.R. (1969) "*A Uniqueness Theorem for Magnetohydrodynamic Duct Flows*", Proc. Camb. Phil. Soc., **65**, pp. 319-327

- Kolmogorov, A.N. (1941) "*The Local Structure of Turbulence in Incompressible Viscous Fluid for Very Large Reynolds Numbers*", Dokl. Akad. Nauk. SSSR **30**, pp. 299-303

- Kraichnan, R.H. (1967) "*Inertial Ranges in Two-Dimensional Turbulence*", Phys. Fluids, **1417**, pp. 1417-1423

- Kraichnan, R.H. and Montgomery, D. (1980) "*Two-Dimensional Turbulence*", Rep. Prog. Phys., **43**, pp. 547-619

- Kraichnan, R.H. (1987) "*An Interpretation of the Yakhot-Orszag Turbulence Theory*", Phys. Fluids A, **30**, p. 2400-2405

- Lam, S.H. (1992) "*On the RNG Theory of Turbulence*", Phys. Fluids A, **4**, pp. 1007-1017

- Landau, L.D., Lifshitz, L.V. and Pitaiievski, E. (1984) "*Electrodynamics of Continuous Media*", Pergammon, Oxford

- Langcope, D.W. and Sudan, R.N. (1991) "*Renormalization Group Analysis of Reduced Magnetohydrodynamics with Application to Subgrid Modeling*", Phys. Fluids B, **3**, pp. 1945-1962

- Lehnert, B. (1955) "*The Decay of Magneto-Turbulence in the Presence Magnetic Field and Coriolis Force*", Quart. Appl. Math., **12**, pp. 321

- Lilly, D.K. (1969) "*Numerical Simulation of Two-Dimensional Turbulence*", Phys. Fluids Supplement II, pp. II-240-249

- Lund, T. (1990) "*Application of the Algebraic RNG Model for Transition Simulation, in Instability and Transition*", Hussaini, M.Y. and Voigt, R.G. (eds.), Springer-Verlag, New York, **2**, p. 463.

- Miyazaki, K., Inoue, H., Kimoto, T., Yamashita, S., Inoue, S. and Yamaoka, N. (1986) "*Heat Transfer and Temperature Fluctuation of Lithium Flowing under Transverse Magnetic Field*", J. Nucl. Sci. Tech., **23**, pp. 582-593

- Mc Williams, J.C. (1983) "*Interactions of Isolated Vortices*", Geophys. Astrophys. Fluid Dyn., **24**, pp. 1-22

- Moffatt, H.K. (1967) "*On the Suppression of Turbulence by a Uniform Magnetic Field*", J. Fluid Mech., **28**, pp. 571-592

- Monin, A.S. and Yaglom, (1972) "*Statistical Fluid Mechanics*", The MIT Press, Cambridge, Massachsetts

- Moreau, R. (1968) "*On Magnetohydrodynamic Turbulence*", Proc. of Symp. on Turbulence of Fluids and Plasmas, Polyt. Inst. Brooklyn, New York pp. 359-379

- Moreau, R. (1990) "*Magnetohydrodynamics*", Kluwer Academic Publishers, The Netherlands

- Nestlerode, J.A. and Lumley, J.L. (1963) "*Initial Response of the Spectrum of Isotropic Turbulence to the Sudden Application of a Strong Magnetic Field*", Phys. Fluids, **6**, pp. 1260-1262

- Patankar, S.V. (1980) "*Numerical Heat Transfer and Fluid Flow*", Hemisphere Publishing Corporation, New York.

- Picologlou, B.F., Reed, C.B., Nygren, R. and Roberts, J. (1985a) "*Magneto-Fluid-Dynamic Issues for Fusion First-Wall and Blanket Systems*", Progress in Astronautics and Aeronautics AIAA, **110**, pp. 496-515

- Picologlou, B.F. (1985b) "*Magnetohydrodynamic Considerations for the Design of Self-Cooled Liquid-Metal Fusion Reactor Blankets*", Fusion Tech., **8**, pp. 276-282

- Picologlou, B.F., Reed, C.B. and Hua, T.Q. (1989) "*Thermal Hydraulic Considerations in Liquid-Metal-Cooled Components of Tokamak Fusion Reactors*", Proc. Fourth International Topical Meeting on Nuclear Reactor Thermal-Hydraulics, **2**, Karlsruhe, F.R.G., Edited by Muller, U., Rehme, K. and Rust, K., pp. 863-870

- Picologlou, B.F. (1992a) "*Heat Transfer in Liquid Metals in Strong Magnetic Fields*", Argonne National Laboratory, Internal Communication, October.

- Picologlou, B.F. (1992b) Private Communication.

- Platnieks and Freibergs (1972) "*Turbulence and Some Questions of Stability in Flows with M-Shaped Velocity Profiles*", Magnitnaya Gidrodinamika, No. 2, p. 29

- Press, W.H., Teukolsky, S.A., Vetterling, W.T. and Flannery, B.P. (1992) "*Numerical Recipes in Fortran*", 2nd ed., Cambridge University Press, USA

- Ramos, J.I. and Winowich, N.S. "*Finite Difference and Finite Element Methods for MHD Channel Flows*", Int. J. Num. Methods in Fluids, **11**, 907-934

- Reed, C.B., Picologlou, B.F. and Dauzvardis, P.V. (1985) "*Experimental Facility for Studying MHD Effects in Liquid Metal Cooled Blankets*", Fusion Technology, **8**, pp. 257-263

- Reed, C.B., Picologlou, B.F., Dauzvardis, P.V. and Bailey, J.L. (1986) "*Techniques for Measurement of Liquid-Metal MHD Flows*", Fusion Technology, **10**, pp. 813-821

- Reed, C.B. and Picologlou, B.F. (1989) "*Sidewall Flow Instabilities in Liquid-Metal MHD Flow under Blankets Relevant Conditions*", Fusion Technology, **15**, pp. 705-715

- Roberts, P.H. (1967) "*An Introduction to Magnetohydrodynamics*", Longmans, London.

- Rogallo, R.S. and Moin, P. (1984) "*Numerical Simulation of Turbulent Flows*", Ann. Rev. Fluid Mech., **16**, pp.99-137

- Schlichting, H. (1979) "*Boundary Layer Theory*", Mc Graw-Hill, New York.

- Shercliff, J.A. (1956) "*The Flow of Conducting Fluids in Circular Pipes under Transverse Magnetic Fields*", J. Fluid Mech., **1**, pp.644-666

- Shercliff, J.A. (1962) "*The Theory of Electromagnetic Flow Measurement*", Cambridge University Press, Great Britain.

- Shercliff, J.A. (1965) "*A Textbook of Magnetohydrodynamics*", Pergamon, Great Britain.

- Schumann, U. (1976) "*Numerical Simulation of the Transition from Three- to Two-Dimensional Turbulence under a Uniform Magnetic Field*", J. Fluid Mech., **74**, pp. 31-58

- Smith, D.L. et al., (1984) "*Blanket Comparison and Selection Study*" Fusion Technol., **8**, p.1

- Smith, L.M. and Reynolds, W.C. (1992) "*On the Yakhot-Orszag Renormalization Group Method for Deriving Turbulence Statistics and Models*" Phys. Fluids, **4**, p.364-390

- Sommeria, J. and Moreau, R. (1982) "*Why, How, and When, MHD Turbulence Becomes Two-Dimensional*", J. Fluid Mech., **118**, pp. 507-518

- Sommeria, J. (1983) "*Two-Dimensional Behavior of MHD Fully Developed Turbulence*", J. Méc. Theorique et Appliquée, Numéro Spécial, pp. 169-190

- Sommeria, J., Nguyen Duc, J.M. and Caperan, Ph. (1989) "*Two-Dimensional MHD Turbulence*", Liquid Metal Magnetohydrodynamics, Lielpeteris, J. and Moreau, R. (eds.) Kluwer Academic Publishers, The Netherlands, pp. 441-448

- Sterl, A. (1990) "*Numerical Simulation of Liquid-Metal MHD Flows in a Rectangular Ducts*", J. Fluid Mech., **216**, pp. 161-191

- Sukoriansky, S., Zilberman, I. and Branover, H. (1986) "*Experimental Studies of Turbulence in Mercury Flows with Transverse Magnetic Fields*", Experiments in Fluids, **4**, pp. 11-16

- Sukoriansky, S. and Branover, H. (1987) "*Turbulent Flows with Inverse Energy Cascade Realizable in a Laboratory. Part II- Numerical Methods*", Unpublished

- Sukoriansky, S. and Branover, H. (1988) "*Turbulence Peculiarities Caused by Interference of Magnetic Fields with the Energy Transfer Phenomena*", Progress in Astronautics and Aeronautics, AIAA, **112**, pp. 87

- Sukoriansky, S., Klaiman, D., Branover, H. and Greenspan, E. (1988) "*MHD Enhancement of Heat Transfer and its Relevance to Fusion Reactor Blanket Design*", Proc. Int. Symp. on Fusion Nucl. Technology, Tokyo, Japan, April 10-15

- Sukoriansky, S., Staroselsky, I., Galperin, B., Roy, S. and Orszag, S.A. (1992) "*Renormalization Group Analysis of MHD Turbulence with Low Magnetic Reynolds Number*", Progress in Astronautics and Aeronautics, AIAA, pp. 151-158

- Talmage, G. and Walker, J.S. (1988) "*Three-Dimensional Laminar Flow in Ducts with Thin Metal Walls and Strong Magnetic Fields*", Progress in Astronautics and Aeronautics, AIAA, **111**, pp. 3-25

- Talmage, G. (1989) "*Liquid Metal Brushes For Homopolar Devices*", Ph.D. Thesis, University of Illinois at Urbana-Champaign, USA

- Talmage, G., Walker, J.S., Brown, S.H., Sondergaard, N.A., Branover, H. and Sukoriansky, S. (1991a) "*Liquid-Metal Flows in Sliding Electrical Contacts: Solution for Turbulent Primary Azimuthal Velocity*", Progress in Astronautics and Aeronautics, AIAA, **148**, p. 165

- Talmage, G., Walker, J.S., Brown, S.H., Sondergaard, N.A., Branover, H. and Sukoriansky, S. (1991b) "*Liquid-Metal Flows in Sliding Electrical Contacts with Arbitrary Magnetic Field Orientations*", Phys. Fluids A, **3**, pp. 1657-1665

- Talmage, G., (1993) "*Heat Conduction in Liquid-Metals: A Comparison of Laminar and Turbulent Effects*", To be published.

- Tennekes, H. and Lumley (1972) "*A First Course in Turbulence*, The MIT Press, Cambridge, Massachussetts.

- Ting, A. (1991) "*Combined Analytical and Numerical Solutions in Liquid-Metal Flows in a Rectangular Duct with Uniform or Non-Uniform, Strong Magnetic Fields*", Ph.D. Thesis, University of Illinois at Urbana-Champaign, USA

- Ting, A., Walker, J.S., Moon, T.J., Reed, C.B. and Picologlou, B.F. (1991) "*Linear Stability Analysis for High-Velocity Boundary Layers in Liquid-Metal Magnetohydrodynamic Flows*", Int. J. Engng. Sci., **29**, pp. 939-948

- Ting, A., Hua, T.Q., Walker, J.S. and Picologlou, B.F. (1993) "*Liquid-Metal Flow in a Rectangular Duct with Thin-Metal Walls and with a Non-Uniform Magnetic Field*", Int. J. Engng. Sci., **31**, pp. 357-372

- Walker, J.S. (1981) "*Magnetohydrodynamic Flows in Rectangular Ducts with Thin Conducting Walls. Part I. Constant Area and Variable Area Ducts with Strong Magnetics Fields*", J. Méc., **20**, pp. 79-112

- Walker, J.S. and Picologlou, B.F. (1985) "*MHD Flow Control as a Design Approach for Self-Cooled Liquid-Metal Blankets of Magnetic Confinement Fusion Reactors*", Fusion Tech., **8**, pp. 270-275

- Walker, J.S. (1992a) "*Fully Developed Turbulent Liquid-Metal Flow in a Rectangular Duct with Thin Metal Walls*", Unpublished notes, University of Illinois at Urbana-Champaign, USA

- Walker, J.S. (1992b) "*Introduction to Spectral Methods*", Unpublished notes, University of Illinois at Urbana-Champaign, USA

- Winowich, N.S. and Hughes, W.F (1982) "*A Finite Element Analysis of Two-Dimensional MHD Flows*", Liquid Metal Flows and MHD, Proc. Third Beer-Sheva Int. Seminar on MHD Flows and Turbulence, Eds. Branover, H., Lykoudis, P.S. and Yakhot, A., Progress in Aeronautics and Astronautics, AIAA, **84**, pp.313-322

- Yakhot, V. and Orszag, S. (1986) "*Renormalization Group Analysis of Turbulence. I. Basic Theory*", J. Sci. Comput., **1**(1), pp. 3-51

- Yakhot, V., Orszag, S. and Yakhot, A. (1987) "*Heat Transfer in Turbulent Fluids-I. Pipe Flow*", Int. J. Heat. Transfer, **30**, pp. 15-22

- Yakhot, V., Orszag, S. and Panda, R. (1988) "*Computational Test of the Renormalization Group Theory of Turbulence*", J. Sci. Comput., **3**, pp. 139-147

- Yakhot, V., Kedar, O. and Orszag, S. (1992) "*An Algebraic-Q4 Turbulent Eddy Viscosity Model: Boundary Layer Flow over a Flat Pipe and Flow in a Pipe*", J. Sci. Comput., **7**(3), pp. 229-239